Manipulating the Properties of Hydrogels to Promote Ependymal Cell Behaviour for Spinal Cord Repair

Catherine Sarah Colquhoun

Submitted in accordance with the requirements for the degree of

Doctor of Philosophy

The University of Leeds

School of Mechanical Engineering

November 2019

The candidate confirms that the work submitted is her own and that appropriate credit has been given where reference has been made to the work of others.

Acknowledgements

Firstly, an enormous thank you to my supervisor Jim Deuchars, for not only giving me the opportunity to undertake a PhD in his group but also for all of his support and guidance over the last five or so years. I would also like to express great thanks to my co-supervisor Sue for all of her invaluable advice and personal support, along with her magical ability to rein Jim in.

I would also like to thank everyone in the Deuchars lab – for teaching me numerous fiddly experimental techniques, fuelling my coffee addiction, and getting me through the long days spent in the lab. Special thanks to Lauryn, Katie, Christian, Emily, Norah, and Nurha who have kept me sane along the way.

To my amazing friends and family who manage to make me smile every day, even if it is at something disgusting; I'm so lucky to have so many incredible people in my life. Thank you to my Mum, Dad, Rob, Jon, Amanda, and my best friend and twin Sarah – I couldn't ask for a better support network. Last but not least, I wouldn't have made it through this PhD without the love and endless support from Laurence and my three little munchkins. Thank you for dragging me out of bed in the morning and dealing with my hormones – let's hope I age like a fine wine rather than a blue cheese.

Abstract

Spinal cord injury (SCI) occurs when the spinal cord is physically crushed, impinged, severed, or otherwise damaged; resulting in irreversible disruption to the neuronal pathways responsible for motor and sensory function. The main obstacles to spinal cord repair include neuronal damage, loss of oligodendrocytes (leading to axonal demyelination), and scar formation with glial and fibrotic components. Despite the prevalence of SCI and its costly impact on society, treatment remains limited.

Ependymal cells (ECs) lining the central canal show promise as a pool of endogenous stem cells within the spinal cord. These cells are found to proliferate, differentiate, and migrate in response to injury, however at present, little is known about this neurogenic niche and how the local microenvironment influences cellular behaviour. This project aims to investigate whether endogenous EC behaviour can be altered by manipulating the properties of the surrounding matrix.

Nestin is a type VI intermediate filament protein and a marker of neural stem and progenitor cells in the central nervous system. Characterisation of transgenic mice expressing green fluorescent protein (GFP) under the control of nestin was carried out within this thesis; identifying these cells as ECs and pericytes in the spinal cord. (Nestin) GFP-positive ECs colocalised with a number of stem cell markers including: CD24, Sox2, and foxJ1.

ECs were also shown to express chemokine receptor type 4 (CXCR4), the main receptor to stromal cell-derived factor-1 (SDF-1); both of which are involved in the directed migration of neural cells through chemotaxis. The results of spinal cord slice cultures and intraspinal injections presented in this thesis suggest that EC behaviour can be manipulated using hydrogels and SDF-1α; towards repair of SCI.

Table of Contents

List of Figures

List of Tables

Abbreviations

13Ph	1,3-Phenylenediacetic acid
4Ph	p-Phenylenediacetic acid
aCSF	Artificial cerebrospinal fluid
Ad	Adipic acid
BrdU	5-bromo-2'-deoxyuridine
CD24	Cluster of differentiation 24
CD31	Cluster of differentiation 31
CD63	Cluster of differentiation 63
CNS	Central nervous system
CSF	Cerebrospinal fluid
CSFcC	Cerebrospinal fluid contacting cell
CSPG	Chondroitin sulphate proteoglycans
CPMG	Carr-Purcell-Meiboom-Gill sequence
CXCR4	Chemokine receptor type 4
DAPI	4', 6-diamidino-2-phenylindole
DG	Dentate gyrus
DMEM	Dulbecco's modified eagle's medium
EC	Ependymal cell
ECM	Extracellular matrix
EDC	1-(3-Dimethylaminopropyl)-3-ethylecarbodiimide hydrochloride
EdU	5-ethynyl-2'-deoxyuridine
FBS	Foetal bovine serum
FG	Fluorogold
FoxJ1	Forkhead-box J1
GABA	γ-ammino butyric acid
GAD-67	Glutamic acid decarboxylase 67
Gal-3	Galectin-3
GFAP	Glial fibrillary acid protein
GFP	Green fluorescent protein
GM	Grey matter
I.P.	Intraperitoneal
LPC	Lysophosphatidylcholine

MS	Multiple sclerosis
NeuN	Neuronal nuclei
NHS	N-hydroxysuccinimide
NSC	Neural stem cell
NSPC	Neural stem/progenitor cell
OPC	Oligodendrocyte progenitor cell
PB	Phosphate buffer
PBS	Phosphate buffered saline
PBST	Phosphate buffered saline with 0.1% Triton-X100
PFA	Paraformaldehyde
PKD2L1	Polycystic kidney disease 2-like 1 protein
PSA-NCAM	Polysialylated neural cell adhesion molecule
SaCSF	Sucrose artificial cerebrospinal fluid
SCI	Spinal cord injury
SDF-1α	Stromal derived factor 1α
SEM	Scanning electron microscopy
SGZ	Sub granular zone
Sox2	Sex determining region Y-Box 2
SVZ	Subventricular zone
T20	Phosphate buffered saline with 0.1% Tween20
TNBS	2,4,6-trinitrobenzene sulfonic acid
WM	White matter
βME	B-mercaptoethanol

Chapter 1 – General Introduction

1.1 The spinal cord

The spinal cord is part of the central nervous system (CNS) and spans the length of the spine; extending caudally from the medulla oblongata (part of the brain stem), enclosed within the foramen magnum and the vertebral column. Three concentric layers of membrane, the meninges, envelop the spinal cord and provide further protection. These layers include the dura mater, arachnoid mater, and the innermost pia mater. The spinal cord is organised along the rostro-caudal axis into four regions: cervical, thoracic, lumbar, and sacral (Figure 1.1 A). The spinal cord can be divided further into the white and grey matter, with the former being comprised of myelinated and unmyelinated axons making up the ascending (sensory) and descending (motor) nerve fibres. These are present in the form of tracts, which allow for the processing of sensory inputs and initiate movement of the body via afferent and efferent neuronal projections. Sensory afferent nerve fibres enter the spinal cord via the dorsal roots whereas the motor and preganglionic efferent nerve fibres exit via the ventral roots (Figure 1.1 B).

The grey matter forms the distinct butterfly shaped area, central to the spinal cord and this is comprised of dendrites and axons as well as glial cells and neuronal cell bodies organised into a series of 10 laminae in the transverse plane (Rexed, 1954). The dorsal horn contains laminae I-VI, the intermediate zone contains lamina VII, and the ventral horn contains laminae VIII-IX. At the centre of the cord is lamina X and the central canal (Figure 1.1 B). This thesis focuses on the central canal, and so the organisation of cells in this region will be detailed further below.

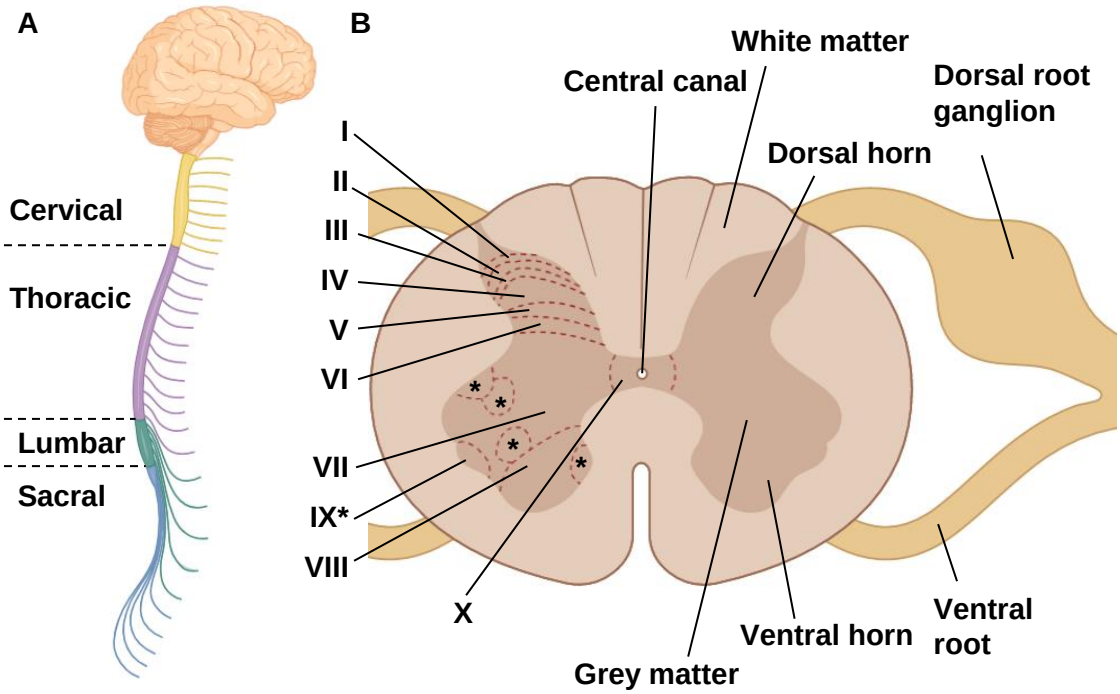

Figure 1.1 Schematic diagram of the spinal cord organisation

(A) Spinal cord segment organisation along the rostro-caudal axis including: cervical, thoracic, lumbar, and sacral regions. (B) Transverse section of the spinal cord and basic anatomical features and laminae (I – X). Drawn using BioRender.

1.1.1 Central canal region cellular organisation

The central canal region resembles a duct as it is surrounded by a heterogeneous cell population, through which the cerebrospinal fluid (CSF) flows. CSF is secreted by ependymal cells lining the choroid plexus and flows caudally from the lateral ventricles down through the spinal cord central canal. The CSF contains a number of ions (Na^+, Cl^-, HCO_3^-, K^+, Mg^{2+}, and Ca^{2+}), vitamins (e.g. folate, ascorbic acid), hormones, and peptides and proteins actively transferred from the blood (e.g. leptin) or synthesised in the choroid plexus (e.g. insulin-like growth factor and brain-derived neurotrophic factor).

The ependymal cells (ECs) are the most abundant cell surrounding the central canal and can be grouped into subtypes depending on their morphology. Ultrastructural

analysis of these cells using transmission electron microscopy identified three EC subtypes: biciliated cuboidal ECs, radial ECs, and tanycytes (Figure 1.2). Typical biciliated cuboidal ECs are the most common subtype and these cells possess motile cilia responsible for CSF propulsion (Alfaro-Cervello et al., 2012a). Radial ECs are found at the ventral and dorsal poles with long basal processes extending along the dorsoventral axis (Alfaro-Cervello et al., 2012a). Lastly, tanycytes are characterised by their single cilium and a long basal process terminating on blood vessels (Hugnot, 2011).

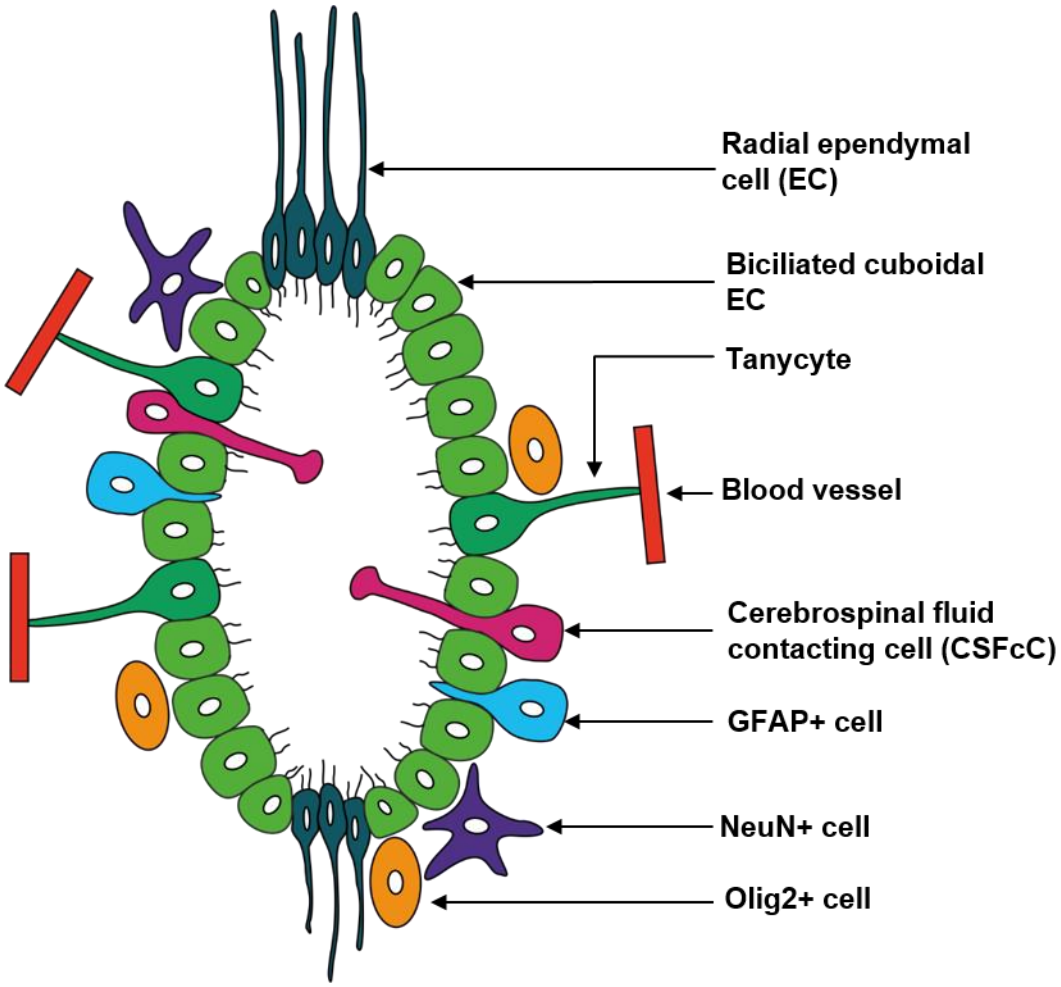

Figure 1.2 Central canal cellular organisation

Schematic of the murine spinal cord central canal, depicting the organisation of: radial ependymal cells (EC), biciliated cuboidal ECs, tanycytes, blood vessels, cerebrospinal fluid contacting cells (CSFcC), glial fibrillary acidic protein+ve (GFAP+) cells, neuronal nuclei+ve (NeuN+) cells, and oligodendrocyte transcription factor+ve (Olig2+) cells. Adapted from (Becker et al., 2018).

Cerebrospinal fluid contacting cells (CSFcCs) are located in the ependymal and subependymal layers within the central canal region and have “bulb-like protrusions” that extend into the CSF (Figure 1.2). In the spinal cord of lamprey and zebrafish these CSFcCs are sensitive to mechanical stimulation and changes in CSF pH (Jalalvand et al., 2016; Orts-Del’Immagine and Wyart, 2017).

Additional cells within the subependymal layer include: astrocytes (glial fibrillary acidic protein - GFAP+ve cells), oligodendrocyte progenitor cells (olig2+ve cells), and neurons (NeuN+ve cells).

1.2 Spinal cord injury

Spinal cord injury (SCI) occurs when the spinal cord is physically damaged due to contusion, laceration, or compression and although complete transection of the spinal cord is a rare occurrence in humans, axonal destruction is often observed, resulting in sensory and motor deficits. Each year in the UK alone, around 2,500 people sustain an SCI, leading to a cost of approximately £500 million per annum in immediate treatment costs resulting in a great social burden (backuptrust.org.uk, 2019).

SCI is typically classified according to its neurological level using the International Standards for Neurological Classification of Spinal Cord Injury. This tests the motor and sensory function of the patient. The level of SCI damage is defined as the most caudal level at which function remains intact (Lee and Thumbikat, 2015). Severity of such an injury is then graded (A-E) according to the American Spinal Cord Association Impairment Scale (NICE, 2016), and grouped according to the cause of damage, with patients presenting contusion or cavity injuries accounting for 49% of cases (Kim and Lee, 2014; Silva et al., 2014).

Despite the prevalence of SCI and its costly impact on society, treatment remains limited, with current therapies focussing on reducing pain and paralysis rather than promotion of spinal cord regeneration (Kim and Lee, 2014). The standard clinical

treatment for SCI consists of stabilisation and decompression of the spinal cord, followed by a high dose of the anti-inflammatory steroid methylprednisolone along with immune modulators (Silva et al., 2014). However, there is considerable debate around the efficacy of this pharmacological intervention (reviewed (Silva et al., 2014)) and so research into alternative strategies for repair still remains crucial.

1.2.1.1 SCI pathophysiology

To effectively design a treatment for SCI, firstly the pathophysiological processes that occur following injury must be understood. In all cases of SCI, the pathological progression can be subdivided into primary, secondary, and chronic phases.

The primary injury phase occurs through the initial insult to the spinal cord and can be grouped according to the morphological type: impact with persistent compression of the cord, impact with transient compression, distraction (separation of adjacent vertebrae), and laceration/transection. This initial insult leads to instantaneous cell death and damage, primarily affecting the softer central grey matter (Freund et al., 2013). Mechanical damage to the spinal cord also leads to haemorrhaging of the vasculature which disrupts blood flow, resulting in local infarction and additional damage due to ischemia (Dumont et al., 2001).

Furthermore, progressive post-traumatic damage also results in loss of motor and sensory function. Secondary acute (0 - 72 h) events include ionic changes, the formation of free radicals, glutamate excitotoxicity, apoptosis, and inflammation brought about by resident cells and invading immune cells when the blood-spinal cord-barrier (BSCB) is damaged (reviewed in more detail by (Silver and Miller, 2004; Oyinbo, 2011; Silva et al., 2014). Damaged cells also release adenosine triphosphate (ATP), thereby mediating chemotaxis of microglia towards the injury (Wu et al., 2007) and reactivity of astrocytes, oligodendrocytes, and oligodendrocyte progenitor cells via the activation of P2 purinergic receptors (James and Butt, 2002).

Mechanical shearing of myelinated axons results in the disruption of the myelin sheath which in turn leads to the accumulation of myelin inhibitors (Nogo-A, Myelin Associated Protein and Oligodendrocyte Myelin Glycoprotein) that hinder axon regeneration via binding to Nogo-66 receptor protein (Wang et al., 2006). Additionally, apoptosis of resident oligodendrocytes leads to further denudation of intact axons, impairing conduction and limiting functional recovery (Grossman et al., 2001; Hulsebosch, 2002).

In the chronic stage of SCI, a fibrous scar is formed at the damaged site in order to prevent further damage and promote repair. The fibrotic component of the scar formed following SCI is located at the centre of the lesion site, and this contains EC-derived astrocytes, stromal cells derived from Glast+ve cells deemed to be type-A pericytes, along with invading meningeal fibroblasts where the BSCB is compromised (Göritz et al., 2011).

The astrocytic response to spinal cord injury is typically referred to as reactive gliosis or astrogliosis. This is characterised by cellular hypertrophy, increased proliferation, process extension, and the production of intermediate filament proteins: GFAP, nestin, and vimentin, in and around the lesion site (Yang et al., 1994). While fibrotic scar formation results in a protective barrier around the site of injury; misalignment of reactive astrocytes occurs during the formation of the glial component at the injury border, followed by deposition of inhibitory chondroitin sulphate proteoglycans (CSPGs) and other extracellular matrix (ECM) proteins, thus creating a chemical and physical barrier to axonal regeneration and limited repair (Rolls et al., 2009; Yuan and He, 2013; Bradbury and Burnside, 2019).

When confronted with the glial scar, the growth cones of regenerating axons undergo dramatic morphological changes and halt elongation (Davies et al., 1999) reportedly via binding of sulphated proteoglycans to the LAR (leukocyte common antigen related gene) family of transmembrane protein tyrosine phosphatases (PTPσ and PTPδ) (Shen et al., 2009; Fisher et al., 2011) and the Nogo receptors: NgR1 and NgR3

(Dickendesher et al., 2012). Degradation of CSPGs via cleavage of glycosaminoglycan (GAG) chains using the bacterial enzyme chondroitinase ABC (ChABC) has previously been investigated to overcome this issue, resulting in the promotion of functional recovery *in vivo* following a bilateral lesion to the dorsal columns (C4 level) in rats (Bradbury et al., 2002). In this study ChABC was administered using a silastic tube inserted intrathecally, rostral to the lesion and recovery was assessed using immunohistochemistry, axon-tract tracing, electrophysiology and behavioural assessment. CSPG formation has also been inhibited *in vivo* using hepatocyte growth factor (HGF) from human mesenchymal stem cells (hMSCs) following a C4 “right over hemisection” injury in rats (Jeong et al., 2012). Transplantation of HGF-hMSCs resulted not only in significantly decreased GAG deposition, but also increased axonal growth beyond the glial scar and functional recovery of the forepaw. Glial scar formation has also been attenuated following experimental SCI using the natural anti-inflammatory agent curcumin, reducing astrogliosis and the presence of inflammatory cells, ultimately leading to improved functional repair (Wang et al., 2014; Jin et al., 2014).

This scar tissue does however, form a protective barrier and these astrocytes reduce secondary degeneration and regulate the injury site by scavenging excess ions (Cui et al., 2001) and protecting neurons from nitric oxide (Chen et al., 2001). Careful consideration must be taken of the scar’s dual and conflicting roles when designing repair strategies (reviewed by (Bradbury and Burnside, 2019)).

1.3 Manipulating neurogenesis post SCI

The production of new neurons as well as astrocytes and oligodendrocytes is typically referred to as neurogenesis. In the adult mammalian brain, postnatal neurogenesis occurs in two neurogenic niches: the dentate gyrus (DG) of the subgranular zone (SGZ) within the hippocampus (Toni et al., 2008), and the subventricular zone (SVZ) within the lateral ventricles (Lois and Alvarez-Buylla, 1994; Curtis et al., 2007).

Under physiological conditions, neuroblasts/type A cells are generated from radial glia-like stem cells within the SVZ and these then migrate along the rostral migratory stream (RMS) towards the olfactory bulb (OB) where they differentiate into interneurons (Lois and Alvarez-Buylla, 1994; Carleton et al., 2003). In the DG of the SGZ, radial glia-like stem cells proliferate and generate neuroblasts that migrate along the SGZ where they differentiate into neuronal and glial cells in the granular layer of the DG.

ECs in the spinal cord share a number of markers associated with the stem cells of the brain, including: sox2, a transcription factor involved in the maintenance of cell pluripotency (Zhang, 2014; Feng and Wen, 2015); nestin, an intermediate filament protein found in precursor cells of the developing and adult CNS (Hockfield and McKay, 1985; Gritti et al., 1996); and vimentin, an intermediate filament expressed in the radial glia of the developing DG (Sancho-Tello et al., 1995; Hamilton et al., 2009).

Nestin+ve cells isolated from the postnatal brain of transgenic mice using fluorescence-activated cell sorting (FACs) formed neurospheres and differentiated into neurons, astrocytes, and oligodendrocytes *in vitro* (Mignone et al., 2004). In the spinal cord of adult mice, nestin is expressed predominantly in dorsal and ventral ECs (Alfaro-Cervello et al., 2012b). Additionally, vimentin is expressed in the cytoplasm and some of the radial processes of ECs at the central canal of adult mice (Alfaro-Cervello et al., 2012b). CD133 (Prominin-1) is also expressed in human and murine embryonic stem cells (Uchida et al., 2000; Kania et al., 2005), and labels ependymal cells in the adult mouse SVZ and central canal (Lee et al., 2005; Coskun et al., 2008; Pfenninger et al., 2011). *In vitro,* ECs were tracked using tamoxifen-induced recombination in cells derived from foxJ1- and nestin-CreER mice; giving rise to inducible and permeant genetic labelling using β-galactosidase (β-gal) and GFP expression. These ECs were shown to form neurospheres that could be serially passaged (> 8 times), and were multipotent; differentiating into astrocytes, oligodendrocytes, and neurons (Meletis et al., 2008).

1.3.1 Neurogenesis following SCI

In the intact spinal cord, proliferation of ECs is restricted to self-renewal (Johansson et al., 1999; Meletis et al., 2008). However, in lower vertebrates ECs contribute significantly to neuronal regeneration and repair, and more recently, stem cell-like activity has been observed in mammals in response to injury (Johansson et al., 1999; Ogai et al., 2014a). ECs are thought to possess *"latent neural stem cell potential"*; proliferating and undergoing multilineage differentiation following SCI (Namiki and Tator, 1999; Takahashi et al., 2003; Lacroix et al., 2014), producing astrocytes responsible for scar formation 4 months post-injury (Barnabé-Heider et al., 2010; Stenudd et al., 2015).

In addition to this, ECs also generate myelinating oligodendrocytes and neurons *in vitro* (Meletis et al., 2008) crucial for the repair of SCI (Qin et al., 2015). 4 weeks following a dorsal funiculus incision in transgenic mice, analysis of the cellular fate of EC progeny using molecular markers and electron microscopy identified β-gal+ve ECs (recombined cells of FoxJ1-CreER mice) expressed Olig2 (oligodendrocyte marker) and these cells were scattered throughout the injury site, indicating EC multipotency *in vivo* (Meletis et al., 2008).

Following compressive injury in the adult rat, ECs proliferate and differentiate at the site of the lesion into reactive astrocytes, with differences observed following injuries of varying severity (Mothe and Tator, 2005a). Delivery of exogenous injury-reactive ECs and oligodendrocyte precursor cells has been investigated in a rat model of severe spinal cord contusion injury. Here the transplanted cells migrated to the lesion site and this resulted in significant motor function recovery (Moreno-Manzano et al., 2009).

1.3.2 Human postnatal neurogenesis

Postnatal human neurogenesis has been widely debated (e.g. (Spalding et al., 2013; Sorrells et al., 2018) and conflicting conclusions have raised questions regarding methodological factors and study design (reviewed in (Bergmann et al., 2015; Kempermann et al., 2018; Snyder, 2019). In a recent study by (Moreno-Jiménez et al., 2019) the post-mortem delay (time between death and tissue fixation) and method of tissue fixation greatly influenced the detection of postnatal neurogenesis in the DG of human tissue. In tissue samples with a post-mortem delay of 24 h and minimal tissue processing (no freezing or paraffin inclusion), the authors identified neurons at a range of maturation stages in the brain as identified by immunofluorescence cell labelling (Moreno-Jiménez et al., 2019). Here, colocalisation of doublecortin (DCX)+ve neurons was seen with both calretinin and calbindin; thereby identifying these cells as immature and more differentiated neurons respectively and indicating the presence of postnatal neurogenesis in the DG of neurologically healthy humans.

Studies have also shown that adult humans have central canal ECs (Mothe et al., 2011; Cawsey et al., 2015). ECs isolated from the human spinal cord immediately following death from stroke or trauma formed neurospheres expressing sox2 and nestin and differentiated into glial cells and neurons *in vitro* (Dromard et al., 2008; Mothe et al., 2011). Additionally, following trauma to the CNS, nestin immunoreactivity at the central canal increases (Cawsey et al., 2015). However, adult human spinal cord ECs aren't thought to proliferate *in vivo* following injury (Cawsey et al., 2015; Paniagua-Torija et al., 2018) suggesting these cells may need manipulating to promote endogenous repair.

1.3.3 Directing stem cell behaviour

Previous research has focussed on the use of stem cell transplants as a means of replacing the cells lost following spinal cord injury, however these are limited due to the safety and ethical issues, as well as the timely nature of stem cell procurement (reviewed by (Li et al., 2008; Sahni and Kessler, 2010). Hofstetter et al. found that

although transplantation of naïve neural stem cells improved motor function recovery within a rat model, allodynia-like hypersensitivity was caused in unaffected forepaws (Hofstetter et al., 2005). Additional problems associated with exogenous administration of neural progenitors include the risk of teratoma formation (Li et al., 2008) and issues related to cell fate when administered without differentiation cues (Panayiotou and Malas, 2013). Additional to this, implanted cell viability has been shown to be as low as 3% for human embryonic stem cell-derived cells in the injured CNS, leading to poor functional outcomes (Kawasaki et al., 2000; Li et al., 2008). Following focal ischemia in rat cerebral cortex, stem cell graft placement was also shown to be a determinant of cell survival, with human CNS-derived neurospheres having a greater survival rate in non-ischemic tissue rather than at the lesion site; highlighting the issue of the oxygen depleted environment into which these cells would be implanted (Kelly et al., 2004). Therefore, a potentially safer and novel approach to spinal cord repair would involve the manipulation of neurogenesis by endogenous stem cells *in situ.*

In the SVZ neurogenic niche, inflammatory signals and the regulation of Wnt activity contribute to adult stem cell quiescence, and therefore regulate the regenerative potential of these cells in the aging brain (Kalamakis et al., 2019). These mechanisms may therefore hold the key to manipulating adult spinal cord neurogenesis for injury repair. Antibody inhibition of the inflammatory cytokine, CXCL10 resulted in the activation of quiescent OB NSCs, and a significant increase in the number of newly born neuroblasts *in vivo* in mice (Kalamakis et al., 2019) (Figure 1.3). Whether spinal cord ECs are retained in a quiescent state by similar mechanisms is currently unknown, however, this study shows the potential for re-activation of stem cells in adult tissue.

The exercise-induced increase in circulating growth factors (Vascular Endothelial Growth Factor - VEGF (Leiter et al., 2019) and Insulin-like growth factor-I (IGF-I) (Carro et al., 2000; Nieto-Estévez et al., 2016)) positively modulates NPC proliferation and the generation of neurons in the DG. Additionally, Activating Transcription Factor 5 (ATF5)

downregulation, via Neural Growth Factor (NGF) or Neurotrophin-3 (NT-3) application, is required for the differentiation of neuronal progenitor cells to neurons (Angelastro et al., 2003) (Figure 1.3). This neurogenic response been enhanced using retinoic acid (RA); whereby RA increased the differentiation of NSCs, and significantly increased the response of stem cells to NT-3 in order to promote the generation of mature neurons (Takahashi et al., 1999).

IGF-I also promotes the proliferation and differentiation of oligodendrocyte-committed progenitor cells (McMorris and Dubois-Dalcq, 1988) and induces oligodendrogenesis from adult NSCs potentially via the blocking of BMP signalling (therefore blocking astrocyte generation – see Figure 1.3) (Hsieh et al., 2004). A number of additional growth factors also direct differentiation of NSCs into myelinating oligodendrocytes in the brain. Experimentally increasing Fibroblast Growth Factor receptor-3 (FGFR) activation, via ligand-independent activation of FGFR in transgenic adult mice, resulted in increased myelin repair following acute focal demyelination of the corpus callosum (induced by lysophosphatidylcholine (LPC) injection) as well as chronic global demyelination (induced by cuprizone diet) (Kang et al., 2019). Additionally, activation of the Epidermal Growth Factor receptor (EGFR) also directs NSC differentiation for the generation of OPCs and myelinating oligodendrocytes *in vitro* and *in vivo.*

In vivo administration of ChABC in combination with EGF, basic Fibroblast Growth Factor (bFGF), and Platelet derived growth factor-AA increased the proliferation of ependymal cells following SCI, promoted oligodendrogenesis, and reduced the differentiation of ECs into astrocytes (Karimi-Abdolrezaee et al., 2012). However, whether these oligodendrocytes were generated from ECs is not clear. Laminin also regulates oligodendrogenesis by increasing OPC survival in the SVZ indicating that the ECM is important in driving beneficial NSC differentiation and survival (Relucio et al., 2012); reviewed further in (Waly et al., 2014).

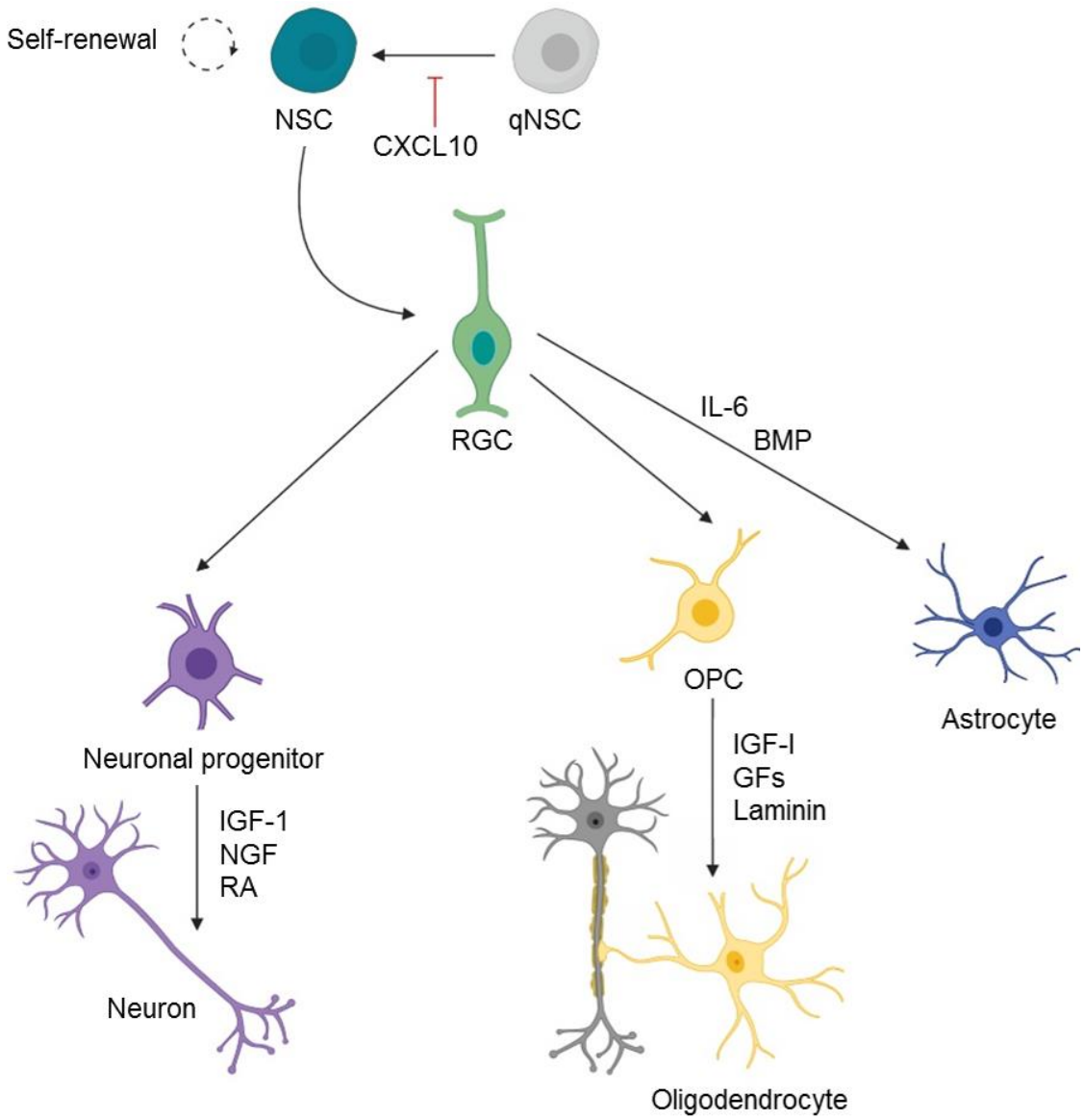

Migration cues		
NSC/RGC	OPC	Neuron
CXCR4 / SDF-1 CCR2 / CCL2 C-Met / HGF GABA	**CXCR4 / SDF-1** Netrin-1 Semaphorin 3A&F CXCL1 / CXCR2 PDGF-A / PDGFRa PSA-NCAM C-Met / HGF	**CXCR4 / SDF-1** Semaphorin 3A&F Netrin-1* PSA-NCAM?

Figure 1.3 Directing stem cell behaviour

Simplified schematic depicting examples of the pathways to neuron, oligodendrocyte, and astrocyte cell differentiation. Examples of the factors regulating differenatiation and migration are detailed. Cell repellants are detailed in red, * indicates a dual action. Created using BioRender.com.

Differentiation of NSCs down an astrocytic lineage is directed by activation of the Janus kinase-signal transducer and activator of transcription (JAK-STAT) pathway. This signalling pathway can be stimulated in NSCs by a number of cytokines from the interleukin-6 (IL-6) family, including: ciliary neurotrophic factor (CTNF) and cardiotrophin-1 (CT-1) (Johe, 1996; Rajan and McKay, 1998). Along with the JAK-STAT pathway, bone morphogenic proteins (BMP) also promote the preferential differentiation of NSCs into astrocytes during the gliogenic phase of development (Gomes et al., 2003; Miller and Gauthier, 2007).

Therefore, targeting growth factor receptors and signalling axes may provide a therapeutic mechanism for directing stem cell fate. Whether the cells within the spinal cord are controlled in a similar fashion is yet to be determined.

In order to manipulate endogenous ECs following injury into differentiating into preferential lineages, first we must attract these cells to the injury site via implantation or injection of molecules that direct cell migration – referred to as chemoattractants.

Directed migration of neural cells towards or away from endogenous and exogenously applied stimuli has been investigated (see examples in Figure 1.3). Interestingly, microglia and astrocytes have been implicated in the inflammatory reactions of a number of pathologies; releasing cytokines for attracting both immune cells along with stem and progenitor cells (Zuena et al., 2019), and these may play a critical role in manipulating the behaviour of ECs following SCI.

Chemokine ligand 2, CCL2, is expressed by microglia and astrocytes following a lesion to the brain and during multiple sclerosis (MS). CCL2 expression is thought to induce leukocyte migration and infiltration into the CNS (Babcock et al., 2003); thus mediating the immune response. CCL2 and Hepatocyte Growth Factor (HGF) also play a role in the migration of adult NSCs in an animal model of MS (Widera et al., 2004; Cohen et al., 2014). Here, the remyelination required for functional improvement following immune-mediated MS (experimental autoimmune encephalomyelitis - EAE model) is

initiated via the recruitment of OPCs to the de-myelinated region, followed by differentiation of these cells into myelin-forming oligodendrocytes. Chemotactic migration of OPCs is triggered via HGF secretion by reactive microglia (Lalive et al., 2005; Li et al., 2012).

Most notable across the neural cell types, is the regulation of directed migration via Stromal derived factor-1α (SDF-1α) signalling (Figure 1.3). SDF-1α activates CXCR4 and CXCR7; two G-protein-coupled receptors expressed in the developing and postnatal CNS (Banisadr et al., 2002; Stumm et al., 2003; Tissir et al., 2004; Cui et al., 2013). Binding of SDF-1α to these receptors is thought to result in the activation of a number of signal transduction pathways leading to calcium flux (Princen et al., 2003) and phosphorylation of focal adhesion components (Ganju et al., 1998; Kucia et al., 2004). Interestingly, CXCR4 is expressed by ependymal cells (Stumm et al., 2002) and therefore, SDF-1α /CXCR4 signalling could be a potential target for the manipulation of endogenous stem cells following spinal cord injury (see Chapter 6 for more detail).

Hydrogels have been identified as potential candidates for delivering chemokines for spinal cord repair. This is due to their physical and mechanical properties closely mimicking the spinal cord, along with the ability of their chemical composition to be adapted and functionalised. How the cells interact with their environment can influence their behaviour dramatically. There is therefore a need to consider EC response to hydrogel stiffness and first we will look at the mechanosensing of other neural stem cells.

1.4 Hydrogels for spinal cord repair

In order to manipulate endogenous stem cells and provide a growth-permissive environment at the site of injury, a tissue engineering approach could be utilised, encompassing both neuroprotection and regeneration. Biomaterials used for neural tissue engineering should meet a number of requirements in order to efficiently achieve this goal. They should be biocompatible, degrade at an appropriate rate *in vivo*, have a suitable mechanical strength, and should be porous in order to permit the flow of nutrients and migration of cells.

Among the various biomaterials available, hydrogels have been identified as promising candidates for spinal cord repair. This is due to their physical and mechanical properties closely mimicking the spinal cord, along with the ability of their chemical composition to be adapted and functionalised. Additionally, a number of hydrogels show promise for SCI repair as they can be delivered to the spinal cord via injection, due to their shear thinning properties and/or *in situ* gelation (Guvendiren et al., 2012; Yang et al., 2014). Previous research has included the release of growth factors, encapsulation of cells, and functionalisation using bioactive motifs to promote specific cell behaviour. The use of hydrogels for the repair of CNS injuries has been widely investigated, and these studies can be grouped according to hydrogel composition.

1.4.1 Synthetic hydrogels

Synthetic hydrogels have the advantage of being relatively simple to manipulate in order to adjust chemical and mechanical properties. While these are typically biocompatible, additional motifs are often required in order to achieve sufficient cell attachment (Table 1.1).

Polyethylene glycol (PEG) hydrogels have been shown to be biocompatible and neuroprotective within the CNS, with chemical modifications allowing for control over degradation rates (Mahoney and Anseth, 2006). Incorporation of peptide motifs such as arginine-glycine-aspartic acid-serine (RGDS), tyrosine-isoleucine-glycine-serine-

arginine (YIGSR), and isoleucine-lysine-valine-alanine-valine (IKVAV) has been achieved in 3D, with cellular extension being greatest on gels with RGDS (Gunn et al., 2005). Additional components such as collagen, poly-l-lysine (PLL) and the signalling molecules basic fibroblast growth factor (FGF-2) and ciliary neurotrophic factor (CNTF) have also been investigated using PEG hydrogels (Mahoney and Anseth, 2006; Burdick et al., 2006; Royce Hynes et al., 2007; Freudenberg et al., 2009). Sustained Neurotrophin-3 release was achieved using a degradable PEG-PLA (polylactic acid) hydrogel for the repair of spinal cord hemisection in rats, resulting in increased functional recovery and regeneration of axons (Piantino et al., 2006).

Poly-hydroxyethylmethacrylate (PHEMA) and poly-hydroxypropylmethacrylate (PHPMA NeuroGel^{TM}) hydrogels have recently been investigated for SCI repair. In an experimental model of SCI, both hydrogel physical properties and functionalisation were found to have a significant impact on axonal and blood vessel ingrowth (Hejčl et al., 2013) which has been shown to be important for oligodendrocyte development in the brain (Dejana and Betsholtz, 2016). PHPMA implantation into a 3 mm cat spinal cord transection resulted in regeneration of the descending supraspinal axons of the ventral funiculus as well as the afferent fibres of the dorsal column across the hydrogel implanted lesion site as identified by axonal labelling (BDA and WGA-HRP) and staining for neurofilaments and myelin basic protein (Woerly et al., 2001).

The peptide RADA16 developed by (Zhang et al., 1993) has been shown to self-assemble under physiological conditions into a hydrogel comprised of nanofiber networks displaying the laminin epitope IKVAV (Tysseling-mattiace et al., 2009). FGL, the neural cell adhesion molecule motif has been recently incorporated into such gels and assessed *in vitro* using a spinal cord-derived neural stem cell (SC-NSC) culture (Wang et al., 2015). A significant increase in cellular adhesion and proliferation was found for the functionalised gels compared to RADA16 gels alone. Furthermore, migration was increased for FGL functionalised gels, indicating a beneficial effect of such modification.

Table 1.1 Synthetic hydrogels investigated for spinal cord injury repair

Hydrogel	Modification	Assessment	Outcomes	Reference
PEG	PEG-diacrylate, RGDS, YIGSR, & IKVAV	PC12 cell culture	Extension of cells was greatest on RGDS functionalised gels.	(Gunn et al., 2005)
	PLA tri-block copolymer	Postmitotic neuron cell culture	Higher metabolic activity and proliferation with increasing percentage of PLA (degradable component - lactic acid) without shift toward glial phenotype.	(Lampe et al., 2010)
PHEMA & PHPMA (NeuroGelTM)	HEMA - MOETACL (positive surface charge), HPMA-SP, PMA-SP-RGD, HPMA-HS-RGD	Rat T8 hemisection	Porous HPMA-SP hydrogels promoted a statistically significant greater ingrowth of axons and less connective tissue elements into the implant. HPMA & RGD promote the ingrowth of blood vessels.	(Hejčl et al., 2013)
PHPMA	-	Cat T6-T7 transection	Axon re-growth, regeneration of descending supraspinal axons of the ventral funiculus and afferent fibres of the dorsal column across the reconstructed lesion.	(Woerly et al., 2001)
Self-assembling peptides	RADA16-FGL	Spinal cord derived NSC cultures	PGL promoted NSC proliferation and migration into the scaffold.	(Wang et al., 2015)
	K2(QL)6K2 (QL6)	Rat T6-T7 clip compression model	Reduced glial scar formation. Promoted axonal preservation/regeneration. Significant functional improvement of axons. Significant neurobehavioral recovery.	(Liu et al., 2013)

Abbreviations: HS: heterophase separation, NSC: neural stem cell, PEG: polyethyleneglycol, PHEMA: polyhydrocyethylmethacrylate[2-(methacryloyloxy)ethyl] trimethylammonium chloride, PHPMA: poly[N-(2-hydrocypropyl) methacrylamide, SP: solid porogen.

K2(QL)6K2 (QL6), another self-assembling peptide has also been investigated *in vivo* using a clip compression model of SCI in the spinal cord of rats (Liu et al., 2013). It was found that not only did this hydrogel significantly reduce astrogliosis and inflammation following injury (as shown by GFAP and Iba1 staining); QL6 injection also resulted in promoted axonal preservation (BDA anterograde and Fluorogold retrograde tracing) along with significantly enhanced functional improvement of axons as measured by electrophysiology. Injection of QL6 resulted in increased conduction velocity, reduced refractoriness and increased high-frequency conduction and significant behavioural/functional recovery occurred for rats receiving this treatment.

1.4.2 Natural hydrogels

A range of hydrogels derived from naturally occurring proteins, peptides, polysaccharides and GAGs have been utilised within the area of CNS repair (Table 1.2). These benefit from their inherent biocompatibility and degradability under physiologically relevant conditions as well as their biological activity.

Agarose is a linear polymer comprised of repeating agarobiose disaccharide subunits derived from algae and forms a hydrogel in the temperature range of 17– 40 ^{o}C. Laminin functionalised agarose hydrogels have been shown to promote dorsal root ganglion (DRG) cell migration and orientated neurite extension when cultured in 3D (Bellamkonda et al., 1995). Additionally, RGDS peptides (found in fibronectin) have been used to create modified channels, leading to orientated axon growth following DRG cell culture (Luo and Shoichet, 2004). More recently, a study by Caron et al. used an arginine-glycine-aspartic acid (RGD) cell adhesion sequence modified agarose/carbomer-based hydrogel for enhanced hMSC attachment, viability, and the delivery of paracrine factors *in vivo* (Caron et al., 2016). hMSCs were grown and these cells deposited ECM over 14 days prior to lyophilisation and re-seeding of the scaffolds for implantation; ultimately modulating the pro-inflammatory environment in a mouse SCI model.

Agarose gels can be loaded with lipid microtubules containing the neurotrophin brain-derived neurotrophic factor (BDNF), encouraging neurite growth into the hydrogels in a dorsal over-hemisection model *in vivo* (Jain et al., 2006).Templated agarose hydrogels have also been investigated in a rat model of SCI for the release of syngeneic marrow stromal cells expressing either BDNF or green fluorescent protein. (Gao et al., 2013) found that these gels organised regenerating axons into fascicles, and BDNF significantly enhanced neurite growth in a directional manner.

Local, sustained release of ChABC (Lee et al., 2010) and Rho GTPases (Cdc42 and Rac1) (Jain et al., 2011) has been achieved using agarose based hydrogels and lipid microtubes, resulting in a beneficial reduction in the inhibitory CSPGs and GFAP+ astrocytes, leading to an improvement in locomotor function when delivered in combination with neurotrophin-3 (in the case of ChABC) *in vivo*.

Also derived from algae is alginate; a linear polysaccharide formed by repeating units of (1–4)-linked β-D-mannuronate and α-L-guluronate. Alginate has a negative charge that forms a hydrogel upon ionic crosslinking with divalent counter-ions (D'Ayala et al., 2008) and can also gel via the stabilisation of a physical network by additional intermolecular hydrophobic interactions.

Alginate has been utilised *in vivo* for the delivery of glial cell line-derived neurotrophic factor (GDNF) using microspheres and normal (free) loading (Ansorena et al., 2013). Controlled release was achieved with both methods; however the release kinetics of the microsphere loaded GDNF resulted in hindered diffusion and reduced repair of the hemisected rats. Free GDNF delivered by this alginate hydrogel resulted in increased neurites surrounding the lesion as well as reduced number of astrocytes and improved functional recovery compared to the control group.

Alginate hydrogels have also been modified using microspheres loaded with alginate lyases; providing a mechanism to modulate degradation. This degradation profile

resulted in a significant increase in the rate of neural progenitor cell (NPC) expansion when cultured *in vitro* compared to the non-degradable control (Ashton et al., 2007).

Directed axonal regeneration has been achieved *in vitro* and *in vivo* using highly anisotropic capillary hydrogels composed of alginate (Prang et al., 2006). Using an entorhino-hippocapal slice culture model these gels were shown to elicit orientated regrowth, resulting in target re-innervation. Following implantation into an acute cervical lesion in an adult rat model, regenerating axons grew into the gels in a longitudinal manner, with aligned axonal and GFAP+ processes.

The use of cellulose hydrogels in spinal cord repair has been limited despite the promising neuronal differentiation of hMSCs *in vitro* (Gu et al., 2010). Methylcellulose, a compound derived from cellulose has been modified via attachment of laminin, giving rise to increased neural stem cell (NSC) survival, neurite outgrowth and differentiation into neuronal and oligodendrocyte lineages (Stabenfeldt et al., 2010).

Chitosan is a biodegradable, cationic polysaccharide produced by deacetylation of chitin found within crustaceans and forms a hydrogel via hydrogen bonding and hydrophobic interactions. Due to receptor-mediated binding of N-acetylglucosamine, chitosan gels stimulate a significant immune response in the brain and so their use is limited (Crompton et al., 2006). In order to mitigate the effects of such a response, modifications have been made to the chemical structure for use in spinal cord repair. Further modifications include pH adjustment and poly-d-lysine (PDL) functionalisation, resulting in increased cell viability (up to 0.05 % PDL) in 3D cultures compared to unfunctionalised controls (Crompton et al., 2007).

Fibrin is a fibrous protein involved in the clotting of blood. This has been used in conjunction with the glycoprotein fibronectin to create injectable hydrogels for the repair of SCI. Following a knife-cut cavity in the rat spinal cord, hydrogels were injected into the lesion cavity and it was found that at 4 weeks axonal growth was the greatest for fibronectin/fibrin gels (King et al., 2010). Fibronectin gels alone however, result in

reduced survival of neurons in the adjacent intact spinal cord, supported by additional evidence indicating a slight inhibitory effect of fibronectin on neurite extension (Deister et al., 2007). Fibrin gels have been investigated for the release of ChABC in the lesioned spinal cord, showing a marked reduction in inhibitory GAGs (reduced by 37 %) compared to injection alone (Hyatt et al., 2010).

Hyaluronic acid (HA) is another naturally derived material used within tissue engineering. This is a non-sulphated GAG found naturally within neural tissue, consisting of repeating D-glucuronic acid and N-acetylglucosamine disaccharide units. The majority of HA present in the CNS is produced by astrocytes, and surrounds the myelinated axons and neuronal cell bodies found within the white and grey matter of the spinal cord (as seen using immunofluorescence in the rat spinal cord) (Bignami et al., 1992).

The biological effects of HA are molecular weight (MW) dependent, with high MW forms of HA being beneficial within the inured spinal cord; reducing epidural scar formation and maintaining astrocytes in an unreactive state (Akeson et al., 2005). High MW HA has also has a suppressive effect on inflammatory cells that may cross the compromised BSCB (Schimizzi et al., 2006; Bollyky et al., 2007). High MW HA however, is degraded into low molecular weight HA following injury (mediated by a family of hyaluronidases), triggering increased proliferation of astrocytes and the formation of a glial scar (Struve et al., 2005).

Both MW variants of HA are capable of binding to the receptor CD44 expressed on the surface of astrocytes (amongst other cells) (Underhill, 1992; Haegel et al., 1993). HA/CD44 binding stimulates Rac1-PKNγ kinase activity; upregulating cortactin phosphorylation, thus attenuating F-actin crosslinking, cytoskeleton activation and astrocyte migration (Bourguignon et al., 2007). RHAMM (receptor for HA-mediated migration) dependent motility has also been detected in cultured astrocytes and

microglia (Turley et al., 1994) and a number of *in vitro* studies suggest the involvement of RHAMM in neurite outgrowth (Nagy et al., 1995; Nagy et al., 1998).

Previously, hydrogels created from pure HA were demonstrated to enhance neural regeneration and reduce glial scar formation in the CNS following experimental SCI (Lin et al., 2009), however, cell attachment remains an issue with such materials. Recently a hyaluronic acid-based hydrogel was found to improve neuronal survival in spinal cord slice cultures, highlighting the potential benefits for the use of this material following SCI (Schizas et al., 2014).

Modification of HA hydrogels using various ECM components including laminin, RGD, IKVAV, PDL and PLL has been achieved. Gels modified with laminin and implanted into brain lesions of rats were shown to improve repair of tissue; reducing the number of reactive astrocytes around the injured area (Hou et al., 2005). Similarly, RGD, PDL, PLL and IKVAV modified HA hydrogels have also been investigated within traumatic brain injury models, resulting in increased cell migration (Tian et al., 2005; Cui et al., 2006; Wei et al., 2007) demonstrating their potential use for the treatment of additional CNS injuries.

HA hydrogels have also been investigated for the release of neurotrophic factors and bioactive agents in the CNS. Anti-NgRs (Nogo receptor antibodies) have been released from HA gels in a pH dependent manner, *in vitro* (Hou et al., 2006) and *in vivo* (Wei et al., 2010). These studies show the beneficial effect the slow release of anti-NgRs has on neurite outgrowth (chick DRG) and axonal ingrowth within an SCI model. Furthermore, sustained release of BDNF has also been achieved using HA based hydrogels in a rat model of SCI (Park et al., 2010). Compared to hydrogels alone and the direct delivery of BDNF, BDNF-containing hydrogels resulted in the greatest improvement of functional recovery as assessed by locomotive testing (Basso-Beattie-Bresnahan (BBB) score).

Table 1.2 Naturally-derived hydrogels investigated for spinal cord injury repair

Hydrogel	Modification	Assessment	Outcomes	Reference
Agarose	Laminin oligopeptide-modified	DRG (E9 chick) & PC12 cell culture	Promotion of neurite extension varied according to peptide sequence.	(Bellamkonda et al., 1995; Bellamkonda et al., 1995)
	GRGDS oligopeptide-modified channels	DRG cell culture	Orientated axonal growth.	(Luo and Shoichet, 2004)
	RGDS & hMSC delivery	Mouse T12 clip compression	Increased M2 macrophage population.	(Caron et al., 2016)
	BDNF delivery	Rat T10 dorsal over-hemisection	Increased neurite growth into hydrogel, reduced astrocytes and CSPGs	(Jain et al., 2006)
	BDNF & Rho GTPase delivery	Rat T8-10 dorsal over-hemisection	Higher percentage of axons from the corticospinal tract spanning the CSPG-rich regions located proximal to the lesion site.	(Jain et al., 2011)
	ChABC & NT-3 delivery	Rat T10 dorsal over-hemisection	Improvement in locomotor function when delivered together.	(Lee et al., 2010)
Alginate	GDNF delivery	Rat T9-10 lateral hemisection	Free GDNF delivery resulted in increased number of neurites, reduced number of astrocytes & improved functional recovery.	(Jain et al., 2006)
	Alginate-based highly anisotropic capillary hydrogels	Entorhino-hippocampal slice culture	Longitudinal axonal growth.	(Prang et al., 2006)
		Rat C3 transection	Axonal profiles grew into gels longitudinally, aligned along GFAP+ processes.	
Cellulose	-	hMSC culture	Neural differentiation of hMSCs.	(Gu et al., 2010)

Hydrogel	Modification	Assessment	Outcomes	Reference
Cellulose	Methylcellulose laminin-1	NSC neurospheres from transgenic mice E14.5	Reduced apoptosis, increased neurite extension and greater neuronal and oligodendrocyte differentiation for laminin functionalised gels.	(Stabenfeldt et al., 2010)
Chitosan	PDL	Cortical cell culture	Neuron survival improved with PDL.	(Crompton et al., 2006)
Fibrin	ChABC delivery	Rat C4 incision	Reduction in sulphated GAGs compared to control and injected ChABC groups.	(Hyatt et al., 2010)
Fibronectin & fibrin	Fibrin and fibronectin gels & mix of the two	Rat T7-9 transection	Gel mixture integrated with the host tissue and supported growth of axons.	(King et al., 2010)
Hyaluronic acid	-	Spinal cord slice cultures	Improved neuronal survival and limited microglial activation.	(Schizas et al., 2014)
	Anti-NgR release	DRG (chick) culture	Improved neural cell attachment and survival and increased neurite outgrowth.	(Hou et al., 2006)
	Anti-NgR & PLL	Rat T8-9 hemisection	Significant increase in axon extension into gel at 8 weeks. Increase in cell number and myelinated axons compared to control. Supported angiogenesis and inhibited glial scar formation.	(Wei et al., 2010)
	BDNF release (& IKVAV)	Rat T10 clip compression	Improvement in BBB score.	(Park et al., 2010)

Abbreviations: BBB: Basso-Beattie-Bresnahan, BDNF: Brain Derived Neurotrophic Factor: ChABC: Chondroitinase ABC enzyme, CSPG: chondroitin sulphate proteoglycan, DRG: dorsal root ganglion, GDNF: Glial Cell Line-Derived Neurotrophic Factor, GFAP+: Glial Fibrillary Acidic Protein positive, hMSC: human mesenchymal stem cell, hEnSC: Human endometrial-derived stromal cells, NSC: neural stem cell, NSPC: neural stem/progenitor cell, PDL: poly-d-lysine, PLL: poly-l-lysine.

1.4.3 Measuring substrate stiffness

Stem cells sense the extent to which a substrate or ECM deforms in response to an applied traction force; essentially measuring the substrate's stiffness and responding accordingly. The stiffness of a material can be measured using a number of methodologies. As hydrogels are viscoelastic, with a combination of solid and fluid phases, these properties are typically assessed using rheology. Rheometers allow the precise measurement of a material's response to applied force (stress) or deformation (strain). In most cases a dynamic (oscillating) shearing force is applied to the material using a frequency or strain sweep (using either a cone or a plate), giving rise to outputs such as complex shear modulus (G*), storage modulus (G') and loss modulus (G'') (described in more detail in Chapter 3.2.3).

The mechanical properties of hydrogels can also be assessed using compressive methods. One popular technique involves compressing the material between parallel plates using a continuous stress or strain. The Young's (compressive elastic) modulus (Ey) is then calculated as the gradient of the stress-strain curve in the linear (elastic) region and is a direct indication of the material's stiffness. Additionally, Ey can be determined using atomic force microscopy (AFM) by quantifying the deflection of a cantilever tip upon indentation at the hydrogel surface, or by using microbead displacement calculations. Additional techniques for CNS tissue are reviewed by (Budday et al., 2019).

1.5 Mechanotransduction in the CNS

Transmembrane proteins, such as integrins, enable cells to bind to the surrounding ECM or substrate, mechanically anchoring the cytoskeleton to the ECM and allowing the transmission of contractile forces required for movement and "sensing" of mechanical stiffness referred to as mechanotransduction (Tsai and Kam, 2009; Moore et al., 2010). The traction forces exerted by cells via these cell surface integrins influence cytoskeletal tension, leading to changes in cell morphology, signalling

cascades, and gene expression; ultimately directing cell fate (Paszek et al., 2005; Huebsch et al., 2010; Lee et al., 2013). Additionally, cell-cell junction adhesion via cadherin-catenin complexes allows cells to communicate forces between the F-actin cytoskeletons of neighbouring cells, further amplifying cellular responses (Figure 1.4) (Buckley et al., 2014). The activity of the ion channel, Piezo1, directs neural stem cell differentiation. Piezo1 opens in response to cell tension mediated by external mechanical stimuli (tensile/shear forces) and changes in traction forces a cell transmits due to ECM stiffness (Pathak et al., 2014).

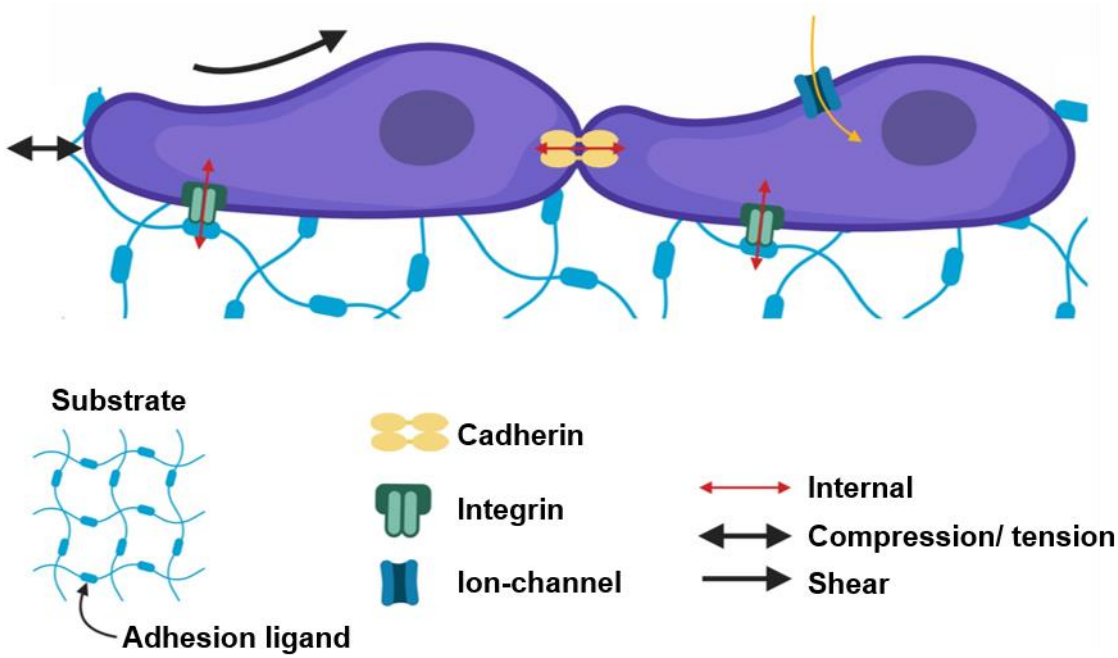

Figure 1.4 Stem cell mechanosensitivity

Stem cells apply traction forces to their surroundings via cell-ECM adhesion ligand (blue matrix) binding to integrin receptors on cells (green). They can also transfer these forces to neighbouring cells via cell-cell junctions, e.g. cadherins (yellow). These internal forces are shown as red arrows. Additionally, cells can sense the external forces applied to them (compression/tension and shear – shown as black arrows), using mechanically-gated ion-channels (blue) and changes to the cell's cytoskeleton. Adapted from (Vining and Mooney, 2017). Created using BioRender.com.

1.5.1 Neural tissue biomechanics

The mechanical properties of biological samples are inherently difficult to characterise and compare due to the heterogeneous nature of tissue, variations in tissue origin between studies, and the differing testing methods employed. CNS tissue has a high water content and is thought to exhibit nonlinear viscoelastic properties, and as such the tissue is strain-stiffening and measurements are influenced by length and time scales of loading (reviewed in detail in (Budday et al., 2019)). Due to the experimental variations and testing inaccuracies, the reported elastic modulus of CNS tissue varies widely, with values ranging from 40 Pa to 20 kPa for the brain (Franze et al., 2013) and a recent study giving a shear modulus of 0.4–1.4 kPa for the human brain (Budday et al., 2017). Despite these limitations, it is widely accepted that CNS tissue is “ultrasoft” and therefore highly susceptible to damage.

Interestingly, in contrast to scars formed elsewhere in the body, the glial scar formed following SCI is significantly softer than uninjured tissue (Franze et al., 2013; Moeendarbary et al., 2017). In a study by (Moeendarbary et al., 2017), the stiffness of uninjured cortical tissue ranged from 50 to 500 Pa, and following a unilateral stab injury to the neocortex of the brain, the tissue either side of the injury was ~15% softer than the contralateral tissue control 9 days post-injury (PI). Uninjured rat spinal cord tissue stiffness was determined to be 420 Pa for grey matter and 177 Pa for white matter. Following a spinal cord crush injury, the stiffness of the lesion site tissue reduced significantly, with the greatest reduction seen in the grey matter (~ 40% reduction in elastic modulus at 3 weeks PI to around 200 Pa). This phenomenon is thought to be due to extensive production of highly hydrated CSPGs at the injury site. Additionally, in contrast to other scar tissue, crosslinked collagen I is absent from the glial scar (Stichel and Müller, 1998) and instead, collagen IV, vimentin, and GFAP are upregulated following injury; potentially contributing to this change in stiffness (Moeendarbary et al., 2017).

1.5.2 Manipulating neural stem cell behaviour using substrate stiffness

A number of studies have demonstrated the sensitivity of neural stem cells to substrate elasticity, with soft matrices comparable to native CNS tissue increasing cell proliferation (Saha et al., 2008a; Banerjee et al., 2009a; Leipzig and Shoichet, 2009a) and inducing neurogenesis (Engler et al., 2006; Seidlits et al., 2010) reviewed by (Lin et al., 2016; Vining and Mooney, 2017).

1.5.2.1 Proliferation and migration

The stiffness of the surrounding substrate also influences stem cell proliferation and migration (Pelham and Wang, 1997). Cell movement requires the generation and transmission of protrusive and contractile forces for lamellipodial extension and uropodal retraction respectively (Thomas and DiMilla, 2000). This occurs via dynamic adhesion and detachment of specific, reversible transmembrane glycoproteins with ECM proteins in the surrounding scaffold.

Human glioblastoma cell migration extent and speed decreases with increasing matrix compliance (Thomas and DiMilla, 2000) and adult rat SEZ NSPCs only migrated from neurospheres when cultured on soft hydrogels with a stiffness of 0.8 kPa (Hynes et al., 2009; Leipzig and Shoichet, 2009b). Additionally, increased NSC/NSPC proliferation occurs on soft hydrogels (< 800 Pa) (Banerjee et al., 2009b)(Leipzig and Shoichet, 2009b). (Saha et al., 2008b) did however, show that adult NSC spreading, self-renewal, and differentiation is inhibited when cultured on hydrogels with a stiffness of 10 Pa, indicating these cells also have a lower stiffness threshold.

1.5.2.2 Differentiation

Neural stem and progenitor cells from embryonic and adult rats and mice have been investigated for their response to substrate modulus. Greatest neuronal differentiation (as indicated by expression of the neuronal marker β-tubulin III) was observed in most

cases to occur on soft gels with moduli under 3 kPa. Glial differentiation was varied across different substrates (Table 1.3).

NSCs from the hippocampus of adult rats differentiated preferentially into neurons when cultured on poly acrylamide (PA) hydrogels with moduli of 100-500 Pa, whereas on stiff gels with moduli of 1-10 kPa, glial differentiation was enhanced (Saha et al., 2008b) (Table 1.3). Neuronal differentiation was greatest when cultured on soft chitosan hydrogels (<1 kPa), and differentiation into astrocytes occurred on hydrogels with stiffnesses ranging from 0.8-3.5 kPa. (Leipzig and Shoichet, 2009b). Here they cultured NSPCs from the sub ependymal zone of adult rats and found that they differentiated mainly into oligodendrocytes, which was increased on hydrogels with an elastic modulus of 7 kPa. Little to no differentiation into neurons or astrocytes was observed when cultured on hydrogels with a stiffness of 7 kPa.

NSCs from embryonic rat (E15.5) cerebral cortices showed an increase in astrocytic differentiation with decreasing stiffness of PDMS hydrogel (Teixeira et al., 2009). Additionally, on all hydrogels, there was a greater number of neurons compared to culture plate controls, (elastic modulus of ~10^9 Pa (Teixeira et al., 2009)), however differentiation into neurons and oligodendrocytes was found to be independent of PDMS stiffness.

Additional studies have investigated the behaviour of stem cells cultured within 3D hydrogels, more reminiscent of the *in vivo* environment. (Banerjee et al., 2009b) found that the greatest enhancement in neuronal differentiation of adult NSCs from the hippocampus of rats was observed when cells were cultured within soft alginate hydrogels with an elastic modulus comparable to that of CNS tissue (180 Pa – Table 1.3). NPCs from the ventral midbrain of embryonic mice (E13.5) differentiated into neurons when co-cultured within soft HA gels, and increased glial differentiation was seen as the substrate modulus increased (Seidlits et al., 2010).

Increased glial differentiation of NPCs from the brain of embryonic rats (E15) was also seen when cultured on PEG/HA hydrogels with increasing stiffness (up to ~15 kPa) (Aurand et al., 2014). However, neuronal differentiation was only observed when these cells were cultured within hydrogels with compressive moduli of ~5 kPa. In the same study, the fate of adult NPCs was investigated. Neuronal differentiation was observed in hydrogels with a stiffness of up to ~20 kPa, and once again, increased differentiation into neurons was seen for cells cultured within soft hydrogels (~5 kPa) (Aurand et al., 2014). Differentiation of adult NPCs into astrocytes was only observed when cultured within hydrogels with compressive moduli of ~5 kPa, opposite to the trend seen for embryonic NPCs (Table 1.3).

Table 1.3 Studies investigating the effect of <u>increasing</u> hydrogel stiffness on the fate of neural stem cells

Hydrogel	Stiffness (Pa)	Tuning of stiffness	Porosity	Cell type, source, location	2D/3D	Neuron	Astrocyte	Olig.	Reference
Chitosan	800 – 20,000 (E_y)	Concentration of photoinitiator	Decreased	NSPCs, adult rat, SEZ of the lateral ventricles	2D	↓↓	↓↓	↑↑	(Leipzig and Shoichet, 2009b)
PA	13.5 – 9,580 (G')	Concentration of acrylamide and bis-acrylamide	N/A	NSCs, adult rat, hippocampus	2D	↓	↑	-	(Saha et al., 2008b)
PDMS	12 - 750 kPa (E_y*)	Crosslinker concentration	N/A	NSC, rat embryo E15.5, cerebral cortices	2D	→	↓	→	(Teixeira et al., 2009)
Alginate	180 – 20,000 (G')	Alginate & $CaCl_2$ concentrations (crosslinking density)	N/A	NSCs, adult rat, hippocampus	3D	↓	-	-	(Banerjee et al., 2009b)
HA	3,000 – 5,100 (compressive bulk modulus)	Crosslinker concentration	N/A	NPCs, embryonic mouse E13.5, ventral midbrain & primary spinal cord astrocytes	3D	↓	↑	-	(Seidlits et al., 2010)
PEG	120 – 31,300 (E_y)	PEG/HA ratio	N/A	NPCs, embryonic rat E15, brain NPCs, adult rat, hippocampus & SVZ	3D	↓ ↓	↑ ↓	- -	(Aurand et al., 2015)

Key: ↓ = *decrease,* ↓↓ = *significant decrease,* ↑ = *increase,* ↑↑ = *significant increase,* → = no change - = not assessed

Abbreviations: E_y: Young's modulus, E_y*: bead displacement method, G': storage modulus, G*: complex modulus, HA: hyaluronic acid, kPa: kilo Pascal, NSC: neural stem cell, NPC: neural progenitor cell, NSPC: neural stem/progenitor cell, Pa: Pascal, PA: polyacrylamide, PEG: polyethylene glycol, PDMS: polydimethylsiloxane, SVZ: sub-ventricular zone, SEZ: sub-ependymal zone.

These studies do however present a number of methodological limitations. As can be seen in the examples presented in Table 1.3, numerous methods have been used to tune and characterise the stiffness of the hydrogels and a variety of cell sources have been used; therefore limiting comparison. Additionally, the porosity is rarely characterised (see Table 1.3), and could contribute to the change in cell behaviour observed. Use of 2D culture techniques may also impact on the cellular response to hydrogel stiffness due to the artificial polarity created between the surfaces of the cell investigated (Cukierman et al., 2001). In addition to this, in most cases the impact of stiffness modulation (i.e. crosslinking density) on the physical properties of the resulting hydrogel (porosity, fibre diameter etc.) has not been addressed and so causal relationships cannot be established conclusively. Similarly, CNS tissue stiffness has also been characterised using various techniques, thus adding further confusion when attempting to accurately match hydrogel properties to native tissue due to a lack of standardisation (Aurand et al., 2012).

From the overall trends seen in the literature, it could be theorised that ependymal cells may exhibit increased proliferation and differentiate preferentially into neurons when cultured on soft hydrogels with a stiffness similar to that of native spinal cord tissue.

1.6 Hypothesis

It is hypothesised that the mechanical properties of hydrogels can be modulated independently of porosity, and that these can be used to deliver SDF-1α to the spinal cord in order to alter the proliferation, differentiation, and migration of spinal cord ependymal cells.

1.6.1 Aims

This project aimed to determine the potential of manipulating endogenous ependymal cells using hydrogels, towards repair for SCI. This included: determining the feasibility of producing a library of collagen hydrogels with varied mechanical properties and constant porosity; characterising a transgenic line for the labelling of spinal cord ependymal cells; developing organotypic spinal cord slice cultures for the assessment of biomaterials; and an investigation into the effects of hydrogels and a chemokine on ependymal cell behaviour *in vitro* and *in vivo* (see Figure 1.5).

1.6.2 Objectives

1. To investigate the potential of synthesising hydrogels with tuneable stiffness within the range of native central nervous system tissue, whilst maintaining porosity
2. To characterise the expression of (nestin) GFP in transgenic mice
3. To optimise a protocol for the detection of EdU incorporated into the dividing cells of fluorescently labelled cells and spinal cord slice culture methods
4. To investigate the effects of hydrogel composition on ependymal cell proliferation and distribution
5. To determine if ependymal cell migration can be manipulated using SDF-1α *in vitro* and *in vivo*

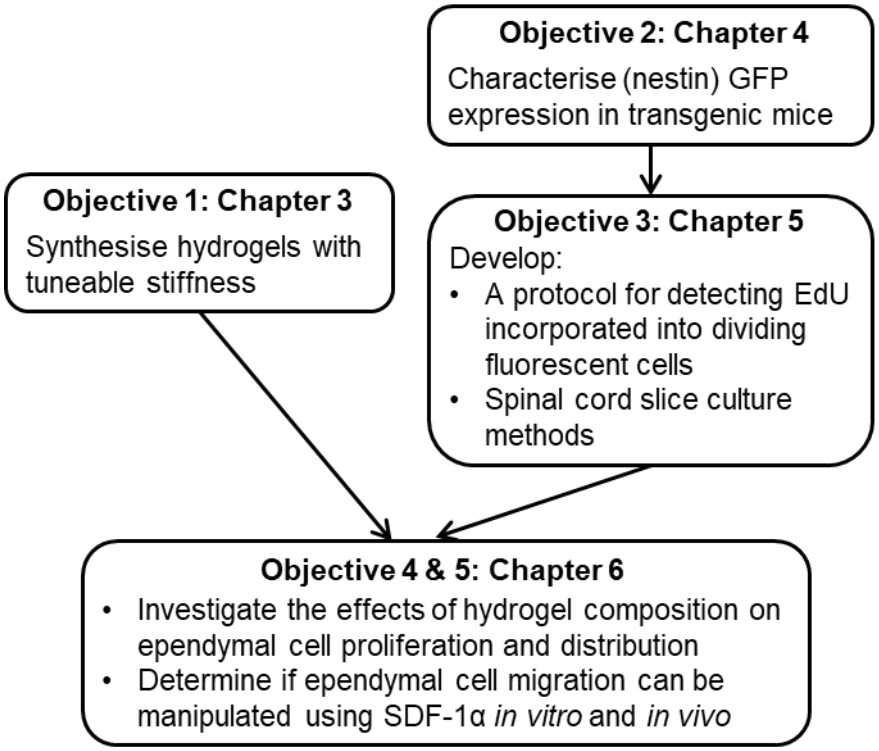

Figure 1.5 Overview of the objectives of this thesis

The development work carried out in chapters 3 to 5 enabled the interrogation of the hypothesis in chapter 6.

Chapter 2 - General Methods

2.1 Materials

The following materials were used throughout this thesis. The chemicals and drugs are detailed in Table 2.1, consumables and glassware are detailed in Table 2.2, and the equipment used are detailed in Table 2.3.

Table 2.1 Chemicals and drugs used within this thesis

Chemical/Drug (abbreviation)	Cat. number	Supplier
1-(3-Dimethylaminopropyl)-3-ethylecarbodiimide hydrochloride (EDC)	A10807	Alfa Aesar. Heysham, UK
2,4,6-Trinitrobenzene Sulfonic Acid (TNBS)	P2297	Sigma-Aldrich. Poole, UK
5-ethynyl-2'-deoxyuridine (EdU)	N/A	Carbosynth, Compton, UK
Acetic Acid	537020	Sigma-Aldrich. Missouri, USA
Agar	A7002	Sigma-Aldrich. Poole, UK
Alexa Fluor secondary antibodies	See chapter 4, Table 4.4	Invitrogen or Life Technologies
AMD3100	ab120718	Abcam, Cambridge, UK
Atipamezole hydrochloride	N/A	Antisedan, Vetoquinol & Orion pharma. Northamptonshire, UK
B27 supplement	17504044	Gibco. NY, USA.
Biotin azide	E3730	Lumiprobe
Biotin picolyl azide	92186	Biotium
Biotin-conjugated secondary antibodies	See chapter 4, Table 4.4	Jackson Immunoresearch

Chemical/Drug (abbreviation)	Cat. number	Supplier
Buprenorphine hydrochloride	N/A	Vetergesic, Ceva animal health Ltd. Buckinghamshire, UK.
β-mercaptoethanol (βME)	M6250	Sigma-Aldrich. Poole, UK
Calibration solutions	pH4: 2626-DA pH7: 2627-DA	Scientific laboratory supplies Ltd
Crosslinkers: p-Phenylenediacetic Acid (4Ph) 1,3-Phenylenediacetic Acid (13Ph) Adipic Acid (Ad) 20115.365	 P23407 A11429 20115.365	 Sigma-Aldrich. Poole, UK Alfa Aesar VWR International. Leicestershire, UK
Dimethyl Sulfoxide (DMSO)	D5879	Sigma-Aldrich
Disodium Hydrogen Phosphate (Na_2HPO_4)	S374-500	Thermofisher. Leicestershire, UK.
Dulbecco's modified eagle's medium (DMEM)	D6546	Sigma-Aldrich. Poole, UK
Ethanol	16368	Sigma-Aldrich. Poole, UK
Fluoroshield	F6182	Sigma-Aldrich. Poole, UK
Fluoroshield with DAPI	F6057	Sigma-Aldrich. Poole, UK
Foetal bovine serum (FBS)	A3912	Sigma-Aldrich. Poole, UK
Gelatin, porcine skin	04055-500G	Sigma-Aldrich. Poole, UK
Glutaraldehyde	36218	Gurr
Hydroxystilbamidine (FG - FluoroGold)	ab138870	Abcam, Cambridge, UK.
Hystem™ Hystem™C	HYS020 HYSC020	Sigma-Aldrich. Poole, UK
Incuwater-Clean	A5219,0100	PanReac AppliChem, ITW Reagents

Chemical/Drug (abbreviation)	Cat. number	Supplier
Ketamine	N/A	Ketavet, Zoetis UK Ltd. London, UK
L-Glutamine	G7513	Sigma-Aldrich. Poole, UK
Magnesium sulphate heptahydrate ($MgSO_4.7H_2O$)	M/1050/53	Fisher Chem. Leics., UK
Medetomidine hydrochloride	N/A	Domitor, Vetoquinol & Orion pharma., UK
Monosodium phosphate monobasic monohydrate ($NaH_2PO_4.H_2O$)	095388	Fluorochem Ltd. Hadfield, UK
Mouse on Mouse Kit	BMK 2202	Vector laboratories, UK
Neurobasal-A medium	10888022	Gilbco, ThermoFisher Scientific,
N-Hydroxysuccinimide (NHS)	804518	Merck. Schuchardt. Hohenbrunn, Germany
Paraformaldehyde (PFA)	15812-7	Sigma-Aldrich. Poole, UK
Penicillin/streptomycin	P44580	Sigma-Aldrich. Poole, UK
Phosphate buffer (PB) sterile	D8537-500	Sigma-Aldrich. Poole, UK
Phosphate-buffered saline (PBS) tablets	BR0014G	Oxoid Ltd., Hampshire, UK
Potassium chloride (KCl)	31248	Sigma-Aldrich. Poole, UK
Recombinant Murine SDF-1α (CXCL12)	250-20A	Peprotech, NJ, USA
Sodium Bicarbonate ($NaHCO_3$)	S6014	Honeywell, Fluka. USA
Sodium Chloride (NaCl,)	S/3120/66	Fisher Chem. Leics., UK
Sodium pentobarbital	N/A	Euthatal, Merial Pentoject, Animalcare, UK
Streptavidin Alexa Fluor^{488}	S32354	Life Technologies
Streptavidin Alexa Fluor^{555}	S32355	Life Technologies
Sucrose	S/8560/60	Fisher Chem. Leics., UK

Chemical/Drug (abbreviation)	Cat. number	Supplier
Triton X-100	X100	Sigma-Aldrich. Poole, UK
Trizma base	T1503	Sigma-Aldrich. Poole, UK
Trizma hydrochloride	T3253	Sigma-Aldrich. Poole, UK
Tween20	P9416	Sigma-Aldrich. Poole, UK
Virkon (Rely+On)	148-0201	Day Impex, VWR, UK
Vitrogel®3D	TWG001	TheWell Bioscience, NJ, USA

Table 2.2 Consumables and glassware used within this thesis

Consumable	Cat. Number	Supplier
Absorbable sutures	W9015	Ethicon, New Jersey, USA.
Culture inserts	PICM0RG50	Millicell, Merck Millipore, Germany.
Curved needle	16mm, W2502	Ethicon, New Jersey, USA.
6 & 48 well plates	140675 & 150687	Thermo Fisher Scientific
Eye lubricant	Lacri-Lube	Allergan, Dublin, Ireland
Non-dissolvable sutures	W2502	Ethicon, New Jersey, USA.
Blades (sterile)	#10	Swann Morton. Sheffield, UK
Blades (non-sterile)	INS4610	VWR, UK.
Blades (vibratome)	752/1/SS/50	Campden instruments, Leics., UK.
Blades (vibratome, ceramic)	7550-1-C	Campden instruments, Leics., UK.
Coverslips (various)	43210.KJ	VWR, UK.
Microscope slides	N/A143	Academy Science Ltd., UK.
Eppendorf tubes	Various	Thermo Fisher Scientific UK. Leics., UK
Falcon tubes (15mL, 50mL)	339650, 339652	Thermo Fisher Scientific UK. Leics., UK
Filter pipette tips	Various	StarLab. Milton Keynes, UK

Consumable	Cat. Number	Supplier
Serological pipettes (sterile)	ARLAPS10	Sigma-Aldrich. Poole, UK.
Pasteur pipettes	Various	SLS, UK.
Separating funnel	527-1222	VWR, UK.

Table 2.3 Equipment used within this thesis

Equipment	Model	Make
Blunt forceps & spring scissors	654558	World Precision Instruments
CD spectrometer	J-715 spectropolarimeter	Jasco
Class II Safety Cabinet	Herasafe,	Heraseus. Germany.
Confocal microscope	LSM880	Zeiss
Culture incubator	N/A	Labtech inc., Massachusetts, USA
Dissection microscope	SMZ-2B	Nikon
Electrode puller	P-97 Flaming/Brown	Sutter Instrument Co. CA, USA
Fine forceps	Dumont tweezers, #55	World Precision Instruments
Fluorescence microscope	E600	Nikon
Fluorescence microscope	M7000	EVOS
Freeze drier	Alpha 2-4 LD plus	SciQuip, UK.
Laminar flow hood	N/A	Astec Microflow. Hampshire, UK
Platinum Sputter Coater	208HR	Cressington
Rheometer	Kinexus Pro	Malvern Instruments. Worcestershire, UK.
Scanning Electron Microscope (SEM)		Quanta FEG
Stereotactic frame	51730U	Stoelting Co., Illinois, USA
Syringe pump	CMA 4004	Harvard apparatus. MA, USA
Vibrating microtome (culture)	Integraslice 7550 PSDS	Campden Instruments Ltd. Leics., UK

Equipment	Model	Make
Vibratome	VT1000S	Leica. Germany.

2.1.1 Common buffers, solutions, and culture medium

The composition, diluent, and pH (where appropriate) of each buffer, solution, drug, and culture medium used throughout this thesis are detailed in Tables 2-4 to 2-7. The pH meter was calibrated before each use at 20°C using pH 4 and 7 calibration solutions.

Table 2.4 General buffers used within this thesis

			Composition	Diluent
Phosphate-buffered saline	PBS	pH 7.4	10 mM Na_2HPO_4, 1.8 mM KH_2PO_4, 137 mM NaCl, 4 mM KCl	diH_2O
Phosphate buffer	PB	0.1 M	$NaH_2PO_4.2H_2O$, Na_2HPO_4	diH_2O
Hydroxymethyl aminomethane (Tris) buffered saline	TBS	0.1 M pH 7.6	Trizma base, Trizma hydrochloride	diH_2O
PBS Triton X-100	PBST	0.1% & 0.2% (v/v)	0.1% & 0.2% (v/v) Triton X-100	PBS
PBS Tween20	T20	0.1% (v/v)	0.1% (v/v) Tween 20	PBS
Sodium phosphate buffer	SPB	0.1 M, pH 7.4	NaH_2PO_4.H2O & Na_2HPO_4	H_2O

Table 2.5 General solutions used within this thesis

	Abbreviation	Composition	Diluent
Acetic acid	N/A	17.4 mM, pH 7.4	diH_2O
Agar	N/A	3% (w/v) – heated to near boiling, bubbles poured off, then left to cool	diH_2O

	Abbreviation	Composition	Diluent
Artificial cerebrospinal fluid	aCSF	Sodium chloride 124 mM, $NaHCO_3$ 26 mM, KCl 3 mM, $MgSO_4.7H_2O$ 2 mM, NaH_2PO_4 2.5 mM, Glucose 10 mM, $CaCl_2$ 2 mM	diH_2O
Ethanol	N/A	70% (v/v)	diH_2O
Gelatin	N/A	10% (w/v) – heated to near boiling, bubbles poured off, then left to cool	diH_2O
Glutamine	N/A	2.5 w/v	PB
$NaHCO_3$	N/A	4 wt.%, pH 8.5	diH_2O
Osmium tetroxide	N/A	1 % w/v	PB
Paraformaldehyde	PFA	4% (w/v)	0.1 M PB
PFA with glutaraldehyde	N/A	0.25% (w/v)	4% PFA
Sucrose artificial cerebrospinal fluid	SaCSF	Sucrose 217 mM, $NaHCO_3$ 26 mM, KCl 3 mM, $MgSO_4.7H_2O$ 2 mM, NaH_2PO_4 2.5 mM, Glucose 10 mM, $CaCl_2$ 1 mM	diH_2O
2,4,6-trinitrobenzenesulfonic acid	TNBS	0.5 wt.%	diH_2O
Virkon	N/A	1% (w/v)	diH_2O

Table 2.6 Drug solutions used within this thesis

	Abbreviation	Concentration	Diluent
Administered I.P – given as: mass of drug/mass of animal			
Atipamezole	N/A	1 mg/kg final	Sterile saline
Buprenorphine	N/A	0.1 mg/kg final	Sterile saline

	Abbreviation	Concentration	Diluent
Hydroxystilbamidine (Fluorogold)	FG	1% (w/v) 50 mg/kg final	Sterile saline
Ketamine	N/A	75 mg/kg final	Sterile saline
Medetomidine	N/A	1.0 mg/kg final	Sterile saline
Sodium pentobarbital	N/A	60 mg/kg final	diH_2O

Table 2.7 Culture media solutions

Medium name	Composition
Dissection medium	Dulbecco's modified eagles medium (DMEM), 1% (v/v) penicillin/streptomycin.
Serum-containing medium	Neurobasal A medium; 1% (v/v) L-Glutamine, 1% (v/v) penicillin/streptomycin, and 10% (v/v) fetal bovine serum.
Serum-free medium	Neurobasal A medium; 1% (v/v) L-Glutamine, 1% (v/v) penicillin/streptomycin, and 2% (v/v) B27 supplement.

2.2 Data analysis

Data were collated in Microsoft Excel and analysed using IBM SPSS statistics 21. Average values were calculated and presented as mean ±SE (unless stated otherwise). Shapiro-Wilk and Levine's tests were applied for distribution and equality of variance analysis respectively. A decision tree was used to determine the appropriate statistical test (Figure 2.1).

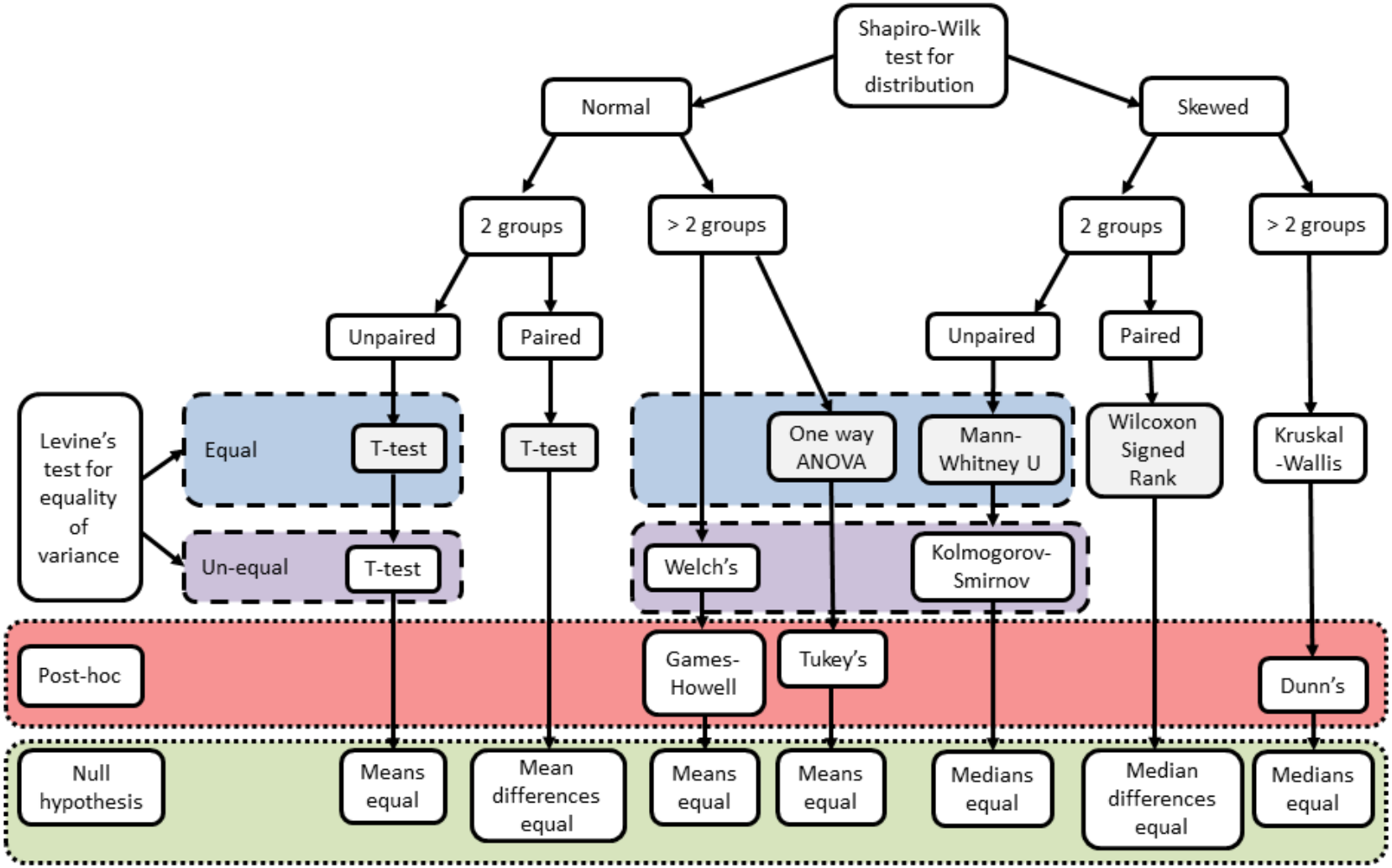

Figure 2.1 Decision tree used to determine the appropriate statistical test depending on the homogeneity of distribution and variance.

Adapted from (Clarkson, 2018).

Chapter 3 – Investigating the potential manipulation of hydrogel mechanical properties

3.1 Introduction

Despite the pressing clinical need for improved spinal cord injury repair, clinical treatment options remain limited. Tissue engineering advancements in the past decade have resulted in a vast library of biomaterials; however, the physical and mechanical factors affecting ependymal cells (ECs) within the spinal cord have not been investigated.

Collagen is the primary component of extracellular matrices and type I collagen has been found to support the growth and differentiation of neurons when used as a hydrogel scaffold *in vitro* (see Table 3.1) (O'Connor et al., 2001; Ma et al., 2004; Huang et al., 2013). Soluble collagen I inhibits glial proliferation in the peripheral nervous system (Eccleston et al., 1989)(as measured by [^{3}H]thymidine incorporation) and so may decrease scarring following SCI (Klapka and Müller, 2006; Macaya and Spector, 2012). Additionally, collagen IV promotes neurite outgrowth in sympathetic neurons of the peripheral nervous system following short term culture (24 hours) as compared to poly-lysine coated coverslips (Lein et al., 1991). In this study collagen IV selectively enhanced only axonal growth whereas dendritic growth was not affected. Furthermore, this activity was found to be associated with the non-collagenous (NC1) domain on collagen, mediated primarily by the transmembrane α1β1 integrin found on these cells.

Collagen hydrogels have been functionalised with hyaluronic acid (HA) and laminin and investigated *in vitro*. Neural stem/progenitor cells (NSPCs) cultured on HA-functionalised hydrogels exhibited greater neuronal differentiation compared to 2D controls (Brännvall et al., 2007). Patterning of collagen I hydrogels using micro-contact

printing of various ECM proteins (aggrecan, fibrinogen, fibronectin, and laminin) resulted in the alignment of astrocyte layers according to protein patterning, ultimately leading to reduced CSPG expression compared to un-patterned gel controls (Hsiao et al., 2015).

Table 3.1 Selection of studies investigating collagen hydrogels for CNS repair

Hydrogel	Culture	Outcomes	Reference
Collagen	3D culture, NSPCs, cerebral cortex or subcortical region, E13 rat	Cells expanded, differentiated into neurons, and formed synapses.	(Ma et al., 2004)
Collagen	3D culture, cortical neurons, E18 rat	Cells exhibited normal neuronal polarity with long neurites (> 500 μm), >50% survival compared to 0% for agarose gel.	(O'Connor et al., 2001)
Collagen	3D culture, NSCs, cerebral cortex, E14 rat	Significant increase in process outgrowth from NSCs cultured in gels compared to control. Differentiation into neurons, astrocytes, and oligodendrocytes.	(Huang et al., 2013)
Collagen & HA	3D culture, NSPCs, cerebral cortex, embryonic; SVZ, P6 & adult mice	Increased neuronal differentiation of embryonic progenitors compared to 2D culture Postnatal progenitors produced mainly mature neurons	(Brännvall et al., 2007)
Collagen & ECM protein patterning	2D culture, astrocytes, cerebral cortex, P2 rats	Alignment of astrocytes with protein pattern. Reduced CSPG expression for collagen gels functionalised with fibronectin.	(Hsiao et al., 2015)

E= embryonic age, P=postnatal age (days)

Although some of the collagen scaffolds detailed above have been investigated as substrates for the promotion of CNS repair, little is known about the response of ECs to such materials. It is hypothesised that by selectively designing and modifying collagen

hydrogels; the migration, proliferation, and differentiation of endogenous ECs could be manipulated, ultimately helping repair damaged spinal cord tissue.

In order to investigate the behaviour of ependymal cells in response to hydrogel mechanical properties, I first aimed to develop and characterise a number of collagen hydrogels, to then use in chapter 6 to investigate the effects of hydrogel composition on ependymal cell behaviour (see Figure 3.1).

3.1.1 Aims and Objectives

This chapter aimed to investigate the feasibility of manipulating the elastic modulus of collagen hydrogels, without changing the hydrogel physical properties. This was achieved by investigating the following objectives:

1. To determine the effect of changing the collagen concentration, crosslinker concentration, and the crosslinker structure (see Table 3.2 for rationale) on the following hydrogel properties:

- Mechanical
  - Rheology to determine the elastic modulus (stiffness)
- Physical
  - TNBS assay to infer the degree of crosslinking/functionalisation
  - Pore spacing assessment using SEM imaging & NMR

2. Determine the effects of post-processing hydrogels (i.e. ethanol disinfectant washes) and whether the methods used for culturing hydrogels (incubation in culture medium at 37 ^{o}C) would alter the hydrogel mechanical properties.

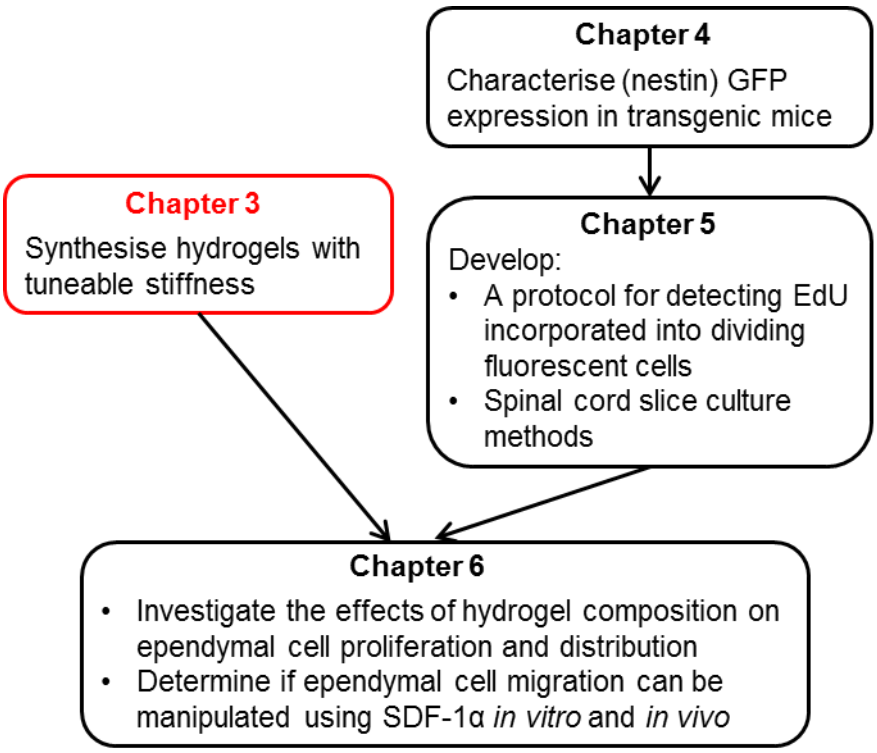

Figure 3.1 Schematic depicting the aim of chapter 3 in relation to the rest of this thesis.

Table 3.2 Conditions trialled in this chapter for manipulating the properties of collagen hydrogels

Variable	**Rationale**
Collagen concentration	Increasing the collagen concentration *should* increase the hydrogel stiffness due to the additional collagen fibrils present. This should also reduce the porosity of the hydrogel. Crosslinking should remain constant (Head et al., 2016).
Crosslinker molar ratio	Increasing the crosslinker molar ratio (compared to collagen lysine groups) *should* increase the degree of functionalisation and increase the hydrogel stiffness due to the additional crosslinks formed. It may also result in a reduction in pore size (Her et al., 2013; Head et al., 2016)
Crosslinker structure	Changing the crosslinker structure may result in a change to the hydrogel mechanical properties due to a change in the crosslinking bond lengths. It is unknown whether the porosity or the degree of crosslinking will change (Head et al., 2016).

3.2 Methods

3.2.1 Isolation of type I collagen

Type I collagen was isolated via acidic treatment of rat tail tendons according to a method used previously (Tronci et al., 2013). Frozen rat tails (obtained from Central Biomedical Services, University of Leeds) were thawed in 70% ethanol (v/v) for 30 minutes to disinfect the skin and transferred into a class II safety cabinet. The skin was removed using a scalpel and locking clamp forceps and tails were then dried for 1 hour at RT. Individual tendons were removed from the tendon sheath, placed in acetic acid (17.4 mM) and stirred for 4 days at 4°C to dissolve (50 mL per tail). The mixture was then centrifuged (38,400 RCF, 4°C) for 40 minutes and the tissue pellets were discarded. The remaining mixture was transferred to a round bottomed flask, frozen overnight at -80°C and then freeze-dried for 7 days to obtain dry collagen.

3.2.1.1 Circular dichroism spectroscopy

Circular dichroism (CD) spectroscopy measures the difference between the absorption of left and right circularly polarised light over a range of wavelengths and is used to study the secondary structure of polypeptides and proteins. CD was carried out on the acid-extracted products to confirm the dichroic properties and assess whether there was any conformational change following extraction.

Extracted collagen and a gelatin (negative) control were dissolved in acetic acid (17.4 mM) at a concentration of 0.002 g/mL. Sample solutions were collected in quartz cells of 10.0 mm path length and CD spectra were obtained with a 2.5 nm bandwidth. Gelatin was used as a control as this is denatured collagen and so should not show any typical peaks associated with triple helices. Acetic acid (17.4 mM) was used as a reference and this solvent spectrum was subtracted from each sample spectrum along with a blank base spectrum of only air.

Ellipticity, θ (millidegrees (mdeg)), was converted into mean residue ellipticity [θ]MRW (deg.cm^2.dmol^{-1}) using equation 1(147).

$$[\theta]MRW = (MRW \times \theta)/(10 \times d \times c)$$ **Equation 1**

Where MRW is the mean residue weight for the peptide bond (94.5 Da for collagen and 91 Da for gelatin (Lopes et al., 2014)), c is the concentration of the sample (g/mL) and d is the path length (1 cm).

3.2.2 Hydrogel synthesis

Collagen hydrogels were created according to the method published by (Tronci et al., 2013; Head et al., 2016), whereby the collagen lysine groups (lys) were directly functionalised using a number of bi-functional monomers and thus, crosslinked. These crosslinkers include: 4-phenylenediacetic acid (4Ph), 1,3-phenylenediacetic acid (13Ph), and adipic acid (Ad) (Figure 3.22).

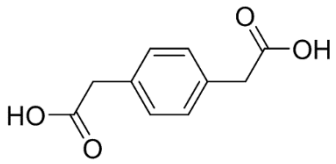

4-Phenylenediacetic acid (4Ph)

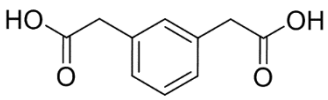

1,3-Phenylenediacetic acid (13Ph)

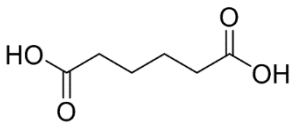

Adipic acid (Ad)

Figure 3.2 Crosslinker molecular structures used for collagen gelation

Chemical structures of the di-acid crosslinkers used in this chapter: 4-phenylenediacetic acid (4Ph), 1,3-phenylenediacetic acid (13Ph), and adipic acid (Ad).

Carboxylic acid groups (COOH) of 4Ph, 13Ph, or Ad (**1** Figure 3.3) were activated using 1-ethyl-3-(3-dimethylaminopropyl) carbodiimide hydrochloride (**2**) (EDC, 1:6 molar ratio carboxylic acid:EDC) and N-hydroxysuccinimide (**4**) (NHS, 1:1 molar ratio carboxylic acid:NHS) at 0°C for 1 hour in sodium phosphate buffer (SPB) (Figure 3.3).

The o-acylisourea active ester intermediate (**3**) formed initially is rapidly hydrolysed in aqueous solutions to form a carboxylate and a urea derivative (**8** & **9** – side reactions), and readily undergoes electron displacement giving rise to an unreactive N-acylurea (**10**). NHS is added to stabilise the reactive intermediate via conversion to an amine-reactive ester (**5**). This therefore increases the reaction efficiency as this ester is reactive towards amine groups and more stable against hydrolysis (Grabarek and Gergely, 1990).

Following activation any remaining unreacted EDC was quenched using 2-mercaptoethanol (βME) for 10 minutes to stop any unwanted side reactions. The NHS-activated crosslinker was then added to a collagen solution (in acetic acid, 17.4 mM), cast into well plates, and allowed to crosslink overnight at room temperature (RT) (Figure 3.3, **iii**). Hydrogels were then washed in 0.1 M PB (3 times) to remove any unreacted chemicals or side products.

Crosslinking collagen lysines

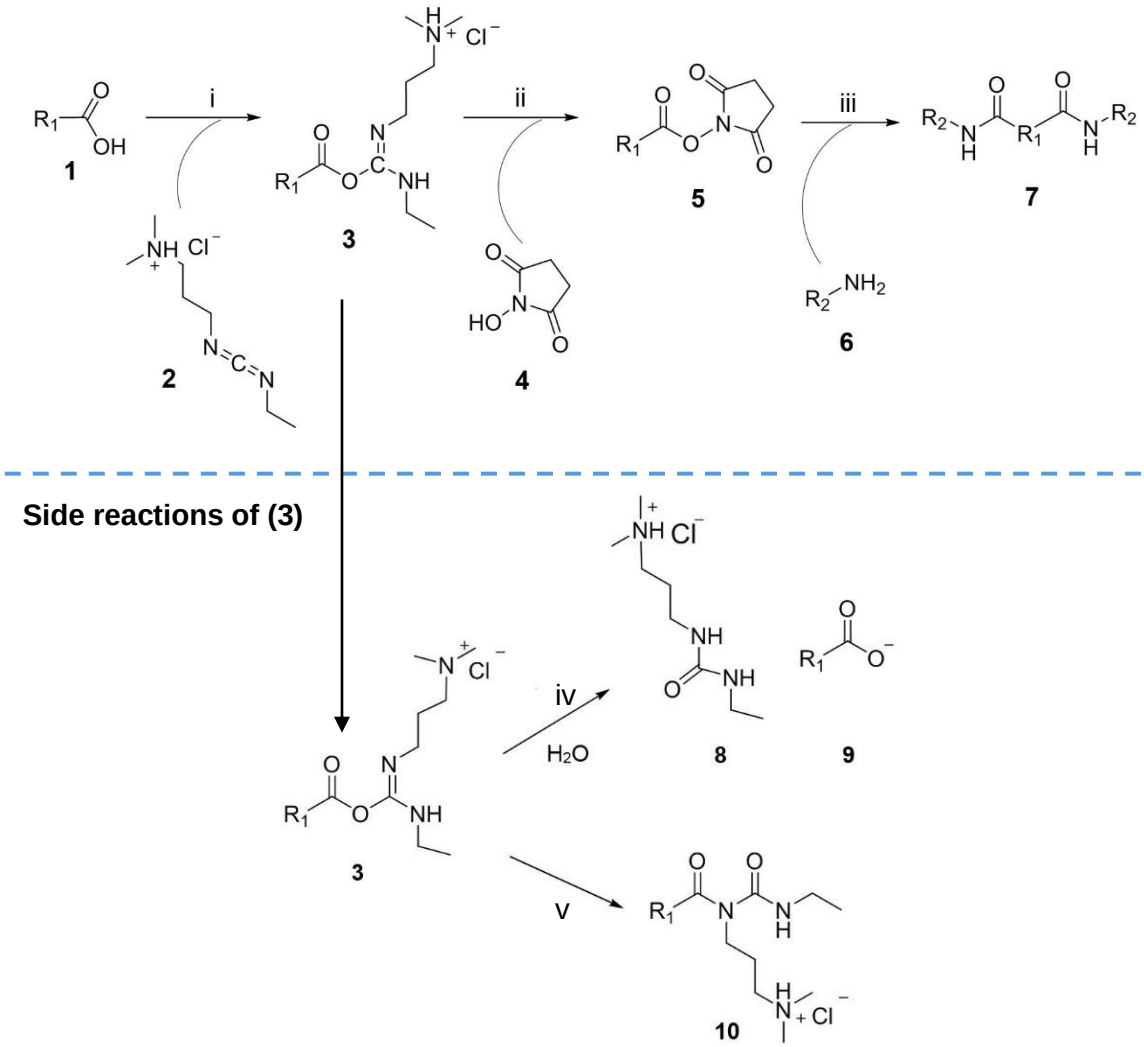

Figure 3.3 Synthetic route adapted for the creation of chemically crosslinked collagen

Collagen hydrogel synthesis involved (i) initial activation of bifunctional carboxylic acid groups of the crosslinker (1) using EDC (2) - forming o-acylisourea active ester intermediate (3). (ii) Reaction with NHS (4) – forming the stable amine-reactive NHS ester (5), followed by (iii) addition of the collagen solution and nucleophilic addition/elimination reaction of collagen lysine amines (6) to the activated diacid. R_1 = bifunctional crosslinker backbone (two reactions per mole of crosslinker), R_2 = collagen backbone.

Side reactions of the o-acylisourea active ester intermediate (iv) Hydrolysis of o-acylisourea active ester (3), yielding a carboxylate and urea derivative (8 & 9) and (v) rearrangement producing N-acylurea (10).

Manipulating hydrogel mechanical and physical properties

A number of crosslinking variables were investigated, including: collagen concentration, crosslinker COOH: collagen lys molar ratio, and the crosslinker structure (Table 3.3).

For hydrogels formed with final collagen concentrations of 0.4, 0.6, and 0.8 wt. % the crosslinker 4Ph was used and the crosslinker carboxylic acid to collagen lysine molar ratio was maintained at 1:1 (Table 3.3, row 1). For hydrogels where the crosslinker COOH:collagen lys molar ratio was varied from 0:5, 1:1 and 1.5:1 the final concentration of collagen was maintained at 0.8 wt.% and the crosslinker used was 4Ph (Table 3.3, row 2). Finally, hydrogels were formed using 4Ph, 13Ph, and Ad crosslinkers. Here, the final collagen concentration was maintained at 0.8 wt. % and the crosslinker COOH:collagen Lys molar ratio was maintained at 1:1 (Table 3.3, experiment 3).

Table 3.3 Conditions trialled in this thesis

Experiment	Collagen concentration /wt.%	Crosslinker COOH: collagen Lys molar ratio	Crosslinker structure
1	**0.4, 0.6, & 0.8**	1:1	4Ph
2	0.8	**0.5:1, 1:1, & 1.5:1**	4Ph
3	0.8	1:1	**4Ph, 13Ph, & Ad**

Conditions trialled in bold, and control variables. Collagen concentration was varied in experiment 1, crosslinker carboxylic acid: collagen lysine group molar ratio was varied in experiment 2, and the crosslinker structure was varied in experiment 3.

Effect of the culture process on hydrogel stiffness

Hydrogels were first washed in PB (3 x 10 minutes) to remove any unreacted chemicals, then disinfected using an ethanol concentration gradient with 15 minute washes in 10, 20, 30, 50, and 70% ethanol solutions. To determine whether the culture process has an impact on hydrogel mechanical properties, rheological characterisation using rheometry was then carried out immediately or hydrogels were stored at 4 °C for 21 days prior to testing. These hydrogels were compared to control samples, where washes were carried out using PB. Additionally, the effect of hydrating hydrogels in

culture medium and incubating them at 37 °C was investigated. Here, hydrogels were washed in PB and disinfected (as described previously) then washed in culture medium with no serum (3 x 10 minutes) and either tested immediately (medium d0), or incubated at 37 °C in a 5% CO_2 enriched environment for 7 days prior to testing (medium d7).

3.2.3 Assessment of mechanical properties using rheology

Hydrogel mechanical properties were assessed using a rheometer. All rheological measurements were performed using a Kinexus Pro rheometer with a parallel plate system. A 20 mm plate with a gap of 3.5 mm were used for all tests. Hydrogels were formed in 24 well plates and cut to size using a 20 mm cylindrical punch. All experiments were performed at 25 ^{o}C unless stated otherwise. Strain amplitude sweeps were carried out at a frequency of 1 Hz from 0.1% to 1000% strain. The linear viscoelastic region (LVER) was identified for each gel as 0.5% strain, where the storage modulus (G') and loss modulus (G") are independent of strain amplitude. G' and G'' are each measures of the solid (elastic) and fluid (viscous) phases of the material respectively. For a self-supporting hydrogel, G' is usually an order of magnitude greater than G'' and so G' is typically quoted alone as an indication of material stiffness (greater G' = increased stiffness) (Borzacchiello and Ambrosio, 2009). Frequency sweeps were then performed on fresh hydrogel samples within this LVER from 0.5 Hz to 5 Hz at 0.5% strain. Storage modulus, G' is quoted at 1 Hz.

3.2.4 Assessment of physical properties

Degree of functionalisation - TNBS assay

A 2,4,6-trinitrobenzenesulfonic acid (TNBS) colorimetric assay was used to determine the number of free primary amino groups following reaction with NHS-activated di-acids, and the consequent degree of collagen functionalisation (grafting) or crosslinking. Trinitrophenyl-L-lysine is a UV chromophore and enables the

quantification of free (unreacted) amino groups at 346 nm via the formation of an orange coloured derivative (Figure 3.4).

Dehydrated hydrogels (0.011 g) were added to a solution of 1 mL sodium hydrogen carbonate ($NaHCO_3$; 4 wt.%, pH 8.5) and 1 mL TNBS solution (0.5 wt.%), covered in foil and reacted at 40 °C under mild agitation for 4 hours. 3 mL hydrochloric acid (HCl, 6 M) was added and heated to 60 °C for 1 hour to hydrolyse and dissolve additional insoluble components.

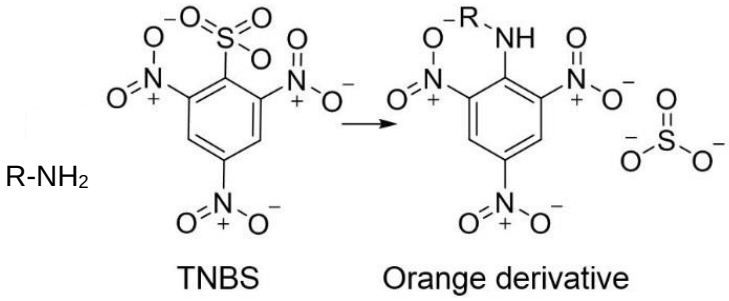

Figure 3.4 Colourimetric 2,4,6-trinitrobenzenesulfonic acid assay schematic

Reaction of trinitrobenzenesulphonic acid (TNBS) with an amine, producing an orange derivative and a sulphite ion. R = collagen backbone.

Solutions were cooled to RT, diluted with 5 mL diH_2O and extracted three times using a separating funnel with 20 mL anhydrous diethylether in order to remove any unreacted TNBS. An aliquot of the aqueous phase (5 mL) was heated at 40 °C to remove excess ether and diluted further using 15 mL diH_2O. Solutions were read against a blank (control) sample, whereby HCl was added prior to the addition of TNBS in order to prevent any protein reaction occurring.

The number of moles of free amino groups per gram of collagen in crosslinked samples was calculated using Equation 2:

$$moles(Lys)_{Crosslinked} = \frac{moles(Lys)}{g(collagen)} = \frac{2 \times Abs(346\ nm) \times V}{\varepsilon \times l \times x} \qquad \textbf{Equation 2}$$

Where: Abs(346 nm) is the absorbance value of the sample at 346 nm, V is the volume of sample solution (0.02 L), ε is the molar absorption coefficient for 2,4,6-trinitrophenyl lysine (1.46 x 10^4 L mol^{-1} cm^{-1}), l is the cell path length (1 cm), x is the sample mass (0.011 g).

From this, the degree of functionalisation/crosslinking (% functionalisation) was calculated as in Equation 3:

$$\%\ functionalisation = \left(1 - \frac{moles(Lys)_{Crosslinked}}{moles(Lys)_{Native\ Collagen}}\right) \times 100 \qquad \textbf{Equation 3}$$

$Moles(Lys)_{Collagen}$ denotes the lysine molar content in native collagen. For rat tail collagen this is 3.24 x 10^{-4} mol/g (Tronci et al., 2013).

Scanning Electron Microscopy (SEM) imaging

Analysis of pore size and internal architecture was carried out using scanning electron microscopy (SEM) following critical point drying (CPD) by Martin Fuller (School of Molecular and Cellular Biology, University of Leeds). Firstly the hydrated hydrogels were fixed in glutaraldehyde (2.5% w/v in PB) overnight, followed by two PB washes and fixed further using osmium tetroxide (1% w/v in PB). Hydrogels were then dehydrated in increasing concentrations of acetone and critically point dried, replacing the solvent with liquid CO_2. This method is typically used for biological specimens as it allows the structural integrity to be maintained (Cohen, 1979). Acetone is used as an intermediate fluid prior to CO_2 phase conversion as this is miscible with CO_2 and also reduces the damage caused by drying due to the reduced surface tension of the solvent with air compared to water. Samples were then sputter coated with platinum at 5 nm thickness and imaged at 50000, 5000, and 1000x magnification.

3 SEM images (5000x magnification) per hydrogel condition were analysed using the BoneJ plugin developed by (Doube et al., 2010) for ImageJ (see Figure 3.5), whereby firstly the scale was set and the scale bars were then removed from the original image (Figure 3.5 A). The images were then smoothed to reduce background noise and converted to binary (Figure 3.5 B). The BoneJ thickness tool was used to generate the fibril thickness (Figure 3.5 C) and the spacing between collagen fibrils (pore spacing) (Figure 3.5 D) (validated for use on hydrogels by (Clarkson, 2018)).

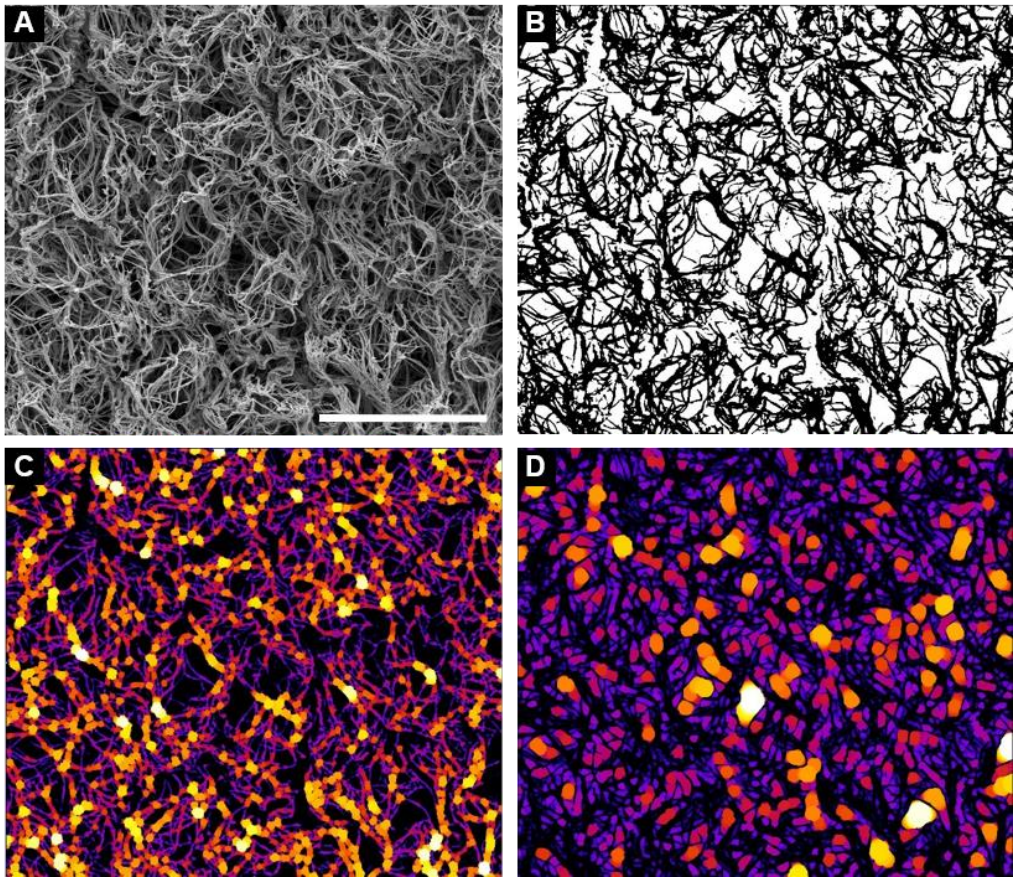

Figure 3.5 SEM image analysis using the BoneJ plugin for ImageJ

(A) The original SEM image used for analysis, scale bar = 20 µm, and (B) the binary conversion. The BoneJ plugin was used to generate: (C) matrix thickness and (D) pore spacing.

Porosity analysis via Carr-Purcell-Meiboom-Gill sequence (CPMG)

SEM pore spacing data were also compared to NMR porosity measurements. Carr-Purcell-Meiboom-Gill sequence (CPMG) experiments allow the measurement of spin-

spin T2 relaxation times of any nucleus within a sample. This gives accurate quantification of the porosity of samples in a non-destructive manner, using nuclear magnetic resonance (NMR). Here, T2 is proportional to pore size, and therefore larger T2 values correspond to larger pore volumes (Coates et al., 1999). CPMG was carried out by Carlos Grattoni (School of Earth and Environment, University of Leeds) at 2 MHz with a field strength of 0.047 Tesla. The software used to get the T2 distributions was WinDXP (Oxford Instruments).

3.3 Results

3.3.1 Collagen extraction

CD spectroscopy confirmed the preservation of the triple helix structure of collagen in acid-extracted products, as indicated by the positive maximum absorption band at 210-230 nm (Figure 3.6). A minimum absorption band was also observed around 190 nm, indicating the single polyproline-II helix conformation.

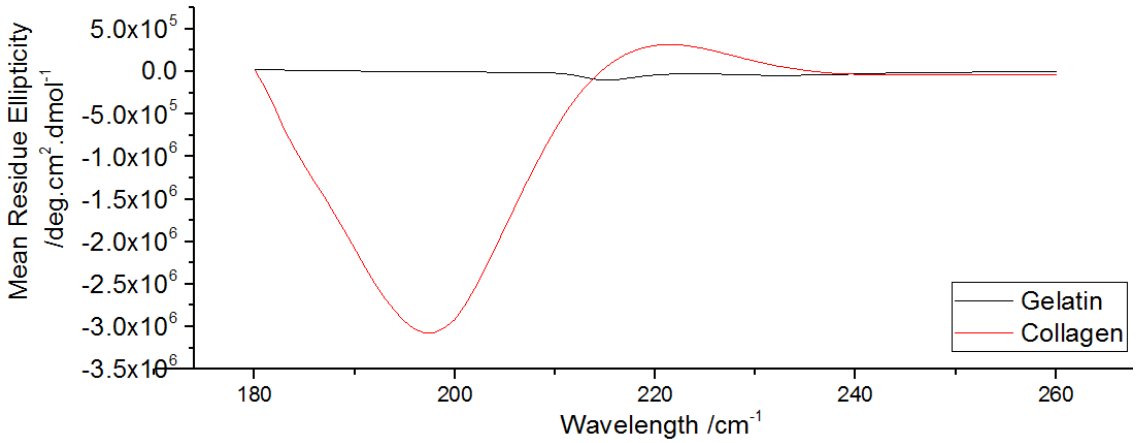

Figure 3.6 Preservation of the collagen triple helix following acid extraction

CD spectra of collagen (black) and gelatin (red) control mean residue ellipticity, indicating the preservation of the collagen triple helix (210-230 nm) and polyproline-II helix conformation (190 nm).

3.3.2 NMR porosity method development

As this method is typically used for porous rocks, the effect of hydrogel solvent was first assessed in order to inform future measurement conditions. Hydrogels were either washed in PBS or H_2O (3 x 10 minutes) prior to NMR porosity measurements. Solvent samples were used as a control and tested using the same method. From the NMR porosity plots, the mean T2 values were calculated for each hydrogel. These are proportional to the porosity of the hydrogel, with greater T2 values corresponding to increased pore volumes.

There was no significant difference in mean T2 values, and therefore hydrogel porosity, between solvents used (n=3, P=0.733). The mean T2 value ±SD was 1393.7 ±57.12 ms for 0.8 wt.% collagen hydrogel in PBS and 1442.0 ±64.51 ms for 0.8 wt.% collagen hydrogel in H_2O. Therefore, future measurements were made using PBS-hydrated hydrogels (Figure 3.7).

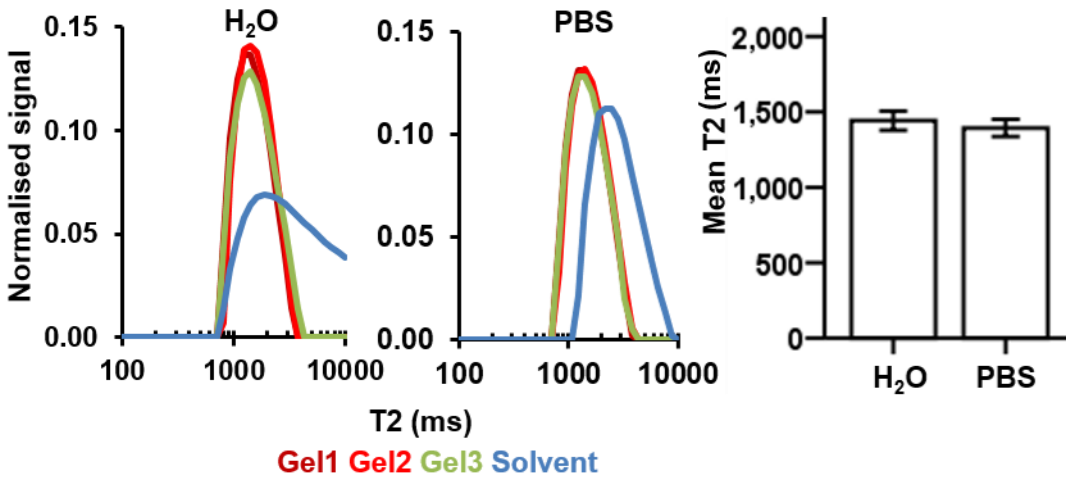

Figure 3.7 NMR porosity measurement using different hydrogel solvents

(A) NMR porosity plot showing normalised signal against T2, and (B) the resulting mean T2 measurements taken from this graph. n=3.

3.3.3 Formation of hydrogels

Collagen hydrogels were formed and the mechanical properties were assessed using rheology. Initial strain sweeps determined 0.5% strain to be within the LVER for each

hydrogel variant (Figure 3.8 A), and so this value was used for the subsequent frequency sweeps (Figure 3.8 B). Additionally, as expected, the storage modulus (G' - Figure 3.8 blue) was around 1 order of magnitude greater than the loss modulus (G'' – Figure 3.8 red); confirming the formation of self-supporting hydrogels (see Supplementary data Table 8.1 for the frequency sweep data for each hydrogel repeat).

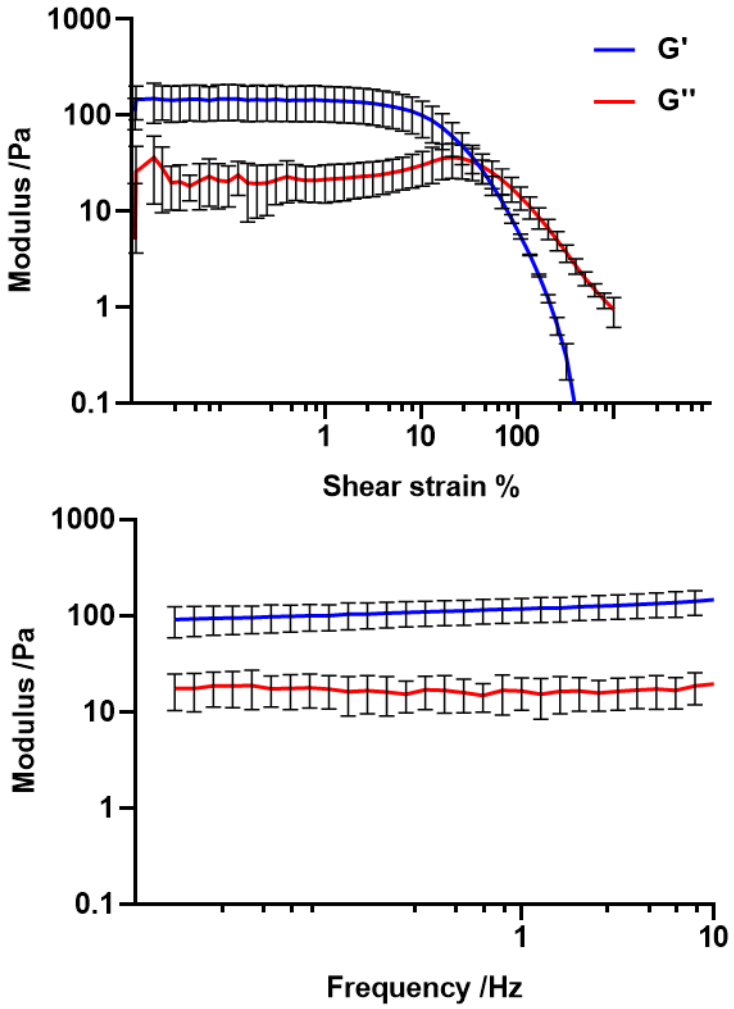

Figure 3.8 Example of rheology data used to characterise hydrogel mechanical properties

The storage moduli (G' blue) and loss moduli (G'' red) measured using: (A) Shear strain amplitude sweep at 10 rad/s from 0.1% to 1000% strain to determine the linear viscoelastic region (LVER). (B) Frequency sweep carried at 0.5% strain. Data taken from 4Ph-crosslinked hydrogel 0.8 wt.% collagen, 1:1 COOH:Lys ratio. Data presented as mean ±SD, n=3.

3.3.4 Manipulating the properties of collagen hydrogels

Collagen concentration, crosslinker molar ratio, and the structure of the crosslinker were investigated as potential routes for forming hydrogels with different mechanical properties, whilst maintaining constant porosity and degree of crosslinking.

3.3.4.1 Effect of collagen concentration

Three collagen concentrations: 0.4, 0.6, and 0.8 wt.% (final concentration) were investigated in order to determine if this variable caused a change in the properties of the resulting hydrogels. For all of these conditions the collagen lys:crosslinker COOH molar ratio was maintained at 1:1.

The collagen concentration did not significantly impact the degree of functionalisation (determined by TNBS assay, Figure 3.9 A). This was expected as the molar ratio of crosslinker to collagen lysine groups was scaled accordingly, and thus remained consistent between groups.

There was a significant difference between the storage modulus of hydrogels created using different collagen concentrations (P= 0.0083 to 0.0002; Figure 3.9 B), with hydrogels formed using 0.8 wt.% collagen exhibiting the greatest storage modulus (mean storage modulus ±SD (Pa): 0.4: 81.45 ±3.119, 0.6: 211.8 ±29.51, 0.8: 351.7 ±51.41).

The spacing between collagen fibrils (as determined using the BoneJ plugin analysis of SEM images) was not significantly different between the collagen concentrations investigated (Figure 3.8 C and D; mean spacing ±SD (μm): 0.4: 0.661 ±0.111, 0.691 ±0.125, 0.741 ±0.112). However, NMR porosity measurements (Figure 3.9 E & F) showed a significant decrease in mean T2 values, and therefore reduced porosity, for 0.8 wt.% collagen hydrogels, indicating these hydrogels had smaller pores (mean T2 ±SD (ms): 0.4: 1771.67 ±101.25, 0.8: 1393.67 ±57.12; n=3, P= 0.0023).

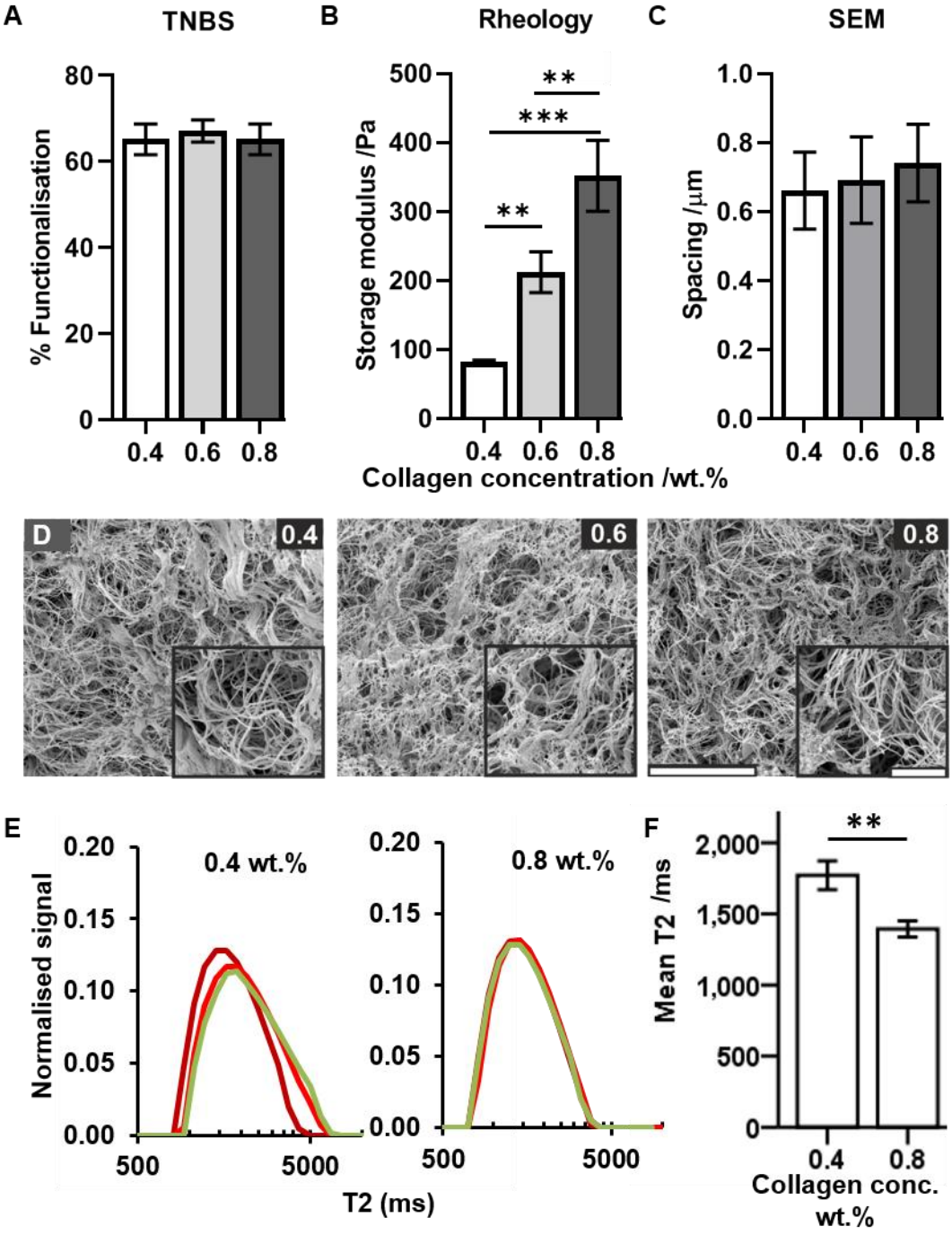

Figure 3.9 Effect of collagen concentration on the physical properties of hydrogels

(A)TNBS assay % functionalisation, (B) storage modulus determined by rheology frequency sweeps, quoted at 10 rad/s (C) pore spacing determined using BoneJ plugin from SEM images (D) representative SEM images, (E) normalised NMR signals, and (F) mean T2 values taken from these plots. Scale bars = 30 μm, inset = 5 μm. 1:1 4Ph crosslinker COOH:collagen lys. Data presented as mean ±SD. n=3, ** P ≤ 0.01, *** P ≤ 0.001.

3.3.4.2 Effect of crosslinker molar ratio

Interestingly, the molar ratio of the carboxylic acid groups of the 4Ph crosslinker used (as compared to collagen lys groups), did not significantly affect the degree of collagen functionalisation (Figure 3.10 A). The storage modulus of gels created using varying crosslinker molar ratios were not significantly different (Figure 3.10 B; n=3, P = 0.3039 to 0.8793). Additionally, there was no significant difference in the mean pore spacing between collagen fibrils (Figure 3.10 C & D).

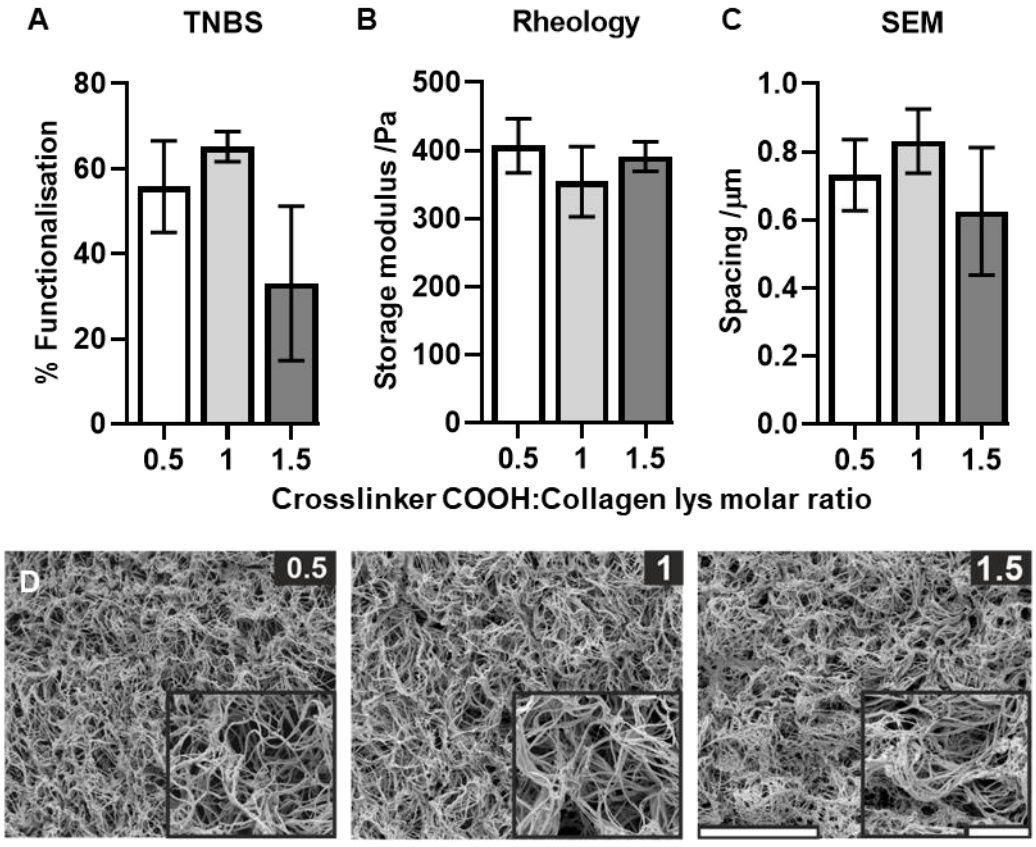

Figure 3.10 Effect of 4Ph crosslinker molar ratio

0.8 wt.% collagen crosslinked using: 0.5, 1, and 1.5 4Ph crosslinker COOH:collagen lys molar ratio. (A)TNBS assay % functionalisation, (B) storage modulus determined by rheology frequency sweeps, quoted at 10 rad/s, (C) mean pore spacing determined using BoneJ plugin from SEM images (D) representative SEM images. Scale bars = 30 µm, inset = 5 µm. Data presented as mean ±SD. n=3, ns P > 0.05.

3.3.4.3 Effect of crosslinker chemical structure on hydrogel properties

The degree of functionalisation remained similar for hydrogels crosslinked using 4Ph, 13Ph, and Ad (Figure 3.11 A) with no significant differences detected. Rheological characterisation showed that hydrogels crosslinked using 4Ph, 13Ph, and Ad had storage moduli (Pa) of 351.7 ±51.42, 395.6 ±80.87, and 332.0 ±37.39 respectively and these were not significantly different. Furthermore, porosity analysis using SEM and NMR measurements also showed that these hydrogels had similar pore spacing and pore volume (Figure 3.11 C – F), once again with no statistically significant differences between the crosslinker variants (SEM pore spacing ±SD (µm): 4Ph: 0.741 ±0.112; 13Ph: 0.774 ±0.101; Ad: 0.650 ±0.031; NMR porosity T2 ±SD (ms): 4Ph: 1416.7 ±107.6; 13Ph: 1418.4 ±55.49; Ad: 1479.6 ±16.35).

3.3.4.4 Effect of culture conditions on hydrogel mechanical properties

To determine the effect of the culture process on hydrogel mechanical properties, hydrogels were washed in PB, disinfected using an ethanol concentration gradient, and tested (using rheology) immediately or following storage at 4 °C for 21 days.

As expected, the process of disinfecting hydrogels in ethanol was shown to increase the storage modulus of the gels significantly when tested immediately (d0: PB: 468.2 ±13.35 Pa; Ethanol: 512.0 ±0.814 Pa; n=3, P = 0.0240) and following 21 days incubation (Figure 3.12) (d21: PB: 420.3 ±19.69 Pa; Ethanol: 549.7 ±16.13 Pa; n=3, P ≤ 0.0001).

Additionally, it was found that storing hydrogels in either solution for 21 days resulted in a significant difference in the hydrogel storage moduli. For PB-hydrated hydrogels, these exhibited a decrease in stiffness over time whereas ethanol storage lead to an increase in stiffness (Figure 3.12). As such, hydrogels were always used/tested immediately and were not stored for prolonged periods (over 2 hours) in ethanol.

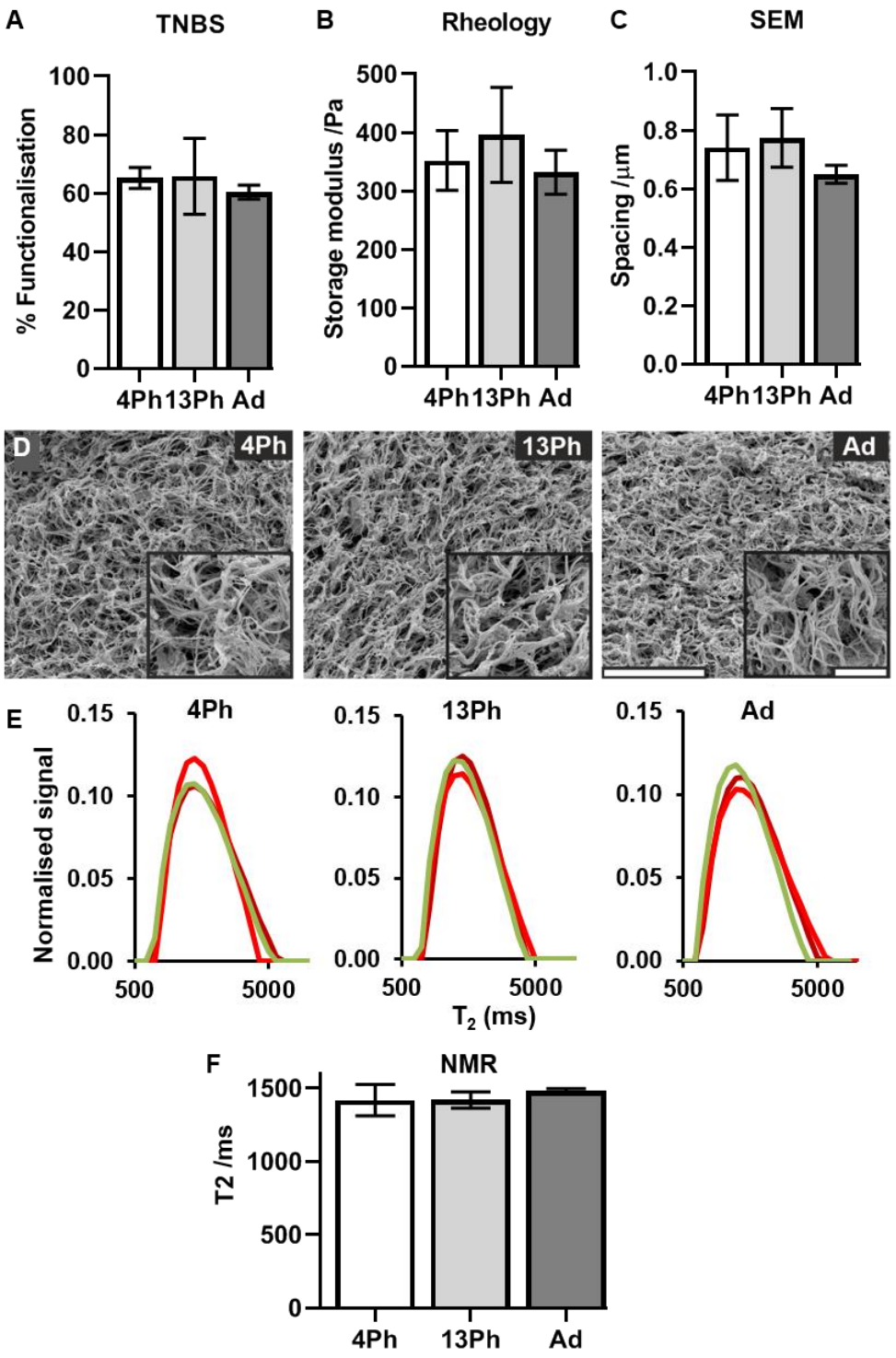

Figure 3.11 Effect of crosslinker structure on hydrogel properties

Characterisation of hydrogels crosslinked using 4-Phenylenediacetic acid (4Ph), 1,3-Phenylenediacetic acid (13Ph) or Adipic acid (Ad). (A)TNBS assay % functionalisation, (B) storage modulus determined by rheology frequency sweeps, quoted at 10 rad/s (C) mean pore spacing determined using BoneJ plugin from SEM images (D) representative SEM images. Scale bars = 30 μm, inset = 5 μm. (E) normalised NMR signals, and (F) mean T2 values. Mean storage moduli determined by rheology frequency sweeps. 4Ph quoted at 10 rad/s. Data presented as mean ±SD. n=3, ns $P > 0.05$.

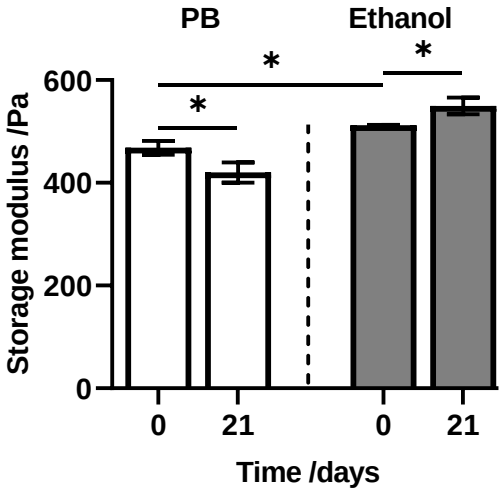

Figure 3.12 Effect of ethanol disinfection on hydrogel storage modulus.

Storage modulus determined by rheology frequency sweeps, quoted at 10 rad/s for hydrogels washed with PB or ethanol and tested immediately (d0) or following 21 days incubation (d21). Data presented as mean ±SD. n=3, * P ≤0.05.

To further assess whether hydrogel mechanical properties change when culturing, the effect of hydrating in culture medium and incubating at 37°C was investigated. Hydrogels were either tested immediately following ethanol disinfection and hydration in medium (medium d0), or heated at 37 °C for 7 days prior to testing (medium d7). The storage modulus of the hydrogels processed this way were compared to hydrogels from the same batch that were washed in PB following ethanol washes and tested immediately (PB). Two crosslinkers: 4Ph and Ad were used to investigate if they differed in response to culture conditions.

There was no significant difference between hydrogel storage modulus for all conditions. There was however, a trend towards reduced storage modulus for 4Ph crosslinked hydrogels maintained in culture. (Figure 3.13; 4Ph PB: 649.7 ±57.01 Pa, medium d0: 556.2 ±40.67, medium d7: 491.6 ±134.9 Pa).

There was a significant difference between the control PB-hydrated hydrogel crosslinked using different crosslinkers (4Ph PB: 649.7 ±57.01 Pa; Ad PB: 434.03 ±13.18 Pa; n=3, P= 0.0178). This trend was not seen previously when assessing the

mechanical properties of hydrogels formed using different crosslinkers, indicating that there could be batch to batch variations.

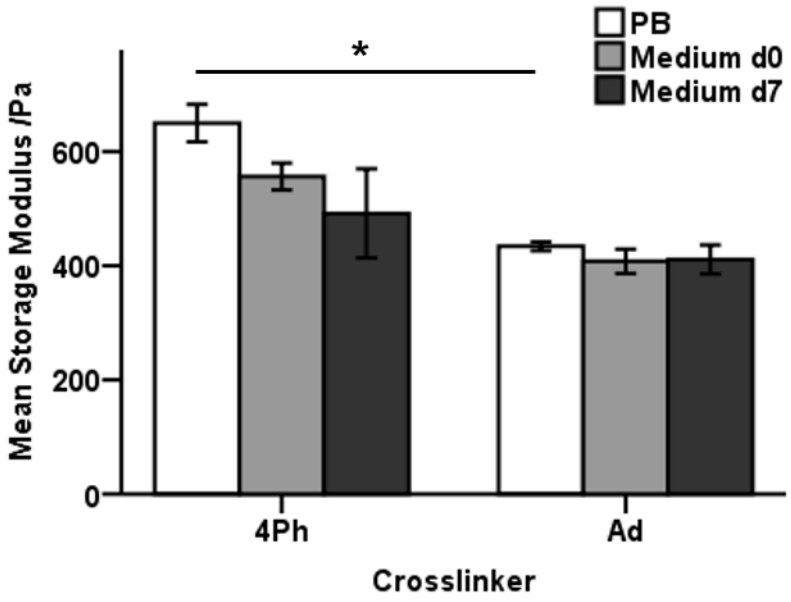

Figure 3.13 Effect of hydrating in culture medium and heating at 37 °C for 7 days on the rheological properties of collagen hydrogels.

Storage modulus of collagen hydrogels crosslinked with 4Ph or Ad and hydrated in phosphate buffer (PB) compared to hydrogels washed in culture medium with no serum and either tested immediately (medium d0), or heated at 37 °C for 7 days prior to testing (medium d7). Storage modulus determined by rheology frequency sweeps, quoted at 10 rad/s. Data presented as mean ±SD. n=3 * $P \leq 0.05$.

3.3.5 Batch reproducibility

It was evident when repeating rheology measurements that the mechanical properties of hydrogels varied between batches (see supplementary Figure 8.1). It wasn't clear however, whether this was due to the collagen or the crosslinker solution batches and so this was investigated.

The batch of crosslinker solution didn't impact the resulting storage modulus of the hydrogels formed (Figure 3.14 A). There was however, a significant difference between the storage modulus of hydrogels created using different batches of collagen solution (same batch of extracted collagen, Figure 3.14 B, **** $P < 0.01$). Interestingly, there was only a significant difference between collagen solution batch 1 and the other hydrogels

formed using collagen solution batch 2 and 3. Collagen solution batch number 1 was a larger volume, indicating that the dissolution of collagen may not be scalable.

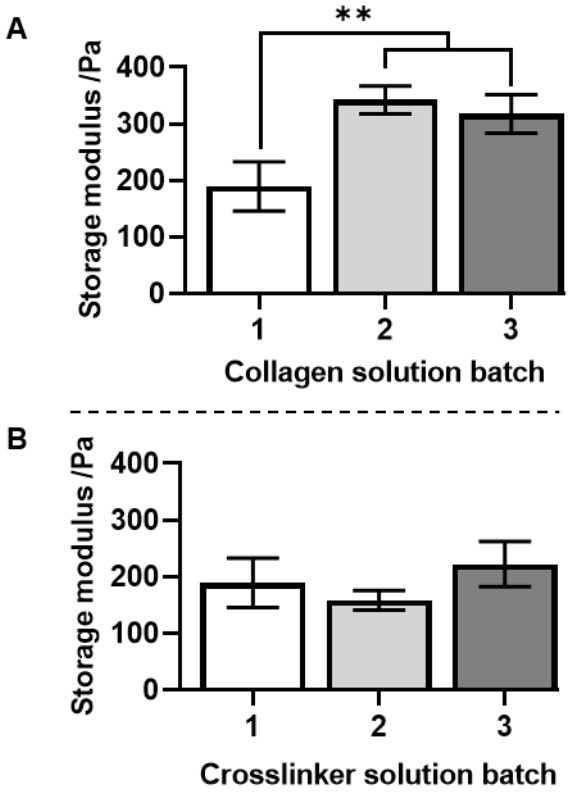

Figure 3.14 Effect of collagen and crosslinker solution batch on hydrogel storage modulus.

Storage modulus determined by rheology frequency sweeps, quoted at 10 rad/s for hydrogels formed from different batches (denoted as 1, 2, and 3) of collagen and 4Ph crosslinker solutions. Data presented as mean ±SD. n=3, ** $P \leq 0.01$.

3.3.5.1 Hydrogel synthesis conditions

To investigate the factors influencing the resulting hydrogel mechanical properties, the starting concentrations of the collagen and activated crosslinker solutions were varied (see Figure 3.15 A). Final concentrations (of the combined collagen and crosslinker mixture) remained constant in all three hydrogel conditions, with a molar ratio of 2:1 collagen: crosslinker.

Firstly, a control hydrogel was created using a 1.2 wt.% initial collagen solution crosslinked with 4Ph at a molar ratio of 1:2 (referred to as Col 1.2 4Ph; Figure 3.15 A).

The effect of a diluted initial collagen solution was then investigated. Here, the same 1.2 wt.% initial collagen solution was diluted to 0.96 wt.%, prior to crosslinking with 4Ph to form a hydrogel (referred to as Col 0.96 4Ph x2; Figure 3.15). To maintain the same final molar ratio of the two solutions (1 4Ph: 2 Col lys), a concentrated crosslinker solution was used (referred to as 4Ph x2).

There was a significant difference between the storage modulus of hydrogels created using different initial collagen solution concentrations. When the initial collagen concentration was diluted to 0.96 wt.% (from the same batch of collagen solution) prior to mixing with the concentrated 4Ph crosslinker (Col 0.96 4Ph x2; Figure 3.15 A), the storage modulus reduced from 521.6 ±9.473 Pa to 200.0 ±6.600 Pa.

To confirm whether this effect was due to the concentration of the collagen solution or the activated crosslinker solution, the concentrated activated 4Ph solution was diluted prior to crosslinking with same 1.2 wt.% initial collagen solution (referred to as Col 1.2 4Ph x2 diluted). The storage modulus was found to be similar to that of the control hydrogel when 4Ph x2 was diluted prior to mixing (525.6 ±21.21 Pa, Figure 3.15 B), thereby confirming this change in stiffness was not due to the concentration of the initial activated crosslinker solution.

These data indicate that the initial collagen concentration in the starting solution, potentially due to the solution viscosity, influences the final storage modulus of hydrogels.

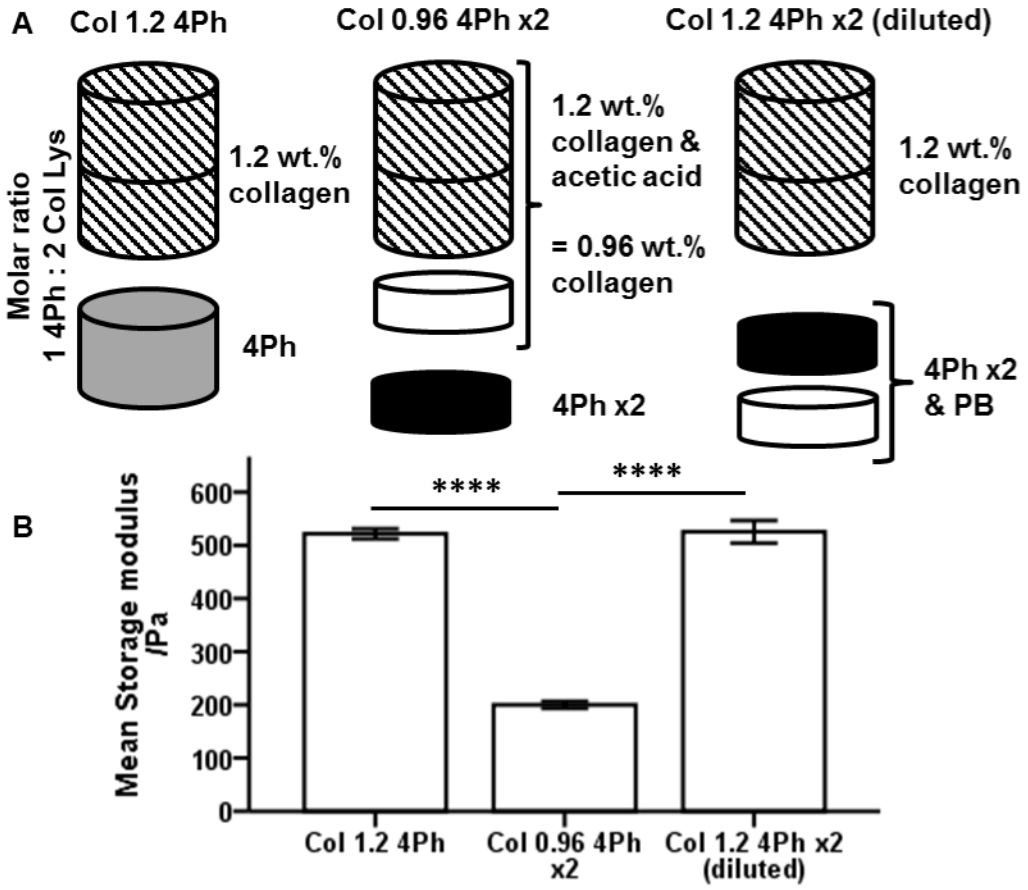

Figure 3.15 Effect of initial collagen concentration on hydrogel rheological properties

(A) Schematic depicting dilution method generating Col 1.2 4Ph (control); Col 0.96 4Ph x2 – created using diluted initial collagen solution mixed with concentrated 4Ph solution; and Col 1.2 4Ph x2 (diluted) – created by diluting the concentrated 4Ph x2 solution prior to mixing with collagen. (B) Storage modulus determined by rheology frequency sweeps, quoted at 10 rad/s. n=3, **** $P \leq 0.0001$.

3.4 Discussion

In this chapter, the potential manipulation of hydrogel mechanical properties was investigated by varying the collagen concentration, the crosslinker molar ratio, and the structure of the crosslinker used.

Hydrogel manipulations

The method of varying the collagen concentration was found to significantly affect the storage modulus of the resulting hydrogels, however, this method is not suitable for the manipulation of hydrogel mechanical properties as it also leads to physical changes. NMR porosity measurements indicated that increasing the collagen concentration in hydrogels significantly reduces the pore volume within hydrogels; thereby rendering it an unsuitable method for independent modulation of mechanical stiffness. Additionally, altering collagen concentration leads to a change in the number of cell-attachment sites, which could potentially impact cell behaviour further. Furthermore, despite the degree of functionalisation remaining constant, it is not clear whether crosslinking occurs in the same fashion in each of these conditions. As the collagen concentration is increased, it is possible that increased grafting (reaction of only one carboxyl group) starts to take place, due to the increased competition between lysine residues.

A previous study aimed to investigate the response of neural stem cells (from the brain of adult rats) to hydrogels of varying stiffnesses, created by altering the concentration of alginate. Here the porosity was not assessed, and as such, it is likely that the change in stem cell behaviour was confounded by the structural changes caused as a result of the change in alginate concentration (Banerjee et al., 2009a).

Varying the crosslinker molar ratio was also investigated. Here it was found that no significant changes were made to the mechanical and physical properties of the resulting hydrogels. As one mole of crosslinker reacts with two moles of collagen lysine groups, an equimolar ratio of crosslinker carboxylic acid groups to collagen lysine

groups should theoretically lead to 100% crosslinking, however, in reality only 65.2% functionalisation was achieved.

The potential manipulation of collagen hydrogel mechanical properties using crosslinkers with structural differences was also investigated in this chapter. The hydrogels formed using 4Ph, 13Ph, and Ad all had storage moduli in the region of 300-400 Pa. These hydrogels also had similar degrees of functionalisation and porosity as measured by SEM imaging and NMR CPMG experiments.

The repeated measurements made in the course of this chapter highlighted the inconsistencies in the hydrogel properties between batches. It was identified that the issues with repeatability are likely to be due to collagen batch variability, with the starting collagen concentration (and the resulting solution viscosity) significantly impacting hydrogel storage modulus. It is also likely that as collagen was extracted in-house from a natural source, the purity and quality may not have been consistent, therefore impacting on hydrogel repeatability. Future studies would therefore benefit from a commercial source of collagen to ensure consistent quality and purity of starting materials.

Impact of culture conditions on hydrogel stiffness

This chapter also aimed to determine if the culture conditions affect the mechanical properties of collagen hydrogels. As expected, ethanol disinfectant washes were shown to lead to a significant increase in hydrogel storage modulus, however this remained in the range of 400 to 600 Pa (Gopinath et al., 2014). Additionally, hydrogels mechanical properties were not shown to significantly change upon hydrating in culture medium and incubating at standard culture conditions (37 ^{o}C and 5% CO_2 enriched environment), therefore indicating that these hydrogels will be suitable culture substrates.

3.5 Conclusions

In this chapter, characterisation of collagen hydrogels developed in-house indicated that the hydrogel stiffness can't be reliably manipulated, independent of physical properties.

Changing the collagen concentration lead to:

- No significant change in the % functionalisation
- A significant change to the storage modulus of hydrogels
- No detectable pore spacing change when assessed using SEM measurements
- A significant change in porosity when assessed using NMR measurements

Changing the crosslinker molar ratio lead to:

- No significant change in the % functionalisation
- No significant change to the storage modulus of hydrogels
- No significant change to the pore spacing - assessed using SEM measurements

Changing the crosslinker structure lead to:

- No significant change in the % functionalisation
- No significant change to the storage modulus of hydrogels
- No significant change to the porosity - assessed using SEM & NMR measurements

Additionally, it was found that disinfecting collagen hydrogels using ethanol washes leads to a significant increase in hydrogel storage modulus, however, culturing these hydrogels for 7 days does not cause a change to the mechanical properties.

Overall, this chapter highlights the issues surrounding creating a tuneable collagen hydrogel for the assessment of mechanical properties independent of physical properties.

Chapter 4 – Characterisation of GFP Expression in the Spinal Cord of (Nestin) GFP Transgenic Mice

4.1 Introduction

4.1.1 Transgenic reporter lines used for studying neurogenesis

Transgenic mouse lines in which the neural stem cells of the embryonic and adult central nervous system express a reporter molecule, such as a fluorescent protein, are useful tools for studying neurogenesis *in vitro* and *in vivo* (Mignone et al., 2004; Encinas et al., 2011; Park et al., 2013). The reporter genes in such transgenic lines can either be expressed constitutively (consistently) or can be induced using an external trigger.

4.1.1.1 Inducible transgenic reporter lines

Spatial and temporal control over transgene expression can be achieved using inducible transgenic reporter lines. These are routinely used to study the molecular and cellular mechanisms involved in stem cell development and behaviour. Tetracycline-controlled transactivator (tTA or Tet-Off) systems (Gossen and Bujard, 1992) are widely used for inducible gene expression, both *in vitro* and *in vivo*. In these systems tTA or reverse tTA (rtTA or Tet-On) is placed downstream from the tetracycline operator (tetO), and tetracycline (or the analogue doxycycline) is used to either block (in the case of tTA) or induce gene expression (in the case rtTA).

4-hydroxytamoxifen (4HT)-regulated expression models are commonly used with Cre recombinase (an enzyme that targets LoxP) for the expression of promotor genes flanked by LoxP DNA sequences. In these systems, a mutated ligand binding domain

of the estrogen receptor is fused with Cre recombinase (CreERT), and this binds to heat shock protein 90 (HSP) in the cytoplasm, rendering it tamoxifen-inducible. As a result, the addition of 4HT or tamoxifen triggers the CreERT-HSP complex to separate, translocation of CreERT into the nucleus, followed by recombination. Overall, this results in either inactivation (and creation of knockout alleles) or activation of gene expression in these animals. A number of Cre/loxP lines have been utilised for studying the lineage of stem cells in the brain. Promoters (DNA sequences that define where transcription of a particular gene by RNA polymerase begins) have included: Nestin (Meletis et al., 2008; Burns et al., 2009; Dhaliwal and Lagace, 2011; Imayoshi et al., 2011; Liang et al., 2012; Sun et al., 2014), Glast1 (Mori et al., 2006), Gli1 (Ahn and Joyner, 2005), FoxJ1 (Meletis et al., 2008; Barnabé-Heider et al., 2010), and Sox2 (Favaro et al., 2009).

More recently, viral gene delivery systems have been developed for the delivery of Cre recombinase using adeno-associated viral-, lentiviral-, and retroviral-based vectors. Using these methods, recombination can be controlled to target specific cell populations using viruses expressing Cre under the promoter of particular genes (e.g. the FoxJ1 gene for targeted recombination in ependymal cells (Carlén et al., 2009)).

4.1.1.2 Constitutive transgenic reporter lines

A number of constitutive transgenic reporter lines have also been developed using a range of constructs and reporters, resulting in varied gene expression (nestin transgenic reporter lines summarised in Table 4.1 and reviewed elsewhere (Walker et al., 2010; Dhaliwal and Lagace, 2011)). The animals used in this chapter were originally created by G. Enikolopov's laboratory. In these mice the regulatory elements of the second intron of the nestin gene were used to create a reporter line expressing green fluorescent protein (GFP) (referred to as (nestin) GFP) (Mignone et al., 2004). Nestin is a type VI intermediate filament protein and a marker of neural stem and progenitor cells in developing and adult animals (Lendahl et al., 1990). In this

transgenic line, (nestin) GFP is selectively expressed in progenitor cells and pericytes (Birbrair et al., 2013; Licht et al., 2016), and diminishes in differentiated cells; allowing for the identification and isolation of neural stem cells (NSCs) (Mignone et al., 2004).

While these GFP-expressing (GFP+ve) cells have been characterised in the brain, the identity of (nestin) GFP+ve cells has not been confirmed elsewhere within the CNS. In this chapter, known markers of ECs and a retrograde tracer for pericyte identification were used to investigate (nestin) GFP expression in the spinal cord.

Since one aim of chapter 6 of this thesis is to use (nestin) GFP mice to track spinal cord ECs and assess their behaviour in response to hydrogels, characterising the fluorescently labelled cells is of great importance. Additionally, identification of cell markers and proteins in (nestin) GFP+ve cells may help inform tissue engineering strategies aimed at manipulating ependymal cell migration and differentiation.

GAD67-GFP transgenic mice were also used in this chapter in order to assess the selectivity of the antibodies used. The enzyme glutamic acid decarboxylase (GAD) is responsible for catalysing decarboxylation of glutamate into ɣ-aminobutyric acid (GABA) and is present in two isoforms: GAD65 and GAD67 (Tamamaki et al., 2003; Gotts et al., 2016). GAD67-GFP has been shown to label CSFcCs, which are also located at the central canal region in the spinal cord of mice (Corns et al., 2015; Gotts et al., 2016). Where possible, immunofluorescence (IF) results were also validated against published RNAseq data (Rosenberg et al., 2018) and Allen Brain Atlas data (Allen Institute for Brain Science, n.d.).

Table 4.1 – Nestin reporter mice used to study neurogenesis

Name	Construct	Reporter	EC labelling	Ref.
(Nestin) GFP	5.8-kb promoter and the 1.8-kb second intron of nestin gene	eGFP	Brain	(Mignone et al., 2004)
pNestin-GFP	2.5 kb nestin promoter, 1.8 kb nestin enhancer 2nd–3rd intron	eGFP	Brain	(Yamaguchi et al., 2000)
E/nestin:eGFP	637-bp (1162–1798) of 2nd intron from nestin, hsp68 min promoter	eGFP	Brain and spinal cord	(Kawaguchi et al., 2001)
NesPlacZ/3	Rat nestin gene; 5-kb upstream and 3 introns	LacZ	Brain and spinal cord	(Johansson et al., 2002)
Nes714tk/lacZ	714-bp of 2nd intron from human nestin, 107-bp of thymidine kinase promoter	LacZ	No	(Johansson et al., 2002)
Nestin-tTA × TetOp-mCREB	5.8-kb upstream to 5.4-kb downstream of nestin gene. Nestin-tTA mouse crossed with TetOp-mCREB-FLAG mice.	CREB	Potentially, brain	(Beech et al., 2004)
Nestin-rtTA-eGFP	5-kb-nestin promoter, 700-bp of 2nd intron of nestin gene	eGFP	Dorsal neural tube	(Yu et al., 2005)
Nestin-CFPnuc	5.8-kb nestin promoter, 1.8-kb nestin enhancer 2nd–3rd intron	CFP	Brain	(Encinas et al., 2006)
Nestin-eGFP	2nd Intron, thymidine kinase promoter	EGFPmut4	Brain	(Walker et al., 2010)

Table adapted from (Dhaliwal and Lagace, 2011)(Walker et al., 2010). (Nestin) GFP transgenic line used in this chapter highlighted in bold.

4.2 Hypothesis and Aims

It is hypothesised that GFP in (nestin) GFP transgenic mice can be used to selectively identify ependymal cells (ECs) in the spinal cord.

This chapter uses immunofluorescence on perfusion-fixed spinal cord slices to:

1. Examine the presence of specific cell markers and proteins in (nestin) GFP labelled cells in the spinal cord of transgenic mice
2. Determine if there are appropriate antibodies to discriminate between ECs and CSFcCs at the central canal
3. Identify if ECs express proteins with potential use for targeting in modulating proliferation and/or migration

The development work carried out in this chapter will enable the hypotheses in chapters 5 and 6 to be interrogated, as shown in Figure 4.1.

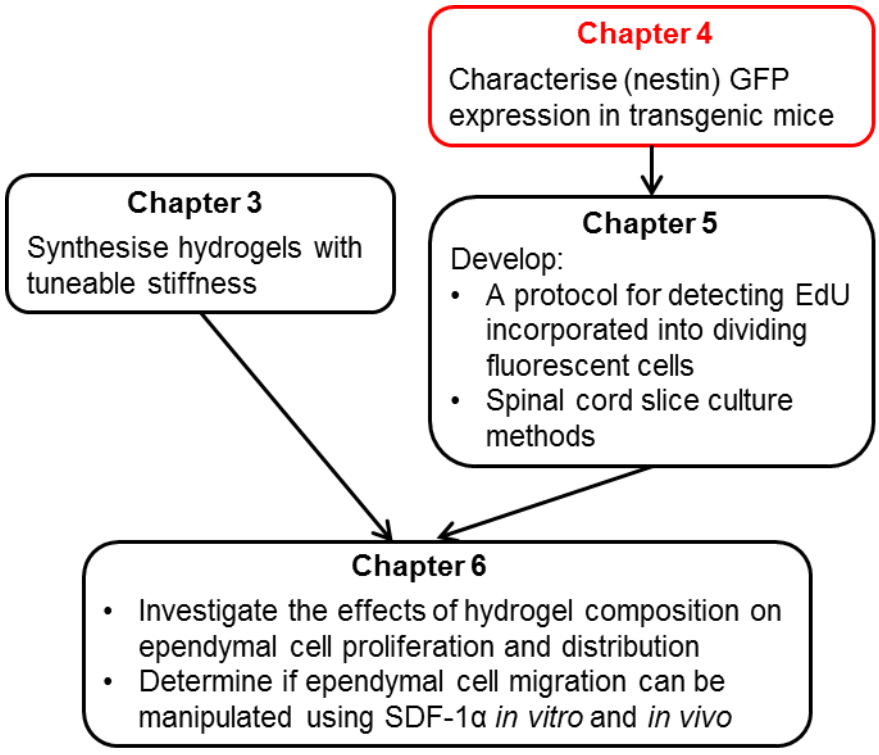

Figure 4.1 Schematic depicting the overall aim of chapter 4 in relation to the rest of this thesis.

4.3 Methods

4.3.1 Animals used

All experiments were carried out under UK Home Office Licence (P1D7A177), in accordance with the UK Animals (Scientific Procedures) Act 1986 and the ethical standards set out by the University of Leeds Ethical Review Committee. Every effort was made to minimise the number of animals used and their suffering.

(Nestin) GFP and GAD67-GFP transgenic mice were bred in-house as heterozygotes, housed in standard conditions with a 12 hour light-dark cycle, and given ad libitum access to food and water.

4.3.2 Hydroxystilbamidine Labelling of Pericytes

Mice received an intraperitoneal (I.P.) injection of 0.05 mL hydroxystilbamidine (Fluorogold, FG) (50 mg/kg) 48 h prior to being perfused to fluorescently label pericytes by retrograde tracing from the periphery (Edwards et al., 2013). FG is directly visible using fluorescence microscopy.

4.3.3 Perfusion fixation and tissue processing

Mice were terminally anaesthetised with sodium pentobarbital (60 mg/kg) I.P. and perfused transcardially with 0.1 M PB to remove blood, then with 4% PFA for tissue fixation. The spinal cord and brain were removed and post fixed overnight at 4 °C in 4% PFA, before being stored in 0.1 M PB at 4 °C.

The pia mater was removed using fine forceps and a dissection microscope, and tissue was sectioned at 40 µm (spinal cord) or 50 µm (brain) on a vibrating microtome. Sections of spinal cord or brain ~1 cm in length were cut using a flat blade, and glued to the vibratome chuck. The chuck was then screwed into place in the water bath containing 0.1 M PB and the blade was attached to the vibratome arm. Sections were

then cut at an amplitude of 0.4 mm/s and vibrating frequency of 80 Hz and tissue sections were transferred into a well plate containing PBS using a paintbrush.

4.3.4 Immunofluorescence

Immunofluorescence (IF) optimisation was carried out to determine the permeabilisation solution and antibody (primary and secondary) concentrations for each antibody used. IF was performed on tissue sections as described in Figure 4.2. Briefly, cell membranes were permeabilised via slice incubation in either 0.1% (v/v) Tween 20 (T20) or 0.1% (v/v) Triton X-100 (PBST) for 30 minutes at RT prior to antibody incubation. All primary antibody incubations were performed for at least 48 h at 4 °C in either 0.1% PBST (Table 4.3) or PBS (for T20 treated sections, Table 4.2). Sections were then washed three times with PBS (10 minutes). Antibodies were detected by incubating sections in the appropriate Alexa Fluor conjugated secondary antibody (1:1000 in PBS) or biotin-conjugated secondary antibody (1:250 in PBS) at RT for 2 h (Table 4.4). In the case of biotinylated secondary antibodies, sections were washed three times with PBS (10 minutes) then incubated with streptavidin Alexa Fluor for 2 h at RT. Finally, sections were washed twice in PBS, followed by a wash in 0.1M PB, and were then mounted on microscope slides, air dried, and covered in Fluoroshield with DAPI (cell nuclei counter-stain) before being coverslipped.

4.3.5 Image capture

Sections (n>3 sections per animal of lumbar and thoracic cord, N=3 animals, Table 4.5) were imaged using a Zeiss LSM880 laser scanning confocal microscope equipped with argon ($\lambda ex = 488$ nm) and He-Ne ($\lambda ex = 543$ nm) lasers. Images were acquired using Carl Zeiss ZEN software (Zeiss Microscopy) and CorelDRAW 2017 was used for image processing - brightness/contrast/intensity and creating figures. DAPI nuclear staining was used to identify each cell and only whole cells were counted. Manual cell counts of the number of (nestin) GFP cells, antibody-labelled cells, and co-localised cells at the central canal were made using the confocal images.

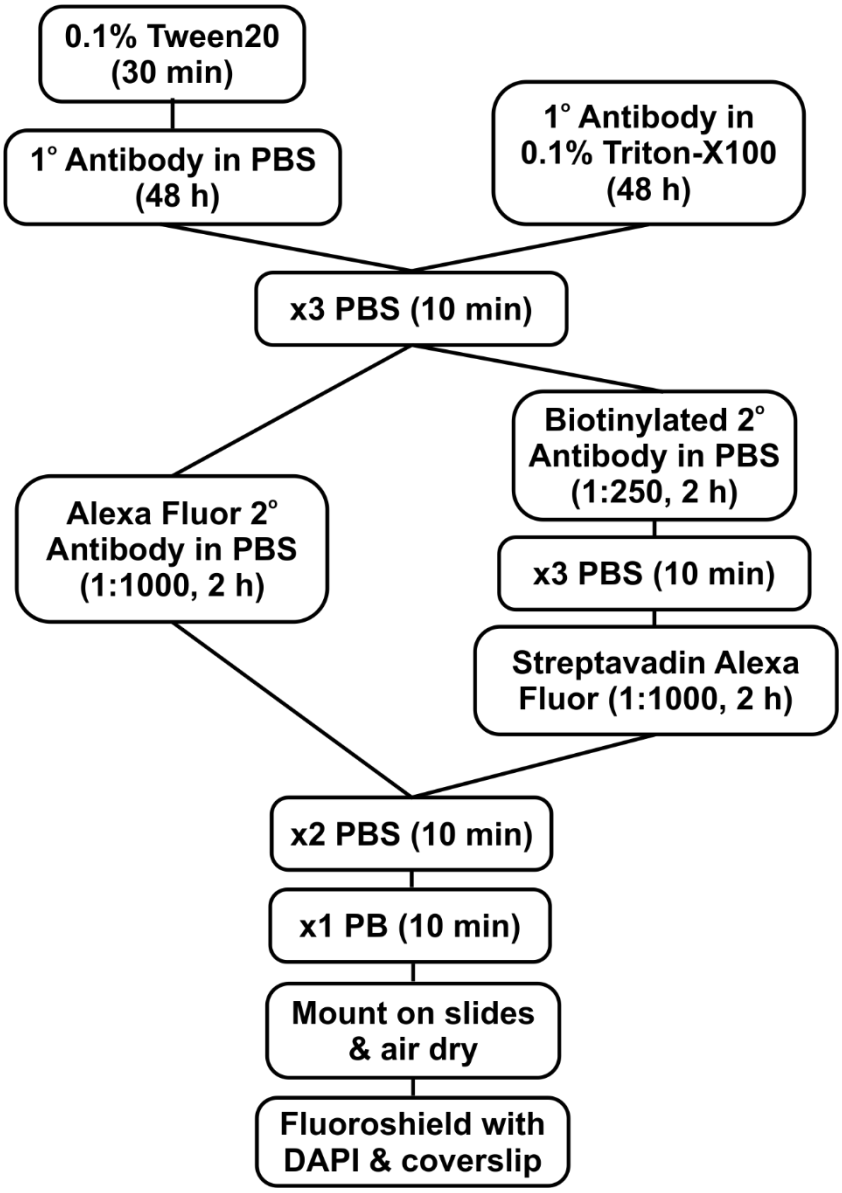

Figure 4.2 Immunofluorescence protocol used for fixed tissue slices

Flow chart detailing the immunofluorescence method used to label proteins within perfusion-fixed tissue slices. Permeabilisation was initially carried out using either Tween20 or Triton-X100, followed by antibody incubation and subsequent antibody detection steps using either a directly conjugated secondary antibody or a biotinylated secondary antibody and streptavidin Alexa Fluor. Slices were then washed and mounted on microscope slides for visualisation

4.3.6 Data Analysis

Cell counts were collated in Microsoft Excel and analysed using IBM SPSS statistics 21. Data presented as mean % colocalisation ± standard error of the mean (SE) where appropriate.

Table 4.2 Antibodies used – permeabilised using Tween20

Target	Raised in	Dilution	Antigen	Evidence	Source & Cat. No
Cluster of differentiation 24 (CD24)*	Mouse	1:100	M1/69 unknown epitope specificity	ECs: adult mice (Pruszak et al., 2009; Pfenninger et al., 2011)	Miltenyi Biotec 130-110-686
Cluster of differentiation 31 (CD31)*	Rat	1:500	129/Sv mouse-derived endothelioma cell line tEnd.1	Endothelial cells (Day et al., 2007)	BD Biosciences 550274
Galectin-3 (Gal-3)*	Goat	1:1000	*E. coli*-derived recombinant mouse Gal-3, Ala2-Ile264, Accession # NP_034835	ECs: adult rat brain (Comte et al., 2011; Yoo et al., 2017)	R&D systems AF1197
Na^+K^+ATPase-α1 (NKA-α1)	Rabbit	1:500	Synthetic non-phosphopeptide derived from human NKA-α1 around the phosphorylation site of serine16 (A-V-SP-E-H)	ECs: adult mice (Edwards et al., 2013; Corns et al., 2015)	AbD Serotec ab58475
Vimentin	Chicken	1:500	Recombinant vimentin	ECs: adult mice (Alfaro-Cervello et al., 2012b) & rats (Schnitzer et al., 1981; Mladinic et al., 2014)	Millipore AB5733

Antibodies marked with an asterisk were detected using biotin-conjugated secondary antibodies followed by streptavidin Alexa Fluor^{555}. Specificity as described by manufacturer.

Table 4.3 Antibodies used – permeabilised using PBST

Target	Raised in	Dilution	Antigen	Evidence	Source
Calbindin-D28k	Rabbit	1:500	Calbindin D-28k	ECs: rat & mouse, not human (Zhang et al., 2016)	Epitomics, ab108404
Cluster of differentiation 63 (CD63)*	Rat	1:1000	HEK293 human embryonic kidney cell line transfected with mouse CD63, Met1-Met238, Accession # P41731	ECs: adult & juvenile mouse spinal cord (Allen Institute for Brain Science, n.d.)	R&D systems MAB5417
Chemokine receptor type 4 (CXCR4)*	Rabbit	1:8000	Non-phosphorylated C-terminus of CXCR4 (residues 341-352)	ECs: (Tysseling et al., 2011; Hugnot, 2011)	RabMab ab124824
Forkhead box protein J1 (FoxJ1)*	Mouse	1:1000	Not detailed	ECs: embryonic, juvenile & adult mouse (Meletis et al., 2008; Alfaro-Cervello et al., 2012a; Li et al., 2018; Franklin et al., 2018)	eBioscience 14-9965-80
Glial fibrillary acidic protein (GFAP)	Mouse	1:100	Synthetic peptide amino acids 411-422 (KTVEMRDGEVIK) of human GFAP	Astrocytes (Gomes et al., 1999) & radial glia (Mamber et al., 2012)	Neuromab 75-240 clone N206/8
Polycystic kidney disease 2-like 1 protein (PKD2L1)	Rabbit	1:250	Synthetic peptide corresponding to N-terminal residues of mouse PDK2L1	CSFcCs (Huang et al., 2006; Orts-Del'Immagine et al., 2012; Orts-Del'Immagine et al., 2014; Djenoune et al., 2014)	Abcam ab56003
Sex determining region Y-box 2 (Sox2)	Goat	1:500	Epitope mapping near the C-terminus of Sox-2 of human origin	ECs: embryonic & adult rat (Graham et al., 2003; Mladinic et al., 2014)	Santa Cruz SC-17320 (Y-17)

Antibodies marked with an asterisk were detected using biotin-conjugated secondary antibodies followed by streptavidin Alexa Fluor^{555}. Specificity as described by manufacturer.

Table 4.4 Secondary antibodies used on tissue sections

Antibody	Raised in	Antigen	Cat. number	Dilution	Source
Alexa Fluor^{555}	Donkey	Mouse	A31570	1:1000	Invitrogen
	Donkey	Rabbit	A32794		
	Goat	Chicken	A21437		
	Goat	Rat	A21437		
Biotinylated	Donkey	Goat	A16003	1:250	Novex
	Donkey	Rabbit	A16039		
	Horse	Mouse*	BMK2202		Vector Laboratories
	Donkey	Rat	712-065-153		Jackson ImmunoResearch
Streptavidin Alexa Fluor^{555}		N/A	532355	1:1000	Invitrogen

The antibody marked with an asterisk is part of the Mouse on Mouse immunodetection kit.

Table 4.5 Animals used in this chapter

Chapter ref.	Strain	Number of animals (N)	Antibody	Sections per condition (n)		Brain (OB, SVZ & SGZ)	Age (weeks)
				Thoracic	Lumbar		
4.5.3.1	(Nestin) GFP	3	CD24	17	18	-	6-8
4.5.3.2			Gal-3	14	16	-	6-8
4.5.3.3			NKA-α1	17	14	-	6-8
4.5.3.4			Sox2	14	15	-	6-8
4.5.3.5			Vimentin	14	18	-	6-8
4.5.4.1			CD63	9		-	6-8
4.5.4.2			CXCR4	9		-	6-8
4.5.4.3			FoxJ1	9		-	6-8
4.5.4.4			Calbindin-D28k	9		-	6-8
4.5.4.5			GFAP	9		-	6-8
4.5.5			PKD2L1	9		-	6-8
4.5.1	(Nestin) GFP*	2	CD31	6		12	6
4.5.5	GAD67-GFP	2	PKD2L1	6		-	6-8
4.5.3.1- 4.5.3.5			CD24- Vimentin	6**		-	6-8

N.B. Tissue was taken from the same 3 (nestin) GFP animals in sections 4.5.3 and 4.4.4. n numbers represent the total number of slices counted/imaged from each spinal cord region, from all animals. * FG-injected. ** Total slices per antibody (CD24, Gal-3, NKA-α1, Sox2, & Vimentin).

4.4 Results

4.4.1 (Nestin) GFP colocalises with markers of pericytes in the spinal cord and brain

(Nestin) GFP expression was present throughout the spinal cord in the white and grey matter, intensifying at the central canal (Figure 4.3 A & B). FG labelling colocalised with (nestin) GFP in the white and grey matter of the spinal cord (Figure 4.3 B) and brain (Figure 4.4) identifying these cells as pericytes (Edwards et al., 2013). As expected, these (nestin) GFP pericytes were also found in close apposition to CD31+ve endothelial cells (Figure 4.3 Ai). (Nestin) GFP+ve cells were located within the hippocampal dentate gyrus (DG) (Figure 4.4 A), as well as the subventricular zone (not shown) and glomerular layer (GL) and subependymal layer (SEL) of the olfactory bulb (Figure 4.4 B), reflecting nestin expression patterns seen elsewhere (Mignone et al., 2004; Encinas et al., 2011).

FG labelling was largely absent from the subgranular zone (SGZ) of the DG, and here (nestin) GFP was expressed mainly in neural stem cells (Figure 4.3 A, white dashed region). A sub-population of (nestin) GFP+ve cells, located at the central canal of the spinal cord, were also CD31-ve and FG-ve (Figure 4.4 A & B, white dashed ovals).

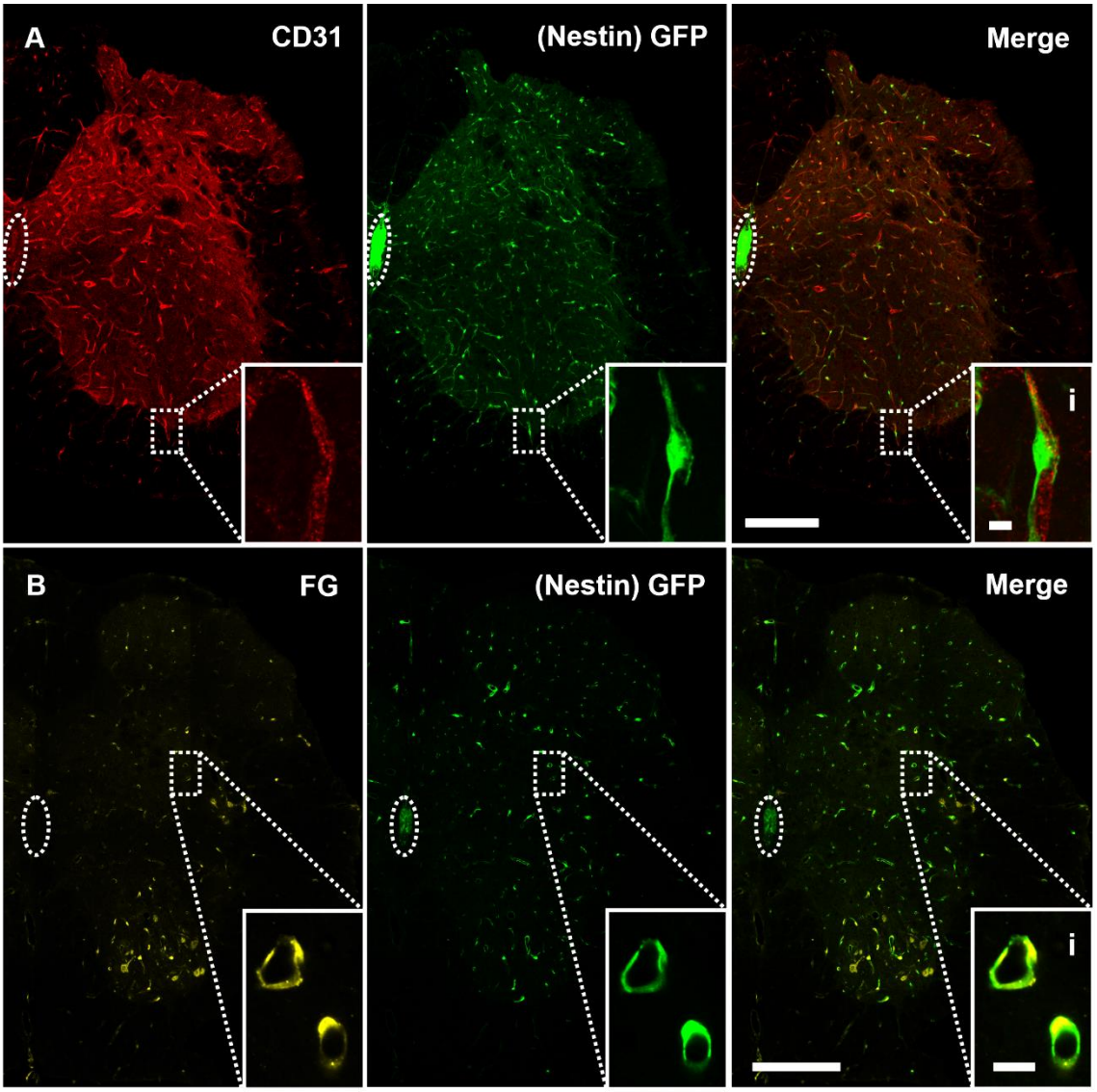

Figure 4.3 (Nestin) GFP labels pericytes and ependymal cells in the spinal cord.

Representative confocal images of (A) CD31 staining (red) and (B) FG-labelled cells (yellow) in the spinal cord of (nestin) GFP mice (green). Scale bars A & B = 200 µm, i = 20 µm.

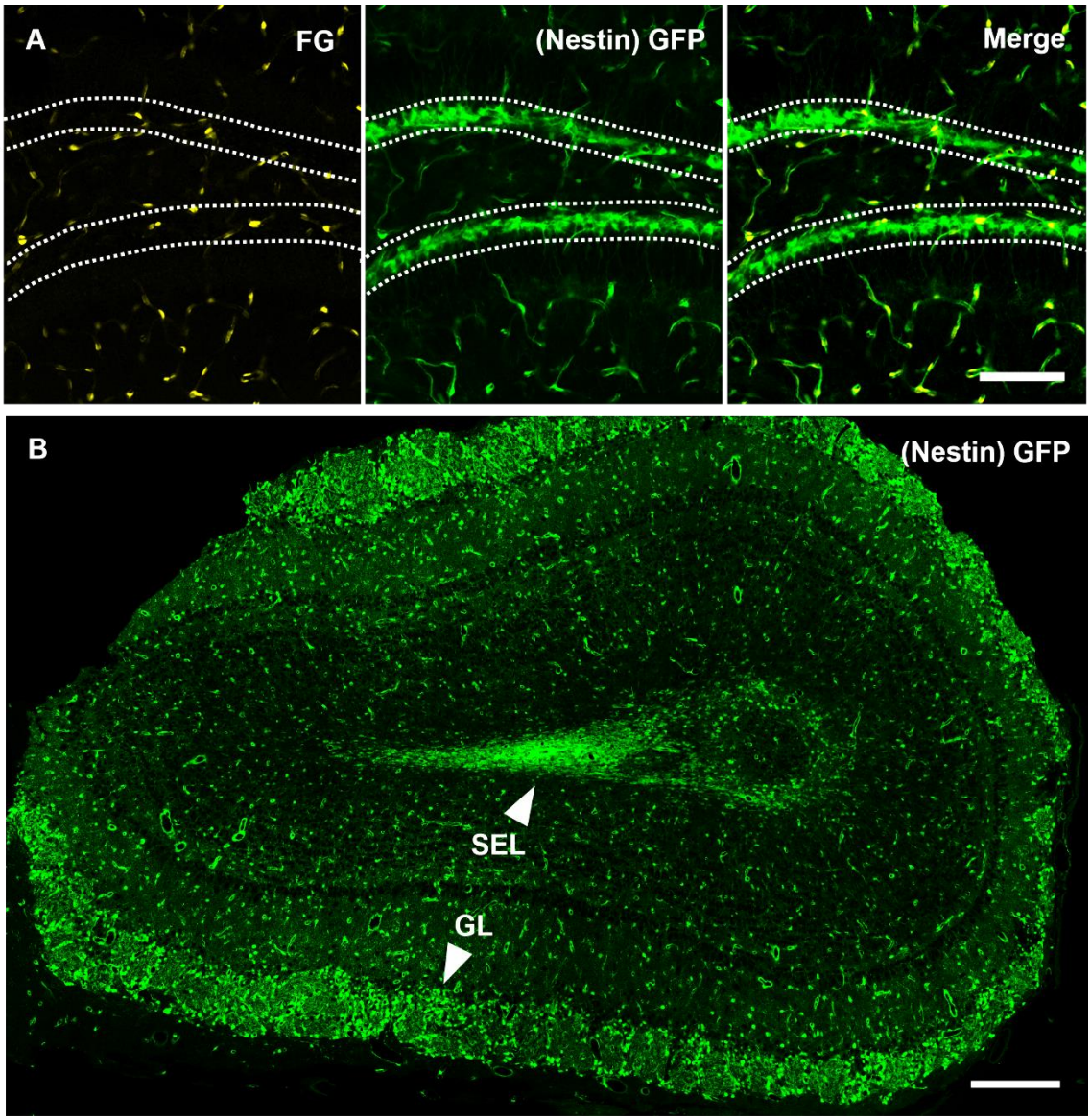

Figure 4.4 (Nestin) GFP labels pericytes and neural stem cells in the brain.

Representative confocal images of (A) FG-labelled cells (yellow) in the subgranular zone (SGZ, dashed region) of the dentate gyrus (DG) of (nestin) GFP mice (green). (B) (nestin) GFP expression in the olfactory bulb (rotated, coronal plane). White arrows denoting the glomerular layer (GL) and subependymal layer (SEL). Scale bars A = 100 µm, B = 200 µm.

4.4.2 (Nestin) GFP colocalises with antibodies labelling ECs in the spinal cord

(Nestin) GFP+ve cells at the central canal of the spinal cord were not labelled by FG or CD31, and various antibodies were used to confirm the identity of these cells as ECs.

Antibodies used to label ECs include: CD24, galectin-3 (gal-3), NKA-α1, sox2, and vimentin. (Nestin) GFP expressing cells at the central canal were immunoreactive against all EC markers, confirming their identity as ECs. GAD67-GFP transgenic tissue was used to assess whether some of the antibodies labelled ECs and/or CSFcCs at the central canal region of the spinal cord.

4.4.2.1 CD24

CD24 has been identified as a neural stem cell surface marker (Pruszak et al., 2009; Yuan et al., 2011) and has been shown to label ependymal cells in the spinal cord (Pfenninger et al., 2011; Alfaro-Cervello et al., 2012b) as well as neuroblasts in the subependymal zone of the adult murine brain (Calaora et al., 1996; Belvindrah et al., 2002). CD24 labelled cells lining the central canal throughout the length of the spinal cord (Figure 4.5 & Figure 4.6 A).

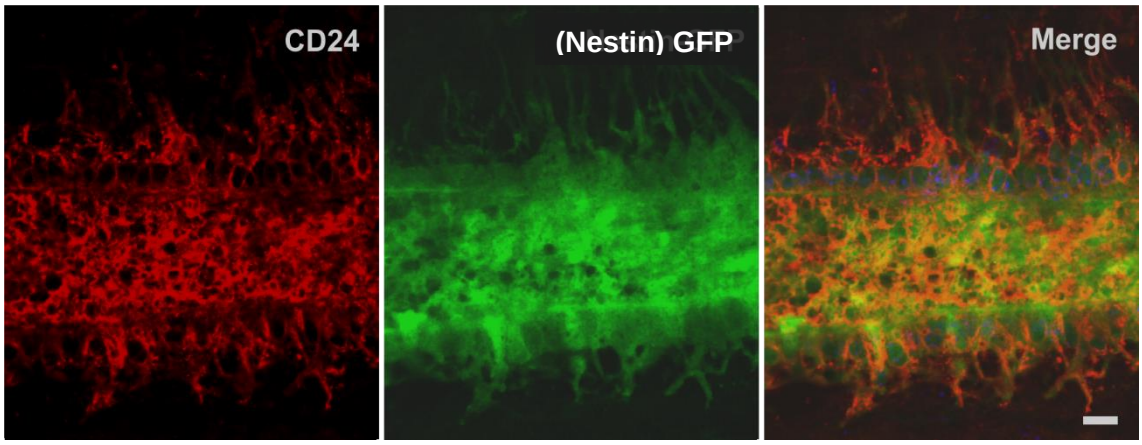

Figure 4.5 CD24 labels ependymal cells along the length of the central canal.

Representative confocal images of saggital central canal CD24 staining (red) and (nestin) GFP (green) colocalisation. Scale bar =10 µm.

On average, cells expressing (nestin) GFP colocalised with over 95% of CD24 labelled cells at the central canal (thoracic= 96.6% ±3.92, lumbar= 95.1% ±1.20; N=3 , n=35) (Figure 4.6 B & D, white arrows with asterisk indicate non-colocalised CD24+ cell). Interestingly, despite being used as an EC marker, CD24 was identified in some GAD67-GFP CSFcCs (Figure 4.6 C, white arrows).

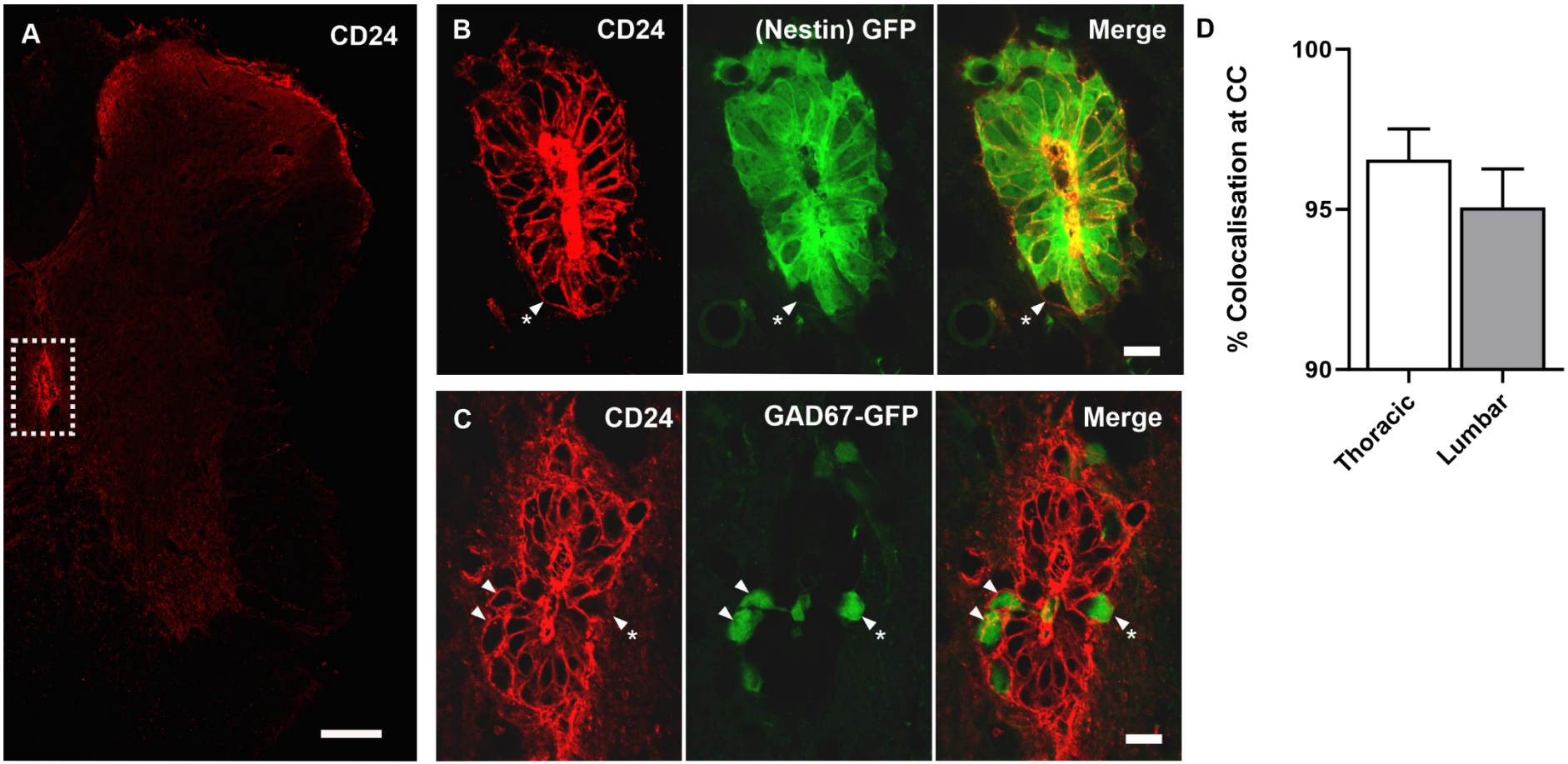

Figure 4.6 CD24 colocalises with (nestin) GFP ECs and some GAD67-GFP CSFcCs at the central canal.

Representative confocal images of CD24 labelling (red) in (A) half a spinal cord slice (central canal in dashed box), central canal of (B) (nestin) GFP and (C) GAD67-GFP tissue (green). (D) Graph showing the percentage of CD24+ve cells colocalised with (nestin) GFP (data presented as mean ±SEM). Arrows indicate co-labelled cells, arrows with asterisk indicate non co-localised cells. Scale bar A = 100 µm, B & C = 20 µm.

4.4.2.2 Galectin-3

In the brain, galectin-3 is expressed in activated microglia (Lalancette-Hébert et al., 2012), neurons (Yoo et al., 2017), and ependymal cells (Comte et al., 2011).

In all spinal cord sections, 100% of (nestin) GFP+ve cells at the central canal colocalised with gal-3 labelling (N=3, n=30) (Figure 4.7 A, B & D). No colocalisation was found between gal-3 and GAD67-GFP+ve CSFcCs, indicating that at the central canal, this Gal-3 antibody is selective for ependymal cells (Figure 4.7 C). Gal-3 also labelled GFP-negative sympathetic preganglionic neurons (SPNs) in the spinal cord (not shown).

4.4.2.3 NKA-α1

Na^+/K^+ATPase (NKA) is a transmembrane protein present in excitable cells (Edwards et al., 2013; Corns et al., 2015). The catalytic α subunits of NKA (isoforms: α1-4) maintain ionic gradients via the exchange of Na^+ and K^+ ions and in the spinal cord of mice the α1 subunit (NKA-α1) is expressed in α-motoneurons, sympathetic preganglionic neurons – SPNs, and ECs (Edwards et al., 2013; Corns et al., 2015).

NKA-α1 staining colocalised with (nestin) GFP+ve cells at the central canal and also labelled GFP-negative terminals in the intermediolateral nucleus (IML, Figure 4.8 A & Ai). Over 90% of NKA-α1 labelled cells colocalised with (nestin) GFP at the central canal (Figure 4.8 B & D) (thoracic= 90.30 ±1.427, lumbar= 94.10 ±1.246; N=3, n=31). A few NKA-α1 labelled cells were GFP-negative or had faint GFP fluorescence and so were not counted as colocalised (Figure 4.7 B, white arrows).

A sub-population of CSFcCs were also immunoreactive for NKA-α1 (not shown), however, this was not seen for all CSFcCs (Figure 4.8 C).

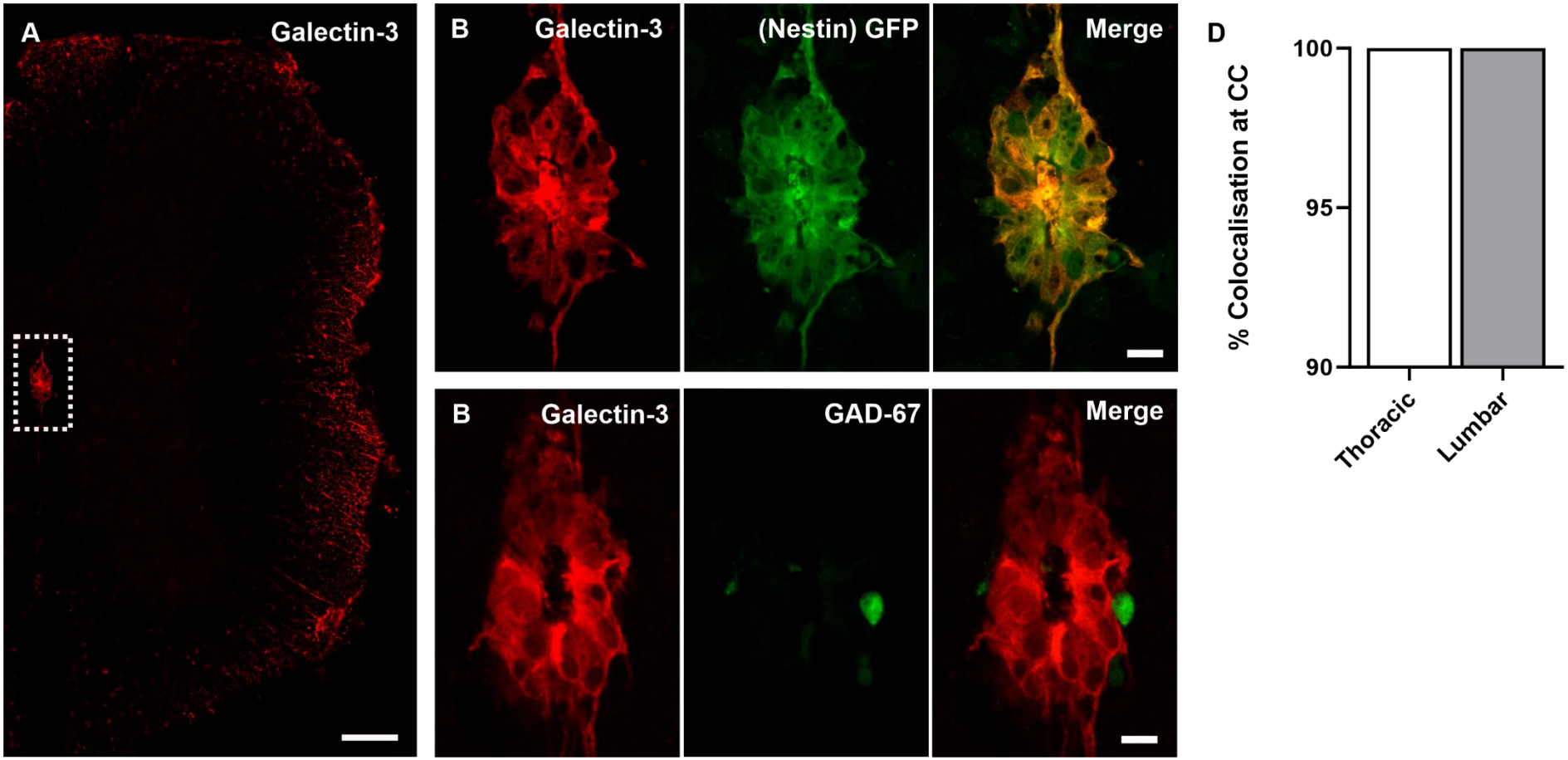

Figure 4.7 Galectin-3 colocalises with (nestin) GFP ECs and but not GAD67-GFP CSFcCs at the central canal.

Representative confocal images of Galectin-3 labelling (red) in (A) half a spinal cord slice (central canal in dashed box), central canal of (B) (nestin) GFP and (C) GAD67-GFP tissue (green). (D) Graph showing the percentage of Galectin-3+ve cells colocalised with (nestin) GFP (data presented as mean ±SEM). Scale bar A = 100 µm, B & C = 20 µm.

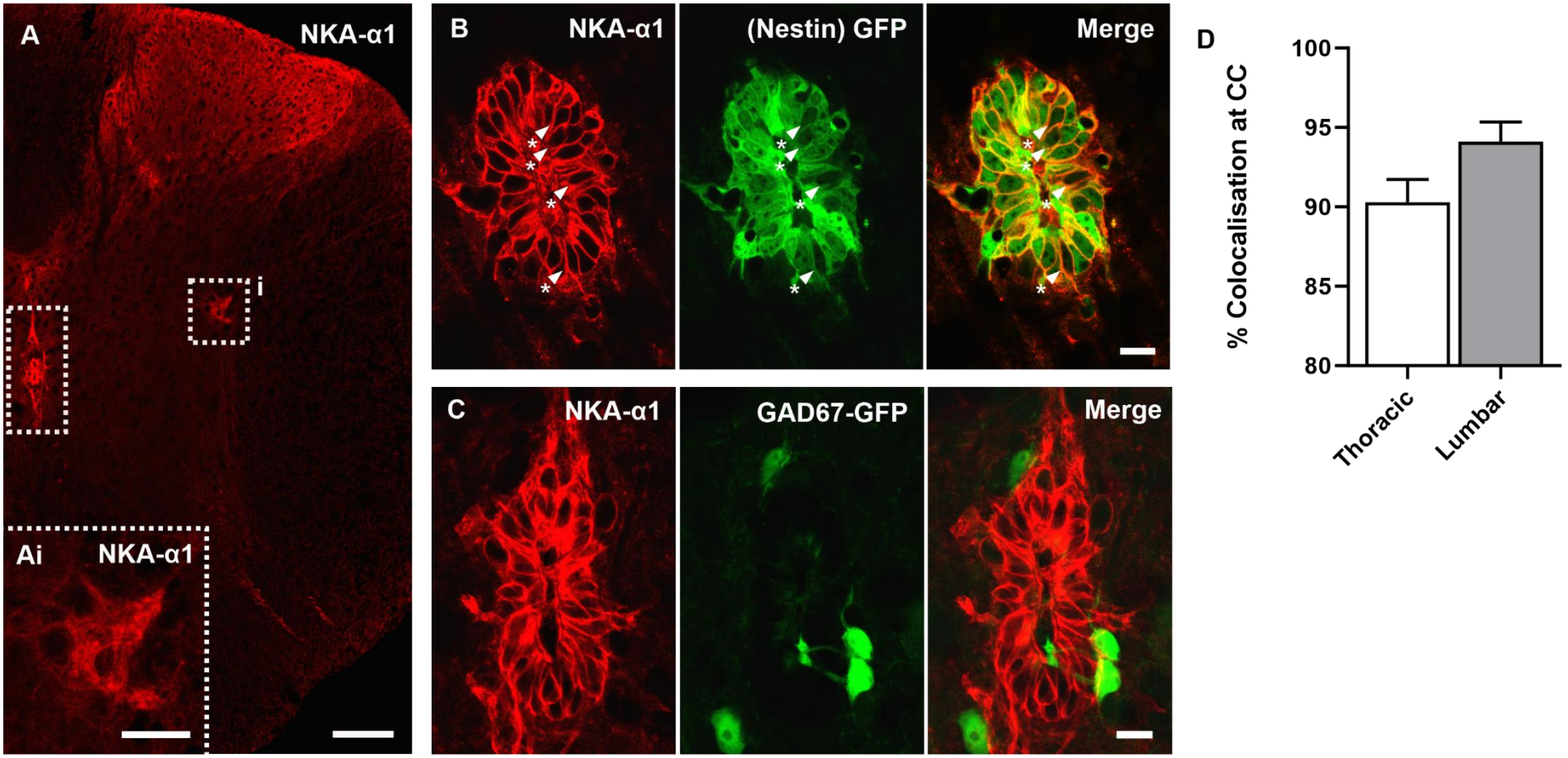

Figure 4.8 NKA-α1 colocalises with (nestin) GFP ECs and some GAD67-GFP CSFcCs at the central canal.

Representative confocal images of NKA-α1 labelling (red) in (A) half a spinal cord slice (central canal in dashed box), central canal of (B) (nestin) GFP and (C) GAD67-GFP tissue (green), (Ai) NKA-α1 labelling of terminal in the IML, (D) Graph showing the percentage of NKA-α1+ve cells colocalised with (nestin) GFP (data presented as mean ±SEM). Arrows with asterisk indicate non co-localised cells. Scale bar A = 100 µm, Ai & B = 20 µm.

4.4.2.4 Sox2

Sox2 (sex determining region Y-box2) is a transcriptional regulator present in pluripotent stem cells (Zhang, 2014; Ogai et al., 2014b).

Sox2 labelled cells at the central canal and throughout the white and grey matter in the spinal cord (Figure 4.9 A). (Nestin) GFP+ve cells at the central canal colocalised with over 90% of sox2+ve cells. In thoracic sections, colocalisation rose to 100% (thoracic= 100.0 ±0.00, lumbar= 91.60 ±1.514; N=3, n=29).

Additional sox2+ve cells that were GFP-negative were found close to the ependymal cell layer in lumbar sections (Figure 4.9 B & D, white arrows). These were identified as CSFcCs, with sox2+ve cells colocalising with GAD67-GFP+ve cells (Figure 4.9 C, white arrows).

4.4.2.5 Vimentin

Vimentin is a class III intermediate filament protein found in fibroblasts and blood vessel cells, as well as ependymal cells and astrocytes in the adult murine brain (Schnitzer et al., 1981).

Approximately 100% of vimentin labelling colocalised with (nestin) GFP+ve cells at the central canal of the spinal cord (thoracic= 99.80± 0.1984, lumbar= 100.3 ± 0.1987; N=3, n=32) (Figure 4.10 A, B & D). No colocalisation was found between vimentin and GAD67-GFP, indicating vimentin labelling is selective to ependymal cells at the central canal of the spinal cord (Figure 4.10 C).

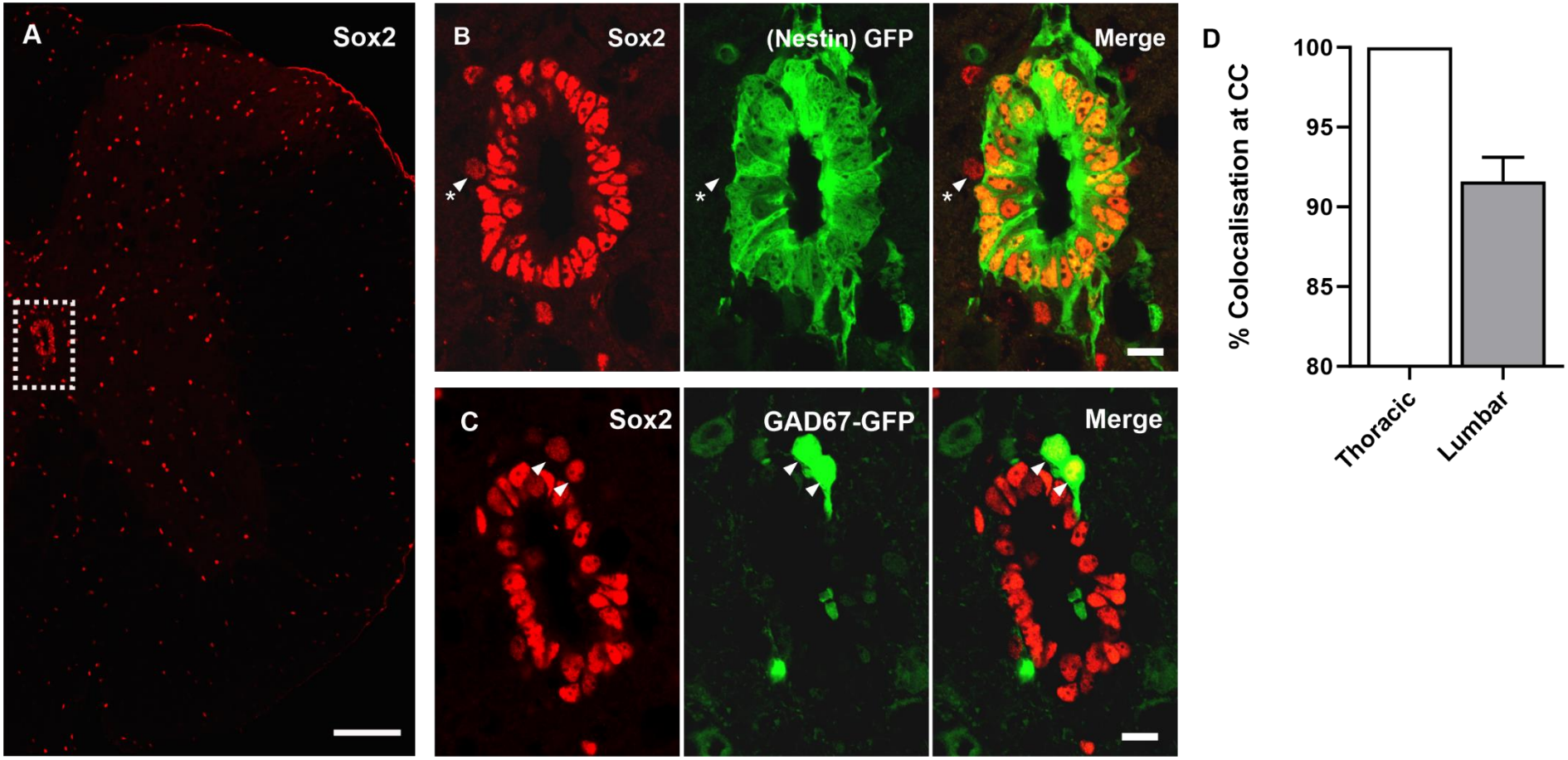

Figure 4.9 Sox2 colocalises with (nestin) GFP ECs and GAD67-GFP CSFcCs at the central canal.

Representative confocal images of Sox2 labelling (red) in (A) half a spinal cord slice (central canal in dashed box), central canal of (B) (nestin) GFP and (C) GAD67-GFP tissue (green). (D) Graph showing the percentage of Sox2+ve cells colocalised with (nestin) GFP (data presented as mean ±SEM). Arrows indicate co-labelled cells, arrows with asterisk indicate non co-localised cells. Scale bar A = 100 µm, B & C = 20 µm.

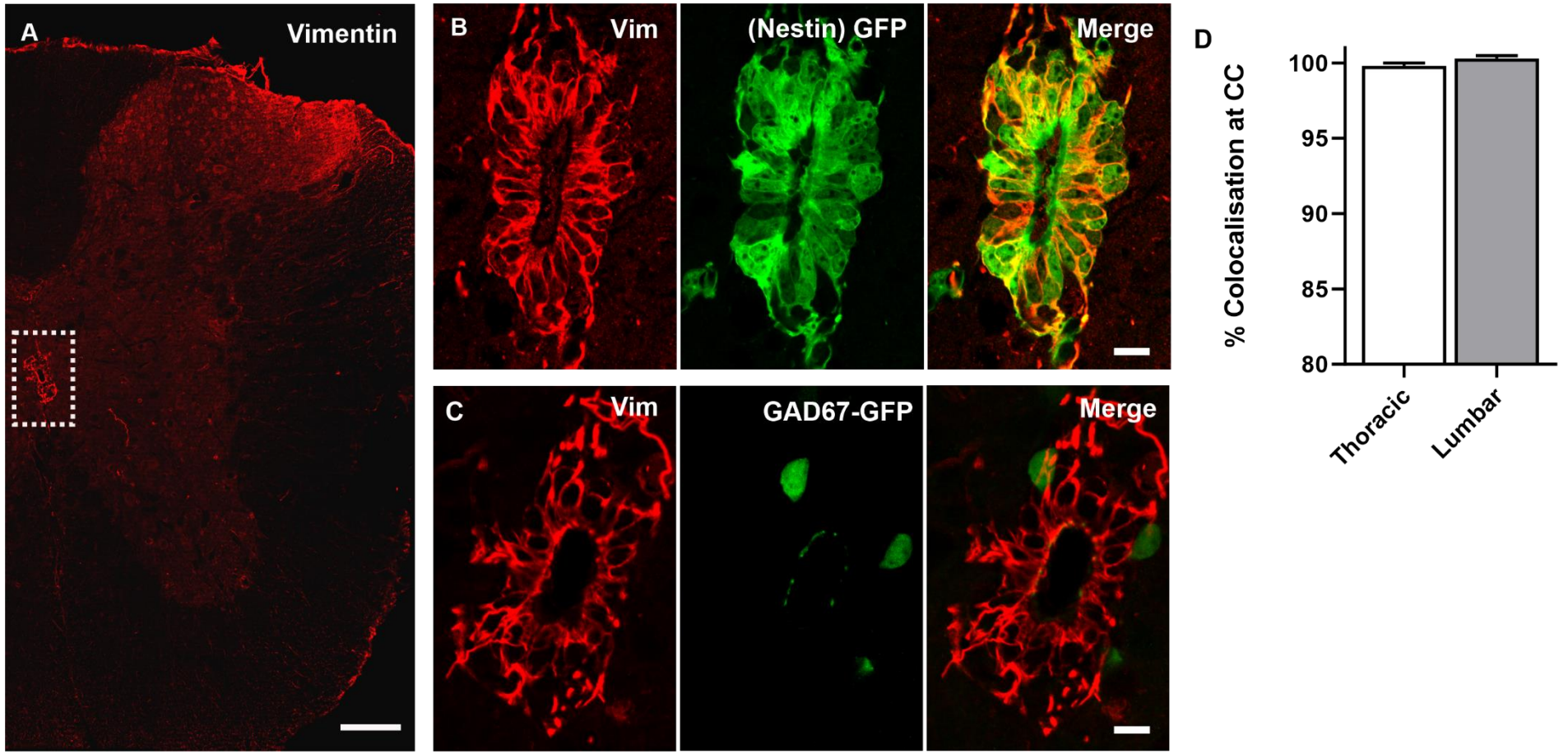

Figure 4.10 Vimentin colocalises with (nestin) GFP ECs but not GAD67-GFP CSFcCs at the central canal

Representative confocal images of vimentin labelling (red) in (A) half a spinal cord slice (central canal in dashed box), central canal of (B) (nestin) GFP and (C) GAD67-GFP tissue (green). (D) Graph showing the percentage of vimentin+ve cells colocalised with (nestin) GFP (data presented as mean ±SEM). Scale bar A = 100 µm, B & C = 20 µm.

4.4.3 Other markers of interest

Other cell markers investigated include: CD63, CXCR4, FoxJ1, Calbindin-D28k, and GFAP. CXC chemokine receptor type 4, also known as CXCR4, is expressed in ECs (Tysseling et al., 2011; Hugnot and Franzen, 2011) and is the main signalling receptor to the chemokine stromal cell-derived factor-1 (SDF-1). Additionally, forkhead box protein J1 (foxJ1) is a transcription factor transiently expressed in progenitor cells within the spinal cord, and is widely used to label ependymal cells in the spinal cord of mice (Jacquet et al., 2009; Li et al., 2016). (Nestin) GFP+ve cells colocalised with CXCR4 and foxJ1 labelling at the central canal (Figure 4.11 B and C).

Additionally, CD63, a marker of exosomes (Kong et al., 2017), appeared to label the cell membrane of (nestin) GFP+ve ECs in contact with CSF (Figure 4.11 A). CalbindinD-28k also appeared to label ependymal (nestin) GFP+ve cells (Figure 4.12 D) and fluorescence was most prominent in the cell membrane in dorsal ependymal cells. Calbindin-D28k is a calcium binding protein present in the ependymal cells of rodents and overexpression of this protein has been shown to promote neuronal differentiation and neurite outgrowth in embryonic and adult hippocampal progenitor cells *in vitro* (Kim et al., 2006).

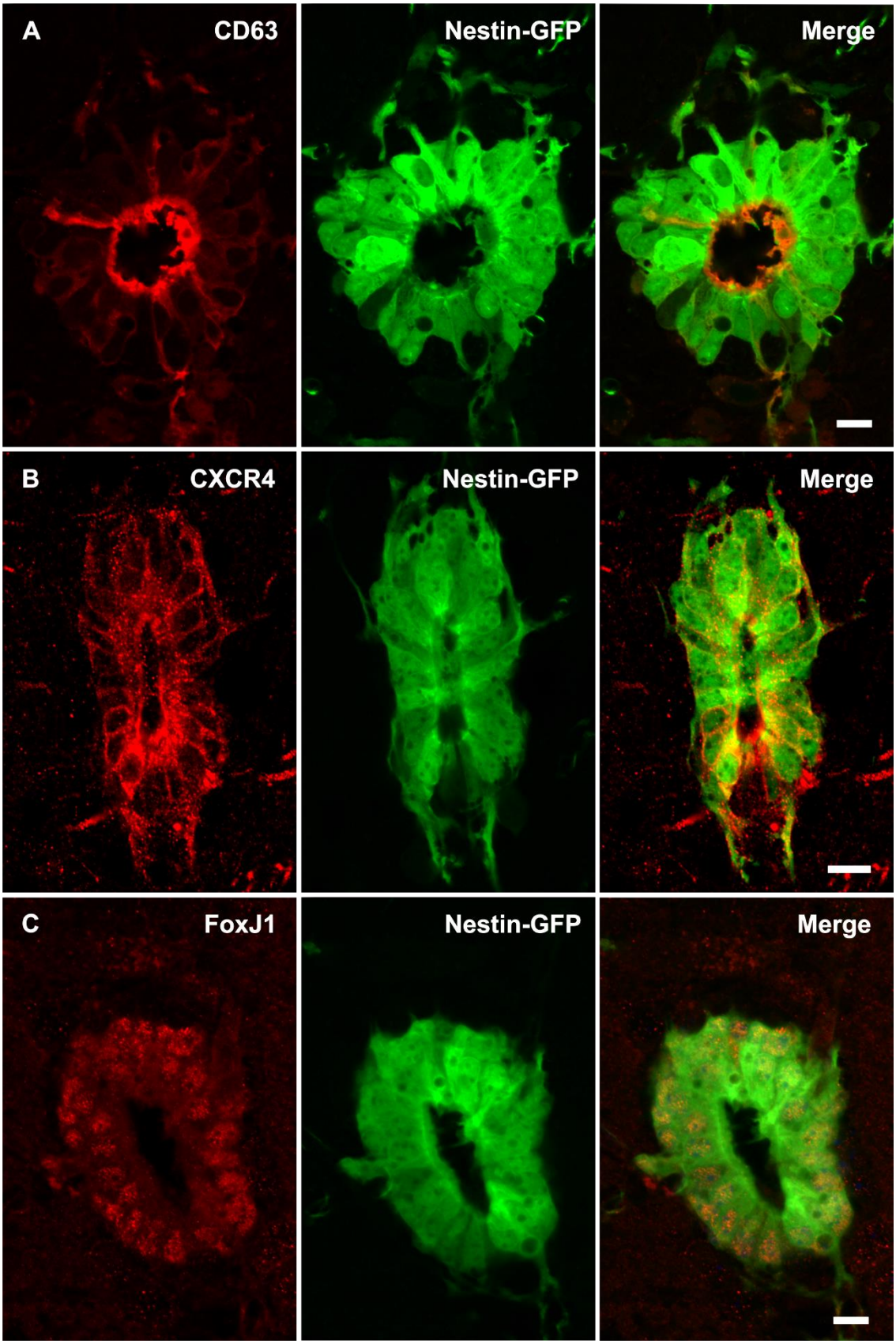

Figure 4.11 (Nestin) GFP colocalises with other antibodies at the central canal.

Representative confocal images of (A) CD63, (B) CXCR4, (C) and FoxJ1 staining (red) at the central canal of (nestin) GFP (green) spinal cord tissue. Scale bar = 20 µm.

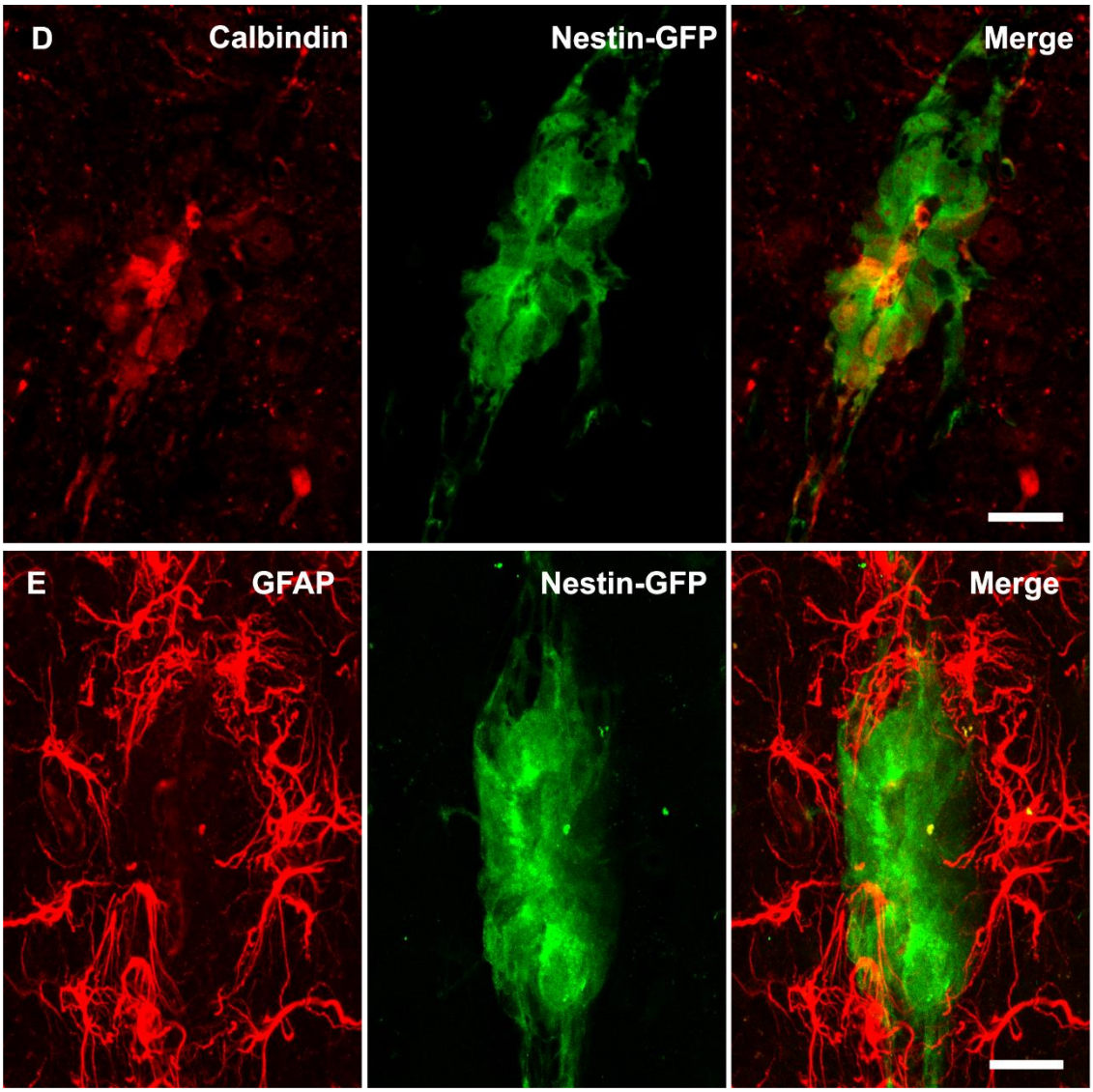

Figure 4.12 (Nestin) GFP colocalises with other antibodies at the central canal.

Representative confocal images of (D) calbindin-D28k and (E) GFAP staining at the central canal of (nestin) GFP (green) spinal cord tissue. Scale bar = 20 µm.

Anti-GFAP was used to identify reactive glial cells around the central canal. Glial fibrillary acidic protein (GFAP) is an intermediate filament found in astrocytes and other glial cells within the CNS (Hol and Pekny, 2015). GFAP labelled processes extended from/around the central canal, however, it wasn't clear whether this staining colocalised with (nestin) GFP+ve cells. (Figure 4.12 E). These results are similar to those seen elsewhere, whereby astrocytic processes are found within the lamina-X and make contact with the ependymal layer (Alfaro-Cervello et al., 2012b). However, as GFAP does not label the cell body, it was difficult to confidently identify which cells these GFAP+ve processes originated from. Ependymal cells are thought to derive from radial glia (Doetsch and Alvarez-Buylla, 1996; Filippov et al., 2003), and published RNA seq. data shows expression of GFAP in ependymal cells (see Table 4.6).

4.4.4 (Nestin) GFP does not label CSFcCs

Anti-PKD2L1 was used as a marker of cerebrospinal fluid contacting cells (CSFcCs) found in the sub-ependymal layer or in close apposition with ECs. No colocalisation of PKD2L1 with (nestin) GFP+ve cells was observed, confirming the identity of (nestin) GFP+ve cells as ECs at the central canal (Figure 4.13 A). As expected, there was colocalisation of PKD2L1+ve cells with GAD67-GFP+ve CSFcCs (Figure 4.13 B). Interestingly, published RNA seq. data unexpectedly shows GAD-67 is expressed in ECs as well as CSFcCs (Rosenberg et al., 2018) (EC: 29.8, CSFcC: 378.7 transcripts per million).

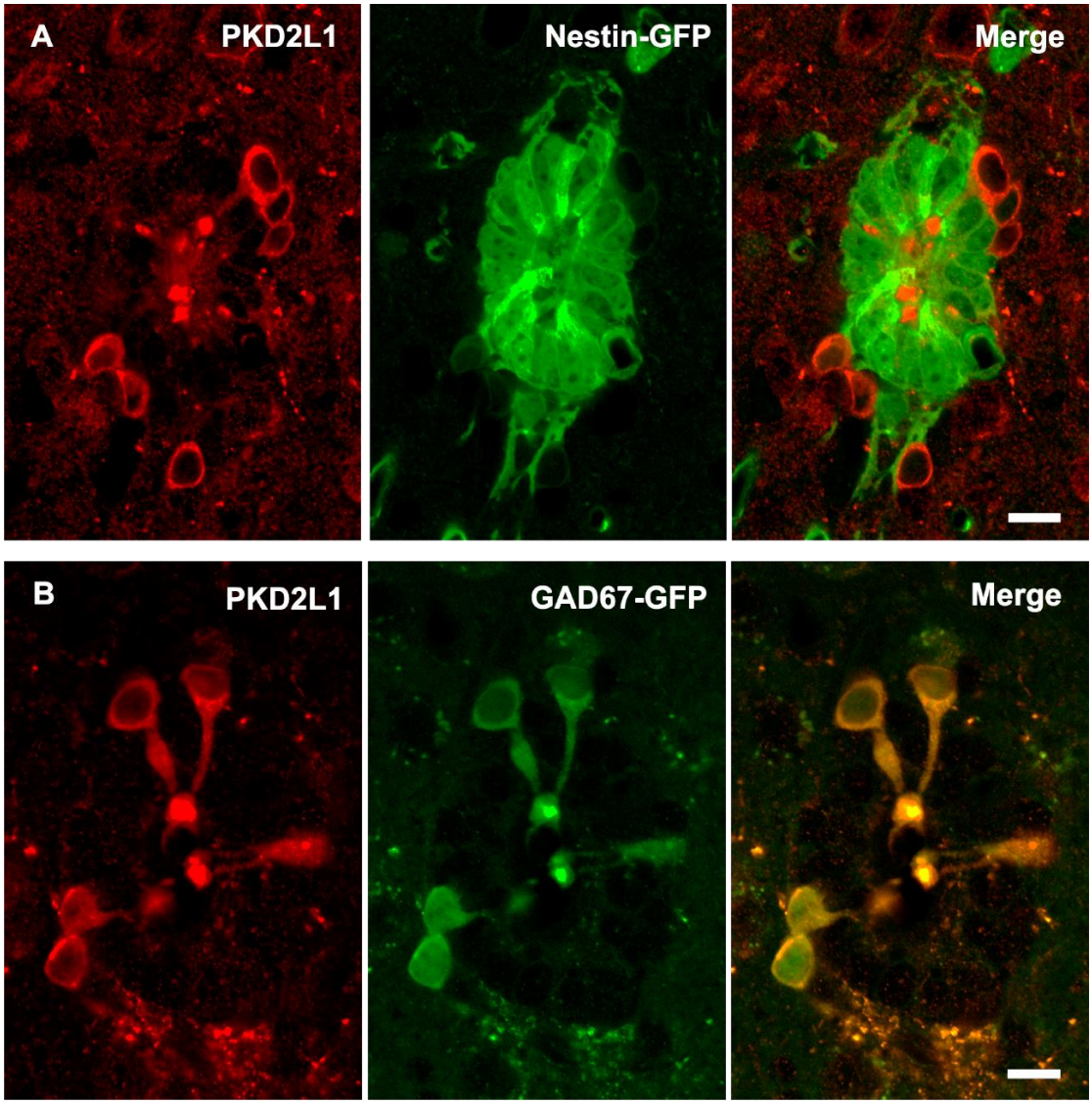

Figure 4.13 (Nestin) GFP does not label CSFcCs at the central canal

Representative confocal images of PKD2L1 staining (red) at the central canal of (A) (nestin) GFP and (B) GAD67-GFP spinal cord tissue. Scale bar = 20 µm.

4.4.5 Allen Brain Atlas and RNA sequencing data

The Allen Brain Atlas (ABA) is a database of gene expression (using RNA in situ hybridization localisation) in spinal cord and brain tissue of juvenile and adult mice (Allen Institute for Brain Science, n.d.). Table 4.6 presents data from the ABA for each gene investigated (where possible), RNA sequencing data from Rosenberg, 2018 (Rosenberg et al., 2018) (presented as transcripts per million), along with the IF presented in this chapter for comparison. It can be seen that ABA and RNA seq. data support our IF results in most cases. There are however, a number of contradicting results in the case of Calbindin-28 and CXCR4 expression in ECs, and CD24 expression in CSFcCs.

Table 4.6 Distinguishing between ECs and CSFcCs at the central canal

Antibody/gene	Ependymal cells			Cerebrospinal fluid contacting cells		
	Immuno.	Allen Brain Atlas	RNA seq.	Immuno.	Allen Brain Atlas	RNA seq.
Calbindin-28k/ CALB1	Yes	Some, adult	1	N.D	Unclear	36.3
CD24	Yes	Juvenile and adult	37.6	Yes	Unclear	1
CD63	Yes	Juvenile and adult	22.7	N.D	Unclear	1
CXCR4	Yes	N.D	1	No	N.D	1
FoxJ1	Yes	N.D	52.9	No	N.D	1
Galectin-3/ LGALS3	Yes	Faint	23.1	No	Unclear	1
GFAP	Unclear	Unclear	120.5	Unclear	Unclear	1
NKA-α1/Atp1a1	Yes	Adult	207.7	Some	Unclear	132.2
PKD2L1	No	No	1	Yes	Juvenile and adult	2424.2
Sox2	Yes	Juvenile and adult	202.1	Yes	Unclear	50.0
Vimentin	Yes	N.D	97.2	No	N.D	1

Immunofluorescence conclusions from this chapter: yes = antibody colocalisation with (nestin) GFP+ve ECs or GAD67-GFP+ve CSFcCs in transgenic tissue. No = no colocalisation. RNA seq data from Rosenberg, 2018 (Rosenberg et al., 2018) values presented as transcripts per million. Allen brain atlas data taken from mRNA localisation pseudo coloured to match expression intensity/in situ hybridization (Allen Institute for Brain Science, n.d.).

4.5 Discussion

The results presented in this chapter demonstrate that (nestin) GFP expression within the SC of these transgenic mice is limited to ECs and pericytes.

(Nestin) GFP expression in this transgenic line has been shown to be present from embryonic day 7, and persist in the progenitor cells of adult mice (Mignone et al., 2004). Nestin immunoreactivity is typically observed in the cytoplasm of a sub-population of ECs at the central canal, with nestin-labelled cellular processes extending dorsally (and in some cases ventrally) along the midline (Hamilton et al., 2009). In this transgenic mouse line, (nestin) GFP is expressed in the cell nucleus as well as the cytoplasm. Additionally, due to the half-life of GFP, fluorescence may be detected after nestin expression is terminated. This difference in nestin labelling could account for the variability in literature with regards to colocalisation of anti-nestin and other stem cell markers.

In this chapter we show labelling of (nestin) GFP+ve ECs with a number of stem cell markers. Sox2 labelling in particular indicates the stemness of ECs as this is a critical factor for directing neural differentiation and stem cell maintenance (Ogai et al., 2014c)(Zhang, 2014). FoxJ1 has been shown to be essential for EC development and transgenic mice under the regulation of the foxJ1 promoter are routinely used to label and track ECs (Jacquet et al., 2009; Li et al., 2016; Muthusamy et al., 2018). FoxJ1 has also been implicated in stem cell potential maintenance and cell fate determination (Li et al., 2018), further supporting the notion that ECs are stem cells.

Additionally, CD24 is a glycosylphosphatidylinositol-anchored membrane glycoprotein expressed in cells of the developing mouse brain as well as in zones of secondary neurogenesis in adult mice (Calaora et al., 1996). CD24 has also been shown to regulate cell proliferation and differentiation in regions of adult neurogenesis *in vitro* and *in vivo* (Nieoullon et al., 2005) and a percentage of CD24+ve ECs have been

shown to generate primary neurospheres, although these cells didn't yield secondary spheres (Coskun et al., 2008).

NKA-α1 aids in the maintenance of cell resting potential, and so could play a role in the hyperpolarisation of ECs associated with cell division (Corns et al., 2013). ECs are depolarised by GABA (Corns et al., 2013) and acetylcholine (Corns et al., 2015) and research has shown potentiation of EC proliferation by the α7 containing nicotinic acetylcholine receptor modulator PNU-120596 (Corns et al., 2015) indicating a potential route for manipulating EC behaviour.

In addition to these stem cell markers, we show that ECs possess proteins involved in the regulation of the neurogenic niche more broadly. CD24 is thought to be involved in cell-cell and cell-matrix interactions (via P-selectin (Aigner et al., 1997; Nieoullon et al., 2005) and L1CAM (Kleene et al., 2001) binding), and act as a neurite growth inhibitor (Shewan et al., 1996) and vimentin is also implicated in neurite formation and is expressed in neurons during axonal regeneration (Cochard and Paulin, 1984; Shea et al., 1993). Together, this indicates ECs may play a role in the regulation of neurite outgrowth, and the manipulation of ECs following injury could help regulate functional repair.

4.5.1 Do ECs sense their environment?

How ependymal cells exert their impact on the neurogenic niche is currently unknown. One potential avenue is via the release of molecules following an injury stimulus. For example, we have shown that ECs may release exosomes (due to the presence of the exosomal marker CD63) and exosomes from the CSF of rats following spinal cord injury have previously been linked to neuron proliferation (Kong et al., 2017). It is therefore possible that ECs "sense" changes in the spinal cord and CSF, and react by releasing cytokines or other molecules via exosomes to manipulate cell behaviour post injury. (Rosenberg et al., 2018) showed that ECs express the membrane protein

aquaporin-4, which is involved in trans-ependymal CSF flow and reabsorption, supporting this hypothesis (Halsey et al., 2018).

In addition to the role CD63 plays in membrane protein trafficking, it is also implicated in the regulation of leukocyte recruitment (Doyle et al., 2011), cell adhesion and migration (Koyama et al., 1998), and the activation of cellular signalling cascades (Tugues et al., 2013).

Additionally, foxJ1 has been shown to regulate ciliogenesis during development (Aamar and Dawid, 2008); these cilia are involved in sonic hedgehog (Shh) signalling and postnatal neurogenesis in the hippocampus (Breunig et al., 2008; Spassky et al., 2008; Han et al., 2008). Elsewhere in the body, cilia are thought to have a mechanosensory role (Nauli et al., 2013), however, it is unclear whether this is the case for neuronal and ependymal cilia within the CNS (Fuchs and Schwark, 2004).

4.5.2 Potential targets for the manipulation of ECs

CXCR4/SDF-1 is thought to direct the migration of ECs in the spinal cord and brain following injury (Itoh et al., 2009; Jaerve et al., 2011; Tysseling et al., 2011). Therefore, this regulatory mechanism could hold the key to successful EC manipulation following injury (discussed further in chapter 5).

Gal-3 is implicated in cell migration from the SVZ to the OB (Comte et al., 2011) and it is thought that Gal-3 regulates neuroblast migration via cell-ECM adhesion, the formation of astrocytic glial tubes, and CSF-flow (as a result of ependymal cell cilia beating) (Sawamoto et al., 2006). In gal-3-depleted mice, EC cilia and SVZ astrocytic glial tubes were disrupted, and as a result, fewer newly born neurons were detected migrating from the SVZ to the OB (Comte et al., 2011). Interestingly, following spinal cord injury, gal-3-depleted mice showed improved functional recovery, tissue preservation, and an increase in the number of neutrophils compared to control WT mice (Mostacada et al., 2015). The presence of gal-3 immunoreactivity suggests the

potential manipulation of ECs using laminin-functionalised tissue engineering strategies for injury repair.

4.5.3 Distinguishing between ECs, CSFcCs, and pericytes

This chapter has also shown that at the central canal, (nestin) GFP is specific to ECs and does not label CSFcCs. Some antibodies (CD24, NKA-α1, and sox2) labelled both ECs and CSFcCs at the central canal, whereas gal-3 and vimentin labelled only ECs.

Interestingly, some GAD67-GFP CSFcCs were immunoreactive against CD24. It is possible this change in staining is due to the use of T20 for cell permeabilisation as opposed to PBST and antigen retrieval used previously (Corns 2015); highlighting the need to consider fixation and permeabilisation protocols in IF for cell characterisation. RNA seq. data (Table 4.6) did not show CD24 expression in CSFcCs and so perhaps only a subset are CD24+ve, with further clarification required.

NKA-α1 also colocalised with a subpopulation of CSFcCs and this observation was supported by RNA seq. data (Table 4.6). Previously, CD24 and NKA-α1 have been used as EC markers, implying proliferation of ECs due to colocalisation with EdU (Corns et al., 2015). However, this may not be the case and these cells may actually have been CSFcCs, emphasising the importance of this transgenic line for the assessment of EC behaviour, as (nestin) GFP only labels ependymal cells at the central canal.

This chapter also demonstrated sox2 labelling of some CSFcCs. Typically sox2 is downregulated upon differentiation (Bylund et al., 2003), however colocalisation of sox2 and PKD2L1 has been seen previously (Petracca et al., 2016) and sox2 expression in CSFcCs was demonstrated by (Rosenberg et al., 2018). If CSFcCs retain plasticity as indicated by sox2 labelling, they too could be a potential target for manipulation.

Increasing evidence has shown that pericytes are also multipotent (Dore-Duffy et al., 2006). Following stroke, isolated pericytes have been shown to express nestin and sox2 (amongst other markers) and generate neural and vascular cells *in vitro* (Nakagomi et al., 2015). This chapter has demonstrated the potential of using this (nestin) GFP transgenic line in combination with FG for the identification of pericytes. Flow cytometry using (nestin) GFP with FG and/or a pericyte-specific antibody (e.g. PDGF-β) could be used for the isolation and exclusion of pericytes, thereby allowing EC isolation. This would be useful for EC implantation as it would remove the requirement of EC antibody labelling (and the blocking of critical cell proteins) prior to implantation or the assessment of EC behaviour.

4.6 Conclusions

The experiments carried out in this chapter show:

1. (Nestin) GFP labels ECs and pericytes throughout the spinal cord and brain.
   - At the central canal, (nestin) GFP is specific to ECs and does not label CSFcCs.
   - Some antibodies (CD24, NKA-α1, and sox2) label both ECs and CSFcCs at the central canal.
   - Galectin-3 and vimentin label only ependymal cells at the central canal.
2. ECs express CXCR4 and galectin-3 which could be used for the manipulation of endogenous cells.

Together, these data suggest that this transgenic line is suitable for studying the response of ECs to biomaterials. This transgenic line will therefore be used in chapter 5 for culture method optimisation and together with the hydrogels developed in chapter 3, will be used to assess the impact of hydrogels on ECs in chapter 6.

Chapter 5 - Optimising Organotypic Spinal Cord Slice Cultures

5.1 Introduction

Organotypic slice culture models provide the opportunity to study cellular behaviour in a context more representative of the *in vivo* environment compared to approaches such as dissociated cell culture. Stoppini *et al.*, 1991 first introduced the membrane-interface culture method whereby the tissue slices are maintained at the interface between culture medium and air. The retention of the native tissue cytoarchitecture *ex vivo* also enables cell-cell and cell-matrix interactions to be studied in response to experimental manipulation over several days or weeks.

A number of organotypic spinal cord slice culture (OSCSC) models have been developed to study cellular response to mechanical insult. Spinal cord contusion/compression has been recapitulated using a weight-drop injury model (Krassioukov et al., 2002; Pandamooz et al., 2019). Stab and transection injury models have also been utilised within OSCSCs (Patar et al., 2019).

OSCSCs enable multiple conditions to be tested from the same animal, therefore limiting the number of animals required for screening different hydrogels. Parameters investigated in response to hydrogels include: motorneuron survival, astrocyte morphology, microglial activation, and axonal growth (Bonnici and Kapfhammer, 2008; Schizas, Rojas, Kootala, Andersson, Pettersson, Hilborn and Nils P. Hailer, 2014). In particular, manipulation of OSCSC EC proliferation and migration using hydrogels and/or chemokines could provide insight into potential regeneration strategies, prior to carrying out *in vivo* experiments.

5.1.1 Identifying proliferating cells

A number of methods can be used to detect DNA synthesis and cell proliferation. Measuring the metabolic activity of cells using tetrazolium salts (e.g. 2-(4,5-Dimethyl-2-thiazolyl)-3,5-diphenyl-2H-tetrazolium bromide (MTT), 2,3-Bis-(2-Methoxy-4-Nitro-5-Sulfophenyl)-2H-Tetrazolium-5-Carboxanilide (XTT), and water-soluble tetrazolium salt-1 (WST-1)) can give an indication of the number of viable cells. Respiring cells convert these salts into dyes that can be quantified using a spectrophotometer, however, these metabolic assays may not accurately represent changes in cell proliferation. Immunohistochemical detection of antigens expressed in proliferating cells (e.g. proliferating cell nuclear antigen (PCNA), Ki67, and minichromosome maintenance (MCM) proteins) can also be used to study cell proliferation. Whilst these proliferation markers are commonly used as an indication of cell proliferation and therefore as diagnostic and prognostic factors for breast carcinoma, the scoring of the results is highly subjective and time consuming (Juríková et al., 2016).

DNA synthesis can be monitored by incorporation and subsequent detection of a thymidine analogue in dividing cells. Two synthetic analogues used for this purpose include: bromodeoxyuridine (BrdU) and 5-ethynyl-2'deoxyuridine (EdU). These are incorporated into dividing cells during G1, S, and G2/M-phases (Buck et al., 2008) (Figure 5.1 A). BrdU detection requires DNA denaturation via hydrolysis using hydrochloric acid or heating (which can destroy antigens, hindering co-staining) (Zeng et al., 2010), whereas EdU can be detected using a click reaction without the need for such harsh staining conditions. Therefore, EdU incorporation was chosen for the detection of proliferating cells in experiments throughout this thesis.

In the case of EdU detection, Cu(II) is first reduced to Cu(I) by ascorbic acid (Figure 5.1 C) and Cu(I) then catalyses the azide-alkyne cycloaddition (CuAAC) of the biotinylated azide and the alkyne present on the EdU moiety (Figure 5.1 B). A streptavidin-conjugated fluorophore (e.g. Alexa Fluor^{555} Streptavidin) can then bind to biotin and

render the cell nucleus fluorescent (Figure 5.1 D). Fluorophores can also be directly conjugated to the azide (not shown).

As Cu(II) is used for the catalysis of EdU detection, any fluorescence present in the tissue is quenched and requires detecting with antibodies against the fluorophore (Bálint et al., 2013). In the case of GFP-transgenic tissue, this quenching mechanism is thought to be a result of Förster resonance energy transfer (FRET) from GFP to Cu(II) (Hötzer et al., 2011). The fluorescence decay time (τ fl) of GFP is Cu(II)-concentration dependent, exhibiting “titration behaviour” and therefore by lowering the Cu(II) concentration, quenching should be reduced, enabling GFP fluorescence retention.

Although the fluorophore can be re-detected using an antibody following EdU detection, this requires additional incubation washes and therefore increases the background fluorescence and tissue fragility. Furthermore, this also limits other antibody labelling and the order of tissue staining. As GFP expressing animal and cell lines are such a critical tool in the study of stem cells within the spinal cord, the experiments presented in this chapter sought to overcome this challenge.

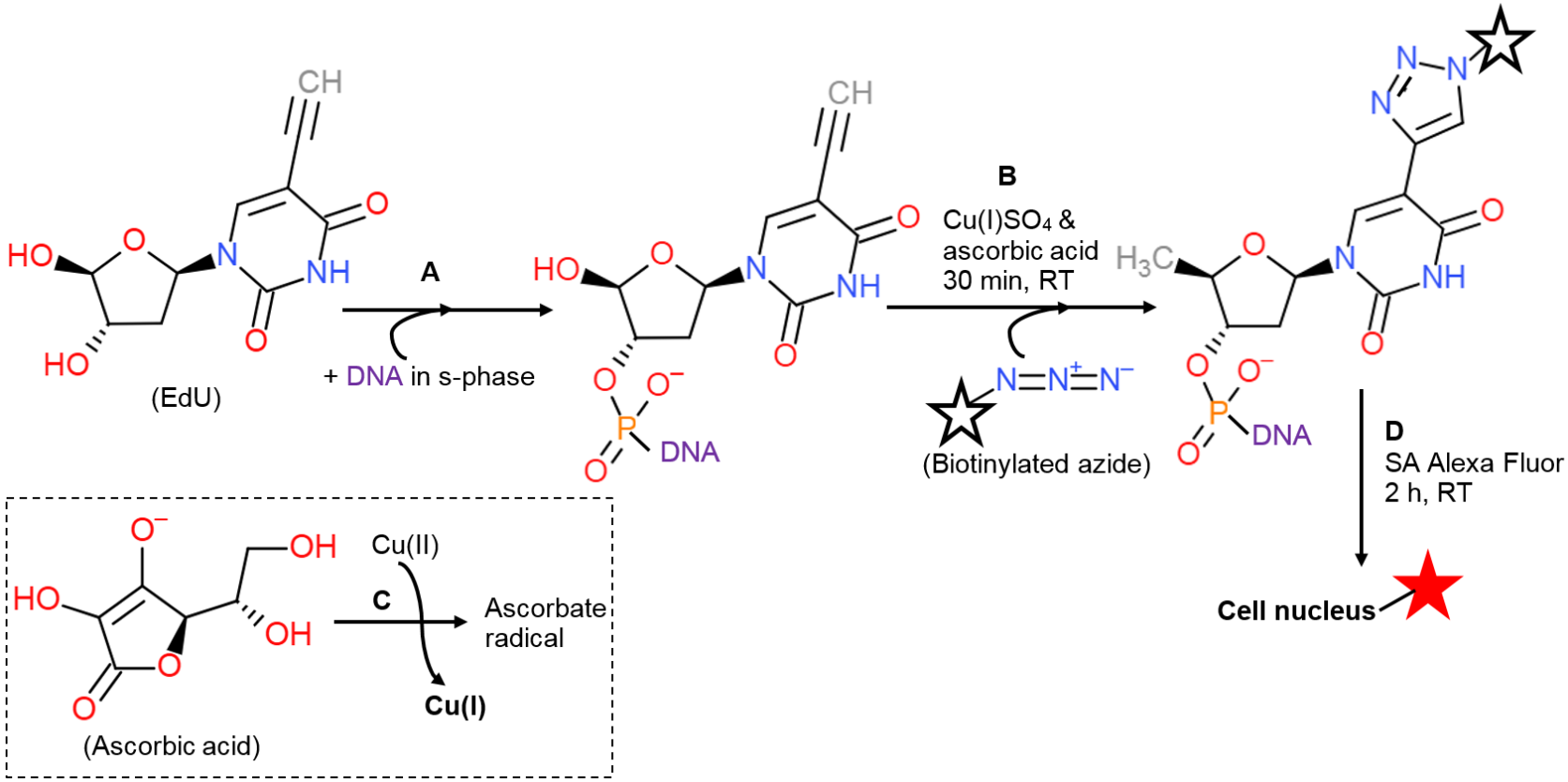

Figure 5.1 EdU detection method schematic.

The thymidine analogue, 5-Ethynyl-2´-deoxyuridine (EdU) is administered to animals via I.P. injection or into culture medium, and this is incorporated into the DNA of cells undergoing division (at the S-phase) (A). EdU is then detected using a copper catalysed azide-alkyne cycloaddition (CuAAC) (B). Cu(II) is reduced to Cu(I) by ascorbic acid (side reaction, C), and this is able to catalyse the cycloaddition of the biotinylated azide with the alkyne present on the EdU moiety. Streptavidin (SA)-conjugated Alexa Fluor is used to bind to biotin (black star) and render the cell nucleus fluorescent (red star) (D). This all occurs at room temperature, in the dark.

5.1.2 Aims

The experiments in this chapter build on the characterisation work carried out in chapter 4; using the nestin transgenic line to optimise and develop methods for use in chapter 6 (Figure 5.2).

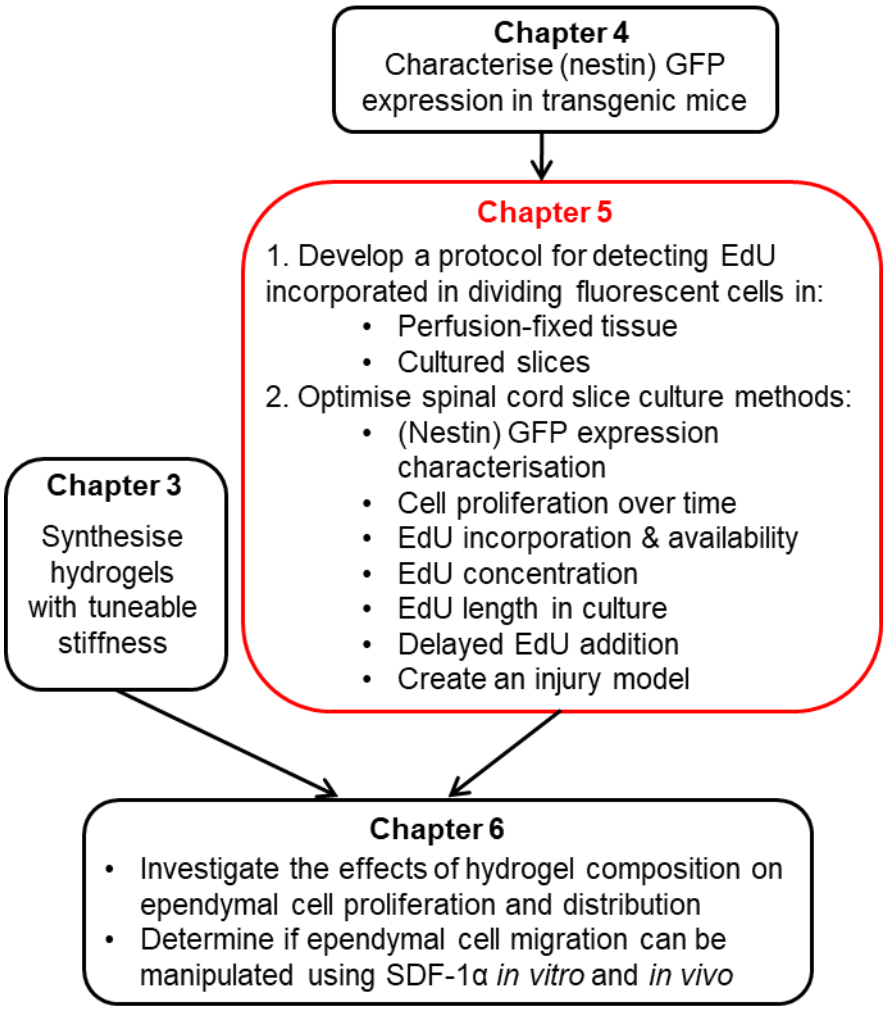

Figure 5.2 Schematic depicting the aims of chapter 5 in relation to the rest of this thesis.

In particular this chapter uses the transgenic line characterised in chapter 4 in order to optimise methods for use in chapter 6.

1. **To develop a method for detecting EdU-labelled cells in (nestin) GFP fluorescent tissue.**

Copper-chelating azides (e.g. picolyl azide) raise the effective concentration of Cu(I) by forming an active complex with/without a water-soluble ligand (THPTA) (Figure 5.3),

resulting in enhanced reaction kinetics of azide-alkyne cycloadditions (Uttamapinant et al., 2012). Therefore, this chapter aimed to use picolyl azide to develop an optimised method for the detection of EdU incorporated into cells, whilst maintaining GFP fluorescence in transgenic tissue.

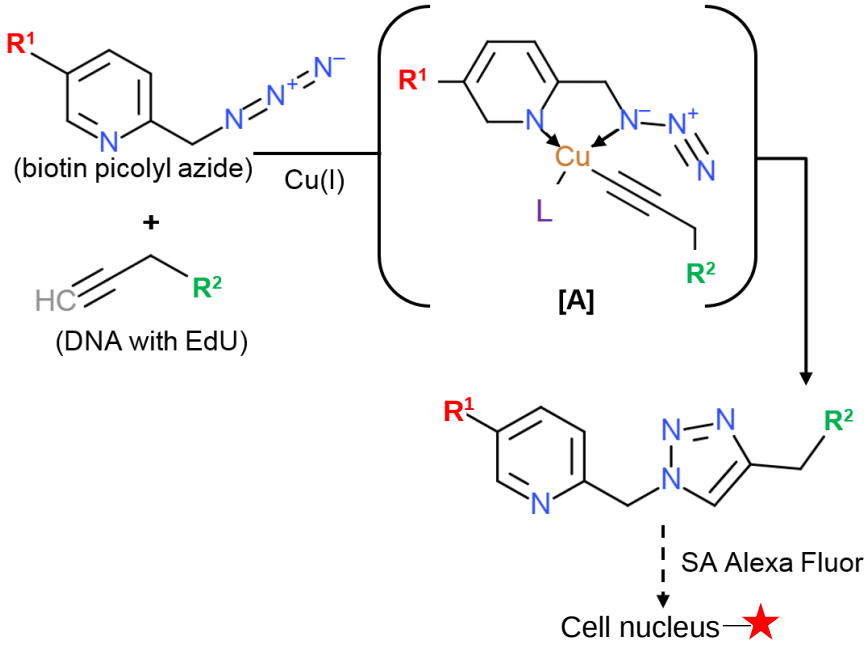

Figure 5.3 Chelation-assisted copper catalysed azide-alkyne cycloaddition for the improved detection of EdU.

The reaction of biotin picolyl azide and the alkyne presented on EdU proceeds via an active complex around Cu(I) [A]. The chelating picolyl azide raises the effective concentration of the Cu(I) catalyst at the reaction site. In turn this allows for a reduction in the Cu(I) concentration. R^1 = rest of the biotin picolyl azide structure. R^2 = rest of the EdU incorporated into the DNA of dividing cells. L = optional water-soluble ligand (THPTA).

2. To determine optimal culture conditions.

We plan to use the organotypic spinal cord slice culture model to assess the impact of hydrogels and SDF-1α delivery on EC behaviour. In order to do so, and to compare to a reliable control, the conditions for culture required optimising. This chapter aimed to determine the optimal EdU concentration and length of time in culture for monitoring the proliferation of ependymal cells.

5.2 Methods

5.2.1 Animals used

All experiments were carried out under a UK Home Office Licence (P1D7A177), in accordance with the UK Animals (Scientific Procedures) Act 1986 and the ethical standards set out by the University of Leeds Ethical Review Committee. Every effort was made to minimise the number of animals used and their suffering.

(Nestin) GFP transgenic mice were bred in-house as heterozygotes, housed in standard conditions with a 12 hour light-dark cycle, and given *ad libitum* access to food and water. Wild-type (WT) C56BL/6 animals were purchased from Central Biomedical Services (University of Leeds).

5.2.2 Organotypic spinal cord slice culture

The laminar flow hood, incubator, and surrounding surfaces were disinfected using 1% (w/v) Virkon followed by 70% (v/v) ethanol prior to use. All tools for *in vitro* and *in vivo* work were cleaned with boiling water, 70% (v/v) ethanol, then autoclaved at 121 °C for 20 minutes under 103 kPa for sterilisation. Where possible, sterile, single use consumables were used and disinfected with 1% Virkon following their use, prior to disposal.

5.2.2.1 Anaesthesia, perfusion, and dissection

Animals were anaesthetised by intraperitoneal (I.P.) injection of sodium pentobarbital (60 mg/kg, See general methods, Table 2.6). Sufficient anaesthesia was identified with the abolishment of pedal and corneal reflexes. A transverse laparotomy was created using spring scissors, the diaphragm was perforated, and the ventral ribcage was removed. The left atrium was cut and the animal was perfused transcardially through the left ventricle using 20 mL ice cold oxygenated (95% O_2, 5% CO_2) sucrose artificial cerebrospinal fluid (SaCSF, See general methods, Table 2.5). Death was confirmed via decapitation using scissors. Following dorsal skin and soft tissue removal to expose the

vertebrae, fine spring scissors were used to remove the dorsal lamina. The spinal cord was then carefully removed and placed in a petri dish containing oxygenated ice cold SaCSF. The meninges were then removed using fine forceps with the aid of a dissection microscope. Thoracic and lumbar spinal sections were used for sectioning.

5.2.2.2 Slice preparation

Tissue was embedded in 3% agar and glued to the chuck with an additional agar block behind for support. The chuck was secured in place in the water bath containing ice cold oxygenated SaCSF and tissue was sectioned at 300 µm in the transverse plane using a vibratome with a ceramic blade. A vibration frequency of 108 Hz was used with 0.8 mm amplitude and 0.5 mm/s speed. Slices were transferred into ice cold dissection medium, Dulbecco's modified eagles medium (DMEM, See general methods, Table 2.7), using a spatula and paint brush.

5.2.2.3 Maintenance of tissue slices

All further work was carried out aseptically in a laminar flow hood. Culture medium was equilibrated at 37°C prior to slice addition. 1 mL culture medium containing serum was added below the insert. Slices within the dissection medium were transferred carefully into a sterile petri dish and 3 to 6 slices were transferred onto each filter insert or gel (placed on top of filter insert) using a P1000 Gilson pipette with the tip cut off to minimise damage to the slice. Excess medium was removed around each slice using a sterile P100 pipette. Plates were cultured in an incubator at 37 °C in a 5% CO_2 enriched environment. Following 1 day *in vitro* (DIV), the medium was exchanged for serum free medium (See general methods, Table 2.7) (Figure 5.4). Medium was then refreshed every 48 h (0.5 mL removed and 0.5 mL fresh added per well).

5.2.2.4 EdU addition

Following 2 DIV (unless specified otherwise, Figure 5.4), EdU was added to the culture medium at a final concentration of 1 µM (unless specified otherwise) allowing for the visualisation of cells that have undergone proliferation with EdU present.

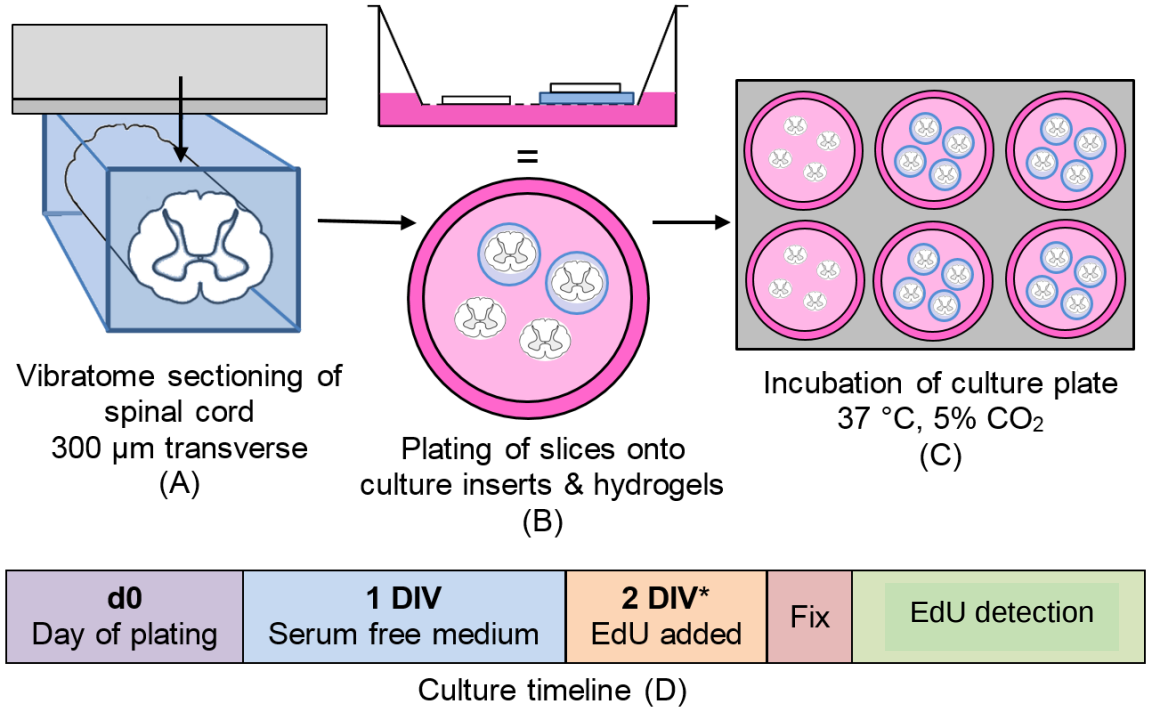

Figure 5.4 Organotypic spinal cord slice culture method.

(A) 300 µm transverse sections cut from agar-embedded spinal cord and (B) transferred onto hydrogels on porous culture inserts, or directly onto the inserts. (C) Culture medium with serum added below the insert and incubated at 37 °C for 24 h. (D) Schematic diagram depicting culture timeline: medium was changed to serum free following 1 day *in vitro* (DIV), and EdU was added to the medium after 2 DIV (*unless stated otherwise) prior to fixation and EdU detection.

5.2.2.5 Fixation

Spinal cord slices were fixed *in situ* on tissue culture inserts using 4% paraformaldehyde (PFA, See general methods, Table 2.7) for 1-2 hours at RT. Following fixation, slices were removed using a paint brush, and transferred into wells containing PBS.

5.2.3 EdU detection

EdU detection reactions and incubation steps (control method detailed in Figure 5.5) were carried out at RT in the dark (See general methods, Table 2.4 for buffer solution compositions). Permeabilisation was carried out with either PBST or T20 depending on the requirements of any antibodies to be used (see antibody table).

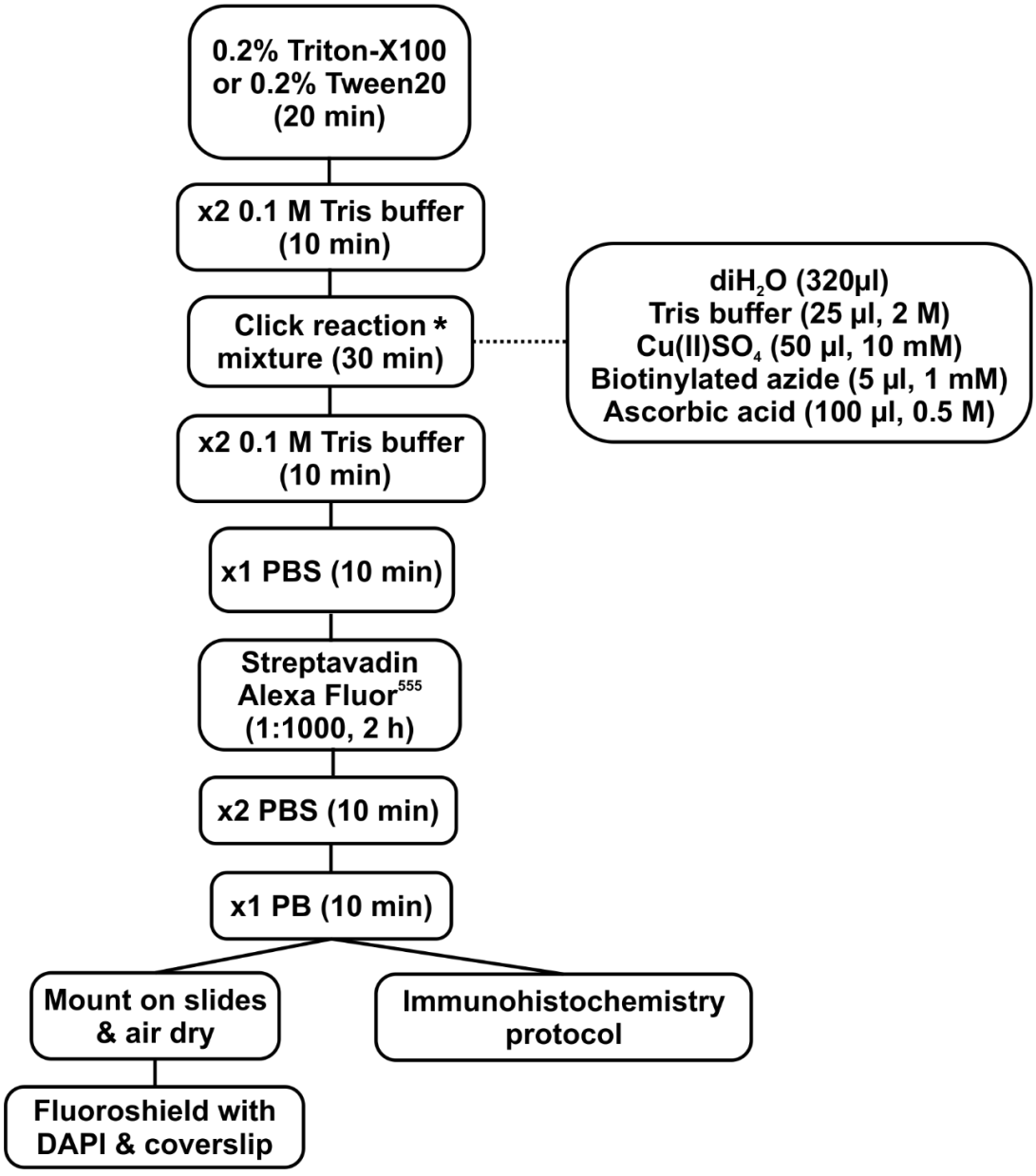

Figure 5.5 EdU detection protocol for fixed tissue slices & cultured slices

*Slices were incubated in the click reaction mixture for 30 minutes unless stated otherwise.

5.2.3.1 Perfusion-fixed tissue

In order to optimise the EdU detection method in perfusion-fixed tissue, firstly, three (nestin) GFP transgenic animals were given EdU in their drinking water at a final concentration of 0.793 mM (0.2 mg/mL), and their water bottle was protected from light using black tape. EdU was administered via the drinking water in order to minimise the distress caused to the animals by repeated injections. Drinking water (with EdU) was refreshed daily for three days prior to perfusion-fixation of the animal. As we couldn't control or guarantee equal water consumption between each animal, slices from each animal were used for all reaction conditions detailed below.

5.2.3.2 Fixation and tissue processing

Mice were terminally anaesthetised with sodium pentobarbital (60 mg/kg) I.P. and perfused transcardially with 0.1 M PB to remove blood, then 4% PFA for fixation. The spinal cord and brain were removed and post fixed overnight at 4 °C in 4% PFA, before being stored in 0.1 M PB at 4 °C. The pia mater was removed using fine forceps and a dissection microscope. Sections of spinal cord were glued to the chuck and this was then screwed into place in the water bath containing 0.1 M PB and the blade was attached to the vibratome arm. The tissue was then sectioned serially at 40 µm in the transverse plane at an amplitude of 0.4 mm/s and vibrating frequency of 80 Hz. Sections were placed into wells containing PBS for EdU labelling.

5.2.4 Optimising EdU detection reaction conditions

5.2.4.1 Perfusion-fixed tissue

A number of reaction conditions (Table 5.1) were trialled using picolyl azide in order to determine the optimal conditions for detecting EdU in tissue with fluorescence. The $Cu(II)SO_4$ concentration was reduced from 1 to 0.01 mM (final concentration) and different reaction lengths were investigated. The original method using a non-conjugating azide was used as a control.

Table 5.1 Conditions used to optimise EdU detection method in fixed tissue

		Time /minutes					
	[Cu(II)SO_4] /mM	**5**	**10**	**30**	**60**	**90**	**120**
Biotin azide	**1**	x	x	x	x	x	x
Biotin picolyl azide	**1**	x	x	x			
	0.5		x	x	x		x
	0.25		x	x	x		x
	0.1			x	x	x	x
	0.01			x	x	x	x

x denotes conditions trialled. n=18 slices per condition, N=3.

5.2.4.2 Cultured tissue

Spinal cord slices were cultured for 2 DIV with EdU added for the final 24 h prior to fixation. Sections were then randomised, and EdU detection performed (Table 5.2).

Table 5.2 Conditions used to optimise EdU detection method in fixed, cultured slices

		Time /minutes				
	[Cu(II)SO_4] /mM	**5**	**10**	**20**	**30**	**45**
Biotin azide	**1**				x	
Biotin picolyl azide	**1**	x			x	
	0.5	x	x	x	x	
	0.1				x	x

x denotes conditions trialled. n=6 slices per condition, N=3.

5.2.5 Immunofluorescence

Immunofluorescence was carried out on fixed cultured slices using the method previously described (Chapter 4.3.4). Antibodies used to characterise (nestin) GFP cellular processes include: CD24, Gal-3, and neural/glial antigen2 (NG2 –also called chondroitin sulphate proteoglycan 4). CD24 and Gal-3 were used to confirm these

processes included ependymal cells originating from the central canal and NG2 was used to identify pericytes (Table 5.3).

Table 5.3 Antibodies used for the labelling of cultured spinal cord slices

Target	Raised in	Dilution	Labels	Source & Cat. No
CD24*	Mouse	1:100	ECs (Pruszak et al., 2009; Pfenninger et al., 2011)	Miltenyi Biotec 130-110-686
Gal-3*	Goat	1:1000	ECs (Comte et al., 2011; Yoo et al., 2017)	R&D systems AF1197
NG2	Rabbit	1:500	Pericytes (Ozerdem et al., 2001)	Millipore AB5320

*detected using biotinylated secondary antibody and Streptavidin AlexaFluor^{555}.

5.2.6 Image capture and analysis

Manual cell counts of EdU-labelled (EdU+ve) cells at the central canal were performed using a Nikon E600 microscope. Images of whole slices were taken using an EVOS fluorescent microscope at x4, x10, and x20 magnification for further quantification.

5.2.6.1 EdU labelled cell quantification

Using ImageJ, images were converted to binary 16 bit and cropped to remove scale bars where applicable. Background fluorescence was removed using the “remove background” tool, and a threshold was applied. The “watershed” tool was applied in order to split any overlapping cells that had been incorrectly identified as a single particle. The “analyse particles” tool was then used to create a total count of all EdU+ve cells (Figure 5.6).

For analysis using quadrants, a line was drawn through the thresholded image along the mid-line, centring the line at the central canal. Five concentric circles were then drawn (centred at the central canal) and each was split into four quadrants using a macro written by Olivier Burri (Burri, 2016). The percentage area (% area of pixels highlighted using threshold limits) for each region of interest (ROI) was then calculated. An average % area was then calculated using the four quadrants, to give a mean %

area as a function of radial distance from the central canal (1= central canal region, 5 = periphery of slice, Figure 5.6).

5.2.7 Data analysis

Data were collated in Microsoft Excel and analysed using IBM SPSS statistics 21. Average EdU+ve cell counts were calculated and presented as mean ±SE unless stated otherwise. Shapiro-Wilk and Levine's tests were applied for distribution and equality of variance analysis respectively. A decision tree was used to determine the appropriate statistical test (See general methods, Figure 2.6).

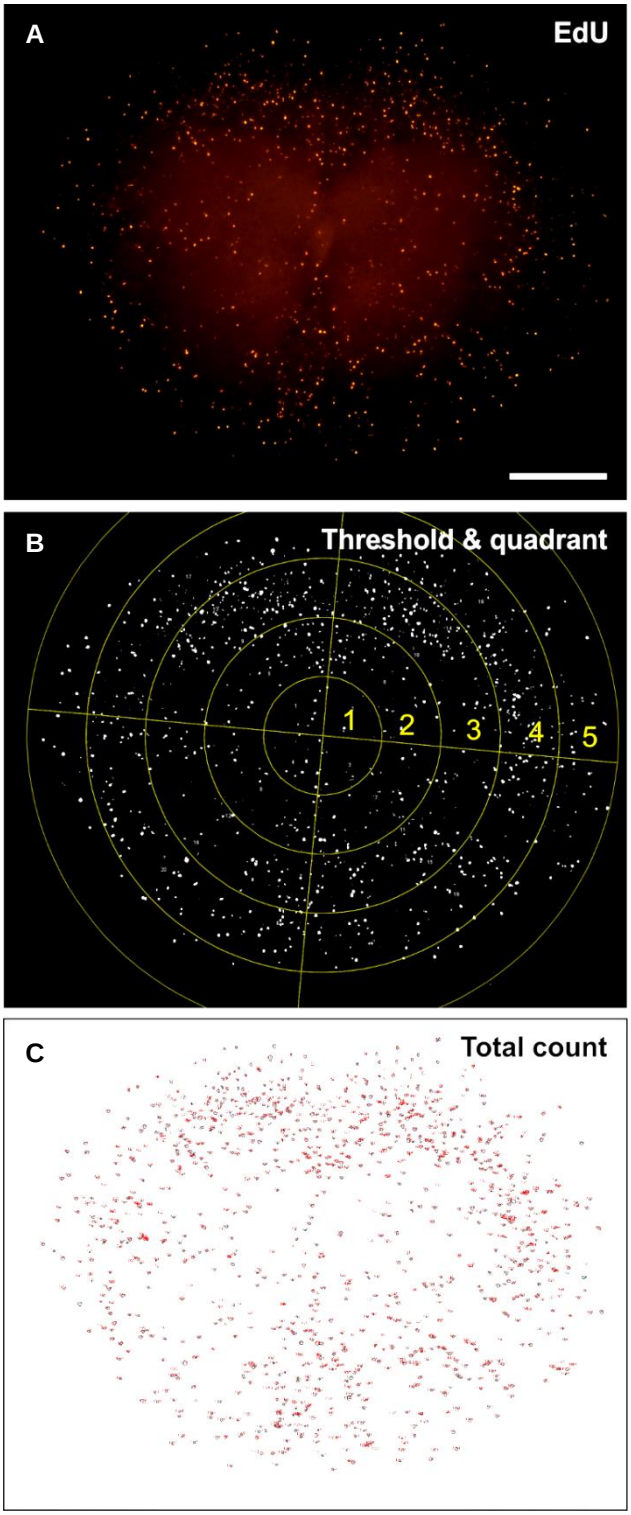

Figure 5.6 Image analysis using ImageJ.

(A) Representative EVOS image of whole cultured spinal cord slice with EdU labelling. (B) Fluorescent images were converted to 16-bit binary, the background was subtracted, the fluorescence was thresholded, and a macro was run to create quadrants and concentric circles, centred at the central canal. % area was calculated for each quadrant and averaged for regions 1 to 5. (C) EdU+ve cells were then counted using the “analyse particles” function on the thresholded images. Scale bar = 500 µm

Table 5.4 Animals used in this chapter for method optimisation

Chapter	Experiment	Strain	Number of animals (N)	Sections per condition (n)	Age
5.3.1	EdU detection optimisation	(Nestin) GFP**	3	18	6-8 weeks
5.3.2	EdU detection optimisation	(Nestin) GFP	3	6	14 ±2 days
5.3.3	Nestin-GFP expression	(Nestin) GFP	9	>3	14 ±4 days
5.3.4	Proliferation over time	(Nestin) GFP	2	>3	12 days
5.5.5	EdU availability - length of time in culture - uptake	(Nestin) GFP	1	>3	18 days
5.5.6	EdU concentration and length of time	(Nestin) GFP	3	>3	15 days
5.5.7	Delayed EdU addition	(Nestin) GFP	1	>2	14 days
5.5.8	Injury model - following 2 DIV, EdU 6 hours	(Nestin) GFP	2	>3	14 days
5.5.8	Injury model - 5 DIV, EdU 18 hours	(Nestin) GFP	2	>3	14 days
5.5.8	Injury model - 3 DIV, EdU 48 hours	(Nestin) GFP	1	>2	13 days

** EdU given in drinking water

5.3 Results

5.3.1 EdU can be detected in perfusion-fixed spinal cord tissue whilst maintaining GFP fluorescence

Out of the 25 combinations of conditions trialled, an optimal reaction length and Cu(II) concentration was found when using biotin picolyl azide. Using 1 mM $CuSO_4$ and reducing the reaction time to 5 minutes resulted in GFP retention and EdU detection comparable with control staining (1 mM, 30 mins) (Table 5.5, Figure 5.7). This protocol was therefore used for EdU detection in perfusion-fixed tissue.

Table 5.5 Optimised EdU detection in fixed tissue

		Time /mins											
	[Cu(II)SO_4] /mM	**5**		**10**		**30**		**60**		**90**		**120**	
Biotin azide	**1**	1	1	1	1	0	3	0	3	0	3	0	0
Biotin picolyl azide	**1**	2	3	1	3	0	3						
	0.5			0	2	0	3	0	3			0	3
	0.25			2	0	1	1	0	3			0	
	0.1					1	0	1	1	0	0	0	1
	0.01					3	1	3	1	2	0	2	0

Staining code: 0 = none, 1 = faint, 2 = good, 3 = best (comparable to control). Green = GFP, EdU = red. Blank cells = not tested.

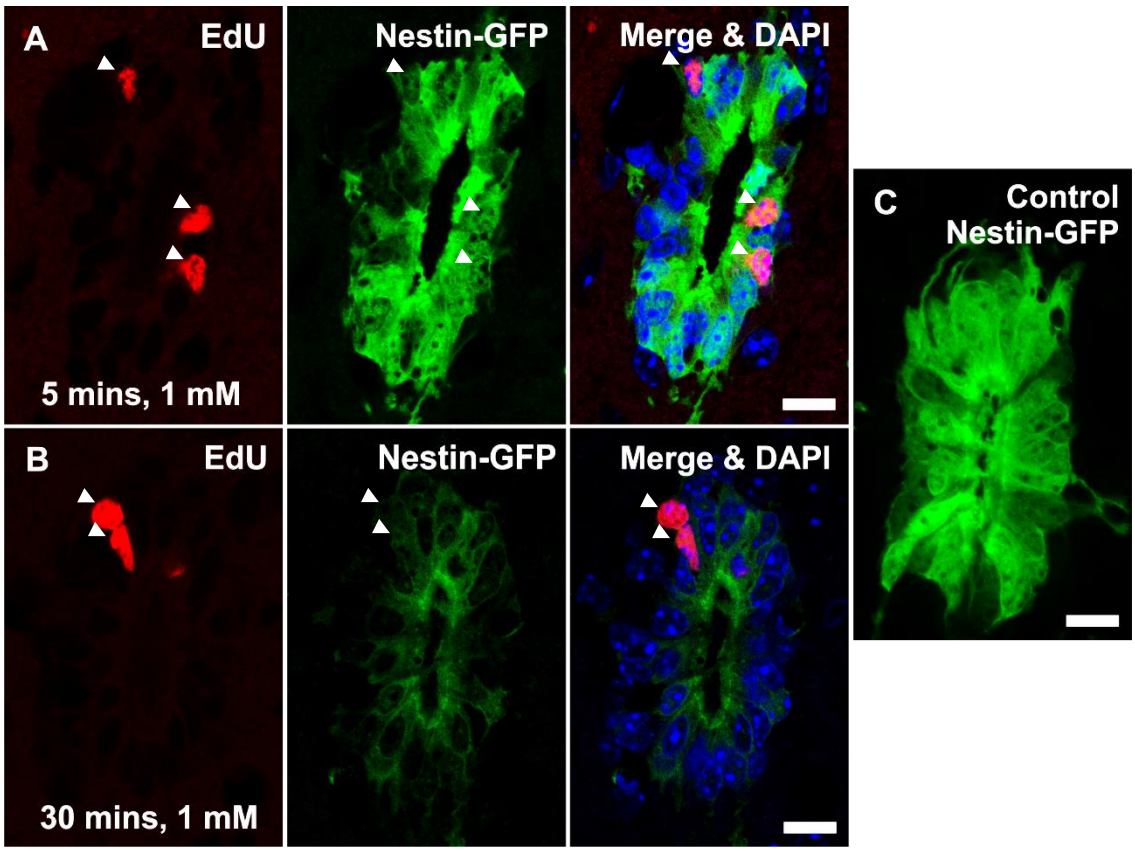

Figure 5.7 EdU detection in nestin-GFP perfusion-fixed tissue using picolyl azide.

Representative confocal images showing EdU detected cells (red), nestin-GFP+ve cells (green), and a merged image with DAPI as a cell nuclei counter stain (blue). (A) 5 minutes click reaction with 1 mM Cu(II) results in good EdU staining and GFP retention allowing for colocalisation counts to be made (white arrows). (B) 30 minutes reaction with 1 mM Cu(II) gives good EdU staining, however GFP fluorescence is quenched and appears faint (white arrows). (C) Control nestin-GFP (no EdU detection) for reference. Scale bars = 20 µm.

5.3.2 EdU can be detected in cultured spinal cord slices whilst maintaining (nestin) GFP fluorescence

Out of the 9 combinations of conditions trialled in cultured tissue, an optimal reaction length and Cu(II) concentration was found. Using a reduced copper concentration (0.5 mM), and reducing the reaction time to 20 minutes resulted in (nestin) GFP retention, and EdU detection comparable with control staining (Table 5.6, image not shown). This protocol was used for subsequent EdU detection in cultured tissue slices.

Table 5.6 Results of optimised EdU detection in fixed, cultured slices

		Time /mins									
	[Cu(II)SO_4] /mM	**5**		**10**		**20**		**30**		**45**	
Biotin azide	**1**							0	3		
Biotin picolyl azide	**1**	2	3*					1	3*		
	0.5	2	3	2	2	3	3	2	3		
	0.1							2	2	1	2

Staining code: 0 = none, 1 = faint, 2 = good, 3 = best (comparable to control). Green = GFP, EdU = red. Blank cells = not tested. *very varied between sections.

5.3.3 (Nestin) GFP fluorescence expression and distribution *ex-vivo*

(Nestin) GFP expression in the white and grey matter of cultured spinal cord slices reduced over 3 days in culture (Figure 5.8, radial segments 2 to 4). Whereas, central canal (nestin) GFP fluorescence remained clearly visible over this time-period, indicating viability of ependymal cells *ex vivo* (Figure 5.8 B).

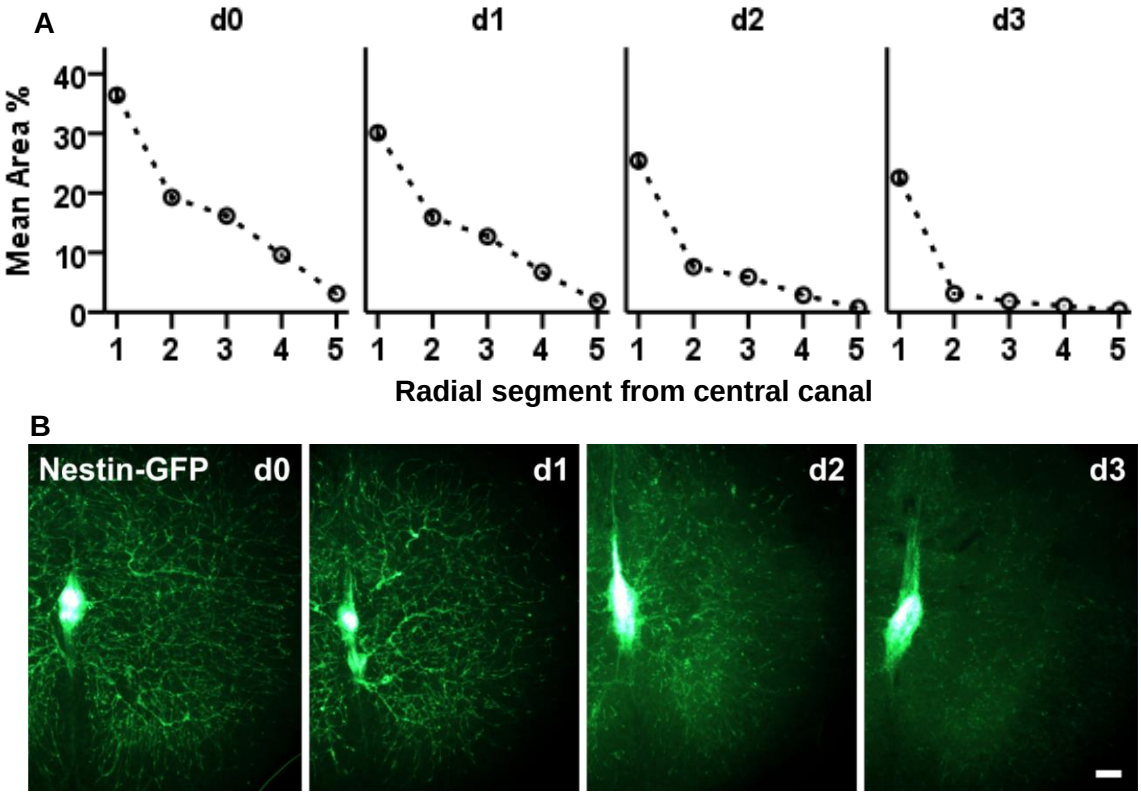

Figure 5.8 (Nestin) GFP expression in cultured spinal cord slices from 0 to 3 days *in vitro*.

(A) (Nestin) GFP mean area % coverage as a function of radial distance from the central canal. Data presented as mean ±SE. N=9, n>3. (B) Representative EVOS images of half a cultured spinal cord slice at day 0 to day 3. Scale bar = 100 µm.

5.3.4 Cell proliferation over time in OSCSCs

1 µM EdU was added to the culture medium on either the day of plating (day 0) or day 1 to day 4 and slices were left for 24 h (from EdU addition) prior to fixation and EdU detection (see Figure 5.9 A).

A peak in the number of EdU+ve cells was observed at d4 for the central canal (11.12 ±1.197) and d3 for the total slice (2360 ±292.0), followed by a decline on day 5 (CC= 3.333 ±1.856, total= 1625 ±289.3; Figure 5.9 B & C). No significant differences were found between EdU+ve cell counts at the central canal, however, there were significantly fewer *total* EdU+ve cells in slices in which EdU had been added on day 0 and fixed on day 1, compared to all other time points (d1= 318.3 ±41.53; P = 0.003 to 0.047). The distribution of EdU+ve cells across the spinal cord slice remained similar for slices fixed on days 2 to 5, with the majority of EdU+ve cells in the white matter (WM) (Figure 5.9 D radial segment 4). Additionally, there were a number of slices with no EdU+ve cells at the CC when fixed on days 1-3 (Figure 5.9 B).

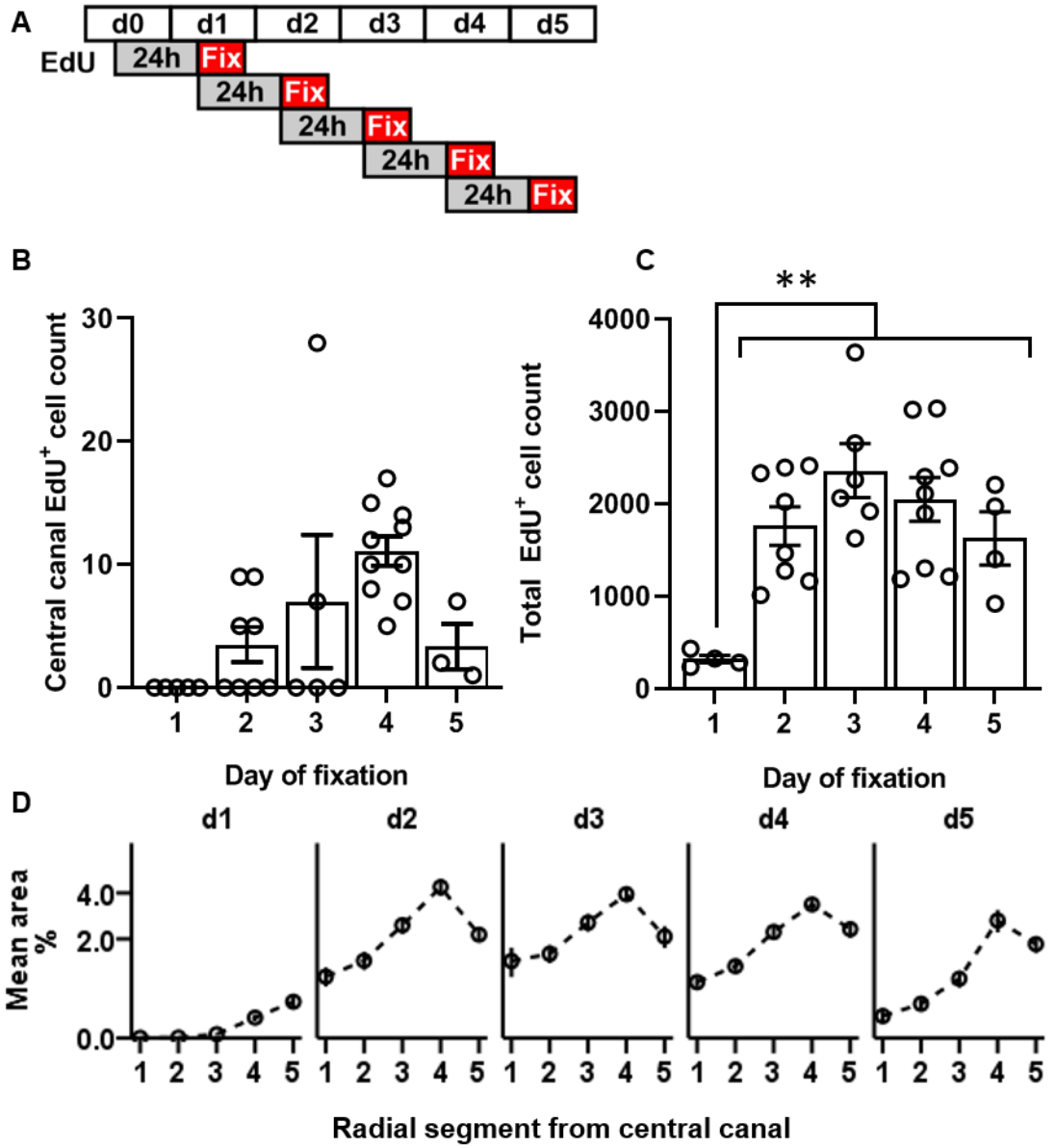

Figure 5.9 EdU+ve cell counts over time and EdU+ve cell distribution throughout the slice.

(A) Schematic diagram depicting EdU addition. (B) Central canal and (C) total EdU+ve cell count per 300 µm slice. (D) EdU mean area % coverage as a function of radial distance from the central canal. Data presented as mean ±SE. N=2, n>3. ** P ≤ 0.01.

5.3.5 EdU incorporation and availability in OSCSCs

To further investigate EdU uptake by dividing cells, and to assess the availability (and remaining concentration) of EdU in the culture medium over time, EdU (1 µM) was added following 2 DIV (on day 2) and slices were fixed on days 3, 4, and 5 (Figure 5.10 A). From the previous trend in EdU cell counts, we should expect a doubling of the number of EdU+ve cells for every 24 h in culture until day 5. No significant difference was found between the mean number of EdU+ve cells in slices cultured for 24 h (1053 ±155.0), 48 h (1166 ±98.51), or 72 h (1445 ±226.3) in the presence of EdU (Figure 5.10 B), however there was a trend towards an increased number of EdU+ve cells over time.

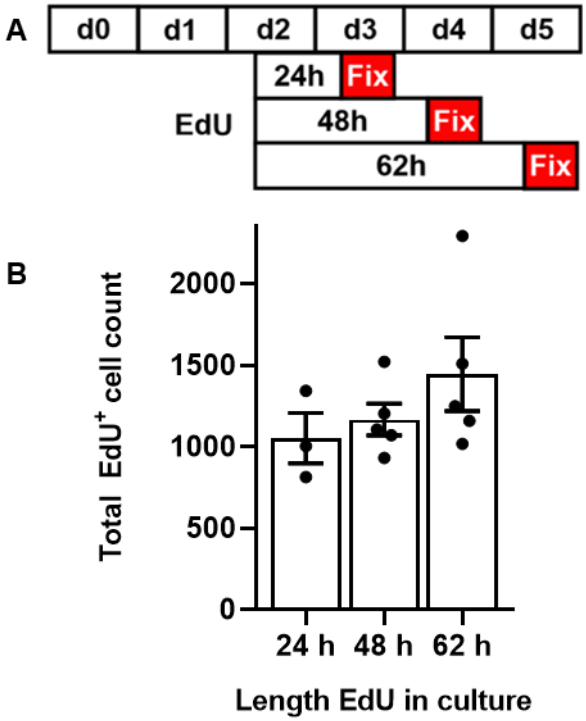

Figure 5.10 Effect of length of time EdU is in culture on EdU+ve cell count

(A) Schematic diagram depicting EdU addition. (B) Total EdU+ve cell count after 24, 48, and 72 hours *in vivo* in the presence of EdU. Data presented as mean total EdU+ve cell count ±SE, N=1, n>3.

Subsequent experiments sought to determine if EdU remained intact in culture medium after 24 and 48 h. Culture medium (and any remaining EdU in solution) from the 24 and 48 h conditions was then transferred to wells containing slices from the same animal (that had not yet had any EdU added), and cultured for a further 24 hours ("1 μM transferred"). This was to see if any EdU was present in the medium after these time points, and if so, how many cells incorporated this EdU compared to slices that had fresh 1 μM EdU added at the same time point ("1 μM control") (Figure 5.10 C).

The mean total number of EdU+ve cells in the 1 μM control and 1 μM transferred conditions were not significantly different when EdU was transferred/added on day 3 (following 24 h in donor well) (Figure 5.11 A, control= 1656 ±219.3, transferred= 1469 ±190.3) indicating the concentration of EdU in culture medium was in excess (more EdU in culture medium than the number of dividing cells) and that EdU remained intact in culture conditions.

As EdU was found to be in excess, the number of EdU+ve cells detected after 48 hours *in vitro* should equal the sum of the number of EdU+ve cells detected after the first 24 hours in the donor condition, plus the number of EdU+ve cells in the transferred condition (when transferred on day 3) or the number of EdU+ve cells in the control 24 h condition. However, we found that the sum of these cell counts (1053 EdU+ve cells + 1469 EdU+ve cells) was more than double the value found after 48 h (1166 EdU+ve cells). These data suggest that some of the cells that incorporated EdU in the first 24 hours of incubation with EdU died or stopped proliferating further in the following 24 hours before detection at 48 h.

Following 48 h in a donor well, the mean total number of EdU+ve cells in the 1 μM transferred condition was significantly lower than in the control condition (Figure 5.11 B, 1 μM control = 1805 ±217.7, 1 μM transferred= 599.4 ±122.5, P = 0.007). An additional control well of slices was cultured in the presence of 0.5 μM EdU ("0.5 μM control") in order to roughly assess how much EdU was available (and incorporated

into cells) in the transferred medium. The number of EdU+ve cells in the transferred condition was not significantly different to the 0.5 µM control, suggesting that the available concentration of EdU had indeed decreased after 48 h in culture (0.5 µM control= 1385 ±316.8, P = 0.06).

These data indicate there is a significant reduction in the availability (concentration) of EdU following 48 hours *in vitro,* and suggests that death of proliferating cells or cessation of proliferation in cells that have incorporated EdU occurs.

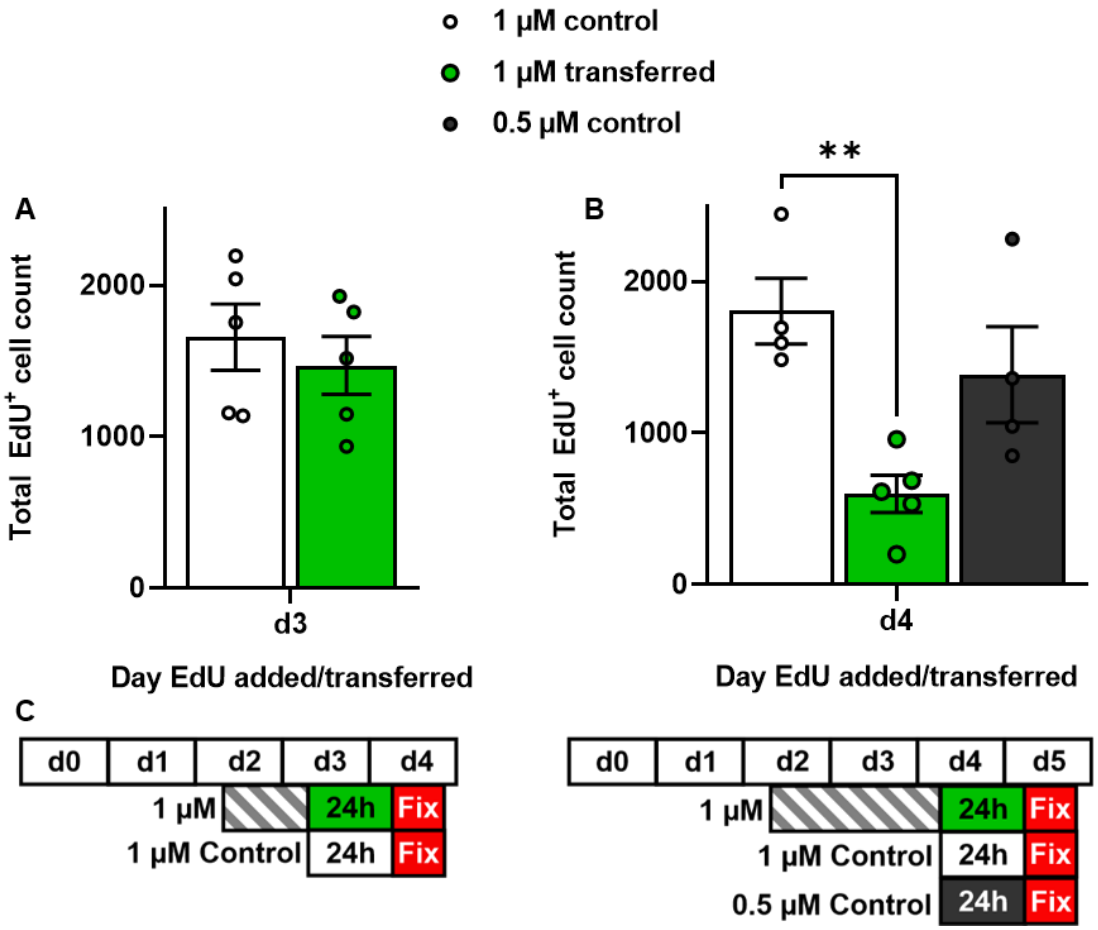

Figure 5.11 Uptake of EdU in cultured spinal cord slices.

Amount of EdU in culture medium, as measured by total EdU+ve cell count following transferral into new well on (A) d3 – 24 h in donor well or (B) d4 – 48 h in donor well. Data presented as mean total EdU+ve cell count ±SE (N=1, n>4). ** P ≤ 0.01. (C) Schematic diagrams depicting EdU addition. Dashed bar corresponds to EdU being in the "donor" well. Solid bar corresponds to EdU being in the experimental well.

5.3.6 Effect of EdU concentration and length in culture

Spinal cord slices were cultured in the presence of 0.1, 0.5, or 1 µM EdU for 24 or 48 hours in order to determine optimal culture conditions and investigate the behaviour of proliferating cells further (Figure 5.12 A). Reduced EdU concentrations were used to determine if the potential toxicity of EdU was causing cell death over this time period.

No significant differences were found between the mean EdU+ve cell counts at the two time points when counted at the central canal or total slice, for any of the EdU concentrations investigated (Figure 5.12 B). However, the average number of EdU+ve cells detected in slices cultured in the presence of 1 µM EdU for 24 or 48 hours was significantly greater than in the 0.1 µM condition (24 h: 0.1 µM= 179 ±38.41, 1 µM= 407.1 ±48.09, P = 0.0140; 48 h: 0.1 µM= 181.7 ±31.04, 1 µM= 412.1 ±55.34, P = 0.0261), indicating EdU concentration is an important and limiting factor.

This finding supports the previous data, indicating death of proliferating cells over this time period as the number of detected proliferating cells remained constant over 24 and 48 hours as previously seen. Additionally, there was no change in the number of EdU+ve cells detected when using 0.5 µM compared to 1 µM control, and so the concentration of EdU over this time period isn't thought to be toxic. Therefore, 1 µM EdU was chosen for experiments assessing the impact of hydrogels on proliferation.

The distribution of proliferating cells also appeared similar over these time points (Figure 5.12 D). In all conditions, proliferating cells were detected at the central canal and within the white matter, whereas the grey matter was seen to be largely devoid of EdU+ve cells. This distribution pattern was more pronounced at greater EdU concentrations. EdU+ve cell chains were also found to extend radially into the grey matter at 24 h (not shown) and 48 h post EdU addition in slices with 0.5 and 1 µM EdU added (Figure 5.12 Ei).

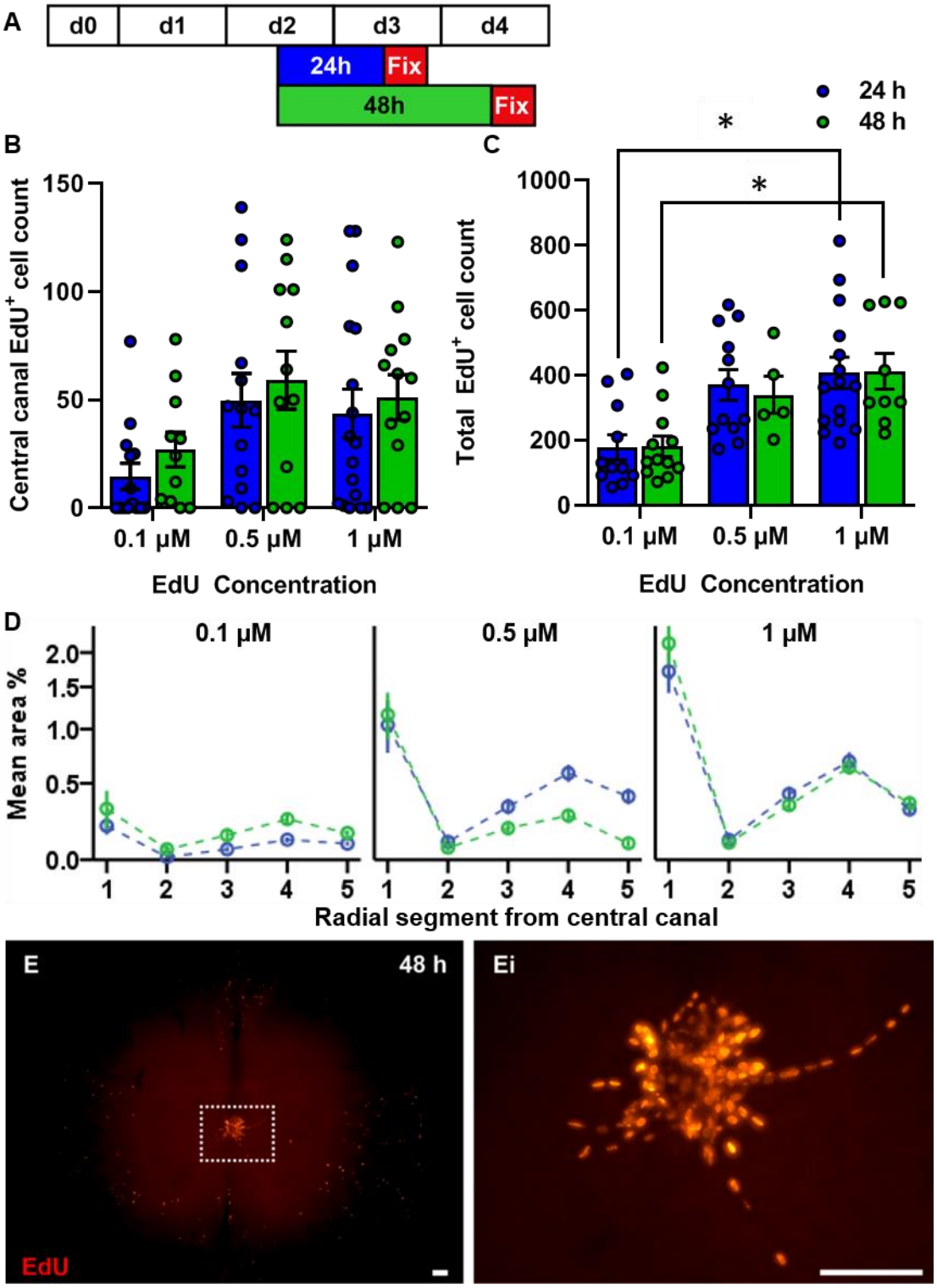

Figure 5.12 Effect of EdU concentration and length in culture on total and central canal EdU+ cell count and EdU distribution.

(A) Schematic diagram depicting EdU addition. (B) Central canal and (C) total EdU+ cell count per 300 µm slice. (D) EdU mean area % coverage as a function of radial distance from the central canal. Data presented as mean ±SE. N=3 n>3, * P ≤ 0.05. (E) Representative EVOS image of spinal cord slice with EdU-labelled cells following 48 h incubation with 1 µM EdU and (Ei) enlarged image of central canal EdU+ve cell chains. Scale bar = 100 µm.

5.3.7 Effect of delaying EdU addition

To investigate the potential benefits of delaying EdU addition until after the initial peak in proliferation (injury response, day 3 to 4), slices were cultured in the presence of EdU over a number of time periods following addition on day 2 (control) or day 4 (delayed) (Figure 5.13 A).

No statistically significant differences were found between any of the conditions investigated, however a trend towards reduced EdU+ve cell counts for increased lengths of time in culture was observed for both control and delayed conditions. There was also a trend towards reduced central canal EdU+ve cell counts in slices where EdU addition was delayed, compared to control (Figure 5.13 B).

The distribution of EdU+ve cells appeared similar in delayed conditions over the three time points investigated (Figure 5.13, blue), whereas the distribution of EdU+ve cells for the control condition appeared to alter over time (Figure 5.13, green). 24 h post-EdU addition, a greater mean area percent of EdU+ve cells was detected in the white and grey matter of the control slices (radial segments 3 and 4). At 120 h post-EdU addition, the central canal region (radial segment 1) exhibited an increased mean area percentage of fluorescence.

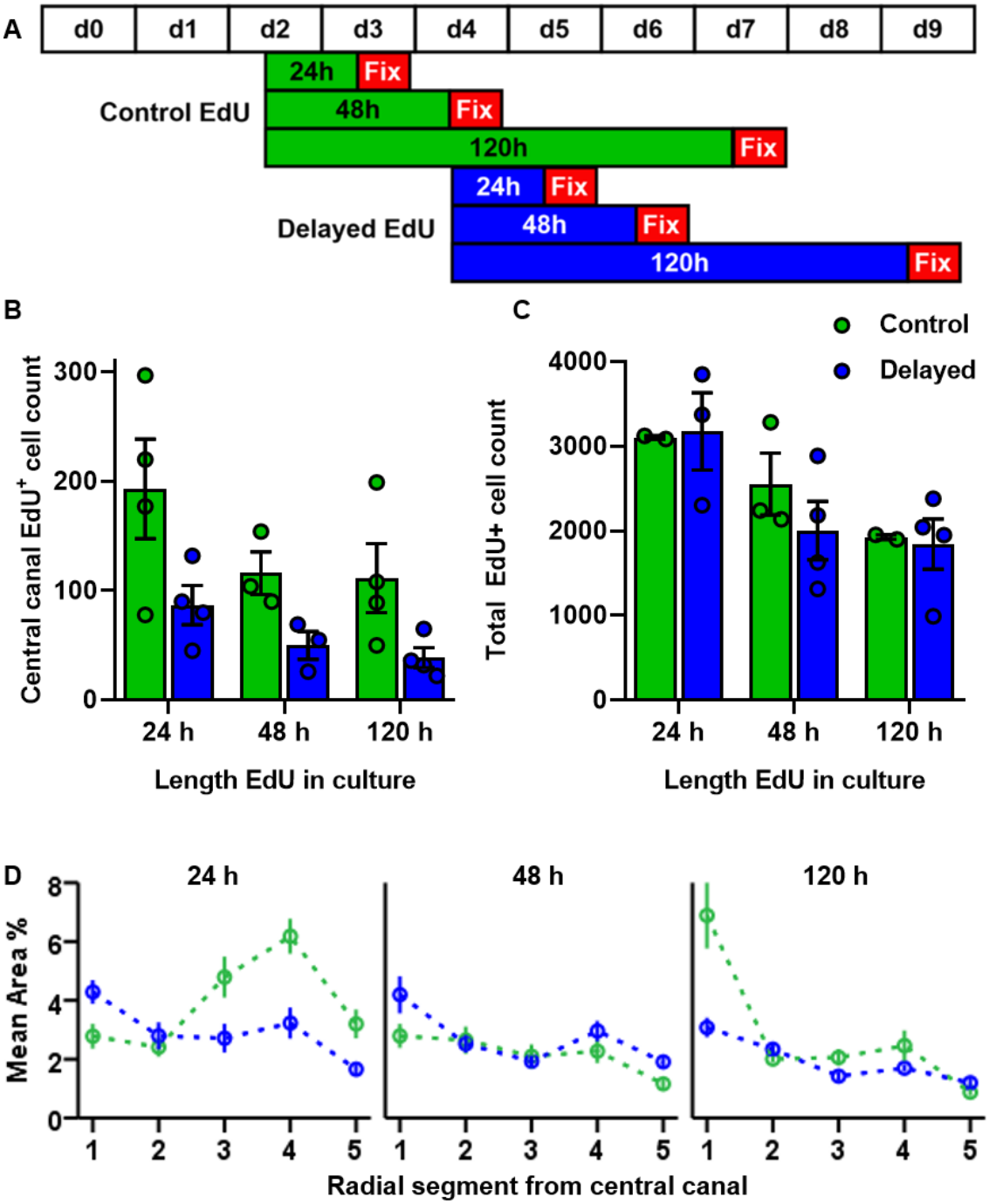

Figure 5.13 Effect of delaying EdU addition on mean total EdU+ cell count and distribution.

(A) Schematic diagram depicting EdU addition. (B) Central canal and (C) total EdU+ve cell count per 300 µm slice for control (green) and delayed (blue) conditions. (D) EdU mean area % coverage as a function of radial distance from the central canal. Data presented as mean ±SE. N=1 n>2.

5.3.8 Creating an injury model in OSCSCs

In an attempt to create an injury model in OSCSCs, slices were cultured for 2, 3, or 5 days *in vitro* (DIV) then scratched using a sterile needle. The scratch was made to the grey and white matter, with care taken to not damage the insert. EdU was added to the culture medium immediately following injury, at a final concentration of 0.1, 0.5, or 1 µM, and cultured slices were fixed following 6, 18, or 48 hours in culture in the presence of EdU.

Injury following 2 DIV, EdU in culture for 6 hours

There was no significant difference between the control and injured EdU+ve cell counts of the central canal or total slice when injured following 2 DIV (Figure 5.14 B & C). The distribution of EdU+ve cells throughout the slice was also similar for both conditions (Figure 5.14 D). The areas with the greatest percentage of fluorescence were shown to be the central canal (radial segment 1) and in the white matter, towards the slice periphery (radial segments 4 and 5, Figure 5.14 D).

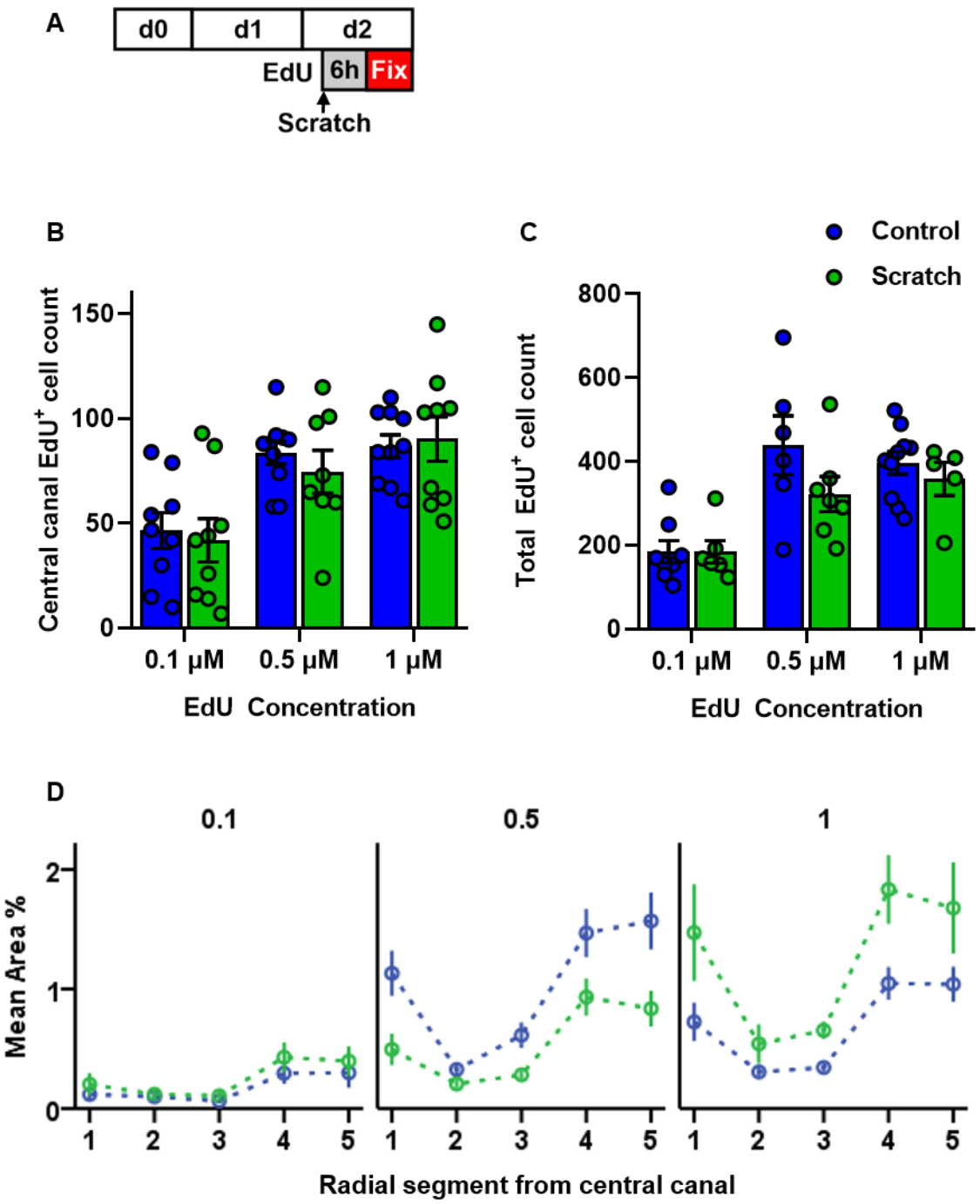

Figure 5.14 Development of a scratch injury model in OSCSCs: Injury following 2 DIV, EdU in culture for 6 hours

(A) Schematic diagram depicting EdU addition following 2 days *in vitro* for 6 hours. (B) Central canal and (C) total EdU+ve cell count per 300 µm for control (blue) and scratched (green) slices. (D) EdU mean area % coverage as a function of radial distance from the central canal. Data presented as mean ±SE. N=2 n>3.

Injury following 5 DIV, EdU in culture for 18 hours

There was also no significant difference between the control and injured EdU+ve cell counts at the central canal or total slice when injured following 5 DIV (Figure 5.15 B & C). The distribution of EdU+ve cells throughout the slice also appeared similar for the control and injured conditions (Figure 5.15 D).

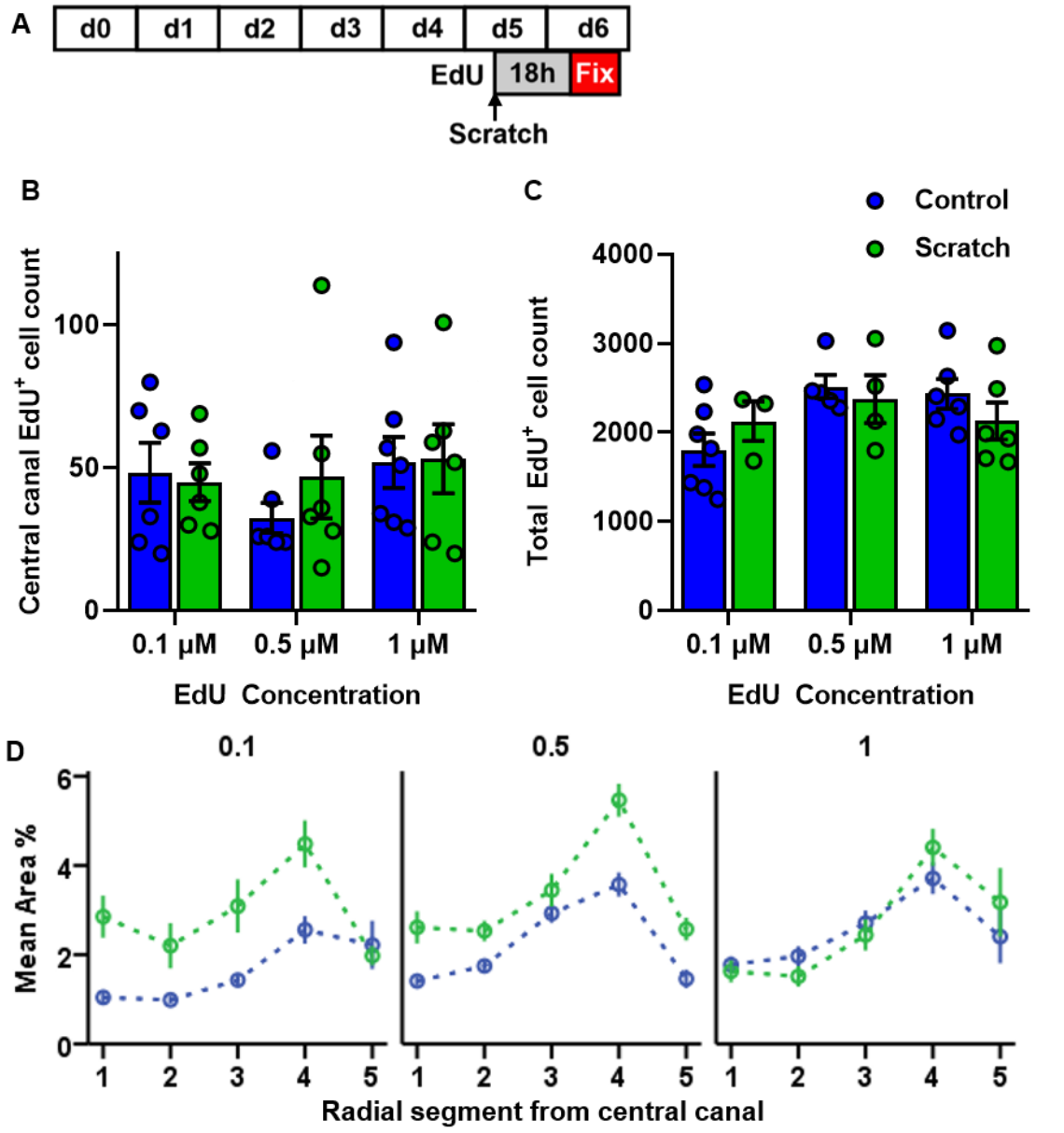

Figure 5.15 Development of a scratch injury model in OSCSCs: Injury following 5 DIV, EdU in culture for 18 hours

(A) Schematic diagram depicting EdU addition following 5 DIV for 18 hours. (B) Central canal and (C) total EdU+ve cell count per 300 µm for control (blue) and scratched (green) slices. (C) EdU mean area % coverage as a function of radial distance from the central canal. Data presented as mean ±SE. N=2 n>3.

Injury following 3 DIV, EdU in culture for 48 hours

When slices were injured following 3 DIV and incubated in the presence of EdU for 48 hours, there were significantly more EdU+ve cells at the injured slice central canal compared to control when detected using 1 µM EdU (Figure 5.16 B; 1 µM control: 11.17 ±2.372, scratch: 29.00 ±2.449, $P = 0.001$). These data suggest that by creating an injury to the spinal cord, we can trigger an increase in central canal cell proliferation (and survival) over 48 hours compared to control.

Whilst there was also a trend towards increased EdU+ve cell counts at the central canal of scratched slices when detected using lower concentrations of EdU, this change in cell proliferation was not statistically significant.

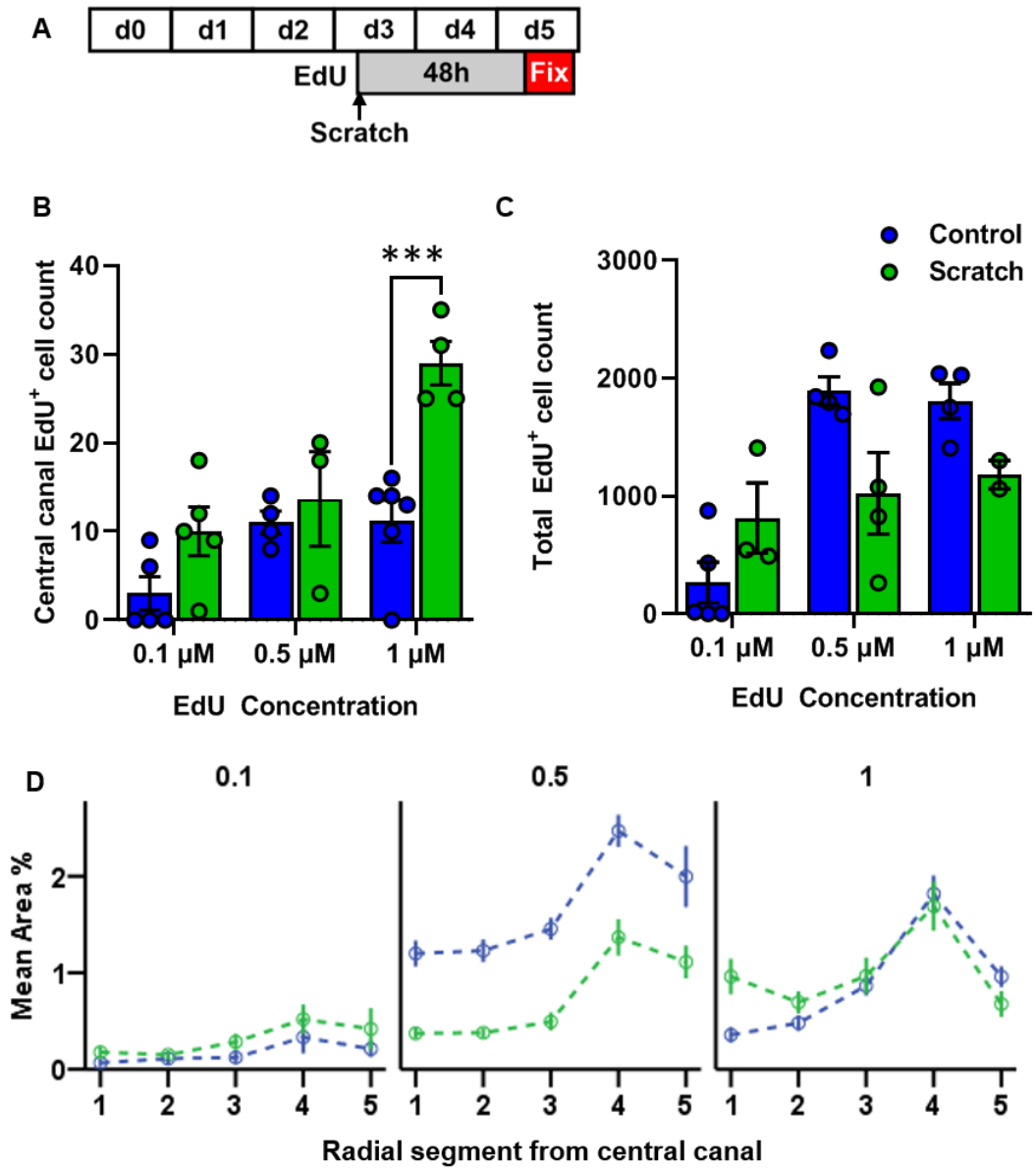

Figure 5.16 Development of a scratch injury model in OSCSCs: Injury following 3 DIV, EdU in culture for 48 hours

(A) Schematic diagram depicting EdU addition following 3 DIV for 48 hours. (B) Central canal and (C) total EdU+ cell count per 300 µm for control (blue) and scratched (green) slices. (C) EdU mean area % coverage as a function of radial distance from the central canal. Data presented as mean ±SE. N=1 n>2, *** P ≤ 0.001.

5.3.9 Characterisation of Cultured Central Canal GFP Projections

(Nestin) GFP processes extending radially away from the central canal were observed in a number of cultured transgenic spinal cord slices (Figure 5.17). These were found to express: CD24 (A), galectin-3 (B), and NG2 (C), and had EdU+ve cells along them (D).

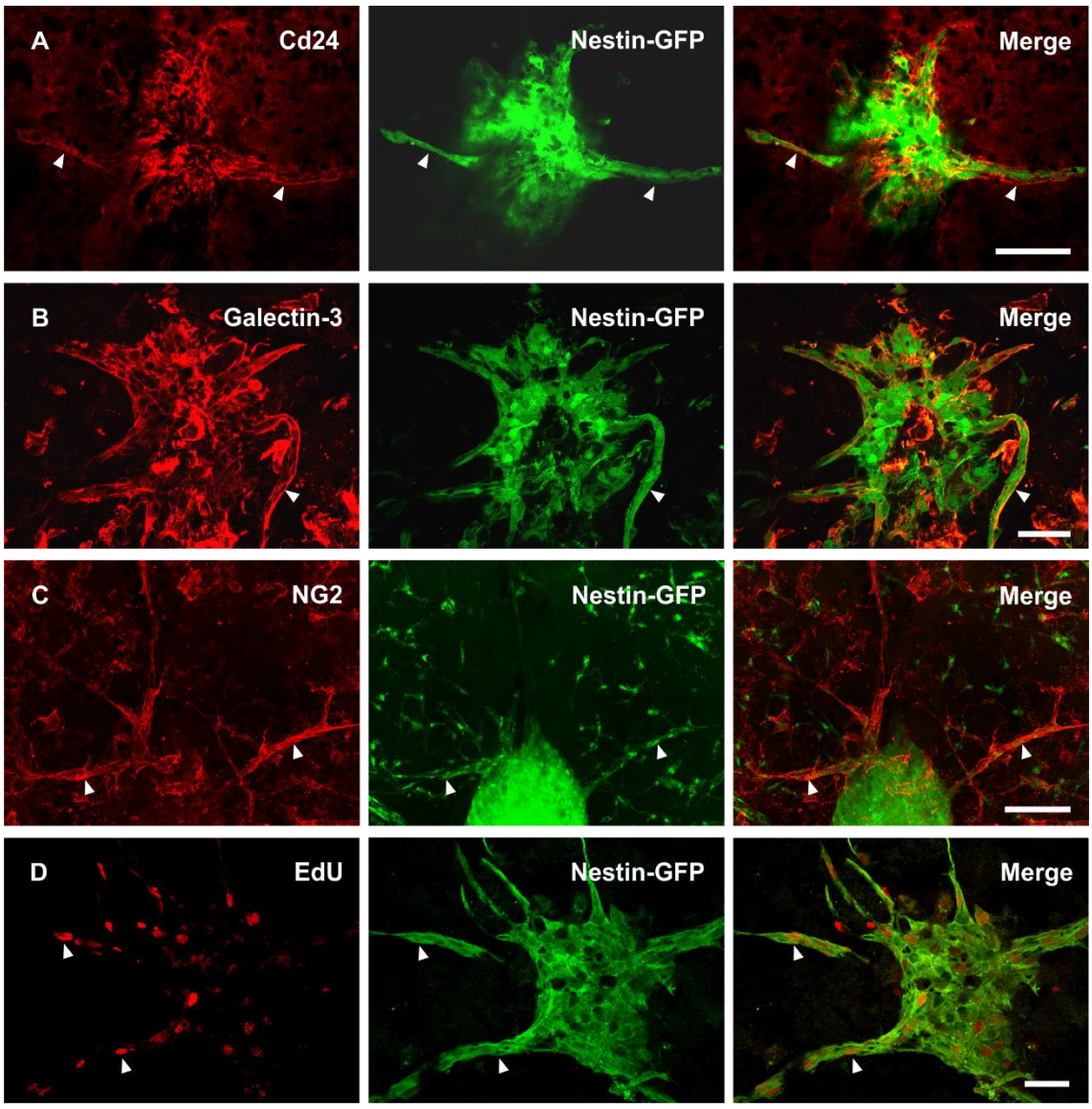

Figure 5.17 Characterisation of (nestin) GFP processes

Representative confocal images of the central canal of cultured (nestin) GFP spinal cord slices stained with antibodies against (A) CD24, (B) Galectin-3, and (C) NG2. Proliferating cells detected using (D) EdU. White arrows indicate a number of colocalised projections/cells. Scale bars= 100 µm

5.4 Discussion

In this chapter a number of culture variables were investigated including: EdU concentration, length in culture, delaying EdU addition, and creating an injury.

Important findings:

1. EdU can be detected in perfusion-fixed and cultured spinal cord tissue whilst maintaining GFP fluorescence. By using a copper chelating azide (picolyl azide) and reducing the reaction time and copper concentration for cultured slices, EdU was successfully detected without quenching the GFP fluorescence needed for identifying ECs.
2. (Nestin) GFP expression in the central canal remains clearly visible over 3 DIV – indicating survival of ECs.
3. (Nestin) GFP expression in the white and grey matter reduces over 3 DIV – indicating death or differentiation of pericytes.
4. There is a peak in the number of proliferating cells on the third/fourth DIV.
5. There is no significant difference in the number of proliferating cells when detected over 24 to 72 hours *in vitro*.
6. The concentration of EdU in culture medium reduces significantly (from 1 µM) following 48 hours *in vitro*.
7. 1 µM EdU is the optimal concentration for our culture experiments.
8. Delaying EdU addition until after the initial peak in proliferation reduces the number of proliferating cells detected at the central canal (but not significantly).
9. Creating an injury to the white and grey matter only results in significantly more proliferating central canal cells when scratched on d3 and monitored over 48 hours, and 1 µM EdU is required to detect this change.
10. Proliferating (Nestin) GFP cells extend radially from the central canal, express CD24 and galectin-3, and colocalise with NG2.

5.4.1 EdU detection in fluorescent tissue

This chapter reveals how to localise EdU in GFP tissue. Considering how widespread GFP use is in studies employing transgenic animals, this is an extremely valuable protocol. High copper concentrations have been shown to inactivate enzymes and quench the fluorescence of GFP and other fluorescent proteins (DsRed, (Rahimi et al., 2008)), and so the findings from this chapter could also be applied to transgenic tissue with other fluorophores. Whilst there are commercial EdU detection kits available (Click-iT Plus kit, Invitrogen) these are costly and still require method optimisation for use in different tissues. This also highlights the importance of the order in which immunofluorescence and EdU labelling is carried out as the fluorophores on secondary antibodies are also quenched using the original EdU protocol.

5.4.2 Nestin GFP expression and distribution *ex vivo*

(Nestin) GFP expression in pericytes in the white and grey matter of spinal cord slices reduced over 3 days in culture, whereas the central canal (nestin) GFP fluorescence remained bright over this time-period. This indicates viability of ependymal cells and maintenance of GFP expression in these cells over time.

It isn't clear however, whether pericyte death, or the loss of pericyte (nestin) GFP expression due to cell differentiation, gives rise to the reduced (nestin) GFP fluorescence over time. Pericyte death could be occurring due to the damage caused to vasculature and lack of blood flow *ex vivo* (Mayo and Bearden, 2015) however, blood vessels have been detected (using the endothelial cell marker RECA-1) in slice cultures of the rat brain (10 days old) up to 14 DIV, indicating the survival of vasculature ex vivo (Schmidt-Kastner and Humpel, 2002). Pericytes have also been shown to behave as stem cells (reviewed in (Andreotti et al., 2019)) and could therefore be differentiating and losing GFP expression.

To investigate this further, FG could be administered to animals prior to culturing slices to label the pericytes. However, FG labelling of pericytes in adult animals (6-8 weeks

old) has been shown to diminish at 48 h post I.P. injection, indicating methodological challenges to this approach (Edwards et al., 2013). Additionally, labelling of neurons typically occurs 3 days post FG I.P. injection and so it is unclear what conditions would be required for the optimal and selective visualisation of pericytes in pre-weaner mice (~14 days) and whether the tracer fluorescence would be retained when cultured *in vitro*. An alternative to this could be the use of a transgenic mouse line in which pericytes display DSRed, even following pericyte differentiation.

5.4.3 EdU availability

To accurately quantify the number of proliferating cells *in vitro*, it was firstly assessed whether the EdU concentration and length in culture was appropriate for our spinal cord slice culture model. When 1 µM EdU was added, the amount of EdU was found to be in excess for the first 24 hours. The concentration of EdU in culture medium then reduced significantly (from 1 µM) following 48 hours *in vitro*. This could be due to the uptake of EdU by cells during this time, leading to a significant reduction in the concentration of EdU remaining in the culture medium. Alternatively, this could be due to the degradation of EdU under these conditions. An ELISA assay or mass spectrometry (for EdU concentration quantification) could be used in order to determine which scenario is occurring. In either case, studies investigating the long-term proliferation of cells will require re-addition of EdU to replenish the EdU taken up or degraded.

5.4.4 Proliferation in spinal cord slice cultures

In pre-weaner mice (under 21 days old), the injury response caused by the sectioning of the spinal cord was found to elicit an increase in the proliferation of cells, peaking at 3/4 days after sectioning, followed by a decline in the number of EdU+ve cells. Other groups (Mothe and Tator, 2005b; Lacroix et al., 2014) also found a peak in EC proliferation at 3 days post injury *in vivo* in adult rodents, followed by a decline in BrdU/Ki67-labelling (markers of proliferation) when detected at 7 days post injury.

We also found a reduced variance in central canal EdU+ve counts for cultures where EdU addition was delayed, suggesting that detecting proliferation a later time point when the injury response has subsided could produce more repeatable data.

5.4.5 Cell death vs cell birth

There was no observed cumulative increase in the total number of dividing cells over the time period investigated, therefore indicating that the proliferating cells were dying before detection. EC proliferation within the intact adult spinal cord has been shown to be limited to self-renewal for the maintenance of cell populations (Meletis et al., 2008). Even following an increase in proliferation induced by an injury, EC turnover eventually reduces to baseline levels, indicating that ECs are no longer required for SCI repair and so these cells die as they are surplus to requirement (Lacroix et al., 2014).

Additionally, EdU incorporation into dividing ECs may also impact their survival. Sensitivity to thymidine analogues, including EdU, has been shown to be cell type specific and dependent on concentration and incubation time. In a number of cell types, EdU addition results in reduced cell viability caused by DNA damage and disruption to cell cycle progression via G2/M cell cycle arrest, ultimately leading to cell death (Diermeier-Daucher et al., 2009; Ross et al., 2011; Kohlmeier et al., 2013).

Alternatively, this EdU toxicity could be halting further cell division of daughter cells, thereby reducing the number of EdU+ve cells detected over time rather than causing cell death. This could be investigated using BrdU to label subsequent proliferation. EdU could be administered for the first 24 hours, followed by BrdU for the second 24 hours; double labelled cells would therefore show that cells are capable of proliferating following EdU incorporation.

5.4.6 Cell migration from the central canal

Cell chains extending from the central canal were observed in a number of spinal cord slices. These newly divided, EdU+ve cells expressed (nestin) GFP and were immuno-

reactive against CD24 and galectin-3; thus identifying them as ependymal cells. In the absence of a pericyte-specific antibody (NG2 also labels oligodendrocyte progenitor cells), NG2 was used to determine if these cells were migrating along vascular structures. We found that NG2 labelling colocalised with (nestin) GFP+ve cells, suggesting a potential guidance mechanism.

Could the EC processes be guided by basement membranes?

Vasculature has been shown to play an important role in the maintenance and regulation of the neurogenic niches within the brain. Within the adult SGZ and SVZ, neurogenesis and the vasculature are interconnected, with clusters of proliferating cells typically found in close proximity to growing capillaries and blood vessels (Palmer et al., 2000; Shen et al., 2008). Neuroblasts have also been shown to migrate along blood vessels in a chain formation; suggesting the vasculature plays a role in the guidance of cell migration (Shen et al., 2008).

In the CNS, two basement membrane (BM) structures have been identified: vascular BMs that ensheath blood vessels, and fractones comprising of bulbs and stems. These BMs are specialised cell-adherent ECMs comprising of laminins, collagen subunits, heparin sulphate proteoglycans (HSPGs), and nidogens (amongst others) and these cell adhesion molecules are critical elements of the neurogenic niches in which they're found (Mercier et al., 2002; Kerever et al., 2007) .

BM HSPGs are thought to play a role in controlling neurogenesis and NPC proliferation via the binding of Bone morphogenic protein-4 and -7 (Douet et al., 2012; Mercier and Douet, 2014), and the neurogenic growth factor FGF-2 (Kerever et al., 2014). Additionally, fractones within the SVZ are enriched in laminin-α5, and have been shown to maintain embryonic stem cells in a non-differentiated state and regulate cell proliferation (Nascimento et al., 2018). Interestingly, ependymal cells adjacent to the SVZ produce the BMP antagonist Noggin, thereby blocking endogenous BMP signalling and promoting neuronal differentiation (Lim et al., 2000).

In addition to the concentration and activation of numerous trophic/growth factors, BMs also provide structural guidance for migrating cells via cell-ECM binding. NSCs adhere to the laminin subtypes (α3/α5) found on BMs via integrin binding; further directing the movement and behaviour of stem cells within the niche (Jacques et al., 1998; Sato et al., 2019).

In the rostral migratory stream (RMS) of the brain, migrating neuroblasts also form chains to migrate through “glial tubes” formed by specialised astrocytes (Sun et al., 2010). Aligned blood vessels provide additional physical guidance as well as molecular signals (PSA-NCAM, etc.) to aid migration along the RMS towards the OB (Whitman and Greer, 2009; Snapyan et al., 2009). Therefore it is reasonable to presume a similar phenomenon could be occurring within the spinal cord; with ependymal cell migration occurring along vascular structures and pericytes.

In a focal photothrombotic cortical stroke model, ECs of the adult mouse forebrain exhibited elongated processes projecting towards the stroke site, however this wasn’t seen in mice with a cortical stab injury (Muthusamy et al., 2018). Further studies are required in order to unpick the mechanisms controlling and directing EC process extension, and investigate whether cell migration could be manipulated for regeneration following injury. As part of this, the vasculature and influence of BMs requires careful consideration.

5.4.7 Creating an injury model

A number of *in vitro* models have been developed to investigate and replicate the cellular response to spinal cord injury (Pandamooz et al., 2019). In this chapter a scratch injury was used as a simple method of damaging the white and grey matter. A significant increase in the number of proliferating central canal cells was found when the slice was injured on day 3, measured over 48 h post injury, and this was detectable when 1 µM EdU was used.

It is unclear whether this enhanced proliferation was due to the injury itself, or because the scratch increased the retention and survival of cells proliferating due to the initial injury response (e.g. by giving them a purpose), or a combination of the two.

Elsewhere in this chapter a peak in central canal cell proliferation was shown to occur at day 3 to 4 (Figure 5.9). It is therefore hypothesised that by creating an injury when central canal cell division is at its greatest, an enhanced injury response can be triggered. Scratching the slice before or after this critical peak in central canal cell proliferation was shown not to elicit an injury response. No significant differences were found between the injured and control cell counts when the slice was scratched on day 2 and measured over 6 hours or when the slice was scratched on day 5 and proliferation was measured over 18 hours. At these time points in un-injured controls, there is minimal central canal proliferation (see Figure 5.9), and therefore, when the white and grey matter were scratched, this caused no increase in central canal proliferation.

Future studies investigating the response of cells to hydrogels in an injury model will benefit from the insight gained in this chapter. In particular this optimised injury protocol (scratching on day 3 and measuring proliferation over 48 hours) will provide a simple method by which to assess the impact of hydrogels on ependymal cell behaviour *in vitro.* These data also support the rationale for using 1 µM EdU in future studies, for the detection of any changes in proliferation.

5.5 Conclusions

The experiments in this chapter built on the characterisation work developed in chapter 4 in order to develop and optimise methods for use in chapter 6, for the investigation into the potential manipulation of ependymal cells.

In this chapter it was concluded that:

1. Picolyl azide raises the effective concentration of Cu(II) in the EdU reaction and therefore enables the detection of EdU incorporated into cellular DNA, whilst retaining fluorescence in transgenic tissue.
2. Cell proliferation in OSCSCs was found to peak at day 3 to 4 at the central canal, and day 2 to 3 when the whole slice was counted.
3. Optimal cell culture conditions were determined:

- 1 µM EdU allows the detection of proliferating cells within spinal cord slices for up to 48 hours *in vitro.*
- After 48 hours *in vitro* the concentration of EdU requires replacing for long-term proliferation detection.
- 1 µM EdU was determined to be optimal for these experiments – enabling changes in central canal proliferation levels to be detected following a scratch injury *in vitro.*

4. An optimised injury model protocol was identified:

- Scratching the white/grey matter on day 3 results in a significant increase in central canal cell proliferation when measured over 48 hours.

5. Ependymal cells may migrate radially from the central canal in OSCSCs, potentially guided by vascular structures.

- Proliferating (Nestin) GFP cells extend radially from the central canal, express CD24 and galectin-3, and colocalise with NG2.

Overall, this chapter identifies the conditions required for organotypic spinal cord slices to be used to study EC behaviour in chapter 6. In addition, results suggest that ECs do migrate and may be manipulated for spinal cord injury repair.

Chapter 6 - Manipulating Ependymal Cells in Organotypic Spinal Cord Slice Cultures and *In Vivo*

6.1 Introduction

SDF-1α/CXCR4 – directing migration and proliferation

The chemokine CXCL12, also known as stromal cell-derived factor-1 (SDF-1), and its signalling receptor C-X-C chemokine receptor type 4 (CXCR4) are reported to have multiple roles within the CNS. CXCR4 is a G protein-coupled receptor, and binding of SDF-1 is thought to lead to downstream effects via modulation of G nucleotide-binding proteins (Wescott et al., 2016). CXCR4 has been implicated in neuronal migration and morphogenesis during development (Lu et al., 2002; Stumm et al., 2003) and adult neurogenesis (Tran et al., 2007). SDF-1/CXCR4 signalling is also thought to function as an axon guidance cue for mammalian motor neurons, dorsal root ganglion (DRG) sensory and sympathetic axons, and retinal ganglion cells of the zebrafish (Chalasani et al., 2003; Lieberam et al., 2005; Chalasani et al., 2007).

Following focal cerebral ischemia in adult rodents, an increase in endogenous neural progenitor cell (NPC) proliferation in the SVZ is seen, followed by SDF-1/CXCR4 mediated neuroblast migration (Robin et al., 2006; Ohab et al., 2006; Wang et al., 2012). Directed migration of new neurons was also shown to be regulated by SDF-1/CXCR4 up to 4 months following stroke-induced neurogenesis in rats (Thored et al., 2006).

Migration of oligodendrocyte progenitor cells (OPCs) is also thought to occur via CXCR4-mediated signalling, with neurospheres formed from CXCR4-defective mice showing reduced outgrowth and cell migration *in vitro* compared to WT mice

(Dziembowska et al., 2005). Cell migration within a viral-induced immune-mediated demyelination model of multiple sclerosis was investigated by (Carbajal et al., 2010; Carbajal et al., 2011). In these animals, NSCs (expressing CXCR4 and CXCR7) were injected into the spinal cord and these were found to migrate to the demyelinated white matter tracts, proliferate extensively, and differentiate into mature oligodendrocytes (~7%) and oligodendrocyte progenitor cells (~29%); ultimately aiding remyelination of axons. SDF-1 immunoreactivity was found in the white matter tracts and astrocytes of infected mice, and blocking studies (using the antagonists: AMD3100 and CCX771) indicated that CXCR4 signalling, rather than CXCR7, was important for NSC migration and proliferation.

In the uninjured spinal cord, SDF-1 is expressed within the meninges and dorsal corticospinal tract, and CXCR4 is expressed in ependymal cells at the central canal (Tysseling et al., 2011). Following a compression injury in adult mice, CXCR4+ve cells appeared to migrate towards the periphery of the spinal cord, towards SDF-1-expressing meningeal cells and the SDF-1-containing dorsal corticospinal tract rostral to the lesion. Fewer CXCR4+ve ependymal cells were found to reside in the central canal following injury, however it was unclear whether the migrating CXCR4+ve cells were ECs or macrophages (Tysseling et al., 2011).

Delivery of SDF-1α using a number of scaffolds has been achieved for various tissue-repair applications (reviewed in (Zhao et al., 2017)). In the brain, the retention of transplanted neural stem/progenitor cells (NSPCs) was significantly increased when cells were incorporated into a hyaluronic acid (HA)-laminin hydrogel compared to bolus delivery. Migration of these cells towards SDF-1α (injected close to the transplantation site) was also significantly increased compared to bolus controls (Addington et al., 2017). This chapter aims to determine whether delivering SDF-1α in a hydrogel promotes endogenous ependymal cell proliferation and/or migration within the spinal cord for potential repair following injury.

6.1.1 Hypothesis

Previous studies have shown that stem cells can be manipulated using tissue engineering strategies involving chemokines and materials with modified mechanical properties. The hypothesis here is that hydrogels and/or SDF-1α can be used for the modulation of ependymal cells within the spinal cord.

The experiments in this chapter build on the work carried out in chapters 3 to 5 and use the methods and transgenic line optimised earlier in this thesis (Figure 6.1).

6.1.2 Aims

1. To investigate the impact of culturing spinal cord slices on hydrogels with regards to cell proliferation and distribution.
2. To assess the effect of SDF-1α on ependymal cell proliferation and migration *in vitro* and *in vivo.*

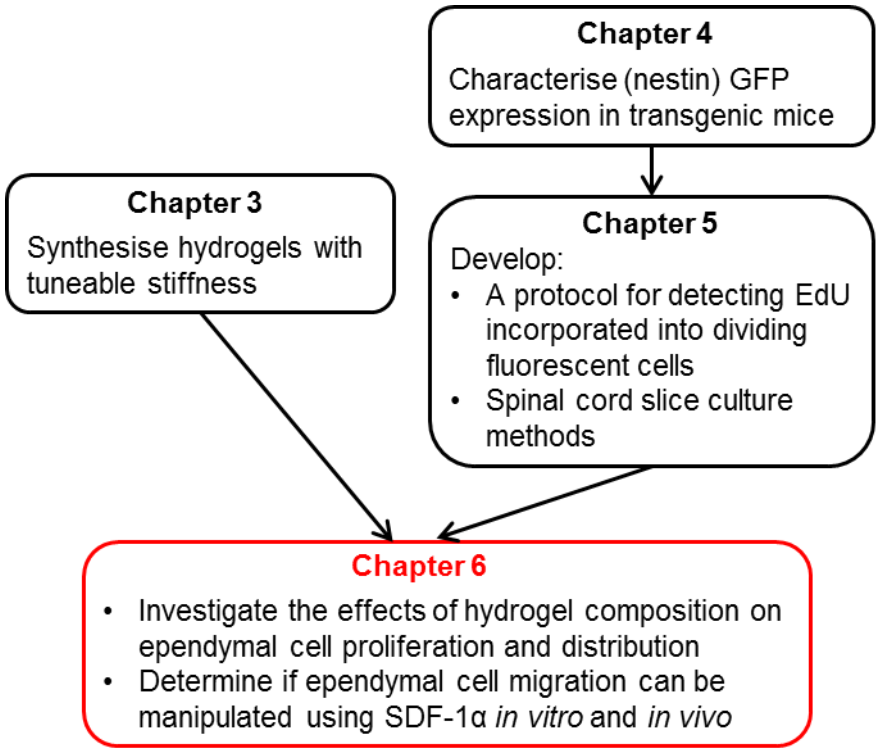

Figure 6.1 Schematic depicting the aims of chapter 6 in reference to the rest of this thesis

The work carried out within this chapter builds-on the methods developed in chapters 3 and 5, and uses the transgenic line characterised in chapter 4.

6.2 Methods

6.2.1 Animals used

All experiments were carried out under a UK Home Office Licence (P1D7A177), in accordance with the UK Animals (Scientific Procedures) Act 1986 and the ethical standards set out by the University of Leeds Ethical Review Committee. Every effort was made to minimise the number of animals used and their suffering.

(Nestin) GFP transgenic mice (characterised in chapter 4) were bred in-house as heterozygotes, housed in standard conditions with a 12 hour light-dark cycle, and given *ad libitum* access to food and water.

6.2.2 Sterilisation and disinfection

The laminar flow hood, incubator, and surrounding surfaces were disinfected using 1% Virkon followed by 70% ethanol prior to use. All tools for *in vitro* and *in vivo* work were cleaned with boiling water, 70% ethanol, and then autoclaved at 121 °C for 20 minutes under 103 kPa for sterilisation. Where possible, sterile, single use consumables were used and disinfected with 1% Virkon following their use, prior to disposal. Collagen hydrogels were disinfected using 70% ethanol washes, all other hydrogels were created aseptically in a laminar flow hood.

6.2.3 Hydrogel synthesis

As we were unable to reliably manipulate the stiffness of collagen hydrogels developed in-house, we compared 4Ph-crosslinked collagen hydrogels to two commercial hydrogels (Table 6.1).

6.2.3.1 Collagen

4Ph crosslinked collagen hydrogels were synthesised as previously described (Chapter 3.3.2). Briefly, rat tail collagen (extracted in-house, 1.2 wt.% in acetic acid) was crosslinked using activated 4Ph at a molar ratio of 1:1 (crosslinker carboxylic acid

groups: collagen lysine groups) to form hydrogels. Prior to tissue culture, collagen hydrogels were washed in diH_2O and 70% ethanol to remove any unreacted species and disinfect the gels.

6.2.3.2 Commercial hydrogels:

VitroGel

According to the manufacturer (TheWell BioScience), VitroGel is “an animal origin-free hydrogel system mimicking the natural ECM” and is “unmodified polysaccharide-based”. This hydrogel is shear-thinning and recoverable, and therefore injectable. VitroGel hydrogels were created by mixing VitroGel with sterile VitroGel dilution solution (ratio of 1:1 VitroGel: dilution solution) and culture medium (no serum) was then added (ratio of 4:1 VitroGel: medium), mixed, and immediately transferred to sterile culture inserts to initiate gelation *in situ.*

HyStem

HyStem hydrogels comprise of a thiol modified HA (Glycosil) and a thiol reactive crosslinker (Extralink), with or without thiol-modified denatured collagen fibrils (Gelin-S) for cellular attachment sites (referred to as HyStemC). HyStem hydrogels were formed according to the manufacturer’s protocol. Each gel component (Glycosil, Extralink, and Gelin-S) was reconstituted under aseptic conditions using degassed sterile water. Glycosil and Gelin-S bottles were placed onto a plate shaker for 1 hr at RT to fully dissolve. Extralink did not require shaking and was prepared immediately prior to hydrogel formation. Extralink and HyStem solutions were mixed at a ratio of 1:4 (Extralink: HyStem) to initiate gelation. For HyStemC hydrogels, HyStem was first mixed with Gelin-S at a ratio of 1:1. Extralink was then added at a ratio of 1:4 (Extralink: HyStem mixture) to initiate gelation.

Table 6.1 Hydrogels used in this chapter and their composition and mechanical properties

Hydrogel	Composition	G' (Pa)	Testing method	Reference
Collagen	4Ph crosslinked rat tail collagen	~ 100 to 650*	Rheology (Kinexus Pro, frequency sweep)	Chapter 3
VitroGel	Unmodified polysaccharide-based	~ 1000**	Rheology (single frequency test, created using DMEM)	(TheWell Bioscience Inc, n.d.)
HyStem	Polyethylene glycol diacrylate-crosslinked hyaluronic acid	~ 110	Contactless rheology (Elastosens, laser, non-shear)	(Advanced BioMatrix, n.d.)
HyStemC	HyStem modified with porcine gelatin	~ 159	Contactless rheology (Elastosens, laser, non-shear)	

*taken from all rheology data, **Incubated at 37°C for 24 hrs before the rheological test

6.2.4 Organotypic spinal cord slice culture

Hydrogels were washed twice (30 minutes) with culture medium, incubated in culture medium containing serum (Chapter 2, Table 2.7) and equilibrated to 37 °C for 2 hours prior to spinal cord slice addition and organotypic spinal cord slice cultures (OSCSCs) were carried out as described in Chapter 5.2.2. Following 1 day *in vitro* (DIV), the medium was exchanged for serum free medium (Chapter 2, Table 2.7) (see Chapter 5, Figure 5.4). EdU was added to the culture medium following 3 DIV at a final concentration of 1 μM, allowing for the visualisation of cells that have undergone proliferation with EdU present.

6.2.4.1 SDF-1α and AMD3100 addition

In this chapter the response of cells to SDF-1α was investigated. Here, collagen hydrogels were used to deliver SDF-1α or AMD3100 in order to determine if cell migration towards a chemokine (through the hydrogel) could be triggered.

For uniform SDF-1α concentration, hydrogels were pre-saturated in SDF-1α (referred to as collagen & SDF; 1 µL of SDF-1α added to the medium used to hydrate the hydrogels; 7.9 kDa, 126.6 nM,) 24 hours prior to culturing. To create a gradient, SDF-1α was also added to the culture medium in the well (referred to as collagen & SDF x2; 2 µL of SDF-1α, 253.2 nM) thereby creating a concentration gradient through the hydrogel due to SDF-1α diffusion (see Addington et al., 2015) (see table 6.2 for more details).

To investigate whether CXCR4 was involved in SDF signalling, the CXCR4 antagonist AMD3100 was used. In this condition, hydrogels were pre-saturated in medium containing 1 µL of AMD3100 (referred to as AMD3100; 794.48 g/mol, 1.259 nM) 24 hours prior to culturing. These experimental conditions were compared to slices from control wells where slices were cultured directly onto the tissue culture insert (no hydrogel) with/without SDF referred to as control and SDF respectively) and those cultured on hydrogels in the absence of exogenous SDF-1α (referred to as collagen: Table 6.2).

Table 6.2 Conditions investigated in this chapter

Condition	Hydrogel	SDF in gel	SDF in medium (1 µM)	SDF in medium (2 µM)	AMD3100
Control	✗	✗	✗	✗	✗
SDF	✗	✗	✓	✗	✗
Collagen	✓	✗	✗	✗	✗
Collagen & SDF	✓	✓	✗	✗	✗
Collagen & SDF x2	✓	✓	✗	✓	✗
AMD3100	✓	✗	✗	✓	✓

See Supplementary Figure 8.2 for more detail regarding the culture set up.

6.2.4.2 Fixation

Spinal cord slices were fixed *in situ* on tissue culture inserts using 4% paraformaldehyde (PFA, Chapter 2, Table 2.5) for 1-2 hours at RT. Following fixation, slices were removed using a paint brush, and transferred into wells containing PBS.

6.2.5 *In vivo* methods

Glass electrodes were used for the delivery of hydrogels to the spinal cord and were pulled using a Sutter P27 micropipette puller. VitroGel was used as it is sterile, shear-thinning and recoverable, and therefore suitable for injecting *in vivo*. Hydrogels were prepared by mixing VitroGel with sterile PBS (±SDF, 12.66 µM) and left to stabilise in a sterile syringe for 18 h at 4 °C prior to injection. Adult (Nestin) GFP mice (6-8 weeks) of either sex were used for *in vivo* experiments. Mice were weighed prior to surgery and anaesthetised with an I.P. injection of ketamine (75 mg/kg, Chapter 2, Table 2.6) and medetomidine (1.0 mg/kg, Chapter 2, Table 2.6) to maintain anaesthesia for approximately 1 hour. Absence of pedal reflexes determined adequate anaesthesia. Fur around the surgery site was removed using electric clippers and ethanol wipes were used to clean the skin. A lubricant was applied to the eyes to prevent drying during surgery and the animal was kept on a heated table at 37 °C.

6.2.5.1 Intraspinal injection

Using a surgical microscope and a sterile blade, a small incision was made through the dorsal skin and muscle, rostral to the rib cage. Blunt forceps were used to resect muscle caudal to the spinal column and retractors were used to hold the site open. The dura and pia mater were then removed using fine forceps.

A stereotactic frame was used to secure the animal in place, and 5 µL hydrogel (VitroGel ± SDF-1α) was drawn up the electrode in preparation using a syringe pump. The electrode was then moved in place above the spinal cord and the frame height was zeroed. The electrode was then lowered to a depth of 300 µm and a syringe pump was used to deliver 1 µL of hydrogel (Figure 6.2). Following surgery the muscle was sutured using absorbable sutures, the skin was closed using non-dissolvable sutures and antibacterial wound powder was applied to the skin.

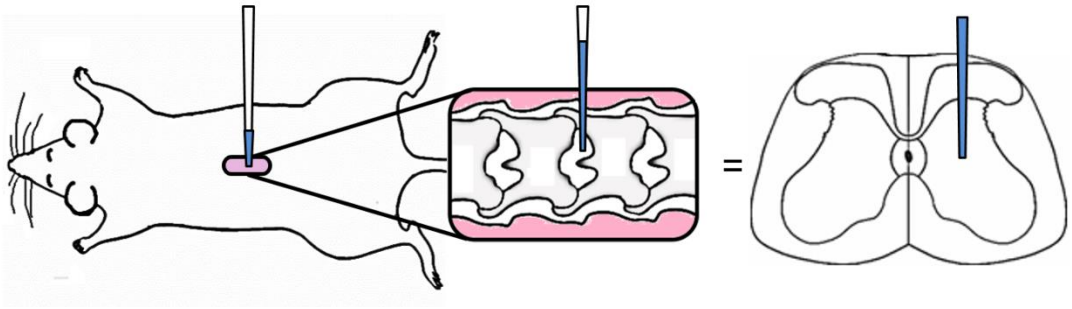

Figure 6.2 Injection of a hydrogel ± SDF-1α into the grey matter of lumbar spinal cord.

A glass electrode was lowered through the intervertebral space into the spinal cord, and a syringe pump was used to deliver 1 µl of hydrogel ± SDF-1α at a depth of 300 µm.

6.2.5.2 Postoperative care and EdU injections

Atipamezole (1 mg/kg, Chapter 2, Table 2.6) was administered I.P. to reverse the effects of medetomidine. Buprenorphine (0.1 mg/kg, Chapter 2, Table 2.6) was given subcutaneously to alleviate post-operative pain, and the animal was transferred to a cage on a heated pad for recovery. Soaked diet was made available and each animal was observed and weighed daily to monitor recovery. 24 hours post-surgery 0.5 mL sterile saline was given I.P. in order to ensure animals were not dehydrated and buprenorphine (0.1 mg/kg, Chapter 2, Table 2.6) was given subcutaneously to ensure pain prevention. EdU (10 mM, 0.1 mL in sterile saline) was delivered via I.P. injection at 24 and 48 h post-surgery (day 1 and 2) to enable detection of proliferating cells.

6.2.5.3 Perfusion-fixation and tissue processing

Mice were terminally anaesthetised 62 h post-surgery with sodium pentobarbital (60 mg/kg) I.P. and perfused transcardially with 0.1 M PB to remove blood, then 4% PFA for fixation. The spinal cord and brain were removed and post fixed overnight at 4 °C in 4% PFA, before being stored in 0.1 M PB at 4 °C. The pia mater was removed using

fine forceps and a dissection microscope, and the injection site and the spinal cord tissue rostral and caudal to it were embedded in gelatin.

6.2.5.4 Gelatin-embedding of tissue and vibratome sectioning

A 1cm block of tissue was cut using a flat blade, and a solution of 10% gelatin (Chapter 2, Table 2.5) was prepared and left to cool slightly. The tissue section was then orientated on the bottom of a glass petri dish placed onto a frozen metal block. The cooled gelatin solution was then carefully pipetted around the tissue until the gelatin was ~1 inch above the tissue section. The block and petri dish containing the embedded section were then transferred into a fridge to set for 2 h. The gelatin was then cut leaving ~2 cm around the tissue section and this was placed into 4% PFA with 0.25% glutaraldehyde overnight at 4 °C. Embedded sections were then washed twice in 0.1 M PB (10 minutes).

Sections of embedded spinal cord were glued to the chuck with the exposed end of tissue facing up. The chuck was then screwed into place in the water bath containing 0.1 M PB and the blade was attached to the vibratome arm. The tissue was then sectioned serially at 40 µm in the transverse plane at an amplitude of 0.4 mm/s and vibrating frequency of 80 Hz. Serial sections were placed into wells containing PBS for EdU labelling.

6.2.6 EdU detection

EdU detection reactions and incubation steps were carried out at RT in the dark as in the optimised method detailed in Chapter 5.2.3, Figure 5.4. Briefly, spinal cord slices were permeabilised using 0.2% PBST, washed twice in 0.1 M Tris buffer (10 minutes each), then incubated in the optimised click reaction mixture (with picolyl azide) for 20 minutes (0.5 mM $Cu(II)SO_4$ for cultured slices) or 5 minutes (1 mM $Cu(II)SO_4$ for *in vivo* slices). Slices were then washed twice in 0.1 M Tris buffer (10 minutes each), followed by 10 minutes in PBS, then incubated in Streptavadin Alexa Fluor^{555} for 2 hours. Finally, slices were washed twice in PBS (10 minutes), washed in PB (10 minutes),

mounted on microscope slides, air-dried, covered in Fluoroshield with DAPI and coverslipped.

6.2.7 Image capture and analysis

6.2.7.1 OSCSC EdU-labelled cell counts

Manual cell counts of EdU-labelled (EdU+ve) cells at the central canal were performed using a Nikon E600 microscope. Images of whole slices were taken using an EVOS fluorescence microscope at x4, x10, and x20 magnification for further quantification. As previously described in Chapter 5.2.6, EdU labelled cells were then quantified using ImageJ to get total counts of all EdU+ve cells, and their radial distribution throughout the slice (see Figure 5.6).

6.2.7.2 (Nestin) GFP process quantification

ImageJ Simple Neurite Tracer was used to create a skeleton of the processes extending from the central canal (Figure 6.3). Processes were manually traced using the plugin, with paths starting from the edge of the central canal region. Branches were mapped and logged (Longair et al., 2011). Outputs included: number and length of projections, and number and length of branches. This was done for five images per condition.

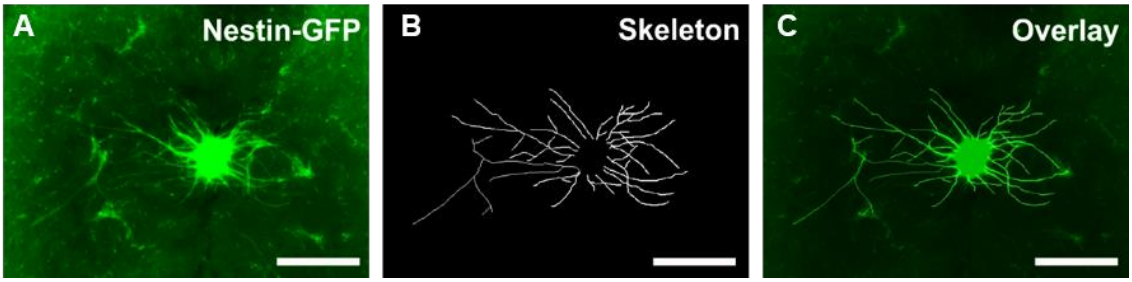

Figure 6.3 ImageJ skeleton creation for analysis of (Nestin) GFP processes.

Representative EVOS image of (Nestin) GFP central canal processes. (B) Manual skeleton application using ImageJ and (C) overlay of the two images. Scale bar = 300 µm

6.2.7.3 In vivo EdU-labelled cell counts

Manual cell counts were performed using a Nikon E600 microscope. EdU labelled cells were counted at the central canal, white, and grey matter regions to allow for comparison between experimental groups. Representative images were taken using a Zeiss LSM880 laser scanning confocal microscope equipped with argon (λex = 488 nm) and He-Ne (λex = 543 nm) lasers. Images were acquired using Carl Zeiss SEN software (Zeiss Microscopy) and CorelDRAW 2017 was used for image processing.

6.2.8 Data analysis

Data were collated in Microsoft Excel and analysed using IBM SPSS statistics 21. Average EdU-positive (EdU+ve) cell counts were calculated and presented as mean ± standard error of the mean (SE) unless stated otherwise. Shapiro-Wilk and Levine's tests were applied for distribution and equality of variance analysis respectively. A decision tree was used to determine the appropriate statistical test (Chapter 2, Figure 2.6).

Table 6.3 Animals used in this chapter to investigate the response of ECs to hydrogels and the chemokine SDF-1α

Chapter	Experiment	Strain	Number of animals (N)	Sections per condition (n)	Age
6.3.1	Hydrogel assessment	(Nestin) GFP	3 2	>9 >6	14 ±2 days
6.3.2	SDF-1α – proliferation	(Nestin) GFP	1	>3	15 days
6.3.2	SDF-1α – (Nestin) GFP CC projections	(Nestin) GFP	1	5	14 days
6.3.2	SDF-1α – (Nestin) GFP distribution	(Nestin) GFP	1	>3	16 days
6.3.3	*In vivo* injection of hydrogel ±SDF-1α	(Nestin) GFP	4	12 (per level)	6-8 weeks

6.3 Results

6.3.1 Effect of Hydrogels on the Proliferation of Cells

Spinal cord slices were cultured on hydrogels in the presence of EdU for 6 hours on d3 (Figure 6.4 A) in order to determine if these materials affected the proliferation of cells. The number of EdU+ve cells was lower in hydrogel conditions compared to control when the central canal or whole slice was counted (Figure 6.4 B & C). There was a statistically significant reduction in the number of EdU+ve cells at the central canal of slices cultured on HyStemC hydrogels compared to control (mean rank difference: -22.33; p=0.0027). The number of EdU+ve cells in the whole slice for those cultured on HyStem and HyStemC hydrogels was also significantly less than control (mean difference ±SE of difference: HyStem= -602.5 ± 162.2, P= 0.0018; HyStemC= -538.6 ±204.1, P = 0.0321).

There were no statistically significant differences between the central canal EdU+ve cell counts of each hydrogel condition, however there were significantly fewer EdU+ve cells when the whole slice was counted, in slices cultured on HyStem gels compared to collagen gels (mean difference ±SE of difference= -494.0 ±146.9; P = 0.0198).

The distribution of EdU+ve cells appeared similar in the control and collagen conditions, with fluorescence throughout the slice and a peak in the area % in the white matter (Figure 6.4 D, radial segment 4 & E). Similarly in the HyStem conditions, the fluorescence was distributed throughout the slice, with a total reduction in area percent coverage corresponding to the lower EdU+ve cell counts.

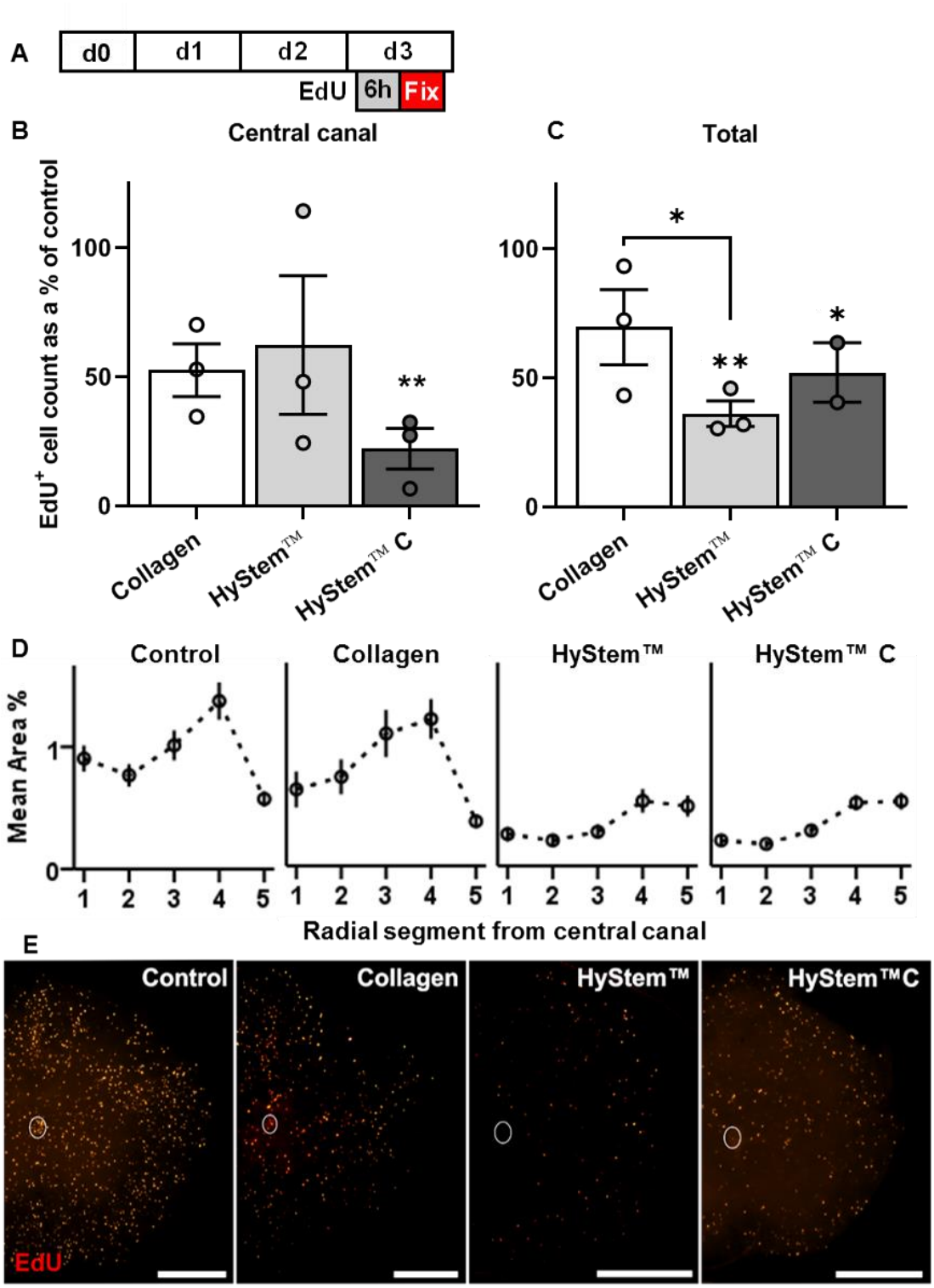

Figure 6.4 Effect of hydrogels on the number and distribution of EdU labelled cells.

Schematic diagram depicting EdU addition following 3 DIV for 6 hours. EdU count as a % of control slices for (B) central canal area and (C) total slices. (D) EdU mean area % coverage as a function of radial distance from the central canal. Data presented as mean ±SE. Individual data points represent mean values from each repeat. N=3, n>3, * P≤0.05, **P≤ 0.01. (E) Representative EVOS images of half a cultured spinal cord slice for each condition, central canal highlighted with dashed circle. Scale bars = 500 µm.

Spinal cord slices were then cultured on hydrogels in the presence of EdU for 18 hours, this time with an additional commercial hydrogel: VitroGel (Figure 6.5 A). Whilst not statistically significant, the number of EdU+ve cells detected at the central canal of slices cultured on VitroGel hydrogels was 37% greater than that of the control. This was however, significantly greater than the corresponding value found for slices cultured on collagen hydrogels (Figure 6.5 B, mean difference ±SE of difference: 12.75 ±4.384; P = 0.0434).

As previously found, there was a reduced number of EdU+ve cells for all slices cultured on collagen and HyStem hydrogels compared to control, with significantly fewer *total* EdU+ve cell counts compared to control (Figure 6.5 C, mean difference ±SE of difference: collagen= -1158 ±318.5, p= 0.0043; HyStem= -1074 ±296.5; P = 0.0045). The mean total number of EdU+ve cells in slices cultured on VitroGel hydrogels was similar to that of control and as found previously, the distribution of EdU+ve cells remained similar in control and hydrogel conditions (Figure 6.5 D and E).

6.3.2 Effect of SDF-1α on spinal cord slice cultures

6.3.2.1 SDF-1α does not affect the number or distribution of EdU-labelled cells *in vitro*

Slices were cultured on collagen hydrogels ±SDF-1α for 4 DIV and EdU was added to the culture medium for the final 18 hours to detect proliferating cells (Figure 6.6 A). Collagen was selected as this previously resulted in the greatest change to proliferating cell numbers (Figure 6.5). SDF-1α did not affect the number of EdU+ve cells or their distribution within the cultured slice compared to collagen hydrogels alone (Figure 6.6 B-E). There was a trend towards reduced EdU+ve cell counts at the central canal and in the total slice compared to control slices for collagen hydrogels with/without SDF-1α as seen previously (Figure 6.6).

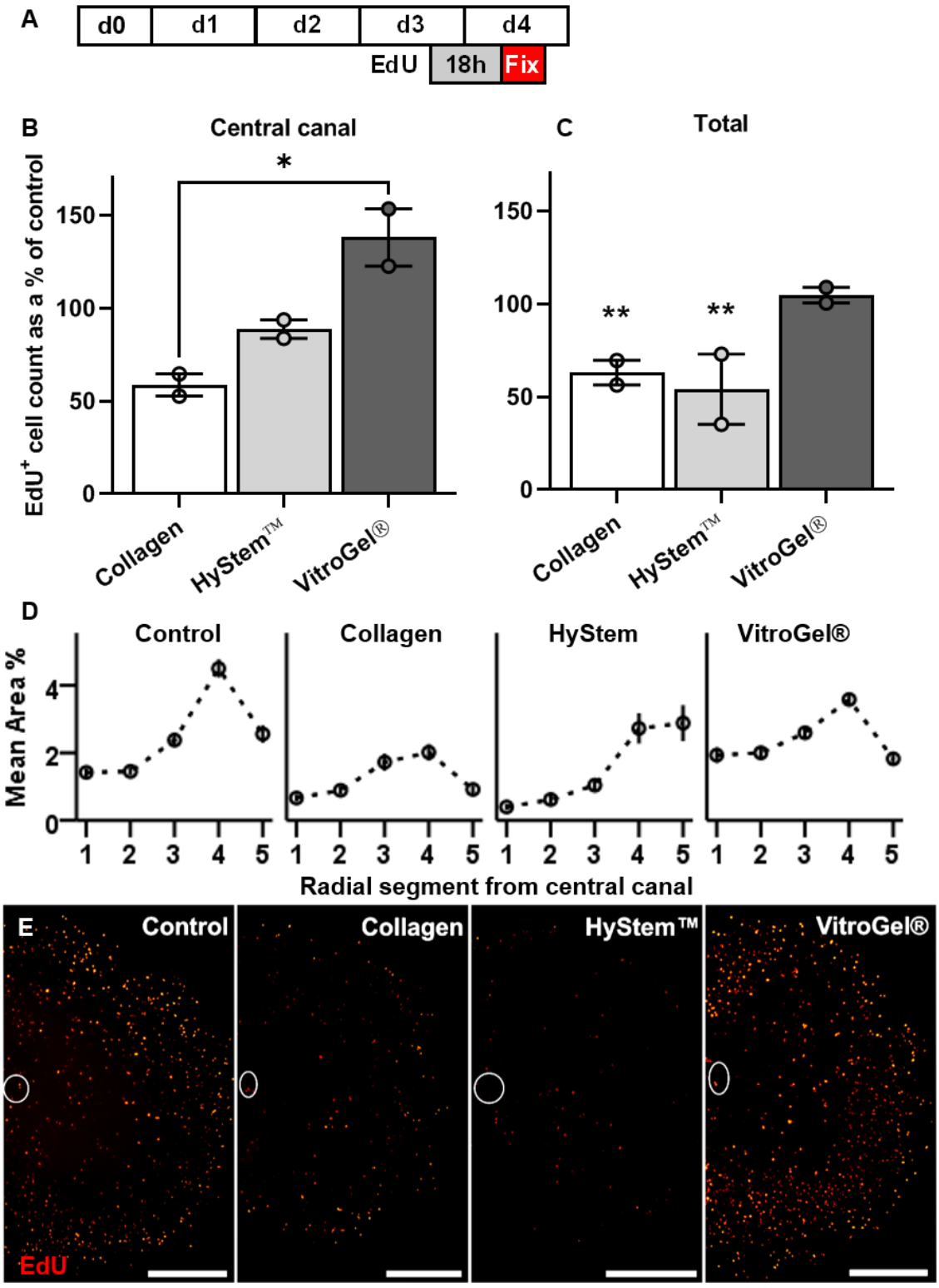

Figure 6.5 Effect of hydrogels on OSCSC EdU labelled cells.

(A) Schematic diagram depicting EdU addition following 3 DIV for 18 hours. EdU count as a % of control slices for (B) central canal area and (C) total slices. (D) EdU mean area % coverage as a function of radial distance from the central canal. Data presented as mean ±SE. Individual data points represent mean values from each repeat. N=2, n>3, * P ≤ 0.05, ** P ≤ 0.01. (E) Representative images of half a cultured spinal cord slice for each condition, central canal highlighted with dashed circle. Scale bars = 500 µm

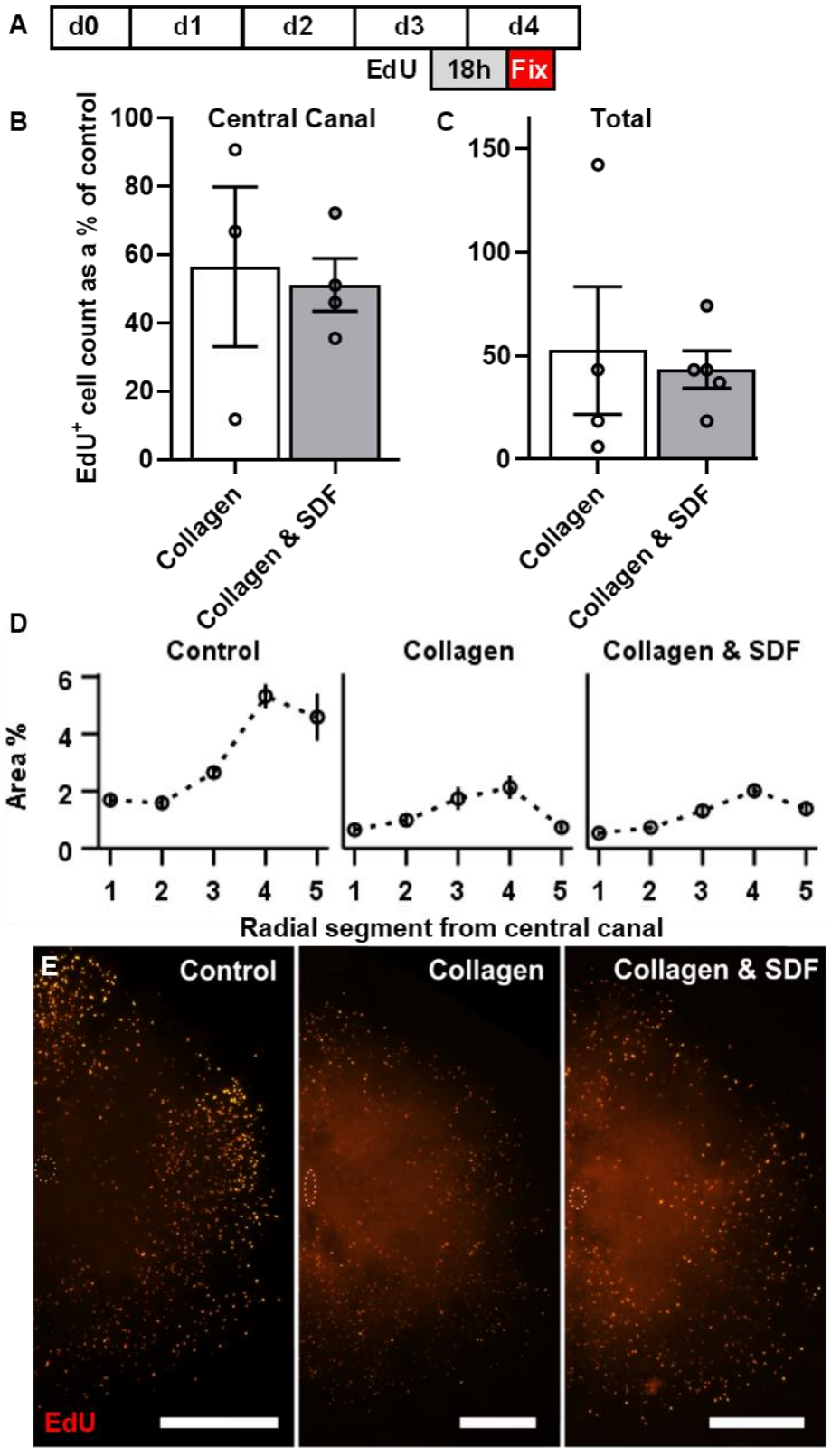

Figure 6.6 Effect of SDF-1α on EdU labelled cell distribution in OSCSCs.

Schematic diagram depicting EdU addition following 3 DIV for 18 hours. EdU count as a % of control slices for (B) central canal area and (C) total slices. (D) EdU mean area % coverage as a function of radial distance from the central canal. Data presented as mean ±SE. N=1, n>3. (E) Representative images of half a cultured spinal cord slice for each condition, central canal highlighted with dashed circle. Scale bars = 500 µm.

6.3.2.2 SDF-1α does not affect the GFP projections from central canal

Following the addition of SDF-1α into the culture medium for either 1 or 2 days *in vitro*, the central canal (nestin) GFP projections were assessed by measuring the number of primary projections, the number of branches, the branch length, and the number of secondary branches compared to control slices (Figure 6.7).

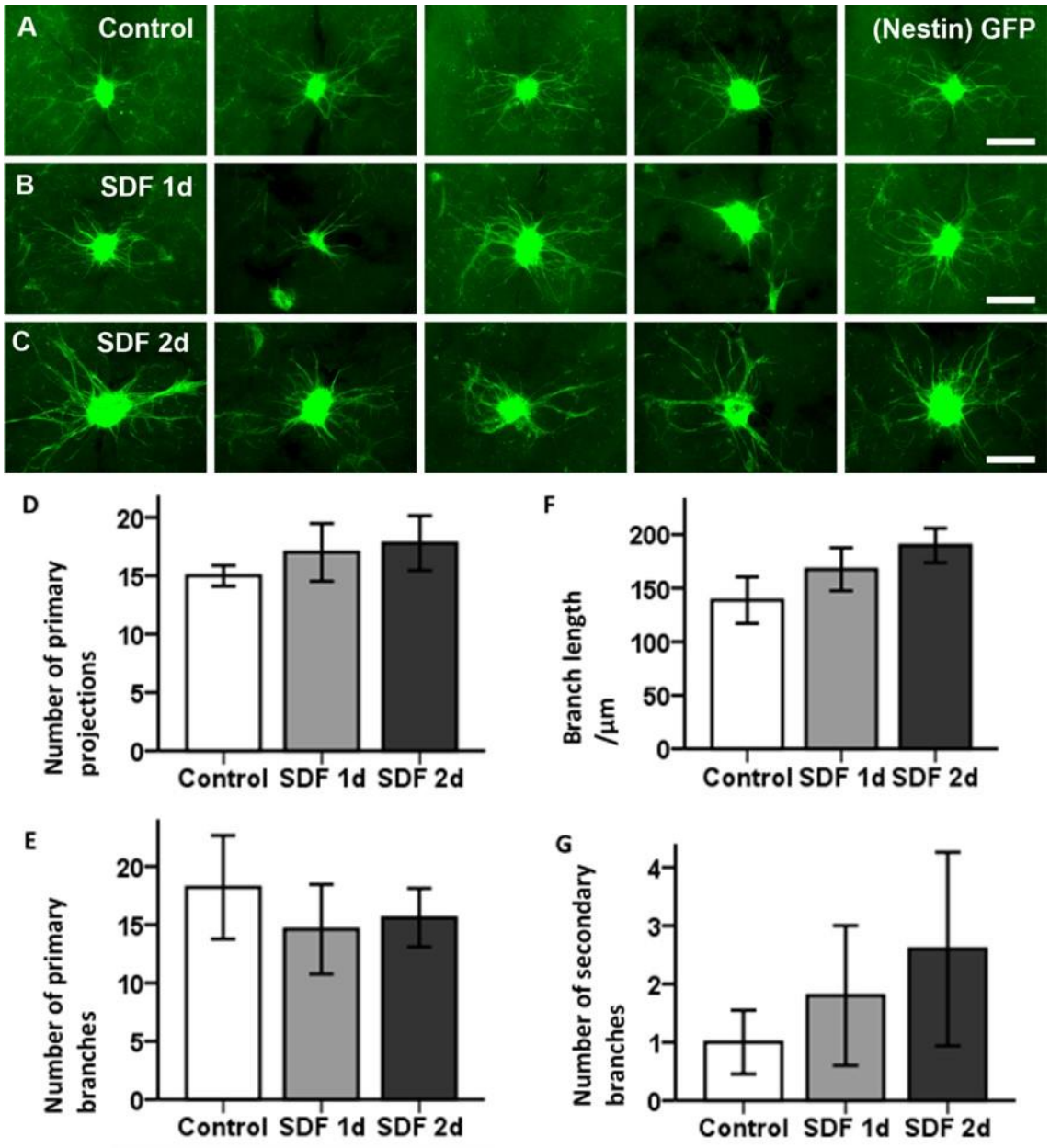

Figure 6.7 Effect of SDF-1α on cultured spinal cord slice central canal (Nestin) GFP projections and branching characteristics.

EVOS images of the central canal region for (A) control and (B & C) SDF treated slices. (D) Mean number of primary projections, (E) branches, (F) length of branches, and (G) number of secondary branches. Data presented as mean ±SE. N=1, n=5. Scale bars = 275 µm. Slices were cultured for 4 days *in vitro* with 1 µM SDF-1α added into the culture medium for either 1 or 2 days prior to fixation and imaging.

Whilst not statistically significant, the number of primary projections, branch length, and the number of secondary branches appeared to increase with increasing SDF addition (Figure 6.7 D, F, and G) indicating SDF may influence (nestin) GFP processes at the central canal. An increased number of repeats would be required in order to investigate this trend further.

6.3.2.3 SDF-1α does not affect the radial distribution of (Nestin) GFP+ve cells *in vitro*, but may influence cell migration

The effect of a concentration gradient of SDF-1α was then investigated using a method developed by (Addington et al., 2015). The radial distribution of (nestin) GFP remained similar for slices cultured on collagen hydrogels with SDF-1α and/or AMD3100 (CXCR4 antagonist), compared to control slices, with the majority of GFP % fluorescence remaining at the central canal (Figure 6.8 A). Interestingly, in slices with a gradient of SDF-1α (SDF x2), there was an increase in (Nestin) GFP fluorescence in the grey matter (Figure 6.8 A, radial segments 2 and 3), however it isn't clear whether this is due to cell migration. When cultured with SDF-1α, GFP+ve cells were also found to migrate through the collagen hydrogels (towards the higher SDF-1α concentration in the culture medium) and attach to the culture insert, similar to when the slice was cultured directly onto the insert (Figure 6.8 B). This was not seen for slices cultured on collagen gels without SDF-1α, or with AMD3100.

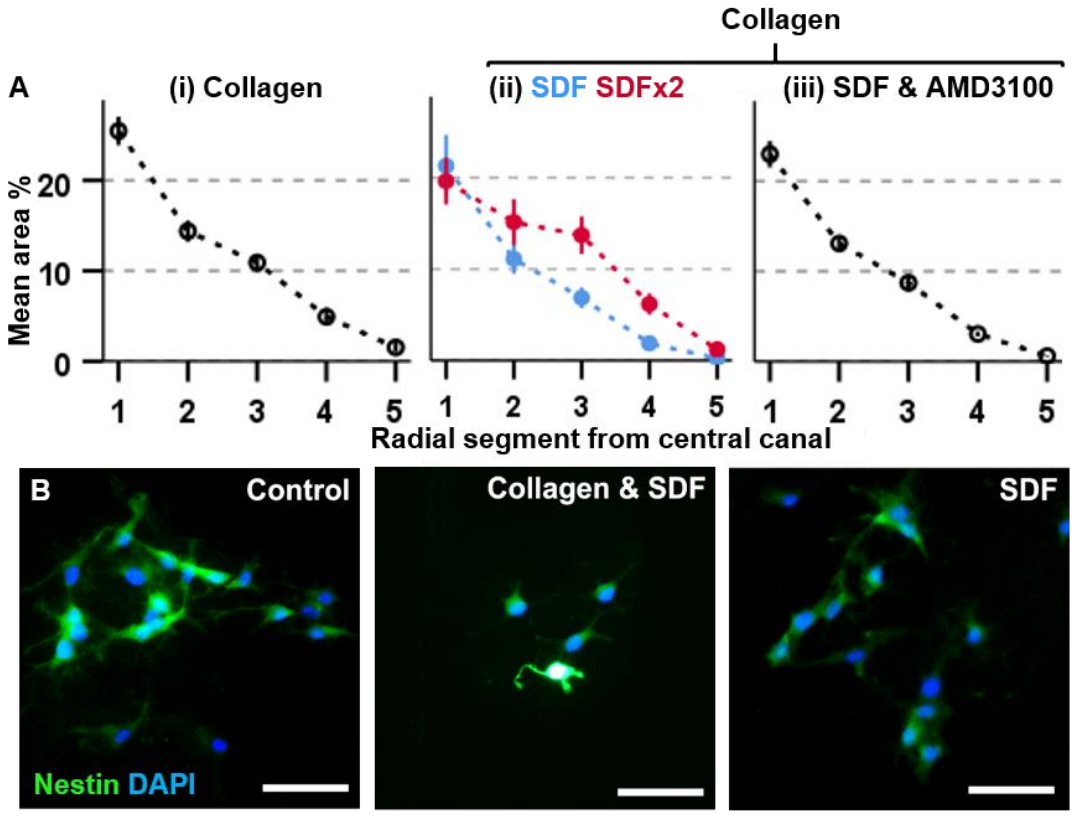

Figure 6.8 Effect of SDF-1α and AMD3100 on (nestin) GFP distribution and migration

(Nestin) GFP mean area % coverage as a function of radial distance from the central canal for slices cultured on collagen hydrogels either (i) alone, (ii) with uniform SDF (blue) or an SDF gradient (SDF x2 - red), or (iii) with SDF & AMD3100. Data presented as mean ±SE. (B) EVOS images of (Nestin) GFP+ve cells on culture inserts (DAPI co-stain) where control= no hydrogel or SDF, and SDF= no hydrogel. N=1, n>3. Scale bars = 20 µm.

6.3.3 Effect of Injecting SDF-1α Intra-Spinally Within a Hydrogel *in Vivo*

The effect of SDF-1α was then assessed *in vivo.* VitroGel was used as it is sterile, shear-thinning and recoverable, and therefore suitable for injecting *in vivo*. VitroGel was injected ±SDF-1α intra-spinally and proliferating cells were labelled via EdU injection at 24 and 48 h post-surgery. A number of EdU+ve cells were detected at the central canal (Figure 6.9 a i) and grey matter surrounding the injection site (Figure 6.9 a ii), presumably due to the injury caused by the needle. (Nestin) GFP+ve cells were also found throughout the spinal cord, with extended GFP processes projecting

dorsoventrally from the central canal (Figure 6.9 b i). (Nestin) GFP+ve cells were also found surrounding the injection sites (Figure 6.9 bii).

The number of proliferating cells was then quantified. When the whole slice was counted, there were significantly more EdU+ve cells at the level of injection (Figure 6.10 A, level 0) in animals injected with hydrogels with SDF-1α (N=2, n=6; 715.83 ±116.7) compared to those injected with hydrogel alone (N=2, n=8, 347.50 ±56.88; P = 0.024). At levels rostral to the injection site (levels -2 to -4), the number of EdU+ve cells in the entire slice was significantly lower in the tissue from the SDF-1α loaded hydrogels, compared to the hydrogel control (P = 0.012 to <0.0001) indicating potential migration of proliferating cells to the injury site.

The same trend in EdU+ve counts was seen in the white and grey matter (WM and GM respectively), when counted separately. There were significantly more EdU+ve cells in the WM at the level of injection (Figure 6.10 B, level 0) in animals injected with hydrogel with SDF-1α (n=8, 191.50 ±13.43) compared to those injected with hydrogel alone (n=6, 82.63 ±4.953; P = 0.0002). Whilst there were more EdU+ve cells at the level of injection in the grey matter of animals injected with hydrogels with SDF-1α compared to the hydrogel control, this was not significantly different (Figure 6.10 C, level 0; P = 0.08).

At the central canal, there was no significant difference in EdU+ve cell counts at the level of injection (Figure 6.10 D, level 0). At levels rostral to the injection site (levels -4 to -2), the number of central canal EdU+ve cells was slightly lower in the hydrogel with SDF-1α condition compared to hydrogel alone, although this was not statistically significant.

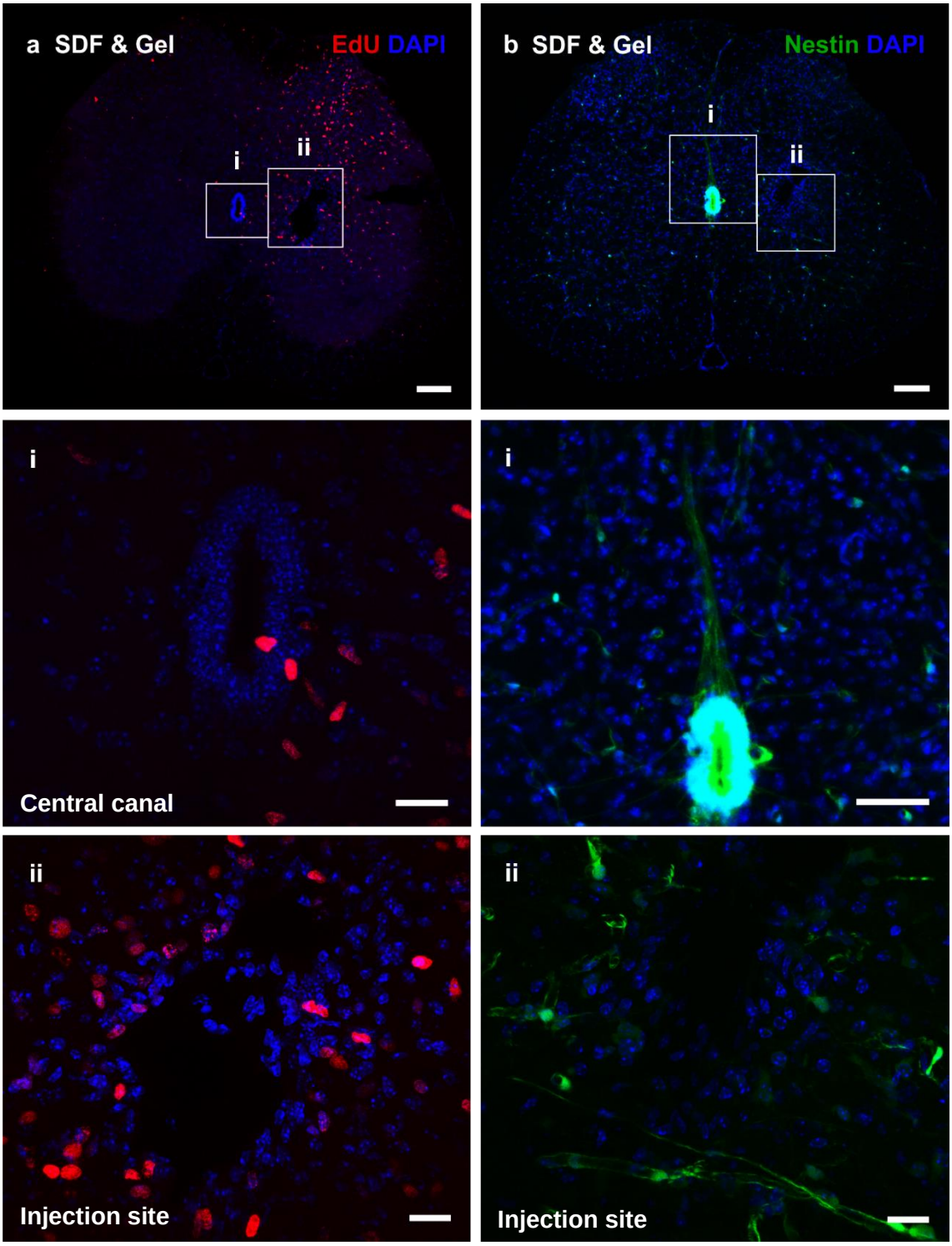

Figure 6.9 Effect of delivering SDF-1α intra-spinally within a hydrogel *in vivo*.

Representative confocal images taken at the level of injection showing EdU labelled cells (red) and DAPI labelled cell nuclei (blue) (b) and (nestin)GFP (green) and DAPI labelled cell nuclei (blue) (c) at the central canal region (i) and injection site (ii). Scale bars: a, b & bi = 100 µm, ai & bi/ii = 20 µm

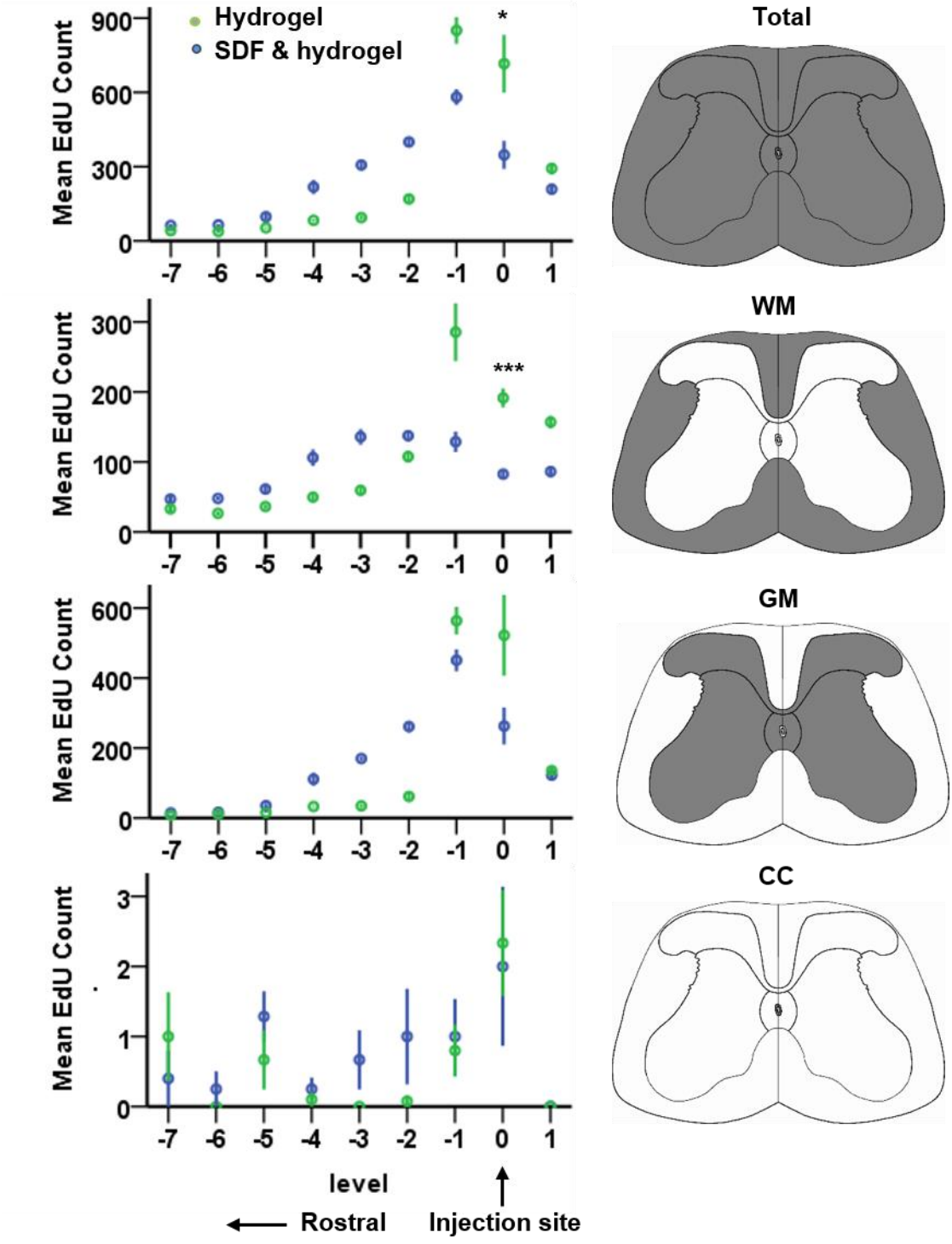

Figure 6.10 Effect of delivering SDF-1α intra-spinally within a hydrogel *in vivo* on EdU counts.

Mean count of EdU+ve cells at the site of injection (0) and levels rostral (negative) and caudal (positive) for control hydrogel-injected animals (blue) and hydrogel & SDF-1α-injected animals (green). Total (A), white matter (WM), grey matter (GM), and central canal (CC) counts. Each level incorporates data from N=2 per condition, n<6 sections, covering a length of ~480 µm spinal cord (a). Data presented as mean ±SE. * P ≤ 0.05, *** P ≤ 0.001.

6.4 Discussion

This chapter aimed to investigate manipulating ependymal cells using hydrogels and the chemokine, SDF-1α. The response of spinal cord cells varied depending on the hydrogel.

Important findings:

- Culturing spinal cord slices on collagen hydrogels leads to a ~50% reduction in central canal cell proliferation compared to control
- Culturing spinal cord slices on collagen hydrogels also leads to an overall reduction of cell proliferation throughout the spinal cord slice, compared to control
- Spinal cord slices cultured on Hystem hydrogels had slightly less proliferation at the central canal and a significant reduction in the proliferation in the whole slice
- Slices cultured on VitroGel hydrogels had significantly more central canal proliferation compared to collagen hydrogels
- The total cell proliferation throughout the spinal cord slice was similar in slices cultured on VitroGel hydrogels and control slices

In OSCSCs, SDF-1α didn't appear to impact:

    - Proliferation levels
    - EdU+ve cell distribution
    - (Nestin) GFP central canal radial processes
    - (Nestin) GFP cell distribution

- However, an SDF-1α concentration gradient may influence ependymal cell migration as (nestin) GFP cells migrated through hydrogels along the concentration gradient
- Injecting SDF-1α within a hydrogel intra-spinally results in significantly more EdU+ve cells at the level of injection in: (a) the whole slice, (b) the white matter (c) the grey matter, compared to control animals.

6.4.1 Effect of hydrogels on ependymal cell behaviour

There was a reduced number of proliferating cells when slices were cultured on hydrogels (with the exception of VitroGel). It is unclear whether this was due to the migration of proliferating cells into the hydrogel that were subsequently not detected; due to a reduction in proliferating cell survival (or overall cell viability); or indeed a true reduction in proliferation, potentially as a result of minimised or alleviated injury response.

We attempted to unpick this trend by labelling and imaging cells within the hydrogels to determine if any migration had occurred, however had minimal success. This was due to the auto fluorescence of collagen fibrils hindering imaging of cells within some hydrogels, along with the processing and re-sectioning of hydrogels and tissue slices leading to tissue fragility and loss. Alternatively, DAB (3,3′-diaminobenzidine) could be used to visualise (using light microscopy) horseradish peroxidase-conjugated secondary antibodies; potentially allowing for the quantification of cells within hydrogels.

In addition to these methodological challenges, it is also unclear what a “good” proliferative response would be. As previously discussed, we observed what we believe to be an injury response in control cultures (see Chapter 5). As such, a reduction in the proliferation of cells when cultured on softer hydrogels may be indicative of the hydrogel having a protective effect on the cells, thus reducing their response to injury. Changes in inflammatory cytokine release (using RNase protection assay and/or enzyme-linked immunosorbent assay) would help confirm this hypothesis. Additionally, immunofluorescence to determine the reactivity state of astrocytes and the cell lineage of differentiated ECs would further determine the protective nature of hydrogels on OSCSCs.

A significant increase in cell proliferation at the central canal of slices cultured on VitroGel hydrogels was observed compared to collagen hydrogels. VitroGel has a

reported elastic modulus of around 1000 Pa (when diluted at 1:1 with VitroGel dilution solution, created using DMEM, and incubated at 37 °C for 24 hours prior to testing), and is therefore the stiffest hydrogel trialled (compared to: collagen ~100-650 Pa, HyStem ~110 Pa, HyStemC ~159 Pa). This difference in hydrogel stiffness could be causing the change in cell proliferation at the central canal, and leading to a total cell proliferation count similar to control slices cultured directly on culture inserts. However, discrepancies between the hydrogel composition reported in literature and that used in this thesis could mean the stiffness reported may not be truly representative of the VitroGel hydrogel used in this experiment. Furthermore, the rheological testing methodologies used to characterise the VitroGel and HyStem hydrogels were not the same as that used to characterise the collagen hydrogels developed in-house (see Table 6.0), and therefore these values may not be directly comparable. Further experiments are required in order to determine a relationship between cell proliferation trends and the mechanical properties of the hydrogel substrate.

6.4.2 Effect of SDF-1α on ependymal cell behaviour

The results in this chapter show the delivery of SDF-1α had no measurable effect on the central canal (nestin) GFP processes extending radially in vitro, however, these were difficult to characterise and varied highly between cultured slices. Migration to a chemotactic gradient of SDF-1α is thought to be concentration-dependent. In this chapter a concentration of 1000 ng/mL (126.6 nM) SDF-1α was selected for in vitro studies, as this concentration has been shown to result in increased proliferation and migration of human neural stem cells in vitro (Imitola et al., 2004), however, this concentration may not be optimal for directing EC migration and proliferation and further optimisation may be required. Interestingly, a gradient of SDF-1α resulted in an increase in a mean area % for the (nestin) GFP fluorescence within the white and grey matter of cultured slices compared to slices with uniform SDF-1α delivery. Additional

chemotaxis experiments are required to confirm this observation (e.g. Boyden chamber assay).

We also show potential cell migration *in vivo* from the area rostral to the injection site, towards SDF-1α. These preliminary data indicate the injection of SDF-1α within a hydrogel could be a potential method for recruiting endogenous ECs to the site of injury. Research in our lab has shown that EC proliferation can be increased *in vivo* using the nicotinic acetylcholine receptor modulator PNU-120596 (Corns et al., 2015). Therefore a combinatorial approach, delivering SDF-1α and PNU, post-injury may give rise to increased migration and proliferation of ECs for spinal cord repair.

Future experiments utilising immunofluorescence for fate mapping would determine if ECs can also be manipulated *in vitro* and *in vivo* into forming oligodendrocytes and/or neurons. Additional *in vivo* experiments are required in order to investigate the potential benefits of directed migration following injury. This could be achieved by creating an injury to the spinal cord followed by delayed injection of a hydrogel with SDF-1α. This study may recreate the injury response seen in human patients and determine if directed migration occurs in an inflamed spinal cord.

The complex balance between stem cell retention and chemotaxis via SDF-1/CXCR4 binding may further complicate regenerative strategies. Functional repair wasn't improved in rats when treated with SDF-1 following spinal cord injury (Pakulska et al., 2017). The CXCR4 antagonist AMD3100 has been shown to mobilise progenitor cells from the bone marrow (Dar et al., 2011) and a similar approach may be required within the CNS for endogenous stem cell recruitment and tissue repair. Whether manipulating ECs in vivo using SDF-1α leads to an improvement in the physiological recovery following spinal cord injury is unclear.

6.5 Conclusions

1. The proliferation of cells within the spinal cord can be manipulated using a number of hydrogels
2. Delivering a concentration gradient of SDF-1α *in vitro* may trigger ependymal cell migration
3. Delivering SDF-1α *in vivo* within a hydrogel leads to an increase in the number of proliferating cells at the level of injection – potentially via recruitment of dividing cells rostral to the injection site

Overall, this results in this suggest that cell proliferation within the spinal cord can be manipulated using hydrogels; and delivering a gradient of the chemoattractant SDF-1α may trigger the directed migration of ependymal cells.

Chapter 7 – General Discussion

7.1 Summary

This study has highlighted the complex nature of spinal cord repair. Injuries to the CNS cause a myriad of cell behaviour changes; all influenced by a number of intrinsic and extrinsic processes and cellular cascades.

Novel developments made include:

- Characterisation of (nestin)GFP expression in the spinal cord of transgenic mice
- Development protocols for the detection of proliferating cells *in vitro* and *in vivo,* reducing the detrimental effect of Cu(II) on GFP fluorescence
- Investigation into the behaviour of ependymal cells in organotypic spinal cord slice culture
- Optimisation of culture conditions for the detection of proliferative changes at the central canal following injury
- Potential manipulation of ependymal cells using hydrogels and SDF-1α

7.1.1 Investigating the potential manipulation of hydrogel mechanical properties

A number of collagen hydrogel variants were synthesised with the aim of manipulating mechanical properties independently of the physical structure of the resulting gel matrix. Altering the collagen concentration was shown not only to impact the mechanical properties of the hydrogel, but also the porosity. Additionally, modulating the crosslinker molar ratio was investigated, however this wasn't shown to impact the mechanical or physical properties of the hydrogels formed. Finally, the crosslinker was varied to see if changes in the chemical structure resulted in changes to the hydrogel

mechanical properties as a result. In contrast to previous research (Head et al., 2016), the storage modulus of hydrogels was not shown to reliably change as a result of crosslinker structural changes. As a result, I was not able to determine the effect of collagen hydrogel stiffness on ependymal cell behaviour as initially planned.

7.1.2 Characterisation of (nestin) GFP expression

Characterisation of (nestin) GFP expression in transgenic mice was carried out within this thesis; identifying the spinal cord ependymal cells as GFP+ve and expressing a number of stem cell markers. ECs were colocalised with antibodies against: CD24, Galectin-3, NKA-α1, Sox2, vimentin, CD63, CXCR4, foxJ1, and calbindin-D28k. I also demonstrate that (nestin) GFP expression within the SC of these transgenic mice is limited to ECs and pericytes, and at the central canal, (nestin) GFP is specific to ECs and does not label CSFcCs. Additionally, I have shown that ECs express the exosomal marker CD63 and therefore may sense changes in the CSF following injury and modulate the neurogenic niche via released exosomes. Immunofluorescence labelling also highlighted that ECs express CXCR4 and galectin-3, targeting of which may prove useful for the manipulation of endogenous cells.

7.1.3 Optimised culture methods

Experiments within chapter 5 enabled the detection of proliferating cells within fluorescent transgenic tissue. Picolyl azide was used to raise the effective concentration of the Cu(II) catalyst for the detection of EdU incorporated within the DNA of dividing cells. Additionally, spinal cord slice culture conditions were investigated and optimised; enabling the detection of injury-induced proliferation changes in pre-weaner mice.

Pre-weaner mice were used in this chapter as our group previously determined optimal cell survival in cultured slices from animals of this age, compared to older animals (unpublished observation). Pre-weaner animals were also used in order to minimise the injury response as a result of slicing, however, for a traumatic injury model adult

animals may have been more appropriate (Pandamooz et al., 2019). Organotypic spinal cord slice cultures, as with other *in vitro* methods, are a simplified system lacking blood supply and therefore exclude the inflammatory response and any blood-borne substances that may be critical in manipulating EC behaviour in vivo. However, they do present a method by which cell-cell and cell-ECM interactions may be investigated, and so offer an insight into tissue engineering opportunities.

7.1.4 Manipulation of ependymal cells using hydrogels and the chemokine SDF-1α

The response of cells within spinal cord slices was shown to vary depending on the hydrogel substrate used. Collagen hydrogels were shown to reduce the central canal cell proliferation by around 50%, and an overall reduction in cell proliferation compared to control culture inserts. Additionally, culturing spinal cord slices on VitroGel hydrogels resulted in significantly more cells proliferating at the central canal compared to control. The trends observed using commercial hydrogels and those developed in-house show promise with regards to cell manipulation. The collagen and HyStem hydrogels used in this thesis have elastic moduli of ~100 to 650 Pa whereas VitroGel hydrogels are reported to have a gel strength of around 1000 Pa. The reduction in cell proliferation when cultured on softer hydrogels (collagen and HyStem) could be due to the mechanical properties of the substrate, however further research is required in order to determine the factors directing this response (e.g. matrix material, porosity, stiffness).

Interestingly, uniform delivery of SDF-1α *in vitro* wasn't shown to significantly affect the number or distribution of proliferating cells within the spinal cord. A concentration gradient of SDF-1α however, was shown to influence ependymal cell migration and injecting SDF-1α (within a hydrogel) into the spinal cord of adult mice resulted in the detection of significantly more proliferating cells at the level of injection in both the whole slice as well as the white matter and grey matter when analysed separately. This

preliminary data therefore shows the promise of ependymal cell migration towards the chemokine SDF-1α.

7.2 Applicability of these results to humans

It was long believed that the postnatal central nervous system of mammals was devoid of newly born neurons. However, following advances in the labelling of proliferating cells; autoradiographic and histological data provided evidence to the contrary (Altman and Das, 1965). The evidence of adult hippocampal neurogenesis in rats propelled postnatal neurogenesis into the forefront of neuroscience research and since then, numerous investigations have also debated the existence of neurogenesis within the spinal cord.

Recent work has shown that the cells around the central canal are capable of proliferating and differentiation into multiple lineages in response to injury (Takahashi et al., 2003; Hugnot, 2011). As such, manipulating the behaviour of the endogenous ependymal cells of the central canal presents an alternative to stem cell therapies for spinal cord repair following injury or disease (Barreiro-Iglesias, 2010).

Proliferation of ependymal cells in response to other neurodegenerative diseases has been investigated. Ependymal cells isolated from symptomatic G93A-SOD1 mice presenting motoneuron degeneration as a model of amyotrophic lateral sclerosis (ALS) showed increased proliferation and migration compared to asymptomatic and wild type (WT) mice (Guan et al., 2007). Additionally, neurosphere-forming ECs from these mice preferentially differentiated into neurons over astrocytes; opposite to the trend seen in WT controls where astrocyte differentiation prevailed.

Ependymal cells are not thought to proliferate in response to demyelination induced by experimental models of multiple sclerosis (MS) (Lacroix et al., 2014); indicating

regenerative strategies aimed at the manipulation of these cells for increased remyelination are required.

Whether humans have ependymal cells that respond in a similar way to animal models is greatly debated (Garcia-Ovejero et al., 2015; Paniagua-Torija et al., 2018). Similar to the spinal cord stem cell niche of mice, some of the ependymal cells of the human central canal express the stem cell markers: nestin, sox2, and CD15 (a marker of SVZ neural stem cells) (Dromard et al., 2008). Recent RNA profiling of ependymal cells also indicated a number of transcription factors and genes are conserved between adult humans and rodents (Ghazale et al., 2019). *In vitro* studies have also evidenced the multipotent nature of human stem cells; with nestin and sox2 expression seen in neurospheres formed when cultured in growth factor (EGF and FGF) supplemented medium (Mothe et al., 2011).

7.3 Future experiments

The experiments in this thesis have set the foundations for future elucidation of the factors influencing ependymal cell behaviour. The data presented indicate that ependymal cells may be manipulated using biomaterials and chemokines however, the fate of such cells is yet to be determined and a number of questions remain:

- What is the origin and ultimate fate of the proliferating cells detected *in vitro* and *in vivo*?

Future studies using transgenic fate mapping in combination with immunofluorescence would further determine the regenerative potential of ependymal cells following SCI and address this question. Additionally, inducible transgenic reporter lines (e.g. under the control of the foxJ1 reporter) whereby ependymal cell progeny are labelled would allow for the assessment of hydrogels and chemokines over longer time frames. This

would also enable further distinction between migratory proliferating ependymal cells and other cells proliferating in the white and grey matter of the spinal cord.

- Which cell response would be desirable following injury (i.e. would an increase or decrease in proliferation be beneficial for repair), and do these cell responses correlate with functional repair and physiological recovery?

Whether manipulating ECs *in vivo* following injury leads to an improvement in the physiological recovery following spinal cord injury is unclear and so behavioural studies in rats would be critical.

Additional studies investigating the response of ependymal cells *in vitro* and *in vivo* are required in order to increase sample sizes, and thus the statistical power of our conclusions. Furthermore, assessment of the hydrogel properties directing ependymal cell behaviour would enable regenerative strategies to be designed according to the cell-response desired. Therefore, the correlation of functional repair with cell behaviour in organotypic slice models would enable the screening of a library of regenerative strategies and minimise the use of animals in future experiments

- What delivery paradigm/injury model would best recapitulate the spinal cord injuries experienced by humans (i.e. when should SDF-1α be delivered following injury)?

Additional factors to consider when translating research to human spinal cord injury regeneration strategies include the delivery paradigm for patients, and how this may impact the potential manipulation of endogenous repair. Patients presenting to A&E with traumatic spinal cord injury often also have life-threatening comorbidities requiring immediate stabilisation and treatment. Referral of these patients to a specialised SCI centre once fit-for-transfer typically occurs within the first 24 hours in the UK, however spinal surgery may not be available immediately; further limiting standardised SCI treatment and restricting the opportunity for delivering regenerative interventions (National Spinal Cord Injury Strategy Board, 2012).

Additionally, non-traumatic spinal cord injury, including spinal cord tumours and prolapsed intervertebral disks impact the spinal cord over longer periods of time; leading to further challenges with regards to repair. Further work is required to establish the optimal time point at which SCI repair strategies should be delivered, in addition to determining the effects deviating from this would cause.

7.4 Conclusions

The studies carried out in this thesis have provided evidence that the ependymal cells of the murine spinal cord possess stem cell markers and can be manipulated using hydrogels and chemokines. Promising preliminary data showed ependymal cell migration may be directed via the delivery of exogenous SDF-1α; indicating the potential for targeting this pool of quiescent stem cells for injury repair. These results also provide an insight into ependymal cell behaviour within organotypic spinal cord slice cultures and the methods developed will be crucial for the assessment of regenerative strategies. As a result, this thesis has provided a platform from which future experiments will be able to assess cell mechanosensory behaviour in response to biomaterial substrate stiffness.

Chapter 8 Supplementary data

Table 8.1 Rheology frequency sweep data for each hydrogel repeat.

0.5, 1, and 1.5 denote the molar ratio of crosslinker: collagen lys groups. 0.6 and 0.4 refer to the collagen concentration (wt.%). Average G' values are quoted at 0.9976 Hz in this thesis.

4Ph 0.5	1		2		3		Average	
Frequency (Hz)	G' (Pa)	G'' (Pa)	G' (Pa)	G'' (Pa)	G' (Pa)	G'' (Pa)	G' (Pa)	G'' (Pa)
0.5000	353.00	39.20	378.00	40.41	433.70	47.48	388.23	42.36
0.6295	358.80	39.51	383.60	40.55	438.60	46.76	393.67	42.27
0.7924	364.20	38.04	388.70	40.08	443.80	46.66	398.90	41.59
0.9976	370.50	38.32	395.80	39.19	447.80	47.52	404.70	41.68
1.2560	376.60	37.38	401.70	39.25	455.40	47.49	411.23	41.37
1.5810	385.40	32.48	402.80	38.69	465.60	49.62	417.93	40.26
1.9910	385.50	37.64	415.20	40.05	467.70	46.63	422.80	41.44
2.5060	392.20	36.54	421.30	39.58	470.70	47.74	428.07	41.29
3.1550	405.80	42.44	433.70	41.16	481.50	52.49	440.33	45.36
3.9720	415.60	41.07	445.30	40.21	496.40	52.25	452.43	44.51
5.0000	429.30	50.93	460.30	42.07	508.90	54.43	466.17	49.14

4Ph 1	1		2		3		Average	
Frequency (Hz)	G' (Pa)	G'' (Pa)	G' (Pa)	G'' (Pa)	G' (Pa)	G'' (Pa)	G' (Pa)	G'' (Pa)
0.5000	309.30	42.86	392.70	46.53	305.30	36.04	335.77	41.81
0.6295	312.70	42.83	399.30	44.46	310.50	35.58	340.83	40.96
0.7924	317.50	41.71	404.70	44.72	316.50	35.78	346.23	40.74
0.9976	321.60	42.82	411.10	44.93	322.50	33.89	351.73	40.55
1.2560	325.80	43.26	417.40	44.68	327.30	34.60	356.83	40.85
1.5810	335.90	46.43	423.30	50.41	335.00	32.08	364.73	42.97
1.9910	332.60	43.66	431.00	44.95	336.80	35.02	366.80	41.21
2.5060	339.30	43.80	436.80	44.67	343.50	35.55	373.20	41.34
3.1550	347.30	46.22	447.60	45.95	358.20	33.19	384.37	41.79
3.9720	357.70	46.45	462.70	50.25	366.00	36.69	395.47	44.46
5.0000	372.40	52.60	476.20	52.71	382.10	43.49	410.23	49.60

4Ph 1.5	1		2		3		Average	
Frequency (Hz)	G' (Pa)	G'' (Pa)	G' (Pa)	G'' (Pa)	G' (Pa)	G'' (Pa)	G' (Pa)	G'' (Pa)
0.5000	375.80	46.45	393.00	46.79	350.00	41.39	372.93	44.88
0.6295	382.90	44.89	399.00	46.17	356.10	39.89	379.33	43.65
0.7924	388.90	44.94	404.80	45.48	361.00	38.16	384.90	42.86
0.9976	395.20	44.67	410.20	45.06	367.70	40.52	391.03	43.42
1.2560	401.50	44.49	417.80	45.73	372.90	40.39	397.40	43.54
1.5810	413.60	44.97	419.40	46.83	387.40	39.62	406.80	43.81
1.9910	415.30	43.95	430.30	45.07	383.90	40.22	409.83	43.08
2.5060	422.10	44.26	435.30	46.20	388.10	41.19	415.17	43.88
3.1550	434.70	43.39	445.30	45.22	399.90	44.50	426.63	44.37
3.9720	447.00	49.84	459.90	46.75	413.40	44.21	440.10	46.93
5.0000	462.60	51.28	477.20	48.98	430.90	50.60	456.90	50.29

4Ph 0.4	1		2		3		Average	
Frequency (Hz)	G' (Pa)	G'' (Pa)	G' (Pa)	G'' (Pa)	G' (Pa)	G'' (Pa)	G' (Pa)	G'' (Pa)
0.5000	80.65	10.01	70.42	8.09	85.90	10.40	78.99	9.50
0.6295	81.18	9.81	72.72	8.36	87.40	9.17	80.43	9.11
0.7924	82.25	10.52	74.72	8.18	86.63	9.02	81.20	9.24
0.9976	83.63	9.15	77.88	7.63	82.85	8.99	81.45	8.59
1.2560	86.20	9.13	79.10	8.35	81.07	11.34	82.12	9.61
1.5810	92.25	10.32	76.49	8.43	76.59	4.75	81.78	7.83
1.9910	90.35	8.72	83.16	7.78	83.95	10.06	85.82	8.85
2.5060	96.16	10.35	88.78	10.28	92.62	9.94	92.52	10.19
3.1550	104.50	12.00	97.52	11.32	104.20	7.57	102.07	10.30
3.9720	109.40	11.90	102.60	10.88	108.00	12.23	106.67	11.67
5.0000	120.10	14.95	114.90	15.01	118.60	9.55	117.87	13.17

4Ph 0.6	1		2		3		Average	
Frequency (Hz)	G' (Pa)	G'' (Pa)	G' (Pa)	G'' (Pa)	G' (Pa)	G'' (Pa)	G' (Pa)	G'' (Pa)
0.5000	196.90	23.82	232.30	25.89	177.00	20.44	202.07	23.38
0.6295	200.70	25.41	236.40	24.91	180.10	20.47	205.73	23.60
0.7924	204.40	22.87	238.90	25.76	183.30	20.28	208.87	22.97
0.9976	206.50	23.38	243.60	25.72	185.30	19.62	211.80	22.91
1.2560	211.80	21.98	246.60	23.84	187.20	19.76	215.20	21.86
1.5810	207.40	23.29	242.40	24.61	182.30	22.55	210.70	23.48
1.9910	214.50	22.58	247.30	24.24	190.60	18.53	217.47	21.78
2.5060	222.80	22.91	254.90	25.31	198.80	20.26	225.50	22.83
3.1550	232.80	25.48	260.30	25.25	204.60	18.30	232.57	23.01
3.9720	241.80	26.09	275.40	29.79	216.30	21.46	244.50	25.78
5.0000	253.20	30.53	288.30	33.46	230.00	26.67	257.17	30.22

13Ph	1		2		3		Average	
Frequency (Hz)	G' (Pa)	G'' (Pa)	G' (Pa)	G'' (Pa)	G' (Pa)	G'' (Pa)	G' (Pa)	G'' (Pa)
0.5000	296.60	38.09	451.50	48.48	382.20	44.42	376.77	43.66
0.6295	302.00	36.88	459.80	49.01	388.00	43.63	383.27	43.17
0.7924	307.10	36.57	467.00	48.16	393.30	42.90	389.13	42.54
0.9976	312.90	36.08	474.50	47.91	399.50	42.30	395.63	42.10
1.2560	317.40	36.20	482.30	47.76	406.20	43.59	401.97	42.52
1.5810	323.50	29.69	485.90	48.50	417.30	39.76	408.90	39.32
1.9910	326.90	35.10	499.50	46.02	418.90	42.11	415.10	41.08
2.5060	333.60	36.48	507.10	46.99	423.70	43.10	421.47	42.19
3.1550	346.00	35.15	518.50	52.17	439.30	44.84	434.60	44.05
3.9720	355.90	39.64	532.80	52.75	448.10	46.60	445.60	46.33
5.0000	368.40	42.97	550.30	56.41	462.00	56.41	460.23	51.93

Ad	1		2		3		Average	
Frequency (Hz)	G' (Pa)	G'' (Pa)	G' (Pa)	G'' (Pa)	G' (Pa)	G'' (Pa)	G' (Pa)	G'' (Pa)
0.5000	274.90	35.21	320.30	38.32	346.10	41.40	313.77	38.31
0.6295	280.20	35.47	326.60	37.83	351.90	40.70	319.57	38.00
0.7924	285.50	34.62	333.20	36.92	358.00	40.54	325.57	37.36
0.9976	291.40	34.67	339.70	36.29	365.00	40.26	332.03	37.07
1.2560	296.90	34.06	346.10	37.10	371.70	39.99	338.23	37.05
1.5810	300.50	39.09	347.20	41.75	382.90	40.41	343.53	40.42
1.9910	310.40	34.10	355.80	38.19	383.50	40.15	349.90	37.48
2.5060	317.50	33.26	362.90	38.70	389.00	39.39	356.47	37.12
3.1550	325.00	35.21	374.60	41.50	400.60	36.32	366.73	37.68
3.9720	338.50	38.43	387.60	44.62	413.70	43.47	379.93	42.17
5.0000	352.60	39.61	402.60	45.92	428.80	46.75	394.67	44.09

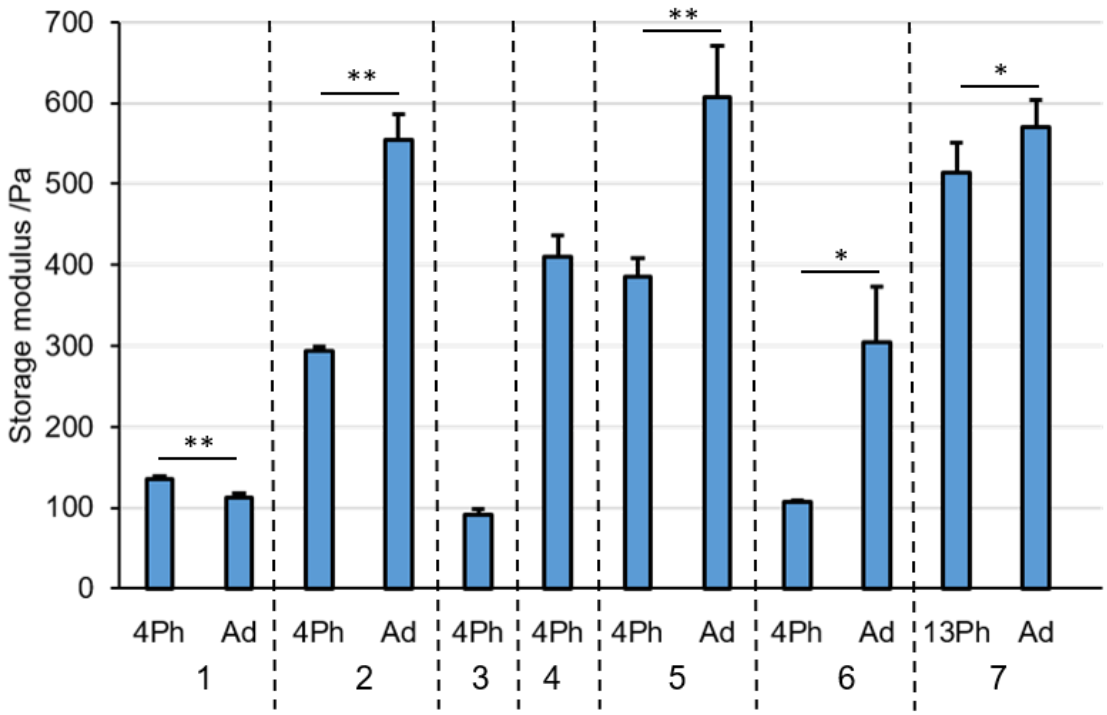

Figure 8.1 Mean storage moduli of hydrogels varies between repeats

Storage modulus determined by rheology frequency sweeps, quoted at 1 Hz. Dashed lines denote separate experiments (i.e. different batches of collagen solution, crosslinker solution batches, and testing dates). Data presented as mean +SD. N=3 for each data point apart from 4Ph, experiments 2 and 6 where N=2. * P ≤ 0.05, ** P ≤ 0.01.

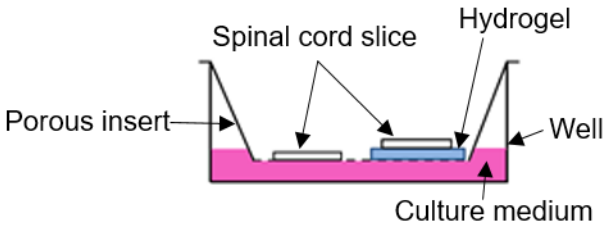

Figure 8.2 Schematic depicting the organotypic spinal cord slice culture set up

Aamar, E. and Dawid, I.B. 2008. Isolation and expression analysis of foxj1 and foxj1.2 in zebrafish embryos. *International Journal of Developmental Biology*. **52**, pp.985–991.

Addington, C.P., Dharmawaj, S., Heffernan, J.M., Sirianni, R.W. and Stabenfeldt, S.E. 2017. Hyaluronic acid-laminin hydrogels increase neural stem cell transplant retention and migratory response to SDF-1α. *Matrix Biology*. **60-61**, pp.206–216.

Addington, C.P., Heffernan, J.M., Millar-Haskell, C.S., Tucker, E.W., Sirianni, R.W. and Stabenfeldt, S.E. 2015. Enhancing neural stem cell response to SDF-1α gradients through hyaluronic acid-laminin hydrogels. *Biomaterials*. **72**, pp.11–19.

Advanced BioMatrix n.d. Mechanical Stiffness Testing of HyStem® Hyaluronic Acid Products.

Ahn, S. and Joyner, A.L. 2005. In vivo analysis of quiescent adult neural stem cells responding to Sonic hedgehog. *Nature*. **437**, pp.894–897.

Aigner, S., Sthoeger, Z.M., Fogel, M., Weber, E., Zarn, J., Ruppert, M., Zeller, Y., Vestweber, D., Stahel, R., Sammar, M. and Altevogt, P. 1997. CD24, a mucin-type glycoprotein, is a ligand for P-selectin on human tumor cells. *Blood*. **89**, pp.3385–3395.

Akeson, W.H., Massie, J.B., Huang, B., Guirea, A., Sah, R., Garfin, S.R. and Kim, C.W. 2005. Topical high-molecular-weight hyaluronan and a roofing barrier sheet equally inhibit postlaminectomy fibrosis. *Spine Journal*. **5**, pp.180–190.

Alfaro-Cervello, C., Soriano-Navarro, M., Mirzadeh, Z., Alvarez-Buylla, A. and Garcia-Verdugo, J.M. 2012b. Biciliated ependymal cell proliferation contributes to spinal cord growth. *Journal of Comparative Neurology*. **520**(15), pp.3528–3552.

Allen Institute for Brain Science n.d. CD63 spinal cord. Available from: http://mousespinal.brain-map.org/imageseries/show.html?id=100020585.

Allen Institute for Brain Science n.d. Mouse Spinal Cord. Available from: http://mousespinal.brain-map.org/.

Altman, J. and Das, G.D. 1965. Autoradiographic and histological evidence of postnatal hippocampal neurogenesis in rats. *Journal of Comparative Neurology*. **124**, pp.319–335.

Andreotti, J.P., Silva, W.N., Costa, A.C., Picoli, C.C., Bitencourt, F.C.O., Coimbra-Campos, L.M.C., Resende, R.R., Magno, L.A.V., Romano-Silva, M.A., Mintz, A. and Birbrair, A. 2019. Neural stem cell niche heterogeneity. *Seminars in Cell and Developmental Biology*. (December 2018), pp.0–1.

Angelastro, J.M., Ignatova, T.N., Kukekov, V.G., Steindler, D.A., Stengren, G.B., Mendelsohn, C. and Greene, L.A. 2003. Regulated expression of ATF5 is required for the progression of neural progenitor cells to neurons. *Journal of Neuroscience*. **23**, pp.4590–4600.

Ansorena, E., De Berdt, P., Ucakar, B., Simón-Yarza, T., Jacobs, D., Schakman, O., Jankovski, A., Deumens, R., Blanco-Prieto, M.J., Préat, V. and Des Rieux, A. 2013. Injectable alginate hydrogel loaded with GDNF promotes functional

recovery in a hemisection model of spinal cord injury. *International Journal of Pharmaceutics*. **455**, pp.148–158.

Ashton, R.S., Banerjee, A., Punyani, S., Schaffer, D. V. and Kane, R.S. 2007. Scaffolds based on degradable alginate hydrogels and poly(lactide-co-glycolide) microspheres for stem cell culture. *Biomaterials*. **28**, pp.5518–5525.

Aurand, E.R., Wagner, J., Lanning, C. and Bjugstad, K.B. 2012. Building biocompatible hydrogels for tissue engineering of the brain and spinal cord. *Journal of functional biomaterials*. **3**(4), pp.839–63.

Aurand, E.R., Wagner, J.L., Shandas, R. and Bjugstad, K.B. 2014. Hydrogel formulation determines cell fate of fetal and adult neural progenitor cells. *Stem Cell Research*. **12**(1), pp.11–23.

Babcock, A.A., Kuziel, W.A., Rivest, S. and Owens, T. 2003. Chemokine expression by glial cells directs leukocytes to sites of axonal injury in the CNS. *Journal of Neuroscience*. **23**, pp.7922–7930.

backuptrust.org.uk 2019. Spinal cord injury paralyses someone every four hours, new estimates reveal. *backuptrust.org.uk*. [Online]. [Accessed 20 October 2019]. Available from: https://www.backuptrust.org.uk/news/spinal-cord-injury-paralyses-someone-every-four-hours-new-estimates-reveal.

Bálint, E.É., Petres, J., Szabó, M., Orbán, C.K., Szilágyi, L. and Ábrahám, B. 2013. Fluorescence of a histidine-modified enhanced green fluorescent protein (EGFP) effectively quenched by copper(II) ions. *Journal of Fluorescence*. **23**(2), pp.273–281.

Banerjee, A., Arha, M., Choudhary, S., Ashton, R.S., Bhatia, S.R., Schaffer, D. V. and Kane, R.S. 2009a. The influence of hydrogel modulus on the proliferation and differentiation of encapsulated neural stem cells. *Biomaterials*. **30**(27), pp.4695–4699.

Banisadr, G., Fontanges, P., Haour, F., Kitabgi, P., Rostène, W. and Parsadaniantz, S.M. 2002. Neuroanatomical distribution of CXCR4 in adult rat brain and its localization in cholinergic and dopaminergic neurons. *European Journal of Neuroscience*. **16**, pp.1661–1671.

Barnabé-Heider, F., Göritz, C., Sabelström, H., Takebayashi, H., Pfrieger, F.W., Meletis, K. and Frisén, J. 2010. Origin of new glial cells in intact and injured adult spinal cord. *Cell Stem Cell*. **7**(4), pp.470–482.

Barreiro-Iglesias, A. 2010. Targeting ependymal stem cells in vivo as a non-invasive therapy for spinal cord injury. *Disease models & mechanisms*. **3**(11-12), pp.667–668.

Becker, C.G., Becker, T. and Hugnot, J.P. 2018. The spinal ependymal zone as a source of endogenous repair cells across vertebrates. *Progress in Neurobiology*. **170**, pp.67–80.

Beech, R.D., Cleary, M.A., Treloar, H.B., Eisch, A.J., Harrist, A. V., Zhong, W., Greer, C.A., Duman, R.S. and Picciotto, M.R. 2004. Nestin promoter/enhancer directs

transgene expression to precursors of adult generated periglomerular neurons. *Journal of Comparative Neurology*. **475**, pp.128–141.

Bellamkonda, R., Ranieri, J.P. and Aebischer, P. 1995. Laminin oligopeptide derivatized agarose gels allow three-dimensional neurite extension in vitro. *Journal of Neuroscience Research*. **41**, pp.501–509.

Bellamkonda, R., Ranieri, J.P., Bouche, N. and Aebischer, P. 1995. Hydrogel-based three-dimensional matrix for neural cells. *Journal of biomedical materials research*. **29**, pp.663–671.

Belvindrah, R., Rougon, G. and Chazal, G. 2002. Increased Neurogenesis in Adult mCD24-Deficient Mice. *Journal of Neuroscience*. **22**, pp.3594–3607.

Bergmann, O., Spalding, K.L. and Frisén, J. 2015. Adult neurogenesis in humans. *Cold Spring Harbor Perspectives in Medicine*. **5**.

Bignami, A., Asher, R. and Perides, G. 1992. The extracellular matrix of rat spinal cord: A comparative study on the localization of hyaluronic acid, glial hyaluronate-binding protein, and chondroitin sulfate proteoglycan. *Experimental Neurology*. **117**(1), pp.90–93.

Birbrair, A., Zhang, T., Wang, Z.M., Messi, M.L., Mintz, A. and Delbono, O. 2013. Type-1 pericytes participate in fibrous tissue deposition in aged skeletal muscle. *American Journal of Physiology - Cell Physiology*. **305**.

Bollyky, P.L., Lord, J.D., Masewicz, S.A., Evanko, S.P., Buckner, J.H., Wight, T.N. and Nepom, G.T. 2007. Cutting Edge: High Molecular Weight Hyaluronan Promotes the Suppressive Effects of CD4 + CD25 + Regulatory T Cells . *The Journal of Immunology*. **179**, pp.744–747.

Bonnici, B. and Kapfhammer, J.P. 2008. Spontaneous regeneration of intrinsic spinal cord axons in a novel spinal cord slice culture model. *European Journal of Neuroscience*. **27**, pp.2483–2492.

Borzacchiello, A. and Ambrosio, L. 2009. Structure-Property Relationships in Hydrogels *In*: R. Barbucci, ed. *Hydrogels: Biological Properties and Applications*. Springer-Verlag Italia, p.14.

Bourguignon, L.Y.W., Gilad, E., Peyrollier, K., Brightman, A. and Swanson, R.A. 2007. Hyaluronan-CD44 interaction stimulates Rac1 signaling and PKNγ kinase activation leading to cytoskeleton function and cell migration in astrocytes. *Journal of Neurochemistry*. **101**, pp.1002–1017.

Bradbury, E.J. and Burnside, E.R. 2019. Moving beyond the glial scar for spinal cord repair. *Nature Communications*. **10**.

Bradbury, E.J., Moon, L.D.F., Popat, R.J., King, V.R., Bennett, G.S., Patel, P.N., Fawcett, J.W. and McMahon, S.B. 2002. Chondroitinase ABC promotes functional recovery after spinal cord injury. *Nature*. **416**, pp.636–640.

Brännvall, K., Bergman, K., Wallenquist, U., Svahn, S., Bowden, T., Hilborn, J. and Forsberg-Nilsson, K. 2007. Enhanced neuronal differentiation in a three-

dimensional collagen-hyaluronan matrix. *Journal of Neuroscience Research*. **85**, pp.2138–2146.

Breunig, J.J., Sarkisian, M.R., Arellano, J.I., Morozov, Y.M., Ayoub, A.E., Sojitra, S., Wang, B., Flavell, R.A., Rakic, P. and Town, T. 2008. Primary cilia regulate hippocampal neurogenesis by mediating sonic hedgehog signaling. *Proceedings of the National Academy of Sciences of the United States of America*. **105**, pp.13127–13132.

Buck, S.B., Bradford, J., Gee, K.R., Agnew, B.J., Clarke, S.T. and Salic, A. 2008. Detection of S-phase cell cycle progression using 5-ethynyl-2′- deoxyuridine incorporation with click chemistry, an alternative to using 5-bromo-2′-deoxyuridine antibodies. *BioTechniques*. **44**, pp.927–929.

Buckley, C.D., Tan, J., Anderson, K.L., Hanein, D., Volkmann, N., Weis, W.I., Nelson, W.J. and Dunn, A.R. 2014. The minimal cadherin-catenin complex binds to actin filaments under force. *Science*. **346**.

Budday, S., Ovaert, T.C., Holzapfel, G.A., Steinmann, P. and Kuhl, E. 2019. Fifty Shades of Brain: A Review on the Mechanical Testing and Modeling of Brain Tissue. *Archives of Computational Methods in Engineering*.

Budday, S., Sommer, G., Birkl, C., Langkammer, C., Haybaeck, J., Kohnert, J., Bauer, M., Paulsen, F., Steinmann, P., Kuhl, E. and Holzapfel, G.A. 2017. Mechanical characterization of human brain tissue. *Acta Biomaterialia*. **48**, pp.319–340.

Burdick, J.A., Ward, M., Liang, E., Young, M.J. and Langer, R. 2006. Stimulation of neurite outgrowth by neurotrophins delivered from degradable hydrogels. *Biomaterials*. **27**, pp.452–459.

Burns, K.A., Murphy, B., Danzer, S.C. and Kuan, C.Y. 2009. Developmental and post-injury cortical gliogenesis: A genetic fate-mapping study with nestin-CreER mice. *GLIA*. **57**, pp.1115–1129.

Burri, O. 2016. Dividing circle into 8 equal areas. *BioImaging & Optics Platform EPFL*. [Online]. [Accessed 19 September 2019]. Available from: http://forum.imagej.net/t/dividing-circle-into-8-equal-areas/1995.

Bylund, M., Andersson, E., Novitch, B.G. and Muhr, J. 2003. Vertebrate neurogenesis is counteracted by Sox1-3 activity. *Nature Neuroscience*. **6**(11), pp.1162–1168.

Calaora, V., Chazal, G., Nielsen, P.J., Rougon, G. and Moreau, H. 1996. mCD24 expression in the developing mouse brain and in zones of secondary neurogenesis in the adult. *Neuroscience*. **73**, pp.581–594.

Carbajal, K.S., Miranda, J.L., Tsukamoto, M.R. and Lane, T.E. 2011. CXCR4 signaling regulates remyelination by endogenous oligodendrocyte progenitor cells in a viral model of demyelination. *GLIA*. **59**, pp.1813–1821.

Carbajal, K.S., Schaumburg, C., Strieter, R., Kane, J. and Lane, T.E. 2010. Migration of engrafted neural stem cells is mediated by CXCL12 signaling through CXCR4 in a viral model of multiple sclerosis. *Proceedings of the National Academy of Sciences of the United States of America*. **107**, pp.11068–11073.

Carlén, M., Meletis, K., Göritz, C., Darsalia, V., Evergren, E., Tanigaki, K., Amendola, M., Barnabé-Heider, F., Yeung, M.S.Y., Naldini, L., Honjo, T., Kokaia, Z., Shupliakov, O., Cassidy, R.M., Lindvall, O. and Frisén, J. 2009. Forebrain ependymal cells are Notch-dependent and generate neuroblasts and astrocytes after stroke. *Nature Neuroscience*. **12**(3), pp.259–267.

Carleton, A., Petreanu, L.T., Lansford, R., Alvarez-Buylla, A. and Lledo, P.M. 2003. Becoming a new neuron in the adult olfactory bulb. *Nature Neuroscience*. **6**, pp.507–518.

Caron, I., Rossi, F., Papa, S., Aloe, R., Sculco, M., Mauri, E., Sacchetti, A., Erba, E., Panini, N., Parazzi, V., Barilani, M., Forloni, G., Perale, G., Lazzari, L. and Veglianese, P. 2016. A new three dimensional biomimetic hydrogel to deliver factors secreted by human mesenchymal stem cells in spinal cord injury. *Biomaterials*. **75**, pp.135–147.

Carro, E., Nuñez, A., Busiguina, S. and Torres-Aleman, I. 2000. Circulating insulin-like growth factor I mediates effects of exercise on the brain. *Journal of Neuroscience*. **20**, pp.2926–2933.

Cawsey, T., Duflou, J., Weickert, C.S. and Gorrie, C.A. 2015. Nestin-Positive Ependymal Cells Are Increased in the Human Spinal Cord after Traumatic Central Nervous System Injury. *Journal of Neurotrauma*. **32**, pp.1393–1402.

Chalasani, S.H., Sabelko, K.A., Sunshine, M.J., Littman, D.R. and Raper, J.A. 2003. A chemokine, SDF-1, reduces the effectiveness of multiple axonal repellents and is required for normal axon pathfinding. *Journal of Neuroscience*. **23**, pp.1360–1371.

Chalasani, S.H., Sabol, A., Xu, H., Gyda, M.A., Rasband, K., Granato, M., Chien, C. Bin and Raper, J.A. 2007. Stromal cell-derived factor-1 antagonizes slit/robo signaling in vivo. *Journal of Neuroscience*. **27**, pp.973–980.

Chen, Y., Vartiainen, N.E., Ying, W., Chan, P.H., Koistinaho, J. and Swanson, R.A. 2001. Astrocytes protect neurons from nitric oxide toxicity by a glutathione-dependent mechanism. *Journal of Neurochemistry*. **77**, pp.1601–1610.

Clarkson, P.E. 2018. *The Effects of Mechanical Properties and Physical Inputs on Stem Cells of the Central Nervous System*.

Coates, G., Xiao, L. and Prammer, M. 1999. NMR logging: principles and applications. *Haliburton Energy Services*., p.234.

Cochard, P. and Paulin, D. 1984. Initial expression of neurofilaments and vimentin in the central and peripheral nervous system of the mouse embryo in vivo. *Journal of Neuroscience*. **4**, pp.2080–2094.

Cohen, A.L. 1979. Critical point drying. Principles and procedures *In*: *Scanning Electron Microscopy*., pp.303–324.

Cohen, M.E., Fainstein, N., Lavon, I. and Ben-Hur, T. 2014. Signaling through three chemokine receptors triggers the migration of transplanted neural precursor cells in a model of multiple sclerosis. *Stem Cell Research*. **13**, pp.227–239.

Comte, I., Kim, Y., Young, C.C., van der Harg, J.M., Hockberger, P., Bolam, P.J., Poirier, F. and Szele, F.G. 2011. Galectin-3 maintains cell motility from the subventricular zone to the olfactory bulb. *Journal of Cell Science*. **124**(14), pp.2438–2447.

Corns, L.F., Atkinson, L., Daniel, J., Edwards, I.J., New, L., Deuchars, J. and Deuchars, S.A. 2015. Cholinergic Enhancement of Cell Proliferation in the Postnatal Neurogenic Niche of the Mammalian Spinal Cord. *Stem Cells*. **33**(9), pp.2864–2876.

Corns, L.F., Deuchars, J. and Deuchars, S.A. 2013. GABAergic responses of mammalian ependymal cells in the central canal neurogenic niche of the postnatal spinal cord. *Neuroscience Letters*. **553**, pp.57–62.

Coskun, V., Wu, H., Blanchi, B., Tsao, S., Kim, K., Zhao, J., Biancotti, J.C., Hutnick, L., Krueger, R.C., Fan, G., de Vellis, J. and Sun, Y.E. 2008. CD133+ neural stem cells in the ependyma of mammalian postnatal forebrain. *Proceedings of the National Academy of Sciences*. **105**(3), pp.1026–1031.

Crompton, K.E., Goud, J.D., Bellamkonda, R. V., Gengenbach, T.R., Finkelstein, D.I., Horne, M.K. and Forsythe, J.S. 2007. Polylysine-functionalised thermoresponsive chitosan hydrogel for neural tissue engineering. *Biomaterials*. **28**(3), pp.441–449.

Crompton, K.E., Tomas, D., Finkelstein, D.I., Marr, M., Forsythe, J.S. and Horne, M.K. 2006. Inflammatory response on injection of chitosan/GP to the brain. *Journal of Materials Science: Materials in Medicine*. **17**, pp.633–639.

Cui, F.Z., Tian, W.M., Hou, S.P., Xu, Q.Y. and Lee, I.S. 2006. Hyaluronic acid hydrogel immobilized with RGD peptides for brain tissue engineering *In*: *Journal of Materials Science: Materials in Medicine*., pp.1393–1401.

Cui, L., Qu, H., Xiao, T., Zhao, M., Jolkkonen, J. and Zhao, C. 2013. Stromal cell-derived factor-1 and its receptor CXCR4 in adult neurogenesis after cerebral ischemia. *Restorative Neurology and Neuroscience*. **31**, pp.239–251.

Cui, W., Allen, N.D., Skynner, M., Gusterson, B. and Clark, A.J. 2001. Inducible ablation of astrocytes shows that these cells are required for neuronal survival in the adult brain. *GLIA*. **34**, pp.272–282.

Cukierman, E., Pankov, R., Stevens, D.R. and Yamada, K.M. 2001. Taking cell-matrix adhesions to the third dimension. *Science*. **294**, pp.1708–1712.

Curtis, M.A., Kam, M., Nannmark, U., Anderson, M.F., Axell, M.Z., Wikkelso, C., Holtås, S., Van Roon-Mom, W.M.C., Björk-Eriksson, T., Nordborg, C., Frisén, J., Dragunow, M., Faull, R.L.M. and Eriksson, P.S. 2007. Human neuroblasts migrate to the olfactory bulb via a lateral ventricular extension. *Science*. **315**, pp.1243–1249.

D'Ayala, G.G., Malinconico, M. and Laurienzo, P. 2008. Marine derived polysaccharides for biomedical applications: Chemical modification approaches. *Molecules*. **13**, pp.2069–2106.

Dar, A., Schajnovitz, A., Lapid, K., Kalinkovich, A., Itkin, T., Ludin, A., Kao, W.M., Battista, M., Tesio, M., Kollet, O., Cohen, N.N., Margalit, R., Buss, E.C., Baleux,

F., Oishi, S., Fujii, N., Larochelle, A., Dunbar, C.E., Broxmeyer, H.E., Frenette, P.S. and Lapidot, T. 2011. Rapid mobilization of hematopoietic progenitors by AMD3100 and catecholamines is mediated by CXCR4-dependent SDF-1 release from bone marrow stromal cells. *Leukemia*. **25**, pp.1286–1296.

Davies, S.J.A., Goucher, D.R., Doller, C. and Silver, J. 1999. Robust regeneration of adult sensory axons in degenerating white matter of the adult rat spinal cord. *Journal of Neuroscience*. **19**, pp.5810–5822.

Day, K., Shefer, G., Richardson, J.B., Enikolopov, G. and Yablonka-Reuveni, Z. 2007. Nestin-GFP reporter expression defines the quiescent state of skeletal muscle satellite cells. *Developmental Biology*. **304**(1), pp.246–259.

Deister, C., Aljabari, S. and Schmidt, C.E. 2007. Effects of collagen 1, fibronectin, laminin and hyaluronic acid concentration in multi-component gels on neurite extension. *Journal of biomaterials science. Polymer edition*. **18**(8), pp.983–97.

Dejana, E. and Betsholtz, C. 2016. Oligodendrocytes follow blood vessel trails in the brain. *Science*. **351**, pp.341–342.

Dhaliwal, J. and Lagace, D.C. 2011. Visualization and genetic manipulation of adult neurogenesis using transgenic mice. *European Journal of Neuroscience*. **33**, pp.1025–1036.

Dickendesher, T.L., Baldwin, K.T., Mironova, Y.A., Koriyama, Y., Raiker, S.J., Askew, K.L., Wood, A., Geoffroy, C.G., Zheng, B., Liepmann, C.D., Katagiri, Y., Benowitz, L.I., Geller, H.M. and Giger, R.J. 2012. NgR1 and NgR3 are receptors for chondroitin sulfate proteoglycans. *Nature Neuroscience*. **15**, pp.703–712.

Diermeier-Daucher, S., Clarke, S.T., Hill, D., Vollmann-Zwerenz, A., Bradford, J.A. and Brockhoff, G. 2009. Cell type specific applicability of 5-ethynyl-2′-deoxyuridine (EDU) for dynamic proliferation assessment in flow cytometry. *Cytometry Part A*. **75**(6), pp.535–546.

Djenoune, L., Khabou, H., Joubert, F., Quan, F.B., Nunes Figueiredo, S., Bodineau, L., Del Bene, F., BurcklÃ©, Cã©., Tostivint, H. and Wyart, C. 2014. Investigation of spinal cerebrospinal fluid-contacting neurons expressing PKD2L1: evidence for a conserved system from fish to primates. *Frontiers in Neuroanatomy*. **8**.

Doetsch, F. and Alvarez-Buylla, A. 1996. Network of tangential pathways for neuronal migration in adult mammalian brain. *Proceedings of the National Academy of Sciences*. **93**(25), pp.14895–14900.

Dore-Duffy, P., Katychev, A., Wang, X. and Van Buren, E. 2006. CNS microvascular pericytes exhibit multipotential stem cell activity. *Journal of Cerebral Blood Flow and Metabolism*. **26**, pp.613–624.

Doube, M., Klosowski, M.M., Arganda-Carreras, I., Cordelières, F.P., Dougherty, R.P., Jackson, J.S., Schmid, B., Hutchinson, J.R. and Shefelbine, S.J. 2010. BoneJ: Free and extensible bone image analysis in ImageJ. *Bone*. **47**, pp.1076–1079.

Douet, V., Arikawa-Hirasawa, E. and Mercier, F. 2012. Fractone-heparan sulfates mediate BMP-7 inhibition of cell proliferation in the adult subventricular zone. *Neuroscience Letters*. **528**, pp.120–125.

Doyle, E.L., Ridger, V., Ferraro, F., Turmaine, M., Saftig, P. and Cutler, D.F. 2011. CD63 is an essential cofactor to leukocyte recruitment by endothelial P-selectin. *Blood*. **118**, pp.4265–4273.

Dromard, C., Guillon, H., Rigau, V., Ripoll, C., Sabourin, J.C., Perrin, F.E., Scamps, F., Bozza, S., Sabatier, P., Lonjon, N., Duffau, H., Vachiery-Lahaye, F., Prieto, M., Tran Van Ba, C., Deleyrolle, L., Boularan, A., Langley, K., Gaviria, M., Privat, A., Hugnot, J.P. and Bauchet, L. 2008. Adult human spinal cord harbors neural precursor cells that generate neurons and glial cells in vitro. *Journal of Neuroscience Research*. **86**, pp.1916–1926.

Dumont, R.J., Okonkwo, D.O., Verma, S., Hurlbert, R.J., Boulos, P.T., Ellegala, D.B. and Dumont, A.S. 2001. Acute spinal cord injury, part I: Pathophysiologic mechanisms. *Clinical Neuropharmacology*. **24**, pp.254–264.

Dziembowska, M., Tham, T.N., Lau, P., Vitry, S., Lazarini, F. and Dubois-Dalcq, M. 2005. A role for CXCR4 signaling in survival and migration of neural and oligodendrocyte precursors. *GLIA*. **50**, pp.258–269.

Eccleston, P.A.N.N., Mirsky, R. and Jessen, K.R. 1989. Type I Collagen Preparations Inhibit DNA Synthesis Cells of the Peripheral Nervous System in Glial During development of the nervous system glial cells proliferate relatively rapidly , while in the mature nervous system glia divide very slowly or are quie. . **182**, pp.173–185.

Edwards, I.J., Bruce, G., Lawrenson, C., Howe, L., Clapcote, S.J., Deuchars, S.A. and Deuchars, J. 2013. Na+/K+ ATPase 1 and 3 Isoforms Are Differentially Expressed in - and -Motoneurons. *Journal of Neuroscience*. **33**(24), pp.9913–9919.

Edwards, I.J., Singh, M., Morris, S., Osborne, L., Le Ruez, T., Fuad, M., Deuchars, S.A. and Deuchars, J. 2013. A simple method to fluorescently label pericytes in the CNS and skeletal muscle. *Microvascular Research*. **89**, pp.164–168.

Encinas, J.M., Michurina, T. V., Peunova, N., Park, J.H., Tordo, J., Peterson, D.A., Fishell, G., Koulakov, A. and Enikolopov, G. 2011. Division-coupled astrocytic differentiation and age-related depletion of neural stem cells in the adult hippocampus. *Cell Stem Cell*. **8**(5), pp.566–579.

Encinas, J.M., Vaahtokari, A. and Enikolopov, G. 2006. Fluoxetine targets early progenitor cells in the adult brain. *Proceedings of the National Academy of Sciences*. **103**, pp.8233–8238.

Engler, A.J., Sen, S., Sweeney, H.L. and Discher, D.E. 2006. Matrix Elasticity Directs Stem Cell Lineage Specification. *Cell*. **126**(4), pp.677–689.

Favaro, R., Valotta, M., Ferri, A.L.M., Latorre, E., Mariani, J., Giachino, C., Lancini, C., Tosetti, V., Ottolenghi, S., Taylor, V. and Nicolis, S.K. 2009. Hippocampal development and neural stem cell maintenance require. *Online*. **12**, pp.1248–56.

Feng, R. and Wen, J. 2015. Overview of the roles of Sox2 in stem cell and development. *Biological Chemistry*. **396**(8), pp.883–891.

Filippov, V., Kronenberg, G., Pivneva, T., Reuter, K., Steiner, B., Wang, L.P., Yamaguchi, M., Kettenmann, H. and Kempermann, G. 2003. Subpopulation of

nestin-expressing progenitor cells in the adult murine hippocampus shows electrophysiological and morphological characteristics of astrocytes. *Molecular and Cellular Neuroscience*. **23**(3), pp.373–382.

Fisher, D., Xing, B., Dill, J., Li, H., Hoang, H.H., Zhao, Z., Yang, X.L., Bachoo, R., Cannon, S., Longo, F.M., Sheng, M., Silver, J. and Li, S. 2011. Leukocyte common antigen-related phosphatase is a functional receptor for chondroitin sulfate proteoglycan axon growth inhibitors. *Journal of Neuroscience*. **31**, pp.14051–14066.

Franklin, R.J.M., Zawadzka, M., Yu, B., Wang, B., Wu, Z., Gonzalez, G., Rawlins, E.L., Zhao, C. and Ma, D. 2018. A Subpopulation of Foxj1-Expressing, Nonmyelinating Schwann Cells of the Peripheral Nervous System Contribute to Schwann Cell Remyelination in the Central Nervous System. *The Journal of Neuroscience*. **38**, pp.9228–9239.

Franze, K., Janmey, P.A. and Guck, J. 2013. Mechanics in Neuronal Development and Repair. *Annual Review of Biomedical Engineering*. **15**, pp.227–251.

Freudenberg, U., Hermann, A., Welzel, P.B., Stirl, K., Schwarz, S.C., Grimmer, M., Zieris, A., Panyanuwat, W., Zschoche, S., Meinhold, D., Storch, A. and Werner, C. 2009. A star-PEG-heparin hydrogel platform to aid cell replacement therapies for neurodegenerative diseases. *Biomaterials*. **30**, pp.5049–5060.

Freund, P., Curt, A., Friston, K. and Thompson, A. 2013. Tracking changes following spinal cord injury: Insights from neuroimaging. *Neuroscientist*. **19**, pp.116–128.

Fuchs, J.L. and Schwark, H.D. 2004. Neuronal primary cilia: A review. *Cell Biology International*. **28**, pp.111–118.

Ganju, R.K., Brubaker, S.A., Meyer, J., Dutt, P., Yang, Y., Qin, S., Newman, W. and Groopman, J.E. 1998. The α-chemokine, stromal cell-derived factor-1α, binds to the transmembrane G-protein-coupled CXCR-4 receptor and activates multiple signal transduction pathways. *Journal of Biological Chemistry*. **273**, pp.23169–23175.

Gao, M., Lu, P., Bednark, B., Lynam, D., Conner, J.M., Sakamoto, J. and Tuszynski, M.H. 2013. Templated agarose scaffolds for the support of motor axon regeneration into sites of complete spinal cord transection. *Biomaterials*. **34**, pp.1529–1536.

Garcia-Ovejero, D., Arevalo-Martin, A., Paniagua-Torija, B., Florensa-Vila, J., Ferrer, I., Grassner, L. and Molina-Holgado, E. 2015. The ependymal region of the adult human spinal cord differs from other species and shows ependymoma-like features. *Brain*. **138**, pp.1583–1597.

Ghazale, H., Ripoll, C., Leventoux, N., Jacob, L., Azar, S., Mamaeva, D., Glasson, Y., Calvo, C.F., Thomas, J.L., Meneceur, S., Lallemand, Y., Rigau, V., Perrin, F.E., Noristani, H.N., Rocamonde, B., Huillard, E., Bauchet, L. and Hugnot, J.P. 2019. RNA Profiling of the Human and Mouse Spinal Cord Stem Cell Niches Reveals an Embryonic-like Regionalization with MSX1 + Roof-Plate-Derived Cells. *Stem Cell Reports*. **12**, pp.1159–1177.

Gomes, F.C.A., Paulin, D. and Neto, V.M. 1999. Glial fibrillary acidic protein (GFAP): Modulation by growth factors and its implication in astrocyte differentiation. *Brazilian Journal of Medical and Biological Research*. **32**, pp.619–631.

Gomes, W.A., Mehler, M.F. and Kessler, J.A. 2003. Transgenic overexpression of BMP4 increases astroglial and decreases oligodendroglial lineage commitment. *Developmental Biology*. **255**, pp.164–177.

Gopinath, A., Reddy, S.M.M., Madhan, B., Shanmguam, G. and Rao, J.R. 2014. Effect of aqueous ethanol on the triple helical structure of collagen. *European Biophysics Journal*. **43**, pp.643–652.

Göritz, C., Dias, D.O., Tomilin, N., Barbacid, M., Shupliakov, O. and Frisén, J. 2011. A pericyte origin of spinal cord scar tissue. *Science*. **333**, pp.238–242.

Gossen, M. and Bujard, H. 1992. Tight control of gene expression in mammalian cells by tetracycline- responsive promoters. *Proceedings of the National Academy of Sciences of the United States of America*. **89**(12), pp.5547–5551.

Gotts, J., Atkinson, L., Yanagawa, Y., Deuchars, J. and Deuchars, S.A. 2016. Co-expression of GAD67 and choline acetyltransferase in neurons in the mouse spinal cord: A focus on lamina X. *Brain Research*. **1646**, pp.570–579.

Grabarek, Z. and Gergely, J. 1990. Zero-length crosslinking procedure with the use of active esters. *Analytical Biochemistry*. **185**, pp.131–135.

Graham, V., Khudyakov, J., Ellis, P. and Pevny, L. 2003. SOX2 functions to maintain neural progenitor identity. *Neuron*. **39**(5), pp.749–765.

Gritti, A., Parati, E.A., Cova, L., Frolichsthal, P., Galli, R., Wanke, E., Faravelli, L., Morassutti, D.J., Roisen, F., Nickel, D.D. and Vescovi, A.L. 1996. Multipotential stem cells from the adult mouse brain proliferate and self-renew in response to basic fibroblast growth factor. *Journal of Neuroscience*. **16**, pp.1091–1100.

Grossman, S.D., Rosenberg, L.J. and Wrathall, J.R. 2001. Temporal-spatial pattern of acute neuronal and glial loss after spinal cord contusion. *Experimental Neurology*. **168**, pp.273–282.

Gu, H., Yue, Z., Leong, W.S., Nugraha, B. and Tan, L.P. 2010. Control of in vitro neural differentiation of mesenchymal stem cells in 3D macroporous, cellulosic hydrogels. *Regenerative Medicine*. **5**, pp.245–253.

Guan, Y.J., Wang, X., Wang, H.Y., Kawagishi, K., Ryu, H., Huo, C.F., Shimony, E.M., Kristal, B.S., Kuhn, H.G. and Friedlander, R.M. 2007. Increased stem cell proliferation in the spinal cord of adult amyotrophic lateral sclerosis transgenic mice. *Journal of Neurochemistry*. **102**, pp.1125–1138.

Gunn, J.W., Turner, S.D. and Mann, B.K. 2005. Adhesive and mechanical properties of hydrogels influence neurite extension. *Journal of Biomedical Materials Research - Part A*. **72**, pp.91–97.

Guvendiren, M., Lu, H.D. and Burdick, J.A. 2012. Shear-thinning hydrogels for biomedical applications. *Soft Matter*. **8**, pp.260–272.

Haegel, H., Tölg, C., Hofmann, M. and Ceredig, R. 1993. Activated mouse astrocytes and T cells express similar CD44 variants. Role of CD44 in astrocyte/T cell binding. *Journal of Cell Biology*. **122**, pp.1067–1077.

Halsey, A., Conner, A., Bill, R., Logan, A. and Ahmed, Z. 2018. Aquaporins and Their Regulation after Spinal Cord Injury. *Cells*. **7**, p.174.

Hamilton, L.K., Truong, M.K. V, Bednarczyk, M.R., Aumont, A. and Fernandes, K.J.L. 2009. Cellular organization of the central canal ependymal zone, a niche of latent neural stem cells in the adult mammalian spinal cord. *Neuroscience*. **164**(3), pp.1044–1056.

Han, Y.G., Spassky, N., Romaguera-Ros, M., Garcia-Verdugo, J.M., Aguilar, A., Schneider-Maunoury, S. and Alvarez-Buylla, A. 2008. Hedgehog signaling and primary cilia are required for the formation of adult neural stem cells. *Nature Neuroscience*. **11**, pp.277–284.

Head, D.A., Tronci, G., Russell, S.J. and Wood, D.J. 2016. In Silico Modeling of the Rheological Properties of Covalently Cross-Linked Collagen Triple Helices. *ACS Biomaterials Science and Engineering*. **2**, pp.1224–1233.

Hejčl, A., Růžička, J., Kapcalová, M., Turnovcová, K., Krumbholcová, E., Přádný, M., Michálek, J., Cihlář, J., Jendelová, P. and Syková, E. 2013. Adjusting the chemical and physical properties of hydrogels leads to improved stem cell survival and tissue ingrowth in spinal cord injury reconstruction: a comparative study of four methacrylate hydrogels. *Stem cells and development*. **22**(20), pp.2794–805.

Her, G.J., Wu, H.C., Chen, M.H., Chen, M.Y., Chang, S.C. and Wang, T.W. 2013. Control of three-dimensional substrate stiffness to manipulate mesenchymal stem cell fate toward neuronal or glial lineages. *Acta Biomaterialia*. **9**, pp.5170–5180.

Hockfield, S. and McKay, R.D.G. 1985. Identification of major cell classes in the developing mammalian nervous system. *Journal of Neuroscience*. **5**, pp.3310–3328.

Hofstetter, C.P., Holmström, N. a V, Lilja, J. a, Schweinhardt, P., Hao, J., Spenger, C., Wiesenfeld-Hallin, Z., Kurpad, S.N., Frisén, J. and Olson, L. 2005. Allodynia limits the usefulness of intraspinal neural stem cell grafts; directed differentiation improves outcome. *Nature neuroscience*. **8**(3), pp.346–53.

Hol, E.M. and Pekny, M. 2015. Glial fibrillary acidic protein (GFAP) and the astrocyte intermediate filament system in diseases of the central nervous system. *Current Opinion in Cell Biology*. **32**, pp.121–130.

Hötzer, B., Ivanov, R., Altmeier, S., Kappl, R. and Jung, G. 2011. Determination of copper(II) ion concentration by lifetime measurements of green fluorescent protein. *Journal of Fluorescence*. **21**, pp.2143–2153.

Hou, S., Tian, W., Xu, Q., Cui, F., Zhang, J., Lu, Q. and Zhao, C. 2006. The enhancement of cell adherence and inducement of neurite outgrowth of dorsal root ganglia co-cultured with hyaluronic acid hydrogels modified with Nogo-66 receptor antagonist in vitro. *Neuroscience*. **137**, pp.519–529.

Hou, S., Xu, Q., Tian, W., Cui, F., Cai, Q., Ma, J. and Lee, I.S. 2005. The repair of brain lesion by implantation of hyaluronic acid hydrogels modified with laminin. *Journal of Neuroscience Methods*. **148**(1), pp.60–70.

Hsiao, T.W., Tresco, P.A. and Hlady, V. 2015. Astrocytes alignment and reactivity on collagen hydrogels patterned with ECM proteins. *Biomaterials*. **39**, pp.124–130.

Hsieh, J., Aimone, J.B., Kaspar, B.K., Kuwabara, T., Nakashima, K. and Gage, F.H. 2004. IGF-I instructs multipotent adult neural progenitor cells to become oligodendrocytes. *Journal of Cell Biology*. **164**, pp.111–122.

Huang, A.L., Chen, X., Hoon, M.A., Chandrashekar, J., Guo, W., Tränkner, D., Ryba, N.J.P. and Zuker, C.S. 2006. The cells and logic for mammalian sour taste detection. *Nature*. **442**(7105), pp.934–938.

Huang, F., Shen, Q. and Zhao, J.T. 2013. Growth and differentiation of neural stem cells in a three-dimensional collagen gel scaffold. *Neural Regeneration Research*. **8**, pp.313–319.

Huebsch, N., Arany, P.R., Mao, A.S., Shvartsman, D., Ali, O.A., Bencherif, S.A., Rivera-Feliciano, J. and Mooney, D.J. 2010. Harnessing traction-mediated manipulation of the cell/matrix interface to control stem-cell fate. *Nature Materials*. **9**, pp.518–526.

Hugnot, J.P. and Franzen, R. 2011. The spinal cord ependymal region: A stem cell niche in the caudal central nervous system. *Frontiers in Bioscience*. **16**, pp.1044–1059.

Hulsebosch, C.E. 2002. Recent advances in pathophysiology and treatment of spinal cord injury. *American Journal of Physiology - Advances in Physiology Education*. **26**, pp.238–255.

Hyatt, A.J.T., Wang, D., Kwok, J.C., Fawcett, J.W. and Martin, K.R. 2010. Controlled release of chondroitinase ABC from fibrin gel reduces the level of inhibitory glycosaminoglycan chains in lesioned spinal cord. *Journal of Controlled Release*. **147**, pp.24–29.

Hynes, S.R., Rauch, M.F., Bertram, J.P. and Lavik, E.B. 2009. A library of tunable poly(ethylene glycol)/poly(L-lysine) hydrogels to investigate the material cues that influence neural stem cell differentiation. *Journal of Biomedical Materials Research - Part A*. **89**, pp.499–509.

Imayoshi, I., Sakamoto, M. and Kageyama, R. 2011. Genetic methods to identify and manipulate newly born neurons in the adult brain. *Frontiers in Neuroscience*., pp.1–11.

Imitola, J., Raddassi, K., Park, K.I., Mueller, F.-J., Nieto, M., Teng, Y.D., Frenkel, D., Li, J., Sidman, R.L., Walsh, C.A., Snyder, E.Y. and Khoury, S.J. 2004. Directed migration of neural stem cells to sites of CNS injury by the stromal cell-derived factor 1alpha/CXC chemokine receptor 4 pathway. *Proceedings of the National Academy of Sciences of the United States of America*. **101**(52), pp.18117–22.

Itoh, T., Satou, T., Ishida, H., Nishida, S., Tsubaki, M., Hashimoto, S. and Ito, H. 2009. The relationship between SDF-1alpha/CXCR4 and neural stem cells appearing in

damaged area after traumatic brain injury in rats. *Neurological research*. **31**(1), pp.90–102.

Jacques, T.S., Relvas, J.B., Nishimura, S., Pytela, R., Edwards, G.M., Streuli, C.H. and Ffrench-Constant, C. 1998. Neural precursor cell chain migration and division are regulated through different β1 integrins. *Development*. **125**, pp.3167–3177.

Jacquet, B. V., Salinas-Mondragon, R., Liang, H., Therit, B., Buie, J.D., Dykstra, M., Campbell, K., Ostrowski, L.E., Brody, S.L. and Ghashghaei, H.T. 2009. FoxJ1-dependent gene expression is required for differentiation of radial glia into ependymal cells and a subset of astrocytes in the postnatal brain. *Development*. **136**(23), pp.4021–4031.

Jaerve, A., Schiwy, N., Schmitz, C. and Mueller, H.W. 2011. Differential effect of aging on axon sprouting and regenerative growth in spinal cord injury. *Experimental Neurology*. **231**(2), pp.284–294.

Jain, A., Kim, Y.T., McKeon, R.J. and Bellamkonda, R. V. 2006. In situ gelling hydrogels for conformal repair of spinal cord defects, and local delivery of BDNF after spinal cord injury. *Biomaterials*. **27**(3), pp.497–504.

Jain, A., McKeon, R.J., Brady-Kalnay, S.M. and Bellamkonda, R. V. 2011. Sustained delivery of activated rho GTPases and BDNF promotes axon growth in CSPG-rich regions following spinal cord injury. *PLoS ONE*. **6**.

Jalalvand, E., Robertson, B., Wallén, P. and Grillner, S. 2016. Ciliated neurons lining the central canal sense both fluid movement and pH through ASIC3. *Nature Communications*. **7**.

James, G. and Butt, A.M. 2002. P2Y and P2X purinoceptor mediated Ca2+ signalling in glial cell pathology in the central nervous system. *European Journal of Pharmacology*. **447**, pp.247–260.

Jeong, S.R., Kwon, M.J., Lee, H.G., Joe, E.H., Lee, J.H., Kim, S.S., Suh-Kim, H. and Kim, B.G. 2012. Hepatocyte growth factor reduces astrocytic scar formation and promotes axonal growth beyond glial scars after spinal cord injury. *Experimental Neurology*. **233**, pp.312–322.

Jin, W., Wang, J., Zhu, T., Yuan, B., Ni, H., Jiang, J., Wang, H. and Liang, W. 2014. Anti-inflammatory effects of curcumin in experimental spinal cord injury in rats. *Inflammation Research*. **63**, pp.381–387.

Johansson, C.B., Lothian, C., Molin, M., Okano, H. and Lendahl, U. 2002. Nestin enhancer requirements for expression in normal and injured adult CNS. *Journal of Neuroscience Research*. **69**, pp.784–794.

Johansson, C.B., Momma, S., Clarke, D.L., Risling, M., Lendahl, U. and Frisén, J. 1999. Identification of a neural stem cell in the adult mammalian central nervous system. *Cell*. **96**(1), pp.25–34.

Johe, K.K. 1996. Single factors direct the differentiation of stem cells from the fetal and adult central nervous system. , pp.3129–3140.

Juríková, M., Danihel, Ľ., Polák, Š. and Varga, I. 2016. Ki67, PCNA, and MCM proteins: Markers of proliferation in the diagnosis of breast cancer. *Acta Histochemica*. **118**, pp.544–552.

Kalamakis, G., Brüne, D., Ravichandran, S., Bolz, J., Fan, W., Ziebell, F., Stiehl, T., Catalá-Martinez, F., Kupke, J., Zhao, S., Llorens-Bobadilla, E., Bauer, K., Limpert, S., Berger, B., Christen, U., Schmezer, P., Mallm, J.P., Berninger, B., Anders, S., del Sol, A., Marciniak-Czochra, A. and Martin-Villalba, A. 2019. Quiescence Modulates Stem Cell Maintenance and Regenerative Capacity in the Aging Brain. *Cell*. **176**, pp.1407–1419.e14.

Kang, W., Nguyen, K.C.Q. and Hébert, J.M. 2019. Transient Redirection of SVZ Stem Cells to Oligodendrogenesis by FGFR3 Activation Promotes Remyelination. *Stem Cell Reports*. **12**, pp.1223–1231.

Kania, G., Corbeil, D., Fuchs, J., Tarasov, K. V., Blyszczuk, P., Huttner, W.B., Boheler, K.R. and Wobus, A.M. 2005. Somatic Stem Cell Marker Prominin-1/CD133 Is Expressed in Embryonic Stem Cell-Derived Progenitors. *Stem Cells*. **23**, pp.791–804.

Karimi-Abdolrezaee, S., Schut, D., Wang, J. and Fehlings, M.G. 2012. Chondroitinase and growth factors enhance activation and Oligodendrocyte differentiation of endogenous neural precursor cells after spinal cord injury. *PLoS ONE*. **7**.

Kawaguchi, A., Miyata, T., Sawamoto, K., Takashita, N., Murayama, A., Akamatsu, W., Ogawa, M., Okabe, M., Tano, Y., Goldman, S.A. and Okano, H. 2001. Nestin-EGFP transgenic mice: Visualization of the self-renewal and multipotency of CNS stem cells. *Molecular and Cellular Neuroscience*. **17**, pp.259–273.

Kawasaki, H., Mizuseki, K., Nishikawa, S., Kaneko, S., Kuwana, Y., Nakanishi, S., Nishikawa, S.I. and Sasai, Y. 2000. Induction of midbrain dopaminergic neurons from ES cells by stromal cell-derived inducing activity. *Neuron*. **28**, pp.31–40.

Kelly, S., Bliss, T.M., Shah, A.K., Sun, G.H., Ma, M., Foo, W.C., Masel, J., Yenari, M.A., Weissman, I.L., Uchida, N., Palmer, T. and Steinberg, G.K. 2004. Transplanted human fetal neural stem cells survive, migrate, and differentiate in ischemic rat cerebral cortex. *Proceedings of the National Academy of Sciences of the United States of America*. **101**, pp.11839–11844.

Kempermann, G., Gage, F.H., Aigner, L., Song, H., Curtis, M.A., Thuret, S., Kuhn, H.G., Jessberger, S., Frankland, P.W., Cameron, H.A., Gould, E., Hen, R., Abrous, D.N., Toni, N., Schinder, A.F., Zhao, X., Lucassen, P.J. and Frisén, J. 2018. Human Adult Neurogenesis: Evidence and Remaining Questions. *Cell Stem Cell*. **23**, pp.25–30.

Kerever, A., Mercier, F., Nonaka, R., de Vega, S., Oda, Y., Zalc, B., Okada, Y., Hattori, N., Yamada, Y. and Arikawa-Hirasawa, E. 2014. Perlecan is required for FGF-2 signaling in the neural stem cell niche. *Stem Cell Research*. **12**, pp.492–505.

Kerever, A., Schnack, J., Vellinga, D., Ichikawa, N., Moon, C., Arikawa-Hirasawa, E., Efird, J.T. and Mercier, F. 2007. Novel Extracellular Matrix Structures in the Neural Stem Cell Niche Capture the Neurogenic Factor Fibroblast Growth Factor 2 from the Extracellular Milieu. *STEM CELLS*. **25**, pp.2146–2157.

Kim, J.H., Lee, J.A., Song, Y.M., Park, C.H., Hwang, S.J., Kim, Y.S., Kaang, B.K. and Son, H. 2006. Overexpression of calbindin-D28K in hippocampal progenitor cells increases neuronal differentiation and neurite outgrowth. *FASEB Journal*. **20**, pp.109–111.

Kim, M.S. and Lee, H.B. 2014. Perspectives on Tissue-Engineered Nerve Regeneration for the Treatment of Spinal Cord Injury. *Tissue Engineering Part A*. **20**(13-14), pp.1781–1783.

King, V.R., Alovskaya, A., Wei, D.Y.T., Brown, R.A. and Priestley, J. V. 2010. The use of injectable forms of fibrin and fibronectin to support axonal ingrowth after spinal cord injury. *Biomaterials*. **31**(15), pp.4447–4456.

Klapka, N. and Müller, H. 2006. Collagen matrix in spinal cord injury. *Journal of neurotrauma*. **23**(3-4), pp.422–435.

Kleene, R., Yang, H., Kutsche, M. and Schachner, M. 2001. The Neural Recognition Molecule L1 is a Sialic Acid-binding Lectin for CD24, Which Induces Promotion and Inhibition of Neurite Outgrowth. *Journal of Biological Chemistry*. **276**(24), pp.21656–21663.

Kohlmeier, F., Maya-Mendoza, A. and Jackson, D.A. 2013. EdU induces DNA damage response and cell death in mESC in culture. *Chromosome Research*. **21**, pp.87–100.

Kong, F.L., Wang, X.P., Li, Y.N. and Wang, H.X. 2017. The role of exosomes derived from cerebrospinal fluid of spinal cord injury in neuron proliferation in vitro. *Artificial Cells, Nanomedicine and Biotechnology*., pp.1–6.

Koyama, Y., Suzuki, M. and Yoshida, T. 1998. CD63, a member of tetraspan transmembrane protein family, induces cellular spreading by reaction with monoclonal antibody on substrata. *Biochemical and Biophysical Research Communications*. **246**, pp.841–846.

Krassioukov, A. V., Ackery, A., Schwartz, G., Adamchik, Y., Liu, Y. and Fehlings, M.G. 2002. An in vitro model of neurotrauma in organotypic spinal cord cultures from adult mice. *Brain Research Protocols*. **10**, pp.60–68.

Kucia, M., Jankowski, K., Reca, R., Wysoczynski, M., Bandura, L., Allendorf, D.J., Zhang, J., Ratajczak, J. and Ratajczak, M.Z. 2004. CXCR4-SDF-1 signalling, locomotion, chemotaxis and adhesion. *Journal of Molecular Histology*. **35**, pp.233–245.

Lacroix, S., Hamilton, L.K., Vaugeois, A., Beaudoin, S., Breault-Dugas, C., Pineau, I., Lévesque, S.A., Grégoire, C.A. and Fernandes, K.J.L. 2014. Central canal ependymal cells proliferate extensively in response to traumatic spinal cord injury but not demyelinating lesions. *PLoS ONE*. **9**(1).

Lalancette-Hébert, M., Swarup, V., Beaulieu, J.M., Bohacek, I., Abdelhamid, E., Weng, Y.C., Sato, S. and Kriz, J. 2012. Galectin-3 is required for resident microglia activation and proliferation in response to ischemic injury. *Journal of Neuroscience*. **32**, pp.10383–10395.

Lalive, P.H., Paglinawan, R., Biollaz, G., Kappos, E.A., Leone, D.P., Malipiero, U., Relvas, J.B., Moransard, M., Suter, T. and Fontana, A. 2005. TGF-β-treated microglia induce oligodendrocyte precursor cell chemotaxis through the HGF-c-Met pathway. *European Journal of Immunology*. **35**, pp.727–737.

Lampe, K.J., Bjugstad, K.B. and Mahoney, M.J. 2010. Impact of degradable macromer content in a poly(ethylene glycol) hydrogel on neural cell metabolic activity, redox state, proliferation, and differentiation. *Tissue engineering. Part A*. **16**(6), pp.1857–66.

Lee, A., Kessler, J.D., Read, T.A., Kaiser, C., Corbeil, D., Huttner, W.B., Johnson, J.E. and Wechsler-Reya, R.J. 2005. Isolation of neural stem cells from the postnatal cerebellum. *Nature Neuroscience*. **8**, pp.723–729.

Lee, H., McKeon, R.J. and Bellamkonda, R. V. 2010. Sustained delivery of thermostabilized chABC enhances axonal sprouting and functional recovery after spinal cord injury. *Proceedings of the National Academy of Sciences of the United States of America*. **107**, pp.3340–3345.

Lee, J., Abdeen, A.A., Zhang, D. and Kilian, K.A. 2013. Directing stem cell fate on hydrogel substrates by controlling cell geometry, matrix mechanics and adhesion ligand composition. *Biomaterials*. **34**(33), pp.8140–8148.

Lee, J. and Thumbikat, P. 2015. Pathophysiology, presentation and management of spinal cord injury. *Surgery (United Kingdom)*. **33**, pp.238–247.

Lein, P.J., Higgins, D., Turner, D.C., Flier, L.A. and Terranova, V.P. 1991. The NC1 domain of type IV collagen promotes axonal growth in sympathetic neurons through interaction with the α1β1 integrin. *Journal of Cell Biology*. **113**, pp.417–428.

Leipzig, N.D. and Shoichet, M.S. 2009a. The effect of substrate stiffness on adult neural stem cell behavior. *Biomaterials*. **30**(36), pp.6867–6878.

Leiter, O., Seidemann, S., Overall, R.W., Ramasz, B., Rund, N., Schallenberg, S., Grinenko, T., Wielockx, B., Kempermann, G. and Walker, T.L. 2019. Exercise-Induced Activated Platelets Increase Adult Hippocampal Precursor Proliferation and Promote Neuronal Differentiation. *Stem Cell Reports*. **12**, pp.667–679.

Lendahl, U., Zimmerman, L.B. and McKay, R.D. 1990. CNS stem cells express a new class of intermediate filament protein. *Cell*. **60**(4), pp.585–595.

Li, J.Y., Christophersen, N.S., Hall, V., Soulet, D. and Brundin, P. 2008. Critical issues of clinical human embryonic stem cell therapy for brain repair. *Trends in Neurosciences*. **31**, pp.146–153.

Li, X., Floriddia, E.M., Toskas, K., Chalfouh, C., Honore, A., Aumont, A., Vallières, N., Lacroix, S., Fernandes, K.J.L., Guérout, N. and Barnabé-Heider, F. 2018. FoxJ1 regulates spinal cord development and is required for the maintenance of spinal cord stem cell potential. *Experimental Cell Research*. **368**(1), pp.84–100.

Li, X., Floriddia, E.M., Toskas, K., Fernandes, K.J.L., Guérout, N. and Barnabé-Heider, F. 2016. Regenerative Potential of Ependymal Cells for Spinal Cord Injuries Over Time. *EBioMedicine*. **13**, pp.55–65.

Li, X., Liu, X., Zhao, W., Wen, X. and Zhang, N. 2012. Manipulating neural-stem-cell mobilization and migration in vitro. *Acta Biomaterialia*. **8**, pp.2087–2095.

Liang, H., Hippenmeyer, S. and Ghashghaei, H.T. 2012. A Nestin-cre transgenic mouse is insufficient for recombination in early embryonic neural progenitors. *Biology Open*. **1**, pp.1200–1203.

Licht, T., Rothe, G., Kreisel, T., Wolf, B., Benny, O., Rooney, A.G., ffrench-Constant, C., Enikolopov, G. and Keshet, E. 2016. VEGF preconditioning leads to stem cell remodeling and attenuates age-related decay of adult hippocampal neurogenesis. *Proceedings of the National Academy of Sciences*. **113**(48), pp.E7828–E7836.

Lieberam, I., Agalliu, D., Nagasawa, T., Ericson, J. and Jessell, T.M. 2005. A Cxcl12-Cxcr4 chemokine signaling pathway defines the initial trajectory of mammalian motor axons. *Neuron*. **47**, pp.667–679.

Lim, D.A., Tramontin, A.D., Trevejo, J.M., Herrera, D.G., García-Verdugo, J.M. and Alvarez-Buylla, A. 2000. Noggin antagonizes BMP signaling to create a niche for adult neurogenesis. *Neuron*. **28**, pp.713–726.

Lin, C.M., Lin, J.W., Chen, Y.C., Shen, H.H., Wei, L., Yeh, Y.S., Chiang, Y.H., Shih, R., Chiu, P.L., Hung, K.S., Yang, L.Y. and Chiu, W.T. 2009. Hyaluronic acid inhibits the glial scar formation after brain damage with tissue loss in rats. *Surgical Neurology*. **72**.

Lin, X., Shi, Y., Cao, Y. and Liu, W. 2016. Recent progress in stem cell differentiation directed by material and mechanical cues. *Biomedical Materials (Bristol)*. **11**.

Liu, Y., Ye, H., Satkunendrarajah, K., Yao, G.S., Bayon, Y. and Fehlings, M.G. 2013. A self-assembling peptide reduces glial scarring, attenuates post-traumatic inflammation and promotes neurological recovery following spinal cord injury. *Acta Biomaterialia*. **9**, pp.8075–8088.

Lois, C. and Alvarez-Buylla, A. 1994. Long-distance neuronal migration in the adult mammalian brain. *Science*. **264**, pp.1145–1148.

Longair, M.H., Baker, D.A. and Armstrong, J.D. 2011. Simple neurite tracer: Open source software for reconstruction, visualization and analysis of neuronal processes. *Bioinformatics*. **27**, pp.2453–2454.

Lopes, J.L.S., Miles, A.J., Whitmore, L. and Wallace, B.A. 2014. Distinct circular dichroism spectroscopic signatures of polyproline II and unordered secondary structures: Applications in secondary structure analyses. *Protein Science*. **23**, pp.1765–1772.

Lu, M., Grove, E.A. and Miller, R.J. 2002. Abnormal development of the hippocampal dentate gyrus in mice lacking the CXCR4 chemokine receptor. *Proceedings of the National Academy of Sciences of the United States of America*. **99**, pp.7090–7095.

Luo, Y. and Shoichet, M.S. 2004. A photolabile hydrogel for guided three-dimensional cell growth and migration. *Nature materials*. **3**(4), pp.249–53.

Ma, W., Fitzgerald, W., Liu, Q.Y., O'Shaughnessy, T.J., Maric, D., Lin, H.J., Alkon, D.L. and Barker, J.L. 2004. CNS stem and progenitor cell differentiation into functional neuronal circuits in three-dimensional collagen gels. *Experimental Neurology*. **190**, pp.276–288.

Macaya, D. and Spector, M. 2012. Injectable hydrogel materials for spinal cord regeneration: a review. *Biomedical Materials*. **7**(1), p.012001.

Mahoney, M.J. and Anseth, K.S. 2006. Three-dimensional growth and function of neural tissue in degradable polyethylene glycol hydrogels. *Biomaterials*. **27**(10), pp.2265–2274.

Mamber, C., Kamphuis, W., Haring, N.L., Peprah, N., Middeldorp, J. and Hol, E.M. 2012. GFAPδ Expression in Glia of the Developmental and Adolescent Mouse Brain. *PLoS ONE*. **7**.

Mayo, J.N. and Bearden, S.E. 2015. Driving the Hypoxia-Inducible Pathway in Human Pericytes Promotes Vascular Density in an Exosome-Dependent Manner. *Microcirculation*. **22**, pp.711–723.

McMorris, F.A. and Dubois-Dalcq, M. 1988. Insulin-like growth factor I promotes cell proliferation and oligodendroglial commitment in rat glial progenitor cells developing in vitro. *Journal of Neuroscience Research*. **21**, pp.199–209.

Meletis, K., Barnabé-Heider, F., Carlén, M., Evergren, E., Tomilin, N., Shupliakov, O. and Frisén, J. 2008. Spinal cord injury reveals multilineage differentiation of ependymal cells. *PLoS Biology*. **6**(7), pp.1494–1507.

Mercier, F. and Douet, V. 2014. Bone morphogenetic protein-4 inhibits adult neurogenesis and is regulated by fractone-associated heparan sulfates in the subventricular zone. *Journal of Chemical Neuroanatomy*. **57-58**, pp.54–61.

Mercier, F., Kitasako, J.T. and Hatton, G.I. 2002. Anatomy of the brain neurogenic zones revisited: Fractones and the fibroblast/macrophage network. *Journal of Comparative Neurology*. **451**, pp.170–188.

Mignone, J.L., Kukekov, V., Chiang, A.-S., Steindler, D. and Enikolopov, G. 2004. Neural stem and progenitor cells in nestin-GFP transgenic mice. *The Journal of comparative neurology*. **469**(3), pp.311–24.

Miller, F.D. and Gauthier, A.S. 2007. Timing Is Everything: Making Neurons versus Glia in the Developing Cortex. *Neuron*. **54**, pp.357–369.

Mladinic, M., Bianchetti, E., Dekanic, A., Mazzone, G.L. and Nistri, A. 2014. ATF3 is a novel nuclear marker for migrating ependymal stem cells in the rat spinal cord. *Stem Cell Research*. **12**(3), pp.815–827.

Moeendarbary, E., Weber, I.P., Sheridan, G.K., Koser, D.E., Soleman, S., Haenzi, B., Bradbury, E.J., Fawcett, J. and Franze, K. 2017. The soft mechanical signature of glial scars in the central nervous system. *Nature Communications*. **8**.

Moore, S.W., Roca-Cusachs, P. and Sheetz, M.P. 2010. Stretchy proteins on stretchy substrates: The important elements of integrin-mediated rigidity sensing. *Developmental Cell*. **19**, pp.194–206.

Moreno-Jiménez, E.P., Flor-García, M., Terreros-Roncal, J., Rábano, A., Cafini, F., Pallas-Bazarra, N., Ávila, J. and Llorens-Martín, M. 2019. Adult hippocampal neurogenesis is abundant in neurologically healthy subjects and drops sharply in patients with Alzheimer's disease. *Nature Medicine*. **25**, pp.554–560.

Moreno-Manzano, V., Rodriguez-Jimenez, F.J., Garcia-Rosello, M., Lainez, S., Erceg, S., Calvo, M.T., Ronaghi, M., Lloret, M., Planells-Cases, R., Sanchez-Puelles, J.M. and Stojkovic, M. 2009. Activated spinal cord ependymal stem cells rescue neurological function. *Stem Cells*. **27**(3), pp.733–743.

Mori, T., Tanaka, K., Buffo, A., Wurst, W., Kühn, R. and Gotz, M. 2006. Inducible gene deletion in astroglia and radial glia - A valuable tool for functional and lineage analysis. *GLIA*. **54**, pp.21–34.

Mostacada, K., Oliveira, F.L., Villa-Verde, D.M.S. and Martinez, A.M.B. 2015. Lack of galectin-3 improves the functional outcome and tissue sparing by modulating inflammatory response after a compressive spinal cord injury. *Experimental Neurology*. **271**, pp.390–400.

Mothe, A.J. and Tator, C.H. 2005a. Proliferation, migration, and differentiation of endogenous ependymal region stem/progenitor cells following minimal spinal cord injury in the adult rat. *Neuroscience*. **131**(1), pp.177–187.

Mothe, A.J. and Tator, C.H. 2005b. Proliferation, migration, and differentiation of endogenous ependymal region stem/progenitor cells following minimal spinal cord injury in the adult rat. *Neuroscience*. **131**, pp.177–187.

Mothe, A.J., Zahir, T., Santaguida, C., Cook, D. and Tator, C.H. 2011. Neural stem/progenitor cells from the adult human spinal cord are multipotent and self-renewing and differentiate after transplantation. *PLoS ONE*. **6**.

Muthusamy, N., Brumm, A., Zhang, X., Carmichael, S.T. and Ghashghaei, H.T. 2018. Foxj1 expressing ependymal cells do not contribute new cells to sites of injury or stroke in the mouse forebrain. *Scientific Reports*. **8**.

Nagy, J.I., Hacking, J., Frankenstein, U.N. and Turley, E.A. 1995. Requirement of the hyaluronan receptor RHAMM in neurite extension and motility as demonstrated in primary neurons and neuronal cell lines. *Journal of Neuroscience*. **15**, pp.241–252.

Nagy, J.I., Price, M.L., Staines, W.A., Lynn, B.D. and Granholm, A.C. 1998. The hyaluronan receptor RHAMM in noradrenergic fibers contributes to axon growth capacity of locus coeruleus neurons in an intraocular transplant model. *Neuroscience*. **86**, pp.241–255.

Nakagomi, T., Kubo, S., Nakano-Doi, A., Sakuma, R., Lu, S., Narita, A., Kawahara, M., Taguchi, A. and Matsuyama, T. 2015. Brain vascular pericytes following ischemia have multipotential stem cell activity to differentiate into neural and vascular lineage cells. *Stem Cells*. **33**, pp.1962–1974.

Namiki, J. and Tator, C.H. 1999. Cell proliferation and nestin expression in the ependyma of the adult rat spinal cord after injury. *Journal of Neuropathology and Experimental Neurology*. **58**, pp.489–498.

Nascimento, M.A., Sorokin, L. and Coelho-Sampaio, T. 2018. Fractone bulbs derive from ependymal cells and their laminin composition influence the stem cell niche in the subventricular zone. *Journal of Neuroscience*. **38**, pp.3880–3889.

National Spinal Cord Injury Strategy Board 2012. The Initial Management of Adults with Spinal Cord Injuries. *National Spinal Cord Injury Strategy Board*., pp.1–32.

Nauli, S.M., Jin, X., Aboualaiwi, W.A., El-Jouni, W., Su, X. and Zhou, J. 2013. Non-motile primary cilia as fluid shear stress mechanosensors *In*: *Methods in Enzymology*., pp.1–20.

NICE 2016. Spinal injury: assessment and initial management. *Nice Guidelines*. **24**, pp.29–43.

Nieoullon, V., Belvindrah, R., Rougon, G. and Chazal, G. 2005. mCD24 regulates proliferation of neuronal committed precursors in the subventricular zone. *Molecular and Cellular Neuroscience*. **28**, pp.462–474.

Nieto-Estévez, V., Defterali, Ç. and Vicario-Abejón, C. 2016. IGF-I: A key growth factor that regulates neurogenesis and synaptogenesis from embryonic to adult stages of the brain. *Frontiers in Neuroscience*. **10**.

O'Connor, S.M., Stenger, D.A., Shaffer, K.M. and Ma, W. 2001. Survival and neurite outgrowth of rat cortical neurons in three-dimensional agarose and collagen gel matrices. *Neuroscience Letters*. **304**(3), pp.189–193.

Ogai, K., Nakatani, K., Hisano, S., Sugitani, K., Koriyama, Y. and Kato, S. 2014b. Function of Sox2 in ependymal cells of lesioned spinal cords in adult zebrafish. *Neuroscience research*. **88**, pp.84–87.

Ohab, J.J., Fleming, S., Blesch, A. and Carmichael, S.T. 2006. A neurovascular niche for neurogenesis after stroke. *Journal of Neuroscience*. **26**, pp.13007–13016.

Orts-Del'Immagine, A., Kastner, A., Tillement, V., Tardivel, C., Trouslard, J. and Wanaverbecq, N. 2014. Morphology, distribution and phenotype of polycystin kidney disease 2-like 1-positive cerebrospinal fluid contacting neurons in the brainstem of adult mice. *PLoS ONE*. **9**.

Orts-Del'Immagine, A., Wanaverbecq, N., Tardivel, C., Tillement, V., Dallaporta, M. and Trouslard, J. 2012. Properties of subependymal cerebrospinal fluid contacting neurones in the dorsal vagal complex of the mouse brainstem. *Journal of Physiology*. **590**, pp.3719–3741.

Orts-Del'Immagine, A. and Wyart, C. 2017. Cerebrospinal-fluid-contacting neurons. *Current Biology*. **27**, pp.R1198–R1200.

Oyinbo, C.A. 2011. Secondary injury mechanisms in traumatic spinal cord injury: A nugget of this multiply cascade. *Acta Neurobiologiae Experimentalis*. **71**(2), pp.281–299.

Ozerdem, U., Grako, K.A., Dahlin-Huppe, K., Monosov, E. and Stallcup, W.B. 2001. NG2 proteoglycan is expressed exclusively by mural cells during vascular morphogenesis. *Developmental Dynamics*. **222**, pp.218–227.

Palmer, T.D., Willhoite, A.R. and Gage, F.H. 2000. Vascular niche for adult hippocampal neurogenesis. *Journal of Comparative Neurology*. **425**, pp.479–494.

Panayiotou, E. and Malas, S. 2013. Adult spinal cord ependymal layer: a promising pool of quiescent stem cells to treat spinal cord injury. *Frontiers in physiology*. **4**(November), p.340.

Pandamooz, S., Salehi, M.S., Zibaii, M.I., Safari, A., Nabiuni, M., Ahmadiani, A. and Dargahi, L. 2019. Modeling traumatic injury in organotypic spinal cord slice culture obtained from adult rat. *Tissue and Cell*. **56**, pp.90–97.

Paniagua-Torija, B., Norenberg, M., Arevalo-Martin, A., Carballosa-Gautam, M.M., Campos-Martin, Y., Molina-Holgado, E. and Garcia-Ovejero, D. 2018. Cells in the adult human spinal cord ependymal region do not proliferate after injury. *Journal of Pathology*. **246**, pp.415–421.

Park, J., Lim, E., Back, S., Na, H., Park, Y. and Sun, K. 2010. Nerve regeneration following spinal cord injury using matrix metalloproteinase-sensitive, hyaluronic acid-based biomimetic hydrogel scaffold containing brain-derived neurotrophic factor. *Journal of Biomedical Materials Research - Part A*. **93**(3), pp.1091–1099.

Park, J.H., Glass, Z., Sayed, K., Michurina, T. V., Lazutkin, A., Mineyeva, O., Velmeshev, D., Ward, W.F., Richardson, A. and Enikolopov, G. 2013. Calorie restriction alleviates the age-related decrease in neural progenitor cell division in the aging brain. *European Journal of Neuroscience*. **37**(12), pp.1987–1993.

Paszek, M.J., Zahir, N., Johnson, K.R., Lakins, J.N., Rozenberg, G.I., Gefen, A., Reinhart-King, C.A., Margulies, S.S., Dembo, M., Boettiger, D., Hammer, D.A. and Weaver, V.M. 2005. Tensional homeostasis and the malignant phenotype. *Cancer Cell*. **8**, pp.241–254.

Patar, A., Dockery, P., Howard, L. and McMahon, S.S. 2019. Cell viability in three ex vivo rat models of spinal cord injury. *Journal of Anatomy*. **234**, pp.244–251.

Pathak, M.M., Nourse, J.L., Tran, T., Hwe, J., Arulmoli, J., Le, D.T.T., Bernardis, E., Flanagan, L.A. and Tombola, F. 2014. Stretch-activated ion channel Piezo1 directs lineage choice in human neural stem cells. *Proceedings of the National Academy of Sciences of the United States of America*. **111**, pp.16148–16153.

Pelham, R.J. and Wang, Y.L. 1997. Cell locomotion and focal adhesions are regulated by substrate flexibility. *Proceedings of the National Academy of Sciences of the United States of America*. **94**, pp.13661–13665.

Petracca, Y.L., Sartoretti, M.M., Di Bella, D.J., Marin-Burgin, A., Carcagno, A.L., Schinder, A.F. and Lanuza, G.M. 2016. The late and dual origin of cerebrospinal fluid-contacting neurons in the mouse spinal cord. *Development*. **143**(5), pp.880–891.

Pfenninger, C. V., Steinhoff, C., Hertwig, F. and Nuber, U.A. 2011. Prospectively isolated CD133/CD24-positive ependymal cells from the adult spinal cord and lateral ventricle wall differ in their long-term in vitro self-renewal and in vivo gene expression. *GLIA*. **59**(1), pp.68–81.

Piantino, J., Burdick, J.A., Goldberg, D., Langer, R. and Benowitz, L.I. 2006. An injectable, biodegradable hydrogel for trophic factor delivery enhances axonal rewiring and improves performance after spinal cord injury. *Experimental Neurology*. **201**, pp.359–367.

Prang, P., Müller, R., Eljaouhari, A., Heckmann, K., Kunz, W., Weber, T., Faber, C., Vroemen, M., Bogdahn, U. and Weidner, N. 2006. The promotion of oriented axonal regrowth in the injured spinal cord by alginate-based anisotropic capillary hydrogels. *Biomaterials*. **27**(19), pp.3560–3569.

Princen, K., Hatse, S., Vermeire, K., De Clercq, E. and Schols, D. 2003. Evaluation of SDF-1/CXCR4-induced Ca2+ signaling by fluorometric imaging plate reader (FLIPR) and flow cytometry. *Cytometry*. **51A**, pp.35–45.

Pruszak, J., Ludwig, W., Blak, A., Alavian, K. and Isacson, O. 2009. CD15, CD24, and CD29 define a surface biomarker code for neural lineage differentiation of stem cells. *Stem Cells*. **27**(12), pp.2928–2940.

Qin, Y., Zhang, W. and Yang, P. 2015. Current states of endogenous stem cells in adult spinal cord. *Journal of Neuroscience Research*. **93**(3), pp.391–398.

Rahimi, Y., Goulding, A., Shrestha, S., Mirpuri, S. and Deo, S.K. 2008. Mechanism of copper induced fluorescence quenching of red fluorescent protein, DsRed. *Biochemical and Biophysical Research Communications*. **370**, pp.57–61.

Rajan, P. and McKay, R.D.G. 1998. Multiple routes to astrocytic differentiation in the CNS. *Journal of Neuroscience*. **18**, pp.3620–3629.

Relucio, J., Menezes, M.J., Miyagoe-Suzuki, Y., Takeda, S. and Colognato, H. 2012. Laminin regulates postnatal oligodendrocyte production by promoting oligodendrocyte progenitor survival in the subventricular zone. *GLIA*. **60**, pp.1451–1467.

Rexed, B. 1954. A cytoarchitectonic atlas of the spinal coed in the cat. *Journal of Comparative Neurology*. **100**, pp.297–379.

Robin, A.M., Zhang, Z.G., Wang, L., Zhang, R.L., Katakowski, M., Zhang, L., Wang, Y., Zhang, C. and Chopp, M. 2006. Stromal cell-derived factor 1α mediates neural progenitor cell motility after focal cerebral ischemia. *Journal of Cerebral Blood Flow and Metabolism*. **26**, pp.125–134.

Rolls, A., Shechter, R. and Schwartz, M. 2009. The bright side of the glial scar in CNS repair. *Nature reviews. Neuroscience*. **10**(3), pp.235–41.

Rosenberg, A.B., Roco, C.M., Muscat, R.A., Kuchina, A., Sample, P., Yao, Z., Graybuck, L.T., Peeler, D.J., Mukherjee, S., Chen, W., Pun, S.H., Sellers, D.L., Tasic, B. and Seelig, G. 2018. Single-cell profiling of the developing mouse brain and spinal cord with split-pool barcoding. *Science*. **360**, pp.176–182.

Ross, H.H., Rahman, M., Levkoff, L.H., Millette, S., Martin-Carreras, T., Dunbar, E.M., Reynolds, B.A. and Laywell, E.D. 2011. Ethynyldeoxyuridine (EdU) suppresses in vitro population expansion and in vivo tumor progression of human glioblastoma cells. *Journal of Neuro-Oncology*. **105**, pp.485–498.

Royce Hynes, S., McGregor, L.M., Ford Rauch, M. and Lavik, E.B. 2007. Photopolymerized poly(ethylene glycol)/poly(L-lysine) hydrogels for the delivery of neural progenitor cells. *Journal of Biomaterials Science, Polymer Edition*. **18**, pp.1017–1030.

Saha, K., Keung, A.J., Irwin, E.F., Li, Y., Little, L., Schaffer, D. V. and Healy, K.E. 2008a. Substrate Modulus Directs Neural Stem Cell Behavior. *Biophysical Journal*. **95**(9), pp.4426–4438.

Sahni, V. and Kessler, J.A. 2010. Stem cell therapies for spinal cord injury. *Nature reviews. Neurology*. **6**(7), pp.363–72.

Sancho-Tello, M., Vallés, S., Montoliu, C., Renau-Piqueras, J. and Guerri, C. 1995. Developmental pattern of GFAP and vimentin gene expression in rat brain and in radial glial cultures. *Glia*. **15**, pp.157–166.

Sato, Y., Kiyozumi, D., Futaki, S., Nakano, I., Shimono, C., Kaneko, N., Ikawa, M., Okabe, M., Sawamoto, K. and Sekiguchi, K. 2019. Ventricular–subventricular zone fractones are speckled basement membranes that function as a neural stem cell niche. *Molecular Biology of the Cell*. **30**, pp.56–68.

Sawamoto, K., Wichterle, H., Gonzalez-Perez, O., Cholfin, J.A., Yamada, M., Spassky, N., Murcia, N.S., Garcia-Verdugo, J.M., Marin, O., Rubenstein, J.L.R., Tessier-Lavigne, M., Okano, H. and Alvarez-Buylla, A. 2006. New neurons follow the flow of cerebrospinal fluid in the adult brain. *Science*. **311**, pp.629–632.

Schimizzi, A.L., Massie, J.B., Murphy, M., Perry, A., Kim, C.W., Garfin, S.R. and Akeson, W.H. 2006. High-molecular-weight hyaluronan inhibits macrophage proliferation and cytokine release in the early wound of a preclinical postlaminectomy rat model. *Spine Journal*. **6**, pp.550–556.

Schizas, N., Rojas, R., Kootala, S., Andersson, B., Pettersson, J., Hilborn, J. and Hailer, N.P. 2014. Hyaluronic acid-based hydrogel enhances neuronal survival in spinal cord slice cultures from postnatal mice. *Journal of biomaterials applications*. **28**(6), pp.825–36.

Schmidt-Kastner, R. and Humpel, C. 2002. Nestin expression persists in astrocytes of organotypic slice cultures from rat cortex. *International Journal of Developmental Neuroscience*. **20**, pp.29–38.

Schnitzer, J., Franke, W.W. and Schachner, M. 1981. Immunocytochemical demonstration of vimentin in astrocytes and ependymal cells of developing and adult mouse nervous system. *Journal of Cell Biology*. **90**(2), pp.435–447.

Seidlits, S.K., Khaing, Z.Z., Petersen, R.R., Nickels, J.D., Vanscoy, J.E., Shear, J.B. and Schmidt, C.E. 2010. The effects of hyaluronic acid hydrogels with tunable mechanical properties on neural progenitor cell differentiation. *Biomaterials*. **31**(14), pp.3930–3940.

Shea, T.B., Beermann, M.L. and Fischer, I. 1993. Transient requirement for vimentin in neuritogenesis: Intracellular delivery of anti-vimentin antibodies and antisense oligonucleotides inhibit neurite initiation but not elongation of existing neurites in neuroblastoma. *Journal of Neuroscience Research*. **36**, pp.66–76.

Shen, Q., Wang, Y., Kokovay, E., Lin, G., Chuang, S.M., Goderie, S.K., Roysam, B. and Temple, S. 2008. Adult SVZ Stem Cells Lie in a Vascular Niche: A Quantitative Analysis of Niche Cell-Cell Interactions. *Cell Stem Cell*. **3**, pp.289–300.

Shen, Y., Tenney, A.P., Busch, S.A., Horn, K.P., Cuascut, F.X., Liu, K., He, Z., Silver, J. and Flanagan, J.G. 2009. PTPσ Is a receptor for chondroitin sulfate proteoglycan, an inhibitor of neural regeneration. *Science*. **326**, pp.592–596.

Shewan, D., Calaora, V., Nielsen, P., Cohen, J., Rougon, G. and Moreau, H. 1996. mCD24, a glycoprotein transiently expressed by neurons, is an inhibitor of neurite outgrowth. *Journal of Neuroscience*. **16**, pp.2624–2634.

Silva, N.A., Sousa, N., Reis, R.L. and Salgado, A.J. 2014. From basics to clinical: A comprehensive review on spinal cord injury. *Progress in Neurobiology*. **114**, pp.25–57.

Silver, J. and Miller, J.H. 2004. Regeneration beyond the glial scar. *Nature Reviews Neuroscience*. **5**, pp.146–156.

Snapyan, M., Lemasson, M., Brill, M.S., Blais, M., Massouh, M., Ninkovic, J., Gravel, C., Berthod, F., Gotz, M., Barker, P.A., Parent, A. and Saghatelyan, A. 2009. Vasculature Guides Migrating Neuronal Precursors in the Adult Mammalian Forebrain via Brain-Derived Neurotrophic Factor Signaling. *Journal of Neuroscience*. **29**(13), pp.4172–4188.

Snyder, J.S. 2019. Recalibrating the Relevance of Adult Neurogenesis. *Trends in Neurosciences*. **42**, pp.164–178.

Sorrells, S.F., Paredes, M.F., Cebrian-Silla, A., Sandoval, K., Qi, D., Kelley, K.W., James, D., Mayer, S., Chang, J., Auguste, K.I., Chang, E.F., Gutierrez, A.J., Kriegstein, A.R., Mathern, G.W., Oldham, M.C., Huang, E.J., Garcia-Verdugo, J.M., Yang, Z. and Alvarez-Buylla, A. 2018. Human hippocampal neurogenesis drops sharply in children to undetectable levels in adults. *Nature*. **555**, pp.377–381.

Spalding, K.L., Bergmann, O., Alkass, K., Bernard, S., Salehpour, M., Huttner, H.B., Boström, E., Westerlund, I., Vial, C., Buchholz, B.A., Possnert, G., Mash, D.C., Druid, H. and Frisén, J. 2013. Dynamics of hippocampal neurogenesis in adult humans. *Cell*. **153**, p.1219.

Spassky, N., Han, Y.G., Aguilar, A., Strehl, L., Besse, L., Laclef, C., Romaguera Ros, M., Garcia-Verdugo, J.M. and Alvarez-Buylla, A. 2008. Primary cilia are required for cerebellar development and Shh-dependent expansion of progenitor pool. *Developmental Biology*. **317**, pp.246–259.

Stabenfeldt, S.E., Munglani, G., García, A.J. and Laplaca, M.C. 2010. Biomimetic microenvironment modulates neural stem cell survival, migration, and differentiation. *Tissue Engineering - Part A*. **16**, pp.3747–3758.

Stenudd, M., Sabelström, H. and Frisén, J. 2015. Role of endogenous neural stem cells in spinal cord injury and repair. *JAMA neurology*. **72**(2), pp.235–7.

Stichel, C.C. and Müller, H.W. 1998. The CNS lesion scar: New vistas on an old regeneration barrier. *Cell and Tissue Research*. **294**, pp.1–9.

Stoppini, L., Buchs, P.A. and Muller, D. 1991. A simple method for organotypic cultures of nervous tissue. *Journal of Neuroscience Methods*. **37**, pp.173–182.

Struve, J., Maher, P.C., Li, Y.Q., Kinney, S., Fehlings, M.G., Kuntz IV, C. and Sherman, L.S. 2005. Disruption of the hyaluronan-based extracellular matrix in spinal cord promotes astrocyte proliferation. *GLIA*. **52**, pp.16–24.

Stumm, R.K., Rummel, J., Junker, V., Culmsee, C., Pfeiffer, M., Krieglstein, J., Höllt, V. and Schulz, S. 2002. A dual role for the SDF-1/CXCR4 chemokine receptor system in adult brain: Isoform-selective regulation of SDF-1 expression modulates CXCR4-dependent neuronal plasticity and cerebral leukocyte recruitment after focal ischemia. *Journal of Neuroscience*. **22**, pp.5865–5878.

Stumm, R.K., Zhou, C., Ara, T., Lazarini, F., Dubois-Dalcq, M., Nagasawa, T., Höllt, V. and Schulz, S. 2003. CXCR4 regulates interneuron migration in the developing neocortex. *Journal of Neuroscience*. **23**, pp.5123–5130.

Sun, M.Y., Yetman, M.J., Lee, T.C., Chen, Y. and Jankowsky, J.L. 2014. Specificity and efficiency of reporter expression in adult neural progenitors vary substantially among nestin-CreERT2 lines. *Journal of Comparative Neurology*. **522**, pp.1191–1208.

Sun, W., Kim, H. and Moon, Y. 2010. Control of neuronal migration through rostral migration stream in mice. *Anatomy & Cell Biology*. **43**, p.269.

Takahashi, J., Palmer, T.D. and Gage, F.H. 1999. Retinoic acid and neurotrophins collaborate to regulate neurogenesis in adult-derived neural stem cell cultures. *Journal of Neurobiology*. **38**, pp.65–81.

Takahashi, M., Arai, Y., Kurosawa, H., Sueyoshi, N. and Shirai, S. 2003. Ependymal cell reactions in spinal cord segments after compression injury in adult rat. *Journal of neuropathology and experimental neurology*. **62**(2), pp.185–194.

Tamamaki, N., Yanagawa, Y., Tomioka, R., Miyazaki, J.I., Obata, K. and Kaneko, T. 2003. Green Fluorescent Protein Expression and Colocalization with Calretinin, Parvalbumin, and Somatostatin in the GAD67-GFP Knock-In Mouse. *Journal of Comparative Neurology*. **467**(1), pp.60–79.

Teixeira, A.I., Ilkhanizadeh, S., Wigenius, J.A., Duckworth, J.K., Inganäs, O. and Hermanson, O. 2009. The promotion of neuronal maturation on soft substrates. *Biomaterials*. **30**, pp.4567–4572.

TheWell Bioscience Inc n.d. Figure 1. Rheological properties of VitroGel RGD with DMEM medium. Available from: https://www.thewellbio.com/product/vitrogel-rgd/.

Thomas, T.W. and DiMilla, P.A. 2000. Spreading and motility of human glioblastoma cells on sheets of silicone rubber depend on substratum compliance. *Medical and Biological Engineering and Computing*. **38**, pp.360–370.

Thored, P., Arvidsson, A., Cacci, E., Ahlenius, H., Kallur, T., Darsalia, V., Ekdahl, C.T., Kokaia, Z. and Lindvall, O. 2006. Persistent Production of Neurons from Adult Brain Stem Cells During Recovery after Stroke. *Stem Cells*. **24**, pp.739–747.

Tian, W.M., Hou, S.P., Ma, J., Zhang, C.L., Xu, Q.Y., Lee, I.S., Li, H.D., Spector, M. and Cui, F.Z. 2005. Hyaluronic acid-poly-D-lysine-based three-dimensional hydrogel for traumatic brain injury. *Tissue Engineering*. **11**, pp.513–525.

Tissir, F., Wang, C.E. and Goffinet, A.M. 2004. Expression of the chemokine receptor Cxcr4 mRNA during mouse brain development. *Developmental Brain Research*. **149**, pp.63–71.

Toni, N., Laplagne, D.A., Zhao, C., Lombardi, G., Ribak, C.E., Gage, F.H. and Schinder, A.F. 2008. Neurons born in the adult dentate gyrus form functional synapses with target cells. *Nature Neuroscience*. **11**, pp.901–907.

Tran, P.B., Banisadr, G., Ren, D., Chenn, A. and Miller, R.J. 2007. Chemokine receptor expression by neural progenitor cells in neurogenic regions of mouse brain. *Journal of Comparative Neurology*. **500**, pp.1007–1033.

Tronci, G., Doyle, A., Russell, S.J. and Wood, D.J. 2013. Triple-helical collagen hydrogels via covalent aromatic functionalization with 1,3-Phenylenediacetic acid. *Journal of materials chemistry. B, Materials for biology and medicine*. **1**(40), pp.5478–5488.

Tsai, J. and Kam, L. 2009. Rigidity-dependent cross talk between integrin and cadherin signaling. *Biophysical Journal*. **96**.

Tugues, S., Honjo, S., König, C., Padhan, N., Kroon, J., Gualandi, L., Li, X., Barkefors, I., Thijssen, V.L., Griffioen, A.W. and Claesson-Welsh, L. 2013. Tetraspanin CD63 promotes vascular endothelial growth factor receptor 2-β1 integrin complex formation, thereby regulating activation and downstream signaling in endothelial cells in Vitro and in Vivo. *Journal of Biological Chemistry*. **288**, pp.19060–19071.

Turley, E.A., Hossain, M.Z., Sorokan, T., Jordan, L.M. and Nagy, J.I. 1994. Astrocyte and microglial motility in vitro is functionally dependent on the hyaluronan receptor RHAMM. *Glia*. **12**, pp.68–80.

Tysseling, V.M., Mithal, D., Sahni, V., Birch, D., Jung, H., Miller, R.J. and Kessler, J.A. 2011. SDF1 in the dorsal corticospinal tract promotes CXCR4+ cell migration after spinal cord injury. *Journal of Neuroinflammation*. **8**(1), p.16.

Tysseling-mattiace, V.M., Sahni, V., Niece, K.L., Birch, D., Fehlings, M.G., Stupp, S.I. and Kessler, J. a 2009. Self-Assembling Nanofibers Inhibit Glial Scar Formation and Promote Axon Elongation after Spinal Cord Injury. *J Neurosci*. **28**(14), pp.3814–3823.

Uchida, N., Buck, D.W., He, D., Reitsma, M.J., Masek, M., Phan, T. V., Tsukamoto, A.S., Gage, F.H. and Weissman, I.L. 2000. Direct isolation of human central nervous system stem cells. *Proceedings of the National Academy of Sciences of the United States of America*. **97**, pp.14720–14725.

Underhill, C. 1992. CD44: The hyaluronan receptor. *Journal of Cell Science*. **103**, pp.293–298.

Uttamapinant, C., Tangpeerachaikul, A., Grecian, S., Clarke, S., Singh, U., Slade, P., Gee, K.R. and Ting, A.Y. 2012. Fast, cell-compatible click chemistry with copper-chelating azides for biomolecular labeling. *Angewandte Chemie - International Edition*. **51**(24), pp.5852–5856.

Vining, K.H. and Mooney, D.J. 2017. Mechanical forces direct stem cell behaviour in development and regeneration. *Nature Reviews Molecular Cell Biology*. **18**, pp.728–742.

Walker, A.S., Goings, G.E., Kim, Y., Miller, R.J., Chenn, A. and Szele, F.G. 2010. Nestin Reporter Transgene Labels Multiple Central Nervous System Precursor Cells. *Neural Plasticity*. **2010**, pp.1–14.

Waly, B. El, Macchi, M., Cayre, M. and Durbec, P. 2014. Oligodendrogenesis in the normal and pathological central nervous system. *Frontiers in Neuroscience*.

Wang, J., Zheng, J., Zheng, Q., Wu, Y., Wu, B., Huang, S., Fang, W. and Guo, X. 2015. FGL-functionalized self-assembling nanofiber hydrogel as a scaffold for spinal cord-derived neural stem cells. *Materials Science and Engineering C*. **46**, pp.140–147.

Wang, X., Baughman, K.W., Basso, D.M. and Strittmatter, S.M. 2006. Delayed nogo receptor therapy improves recovery from spinal cord contusion. *Annals of Neurology*. **60**, pp.540–549.

Wang, Y., Huang, J., Li, Y. and Yang, G.-Y. 2012. Roles of Chemokine CXCL12 and its Receptors in Ischemic Stroke. *Current Drug Targets*. **13**, pp.166–172.

Wang, Y.F., Zu, J.N., Li, J., Chen, C., Xi, C.Y. and Yan, J.L. 2014. Curcumin promotes the spinal cord repair via inhibition of glial scar formation and inflammation. *Neuroscience Letters*. **560**, pp.51–56.

Wei, Y.T., He, Y., Xu, C.L., Wang, Y., Liu, B.F., Wang, X.M., Sun, X.D., Cui, F.Z. and Xu, Q.Y. 2010. Hyaluronic acid hydrogel modified with nogo-66 receptor antibody and poly-L-lysine to promote axon regrowth after spinal cord injury. *Journal of Biomedical Materials Research - Part B Applied Biomaterials*. **95**, pp.110–117.

Wei, Y.T., Tian, W.M., Yu, X., Cui, F.Z., Hou, S.P., Xu, Q.Y. and Lee, I.-S. 2007. Hyaluronic acid hydrogels with IKVAV peptides for tissue repair and axonal regeneration in an injured rat brain. *Biomedical materials (Bristol, England)*. **2**(3), pp.S142–S146.

Wescott, M.P., Kufareva, I., Paes, C., Goodman, J.R., Thaker, Y., Puffer, B.A., Berdougo, E., Rucker, J.B., Handel, T.M. and Doranz, B.J. 2016. Signal transmission through the CXC chemokine receptor 4 (CXCR4) transmembrane helices. *Proceedings of the National Academy of Sciences of the United States of America*. **113**, pp.9928–9933.

Whitman, M.C. and Greer, C.A. 2009. Adult neurogenesis and the olfactory system. *Progress in Neurobiology*. **89**, pp.162–175.

Widera, D., Holtkamp, W., Entschladen, F., Niggemann, B., Zänker, K., Kaltschmidt, B. and Kaltschmidt, C. 2004. MCP-1 induces migration of adult neural stem cells. *European Journal of Cell Biology*. **83**, pp.381–387.

Woerly, S., Doan, V.D., Sosa, N., De Vellis, J. and Espinosa, A. 2001. Reconstruction of the transected cat spinal cord following NeuroGel™ implantation: axonal tracing, immunohistochemical and ultrastructural studies. *International Journal of Developmental Neuroscience*. **19**, pp.63–83.

Wu, L.J., Vadakkan, K.I. and Zhuo, M. 2007. ATP-induced chemotaxis of microglial processes requires P2Y receptor-activated initiation of outward potassium currents. *GLIA*. **55**, pp.810–821.

Yamaguchi, M., Saito, H., Suzuki, M. and Mori, K. 2000. Visualization of neurogenesis in the central nervous system using nestin promoter-GFP transgenic mice. *Neuroreport*. **11**(9), pp.1991–1996.

Yang, H.Y., Lieska, N., Shao, D., Kriho, V. and Pappas, G.D. 1994. Proteins of the intermediate filament cytoskeleton as markers for astrocytes and human astrocytomas. *Molecular and Chemical Neuropathology*. **21**, pp.155–176.

Yang, J.A., Yeom, J., Hwang, B.W., Hoffman, A.S. and Hahn, S.K. 2014. In situ-forming injectable hydrogels for regenerative medicine. *Progress in Polymer Science*. **39**(12), pp.1973–1986.

Yoo, H. Il, Kim, E.G., Lee, E.J., Hong, S.Y., Yoon, C.S., Hong, M.J., Park, S.J., Woo, R.S., Baik, T.K. and Song, D.Y. 2017. Neuroanatomical distribution of galectin-3 in the adult rat brain. *Journal of Molecular Histology*. **48**(2), pp.133–146.

Yu, T.S., Dandekar, M., Monteggia, L.M., Parada, L.F. and Kernie, S.G. 2005. Temporally regulated expression of Cre recombinase in neural stem cells. *Genesis*. **41**, pp.147–153.

Yuan, S.H., Martin, J., Elia, J., Flippin, J., Paramban, R.I., Hefferan, M.P., Vidal, J.G., Mu, Y., Killian, R.L., Israel, M.A., Emre, N., Marsala, S., Marsala, M., Gage, F.H., Goldstein, L.S.B. and Carson, C.T. 2011. Cell-surface marker signatures for the Isolation of neural stem cells, glia and neurons derived from human pluripotent stem cells. *PLoS ONE*. **6**(3).

Yuan, Y.M. and He, C. 2013. The glial scar in spinal cord injury and repair. *Neuroscience Bulletin*. **29**, pp.421–435.

Zeng, C., Pan, F., Jones, L.A., Lim, M.M., Griffin, E.A., Sheline, Y.I., Mintun, M.A., Holtzman, D.M. and Mach, R.H. 2010. Evaluation of 5-ethynyl-2′-deoxyuridine staining as a sensitive and reliable method for studying cell proliferation in the adult nervous system. *Brain Research*. **1319**, pp.21–32.

Zhang, M.D., Barde, S., Szodorai, E., Josephson, A., Mitsios, N., Watanabe, M., Attems, J., Lubec, G., Kovács, G.G., Uhlén, M., Mulder, J., Harkany, T. and Hökfelt, T. 2016. Comparative anatomical distribution of neuronal calcium-binding protein (NECAB) 1 and -2 in rodent and human spinal cord. *Brain Structure and Function*. **221**(7), pp.3803–3823.

Zhang, S. 2014. Sox2, a key factor in the regulation of pluripotency and neural differentiation. *World Journal of Stem Cells*. **6**, p.305.

Zhang, S., Holmes, T., Lockshin, C. and Rich, A. 1993. Spontaneous assembly of a self-complementary oligopeptide to form a stable macroscopic membrane.

Proceedings of the National Academy of Sciences of the United States of America. **90**, pp.3334–3338.

Zhao, W., Jin, K., Li, J., Qiu, X. and Li, S. 2017. Delivery of stromal cell-derived factor 1α for in situ tissue regeneration. *Journal of Biological Engineering*. **11**.

Zuena, A.R., Casolini, P., Lattanzi, R. and Maftei, D. 2019. Chemokines in Alzheimer's disease: New insights into prokineticins, chemokine-like proteins. *Frontiers in Pharmacology*. **10**.